Advances in Experimental Medicine and Biology 1140

Urs F. Greber *Editor*

Physical Virology

Virus Structure and Mechanics

Springer

Advances in Experimental Medicine and Biology

Volume 1140

More information about this series at http://www.springer.com/series/5584

Urs F. Greber
Editor

Physical Virology

Virus Structure and Mechanics

Springer

Editor
Urs F. Greber
Department of Molecular Life Sciences
University of Zurich
Zurich, Switzerland

ISSN 0065-2598 ISSN 2214-8019 (electronic)
Advances in Experimental Medicine and Biology
ISBN 978-3-030-14740-2 ISBN 978-3-030-14741-9 (eBook)
https://doi.org/10.1007/978-3-030-14741-9

This Springer imprint is published by the registered company Springer Nature Switzerland AG.
The registered company address is: Gewerbestrasse 11, 6330 Cham, Switzerland

Contents

Chapter 1
Editorial: Physical Virology and the Nature of Virus Infections

Urs F. Greber

Abstract Virus particles, 'virions', range in size from nano-scale to micro-scale. They have many different shapes and are composed of proteins, sugars, nucleic acids, lipids, water and solutes. Virions are autonomous entities and affect all forms of life in a parasitic relationship. They infect prokaryotic and eukaryotic cells. The physical properties of virions are tuned to the way they interact with cells. When virions interact with cells, they gain huge complexity and give rise to an infected cell, also known as 'virus'. Virion–cell interactions entail the processes of entry, replication and assembly, as well as egress from the infected cell. Collectively, these steps can result in progeny virions, which is a productive infection, or in silencing of the virus, an abortive or latent infection. This book explores facets of the physical nature of virions and viruses and the impact of mechanical properties on infection processes at the cellular and subcellular levels.

Keywords Physics · Cell biology · Virus · Virion · Computational virology · Modelling · Tracking · Trafficking · Uncoating · Genome release · Reverse transcription · Structural evolution · Viral lineage · Active matter · Liquid unmixing · Inclusion bodies · Virion morphogenesis · Maturation · Mechanical properties · Stiffness · Pressure · Water wire · Acidic pH · Alkaline pH · Proton diode · Anisotropic mechanics

1.1 Introduction

The chapters in this book are written by physicists, chemists, computational scientists and biologists. Joining forces across disciplines has been a long-standing and fruitful approach to advancing the life sciences and furthering understanding of infectious disease. For example, biology, chemistry and physics have debated about the nature and the general principles of living matter [1–3]. We now realize

U. F. Greber (✉)
Department of Molecular Life Sciences, University of Zurich, Zurich, Switzerland
e-mail: urs.greber@imls.uzh.ch

U. F. Greber (ed.), *Physical Virology*, Advances in Experimental Medicine and Biology 1140, https://doi.org/10.1007/978-3-030-14741-9_1

that important aspects of living matter are governed by self-organization of their components. This insight has been largely based on a combination of wet lab experimental biology and mathematical modelling merging concepts of discrete particle physics and fluid dynamics [4–6]. It has given rise to a field of 'active matter', which aims to assemble a theory of living matter in biology incorporating the rules of mechanics and statistics. Not surprisingly, viruses have been long known to use self-organizing processes to assemble virions from protein and nucleic acid building blocks produced in excess in the infected cell [7, 8].

Alone, viruses have other intriguing properties relating them to active matter. For example, they are a swarm of genetically related elements and give rise to a productive infection when thousands of particles enter an organism [9, 10]. How this relates to the fact that cellular life is based on self-propelled entities from which large-scale structures and movements arise has remained unknown. The question is critical, however, since viruses gain importance in an increasingly globalized world where they emerge and spread unpredictably between animals, humans and plants [11, 12]. Furthermore, increasingly powerful strategies are designed to engineer viruses for the treatment of disease by gene therapy approaches and antagonizing pathogenic bacteria in humans and livestock [13–15].

The book here brings together an interdisciplinary group of physicists, chemists, mathematicians and biologists and explores how the physical nature of virus particles impacts on virus infections. It covers a select range of viruses, including enveloped and non-enveloped viruses, human immunodeficiency virus (HIV), rotavirus (RV), rabies virus (RABV), adenovirus (AdV) and the insect virus *Triatoma virus* (TrV).

1.2 Chapter 2: Virion Tracking in Entry

The chapter by Susan Daniel and Lakshmi Nathan describes some of the intricate pathways, by which virions enter into host cells [16]. The authors contrast single virus tracking experiments in cells and on biomimetic membranes assembled *in vitro* and discuss the pros and cons of both settings by highlighting examples of enveloped virus membrane fusion assays. They also discuss the power of high-resolution single virus experiments and put this in contrast to biochemical assays lacking spatial and temporal resolution at large but providing population average data.

1.3 Chapter 3: Uncoating of Rotavirus

Daniel Luque and Javier Rodriguez provide a comprehensive overview of the structural changes of the rotavirus (RV) particle in the course of entry into cells [17]. RV is a medium-sized 100 nm large, triple-layered non-enveloped particle with a segmented double-stranded (ds) RNA genome. The particle is primed for entry and

uncoating by limited proteolysis during egress and release. It undergoes a series of remarkable conformational changes triggered by interactions with host cell receptors and ionic cues. These limited uncoating steps activate the membrane penetration machinery, leading to the disruption of the limiting endosomal membrane and release of the dsRNA segments into the cytosol. Intriguing questions arise, for example, whether the outer capsid protein VP7 serves as a quasi-enveloped fusion protein, or how the virion structures in high and low calcium ions inform about the disassembly mechanism in endosomes.

1.4 Chapter 4: Host Factors in HIV Capsid Interactions

Leo James provides an atomistic level view of the interactions of critical host factors with the incoming capsid of HIV during entry [18]. The author raises arguments to diffuse the long-held notion in the field that the capsid is dismantled soon after virion fusion with the plasma membrane or an endosomal non-acidified membrane. Rather, it is now emerging that the capsid serves as a shield to contain the viral genome during trafficking throughout the cytosol. It thereby acts akin to the capsids of icosahedral DNA viruses, such as AdV, herpes virus, parvovirus and hepatitis B virus, all of which contain their viral genome up to the critical uncoating step close to the site of viral replication (for reviews, see [19–23]). This similarity is reinforced by the notion that capsid interacts with a range of host factors. These views open ways towards designing new virus inhibitors targeting the interface between the virion and host factors in the cytosol, or triggering premature viral uncoating distant from the replication site. The chapter also describes exciting new insights into yet another fundamental question in lentivirus infection biology, namely how and where the reverse transcription of the positive sense RNA genome into DNA occurs. Analyses of the available structures of the HIV capsid and new structures of purified capsid protein hexamers revealed a cluster of positively charged arginine residues at the center of each hexamer, potentially providing hundreds of gatable portals, through which to recruit nucleotides into the lumen of the capsid [24]. The concept emerges that the capsids of all lentiviruses are functioning as a semipermeable reaction chamber for importing and consuming nucleotide triphosphates for reverse transcription of the viral genome. This would be reminiscent of bacterial microcompartments, which isolate toxic reaction products from the rest of the cytoplasm [25] and consume metabolites by sequestering appropriate enzymes into dedicated protein cages [26].

1.5 Chapter 5: Virus Structure, Lineage and Evolution

Nicola Abrescia and Hanna Oksanen delve into the nature and evolutionary lineages of membrane-bearing icosahedral viruses, inspired by studies on the PRD1 bacteriophage, a distant relative of AdV [27]. Membrane-bearing phages are different from

eukaryotic enveloped viruses as they contain an internal rather than external membrane [28]. The authors discuss this feature. They also highlight the concept of 'structural evolution', which entails a relationship of structure to function across viral lineages spanning the three domains of life, notably in the absence of any discernable relationship in the sequence of the viral genomes [29]. This concept is also important for human viruses, for example the highly divergent picornaviruses, which comprise enteroviruses and respiratory viruses with common structural determinants, and mechanisms of membrane-bound replication [30, 31]. It is interesting to note that the structure of PRD1 is evolutionarily related to AdV [32]. This does not necessarily imply, however, that the two virions also function the same way in entry and assembly. For example, PRD1 is bearing a striking unique vertex, through which the viral genome is packaged and released in an ATP- and pressure-dependent manner, respectively [33]. In contrast, current evidence for AdV does not indicate a unique vertex in the icosahedral structure [34, 35]. This implies that AdV may not package its genome through a specialized vertex structure into a preformed capsid, unlike other eukaryotic DNA viruses, such as herpes simplex virus type 1 which bears a unique portal [36]. Rather, AdV may use a co-assembly process of capsomers and viral genome to give rise to virions [37]. In fact, the conditional genetic ablation of the DNA-organizing viral protein VII does not abrogate the formation of stable virions but gives rise to particles that are indistinguishable from wild type, except lacking protein VII, and some processing defects inside the capsid [38]. To our knowledge, there is no precedence for a viral DNA packaging machine that would accept both protein-bound and protein-free DNA. The evidence in case of AdV therefore strongly argues against a mechanism that packages viral DNA into a preformed virion but favors a model of co-packaging DNA and protein to form particles.

1.6 Chapter 6: Virus Assembly and Liquid Unmixed Compartments

In the next chapter, Jovan Nicolic, Danielle Blondel, Yves Gaudin and colleagues describe principles of particle assembly involving liquid–liquid phase separated, membrane-free compartments in the virus [39]. They elaborate on the structure and the function of viral assembly zones, often referred to as inclusion bodies. These liquid unmixed zones are considered as 'active matter', much like the nucleolus, stress granules or P-bodies, and contain intrinsically disordered proteins poised to interact with key proteins and RNAs to give rise to new virions. Viral factories formed by liquid–liquid phase separation ensure that the virus distinguishes self from non-self in the infected cell.

1.7 Chapter 7: Virus Maturation

Newly synthesized virions are often not readily infectious, unless they undergo a process called maturation, driven by limited proteolysis. Immature particles are protected against untimely uncoating cues in the assembly or egress pathways and traffic in a quasi-undisturbed manner through the cytosol or secretory pathways. Carmen San Martín describes how virion maturation entails conformational and structural changes to control the stability of the particle [40]. This is important because predominantly the mature virions are susceptible to cues from the host triggering productive virion entry into cells [41–44]. The author explores the biochemical process of virion maturation in icosahedral viruses from four lineages according to the structure of their capsid proteins (picornavirus-like, bluetonguevirus-like, HK97-like and PRD1-like), as well as alpha-, flavi- and retroviruses. San Martín further discusses how virion maturation changes the physical properties of particles and how this affects the response of the virions to uncoating cues.

1.8 Chapter 8: Mechanics of Virions

Mechanical properties of the virion determine both the strength and the unpacking mechanism of the viral genome. They represent key features of any infectious virus particle. Viral mechanics are dominated by the stiffness of the capsid shell, often in combination with the internal pressure from the tightly packed genome [45, 46], and can be tuned in the course of infectious entry into cells, for example by low pH, as shown for influenza A virus [47, 48]. Pedro de Pablo and Iwan Schaap explain how atomic force microscopy (AFM) helps to explore the surface topology and the mechanical properties of virions and how AFM identifies domains of the virion with distinct stiffness and particular susceptibility to cues from the host [49]. This is remarkable since virion stiffness has been shown to regulate the entry of immature HIV-1 particles [50]. Further to this, mechanical host cues occur on the AdV particles at the cell surface and catalyse a stepwise disassembly process of the virion. The process delivers leaky capsid shells containing the viral DNA to the cytosol, and the particles dock to nuclear pore complexes and deliver their DNA cargo into the nucleus upon rupture [20, 51–53]. At the stage of virion docking to the nuclear pore complex, the capsid is still pressurized by the entropic energy of the condensed viral genome, and this may impact on how the genome eventually transits through the nuclear pore complex into the nucleus upon the disassembly of the capsid [54–56]. This concept is built on prior studies with bacteriophage phi29 which showed that the pressure inside the virion is affected by DNA condensation, which was reversibly tuned by the DNA binding agent spermidine added to the virion in solution [57].

1.9 Chapter 9: Proton Diode and Alkaline pH in Insect Viruses

The chapter written by María Branda and Diego Guérin explores the physico-chemical mechanisms for proton conductance through protein cavities in the virion shell of the insect virus *Triatoma virus* (TrV) [58]. TrV is a picornavirus-like particle of the *Dicistroviridae* replicating in insects but not in humans. TrV is exposed to alkaline pH in the insect intestines, and excreted in large amounts in the insect feces, from where virions can be isolated and subjected to structural analyses. Such analyses showed that under extreme natural conditions, such as drying, the particles do not disintegrate but are held intact by the internal genome, which prevents capsid collapse [59]. In addition, the virion responds to changes in pH. Based on the atomic structure of TrV, quantum mechanics and molecular dynamic calculations, the authors put forward a model of water wires across the capsid shell at the fivefold axes of the icosahedral particles. In alkaline pH, this wire conducts protons from the inside of the virion to the outside. The wire is selective for protons due to a narrow restriction leading it to behave like a 'proton diode'. Remarkably, the diode does not allow protons to enter the virion lumen, which is consistent with the notion that the TrV particles are stable at pH up to 3.5. The particles become unstable at alkaline pH, which extracts protons from the virions. The model indicates that proton efflux increases the negative charges on the proteins inside the virion. This in turn removes positive inorganic ions, such as magnesium ions, from the RNA genome, which leads to RNA decondensation, expansion and eventually release from the virion. The authors use their model to estimate that at pH 8.5, the export of protons increases the charge excess on RNA by about 16%. Concomitant with RNA release, the internal protein VP4 is extruded and becomes membrane disruptive in a dose-dependent manner. These events likely mimic the situation in the insect rectum, where the virion is exposed to alkaline pH. By this elaborate unidirectional machinery, the virion selectively responds to changes in the environment to execute the RNA uncoating process, yet remains stable in dry conditions. The chapter impressively illustrates the power of combined experimental and theoretical approaches in analysing structure–function relationship in virus particles under harsh chemical conditions. Remarkably, this contrasts other viruses that are exposed to less harsh chemical environments in their life cycle. For example, during entry and uncoating AdV breaks off entire penton capsomers at the fivefold axes, the weakest part of the virion [60–63]. This exposes the membrane lytic protein but leaves the virion DNA in the capsid shell, well protected from the DNA sensors in the cytoplasm [52, 64].

1.10 Chapter 10: Multilayered Computational Modelling of Viruses

The final chapter by Elisabeth Jefferys and Mark Sansom describes how computer simulations can guide the exploration of virion properties and virion interactions with host components [65]. Computational virology opens the field to predictions that go beyond the readily doable wet lab experiments but remain testable by empirical approaches. The authors delve into the detailed mapping of mechanical properties of single virions, including the behaviour of fusion peptides of enveloped viruses, modelling of viral capsid assembly and genome encapsidation over extended periods of time, and end up with a discussion of whole viral particle simulations. They conclude by providing a high-level view on the power of computational approaches in virology. Computational approaches allow asking questions, such as: is a protein in the virion envelope directly exposed to the environment, and hence a good drug target? Or what is the impact of N- and O-linked glycosylation on the antigenic variation in the ectodomain of viral envelope proteins, and how do they contribute to the shielding of the epitopes on the virion? Such questions are relevant for the identification of neutralizing anti-HIV antibodies or other molecules directed to the virion, a notoriously difficult task. Computational virology can also use information about protein–protein contacts from the crystal structures of icosahedral particles and simulate the mechanics of the capsids to predict anisotropic properties of the virion. Anisotropy in virion mechanics is increasingly recognized as a key property of virions to respond to chemical or mechanical cues from the cell during entry. Simulations of viral structures and dynamics have implications for cell biology and imaging, two distinct fields with increasing overlaps [22, 66, 67]. The approach outlined by Jefferys and Sansom also illustrates the power of simultaneously combining models at different resolutions to focus available computing power on specific components of interest, and deepen mechanistic insights into the biophysical and biochemical processes that enable infectious agents to usurp the functions of host cells and cause disease. Computational implementations of mathematical models will thereby enhance causal insights into virus infection biology.

1.11 Outlook

Physical virology has been pioneered in the phage community, enhanced by powerful genetics and biochemical approaches [68]. It has become an emerging field of interest for mammalian cell biology, medicine and nano-science, with an impact on disease mechanisms, precision medicine and controlled drug delivery [69, 70]. Nowadays, the power of physical virology is perhaps most impressive, when the physical nature of the particles is linked to dynamic changes in the virions during the entry, assembly and maturation processes of the particles in host cells. We are looking

forward to new surprising and enriching interactions between virologists, physicists and computational scientists for further insights into the nature of infectious disease.

Acknowledgement I would like to thank all the authors for their valuable contributions, the reviewers of the chapters for insightful and constructive comments and Maarit Suomalainen for comments to the editorial text.

References

1. Beadle GW, Tatum EL (1941) Genetic control of biochemical reactions in Neurospora. Proc Natl Acad Sci U S A 27:499–506. https://doi.org/10.1073/pnas.27.11.499
2. Dronamraju KR (1999) Erwin Schrodinger and the origins of molecular biology. Genetics 153:1071–1076
3. Luria SE, Delbruck M (1943) Mutations of bacteria from virus sensitivity to virus resistance. Genetics 28:491–511
4. Nedelec FJ, Surrey T, Maggs AC, Leibler S (1997) Self-organization of microtubules and motors. Nature 389:305–308. https://doi.org/10.1038/38532
5. Toner J, Tu Y (1995) Long-range order in a two-dimensional dynamical XY model: how birds fly together. Phys Rev Lett 75:4326–4329. https://doi.org/10.1103/PhysRevLett.75.4326
6. Vicsek T, Czirok A, Ben-Jacob E, Cohen II, Shochet O (1995) Novel type of phase transition in a system of self-driven particles. Phys Rev Lett 75:1226–1229. https://doi.org/10.1103/PhysRevLett.75.1226
7. Caspar DL, Klug A (1962) Physical principles in the construction of regular viruses. Cold Spring Harb Symp Quant Biol 27:1–24. https://doi.org/10.1101/SQB.1962.027.001.005
8. Johnson JE, Speir JA (1997) Quasi-equivalent viruses: a paradigm for protein assemblies. J Mol Biol 269:665–675. https://doi.org/10.1006/jmbi.1997.1068
9. Domingo E, Sabo D, Taniguchi T, Weissmann C (1978) Nucleotide sequence heterogeneity of an RNA phage population. Cell 13:735–744. https://doi.org/10.1016/0092-8674(78)90223-4
10. Eigen M (1993) Viral quasispecies. Sci Am 269:42–49
11. Greber UF, Bartenschlager R (2017) An expanded view of viruses. FEMS Microbiol Rev 41:1–4. https://doi.org/10.1093/femsre/fuw044
12. Lederberg J (2000) Infectious history. Science 288:287–293. https://doi.org/10.1126/science.288.5464.287
13. Cisek AA, Dabrowska I, Gregorczyk KP, Wyzewski Z (2017) Phage therapy in bacterial infections treatment: one hundred years after the discovery of bacteriophages. Curr Microbiol 74:277–283. https://doi.org/0.1007/s00284-016-1166-x
14. Schmid M, Ernst P, Honegger A, Suomalainen M, Zimmermann M, Braun L, Stauffer S, Thom C, Dreier B, Eibauer M et al (2018) Adenoviral vector with shield and adapter increases tumor specificity and escapes liver and immune control. Nat Commun 9:450. https://doi.org/10.1038/s41467-017-02707-6
15. Young R, Gill JJ (2015) Microbiology. Phage therapy redux – what is to be done? Science 350:1163–1164. https://doi.org/10.1126/science.aad6791
16. Nathan L, Daniel S (2019) Single virion tracking microscopy for the study of virus entry processes in live cells and biomimetic platforms. In: Greber UF (ed) Physical virology – virus structure and mechanics. Springer, Berlin
17. Rodríguez JM, Luque D (2019) Structural insights into rotavirus entry. In: Greber UF (ed) Physical virology – virus structure and mechanics. Springer, Berlin
18. James LC (2019) The HIV-1 capsid: more than just a delivery package. In: Greber UF (ed) Physical virology – virus structure and mechanics. Springer, Berlin

19. Fay N, Pante N (2015) Old foes, new understandings: nuclear entry of small non-enveloped DNA viruses. Curr Opin Virol 12:59–65. https://doi.org/10.1016/j.coviro.2015.03.017
20. Flatt JW, Greber UF (2017) Viral mechanisms for docking and delivering at nuclear pore complexes. Semin Cell Dev Biol 68:59–71. https://doi.org/10.1016/j.semcdb.2017.05.008
21. Radtke K, Dohner K, Sodeik B (2006) Viral interactions with the cytoskeleton: a Hitchhiker's guide to the cell. Cell Microbiol 8:387–400. https://doi.org/10.1111/j.1462-5822.2005.00679.x
22. Wang IH, Burckhardt CJ, Yakimovich A, Greber UF (2018) Imaging, tracking and computational analyses of virus entry and egress with the cytoskeleton. Viruses 10(4):166. https://doi.org/10.3390/v10040166
23. Yamauchi Y, Greber UF (2016) Principles of virus uncoating: cues and the snooker ball. Traffic 17:569–592. https://doi.org/10.1111/tra.12387
24. Jacques DA, McEwan WA, Hilditch L, Price AJ, Towers GJ, James LC (2016) HIV-1 uses dynamic capsid pores to import nucleotides and fuel encapsidated DNA synthesis. Nature 536:349–353. https://doi.org/10.1038/nature19098
25. Tanaka S, Sawaya MR, Yeates TO (2010) Structure and mechanisms of a protein-based organelle in *Escherichia coli*. Science 327:81–84. https://doi.org/10.1126/science.1179513
26. Chowdhury C, Chun S, Pang A, Sawaya MR, Sinha S, Yeates TO, Bobik TA (2015) Selective molecular transport through the protein shell of a bacterial microcompartment organelle. Proc Natl Acad Sci U S A 112:2990–2995. https://doi.org/10.1073/pnas.1423672112
27. Oksanen HM, Abrescia NGA (2019) Membrane-containing Icosahedral Bacteriophage PRD1: the dawn of viral lineages. In: Greber UF (ed) Physical virology – virus structure and mechanics. Springer, Berlin
28. Espejo RT, Canelo ES (1968) Properties of bacteriophage PM2: a lipid-containing bacterial virus. Virology 34:738–747. https://doi.org/10.1016/0042-6822(68)90094-9
29. Bamford DH, Burnett RM, Stuart DI (2002) Evolution of viral structure. Theor Popul Biol 61:461–470. https://doi.org/10.1006/tpbi.2002.1591
30. Rossmann MG, Arnold E, Erickson JW, Frankenberger EA, Griffith JP, Hecht HJ, Johnson JE, Kamer G, Luo M, Mosser AG et al (1985) Structure of a human common cold virus and functional relationship to other picornaviruses. Nature 317:145–153. https://doi.org/10.1038/317145a0
31. Roulin PS, Lotzerich M, Torta F, Tanner LB, van Kuppeveld FJ, Wenk MR, Greber UF (2014) Rhinovirus uses a phosphatidylinositol 4-phosphate/cholesterol counter-current for the formation of replication compartments at the ER-Golgi interface. Cell Host Microbe 16:677–690. https://doi.org/10.1016/j.chom.2014.10.003
32. Benson SD, Bamford JK, Bamford DH, Burnett RM (1999) Viral evolution revealed by bacteriophage PRD1 and human adenovirus coat protein structures. Cell 98:825–833. https://doi.org/10.1016/S0092-8674(00)81516-0
33. Stromsten NJ, Bamford DH, Bamford JK (2003) The unique vertex of bacterial virus PRD1 is connected to the viral internal membrane. J Virol 77:6314–6321. https://doi.org/10.1128/JVI.77.11.6314-6321.2003
34. Liu H, Jin L, Koh SB, Atanasov I, Schein S, Wu L, Zhou ZH (2010) Atomic structure of human adenovirus by cryo-EM reveals interactions among protein networks. Science 329:1038–1043. https://doi.org/10.1126/science.1187433
35. Yu X, Veesler D, Campbell MG, Barry ME, Asturias FJ, Barry MA, Reddy VS (2017) Cryo-EM structure of human adenovirus D26 reveals the conservation of structural organization among human adenoviruses. Sci Adv 3:e1602670. https://doi.org/10.1126/sciadv.1602670
36. Cardone G, Winkler DC, Trus BL, Cheng N, Heuser JE, Newcomb WW, Brown JC, Steven AC (2007) Visualization of the herpes simplex virus portal in situ by cryo-electron tomography. Virology 361:426–434. https://doi.org/10.1016/j.virol.2006.10.047
37. Condezo GN, San Martin C (2017) Localization of adenovirus morphogenesis players, together with visualization of assembly intermediates and failed products, favor a model where assembly and packaging occur concurrently at the periphery of the replication center. PLoS Pathog 13:e1006320. https://doi.org/10.1371/journal.ppat.1006320

38. Ostapchuk P, Suomalainen M, Zheng Y, Boucke K, Greber UF, Hearing P (2017) The adenovirus major core protein VII is dispensable for virion assembly but is essential for lytic infection. PLoS Pathog 13:e1006455. https://doi.org/10.1371/journal.ppat.1006455
39. Nikolic J, Lagaudrière-Gesbert C, Scrima N, Blondel D, Gaudin Y (2019) Structure and function of Negri bodies. In: Greber UF (ed) Physical virology – virus structure and mechanics. Springer, Berlin
40. San Martín C (2019) Virus maturation. In: Greber UF (ed) Physical virology – virus structure and mechanics. Springer, Berlin
41. Greber UF, Singh I, Helenius A (1994) Mechanisms of virus uncoating. Trends Microbiol 2:52–56. https://doi.org/10.1016/0966-842X(94)90126-0
42. Imelli N, Ruzsics Z, Puntener D, Gastaldelli M, Greber UF (2009) Genetic reconstitution of the human adenovirus type 2 temperature-sensitive 1 mutant defective in endosomal escape. Virol J 6:174. https://doi.org/10.1186/1743-422X-6-174
43. Kilcher S, Mercer J (2015) DNA virus uncoating. Virology 479–480:578–590. https://doi.org/10.1016/j.virol.2015.01.024
44. Suomalainen M, Greber UF (2013) Uncoating of non-enveloped viruses. Curr Opin Virol 3:27–33. https://doi.org/10.1016/j.coviro.2012.12.004
45. Evilevitch A, Roos WH, Ivanovska IL, Jeembaeva M, Jonsson B, Wuite GJ (2011) Effects of salts on internal DNA pressure and mechanical properties of phage capsids. J Mol Biol 405:18–23. https://doi.org/10.1016/j.jmb.2010.10.039
46. Klug WS, Roos WH, Wuite GJ (2012) Unlocking internal prestress from protein nanoshells. Phys Rev Lett 109:168104. https://doi.org/10.1103/PhysRevLett.109.168104
47. Greber UF (2014) How cells tune viral mechanics – insights from biophysical measurements of influenza virus. Biophys J 106:2317–2321. https://doi.org/10.1016/j.bpj.2014.04.025
48. Li S, Sieben C, Ludwig K, Hofer CT, Chiantia S, Herrmann A, Eghiaian F, Schaap IA (2014) pH-controlled two-step uncoating of influenza virus. Biophys J 106:1447–1456. https://doi.org/10.1016/j.bpj.2014.02.018
49. de Pablo PJ, Schaap IAT (2019) Atomic force microscopy of viruses. In: Greber UF (ed) Physical virology – virus structure and mechanics. Springer, Berlin
50. Pang HB, Hevroni L, Kol N, Eckert DM, Tsvitov M, Kay MS, Rousso I (2013) Virion stiffness regulates immature HIV-1 entry. Retrovirology 10:4. https://doi.org/10.1186/1742-4690-10-4
51. Burckhardt CJ, Greber UF (2009) Virus movements on the plasma membrane support infection and transmission between cells. PLoS Pathog 5:e1000621. https://doi.org/10.1371/journal.ppat.1000621
52. Burckhardt CJ, Suomalainen M, Schoenenberger P, Boucke K, Hemmi S, Greber UF (2011) Drifting motions of the adenovirus receptor CAR and immobile integrins initiate virus uncoating and membrane lytic protein exposure. Cell Host Microbe 10:105–117. https://doi.org/10.1016/j.chom.2011.07.006
53. Strunze S, Engelke MF, Wang IH, Puntener D, Boucke K, Schleich S, Way M, Schoenenberger P, Burckhardt CJ, Greber UF (2011) Kinesin-1-mediated capsid disassembly and disruption of the nuclear pore complex promote virus infection. Cell Host Microbe 10:210–223. https://doi.org/10.1016/j.chom.2011.08.010
54. Bauer DW, Huffman JB, Homa FL, Evilevitch A (2013) Herpes virus genome, the pressure is on. J Am Chem Soc 135:11216–11221. https://doi.org/10.1021/ja404008r
55. Greber UF (2016) Virus and host mechanics support membrane penetration and cell entry. J Virol 90:3802–3805. https://doi.org/10.1128/JVI.02568-15
56. Luisoni S, Greber UF (2016) Biology of adenovirus cell entry – receptors, pathways, mechanisms. In: Curiel D (ed) Adenoviral vectors for gene therapy. Academic Press, London, pp 27–58. ISBN: 9780128002766
57. Hernando-Perez M, Miranda R, Aznar M, Carrascosa JL, Schaap IA, Reguera D, de Pablo PJ (2012) Direct measurement of phage phi29 stiffness provides evidence of internal pressure. Small 8:2366–2370. https://doi.org/10.1002/smll.201200664

58. Branda MM, Guérin DMA (2019) Alkalinization of Icosahedral nonenveloped viral capsid interior through proton channeling. In: Greber UF (ed) Physical virology – virus structure and mechanics. Springer, Berlin
59. Martin-Gonzalez N, Guerin Darvas SM, Durana A, Marti GA, Guerin DMA, de Pablo PJ (2018) Exploring the role of genome and structural ions in preventing viral capsid collapse during dehydration. J Phys Condens Matter 30:104001. https://doi.org/10.1088/1361-648X/aaa944
60. Greber UF, Willetts M, Webster P, Helenius A (1993) Stepwise dismantling of adenovirus 2 during entry into cells. Cell 75:477–486. https://doi.org/10.1016/0092-8674(93)90382-Z
61. Nakano MY, Boucke K, Suomalainen M, Stidwill RP, Greber UF (2000) The first step of adenovirus type 2 disassembly occurs at the cell surface, independently of endocytosis and escape to the cytosol. J Virol 74:7085–7095. https://doi.org/10.1128/JVI.74.15.7085-7095.2000
62. Ortega-Esteban A, Bodensiek K, San Martin C, Suomalainen M, Greber UF, de Pablo PJ, Schaap IA (2015) Fluorescence tracking of genome release during mechanical unpacking of single viruses. ACS Nano 9:10571–10579. https://doi.org/10.1021/acsnano.5b03020
63. Snijder J, Reddy VS, May ER, Roos WH, Nemerow GR, Wuite GJ (2013) Integrin and defensin modulate the mechanical properties of adenovirus. J Virol 87:2756–2766. https://doi.org/10.1128/JVI.02516-12
64. Wang IH, Suomalainen M, Andriasyan V, Kilcher S, Mercer J, Neef A, Luedtke NW, Greber UF (2013) Tracking viral genomes in host cells at single-molecule resolution. Cell Host Microbe 14:468–480. https://doi.org/10.3390/v10040166
65. Jefferys EE, Sansom MPS (2019) Computational virology: molecular simulations of virus dynamics and interactions. In: Greber UF (ed) Physical virology – virus structure and mechanics. Springer, Berlin
66. Sbalzarini IF, Greber UF (2018) How computational models enable mechanistic insights into virus infection. Methods Mol Biol 1836:609–631. https://doi.org/10.1007/978-1-4939-8678-1_30
67. Witte R, Andriasyan V, Georgi F, Yakimovich A, Greber UF (2018) Concepts in light microscopy of viruses. Viruses 10(4):202. https://doi.org/10.3390/v10040202
68. Summers WC (1993) How bacteriophage came to be used by the Phage Group. J Hist Biol 26:255–267. https://doi.org/10.1128/9781555816506.ch1
69. Evilevitch A (2013) Physical evolution of pressure-driven viral infection. Biophys J 104:2113–2114. https://doi.org/10.1016/j.bpj.2013.03.062
70. Yin J, Redovich J (2018) Kinetic modeling of virus growth in cells. Microbiol Mol Biol Rev 82: e00066–00017. https://doi.org/10.1128/MMBR.00066-17

Chapter 2
Single Virion Tracking Microscopy for the Study of Virus Entry Processes in Live Cells and Biomimetic Platforms

Lakshmi Nathan and Susan Daniel

Abstract The most widely-used assays for studying viral entry, including infectivity, cofloatation, and cell-cell fusion assays, yield functional information but provide low resolution of individual entry steps. Structural characterization provides high-resolution conformational information, but on its own is unable to address the functional significance of these conformations. Single virion tracking microscopy techniques provide more detail on the intermediate entry steps than infection assays and more functional information than structural methods, bridging the gap between these methods. In addition, single virion approaches also provide dynamic information about the kinetics of entry processes. This chapter reviews single virion tracking techniques and describes how they can be applied to study specific virus entry steps. These techniques provide information complementary to traditional ensemble approaches. Single virion techniques may either probe virion behavior in live cells or in biomimetic platforms. Synthesizing information from ensemble, structural, and single virion techniques ultimately yields a more complete understanding of the viral entry process than can be achieved by any single method alone.

Keywords Fluorescence microscopy · Virion tracking · Lipid bilayer · Virus entry · Single virus particle · Enveloped virus · Non-enveloped virus · Infection · Membrane fusion · Imaging · Live cells · Biomimetics · Tracking

2.1 Overview of Virus Entry

Viruses can be broadly classified as non-enveloped or enveloped. Non-enveloped viruses are encapsulated by a protein coat, called a capsid, while enveloped viruses are encapsulated in a host-derived lipid membrane implanted with viral proteins

L. Nathan (✉) · S. Daniel (✉)
Robert Frederick Smith School of Chemical and Biomolecular Engineering, Cornell University, Ithaca, NY, USA
e-mail: ln258@cornell.edu; sd386@cornell.edu

U. F. Greber (ed.), *Physical Virology*, Advances in Experimental Medicine and Biology 1140, https://doi.org/10.1007/978-3-030-14741-9_2

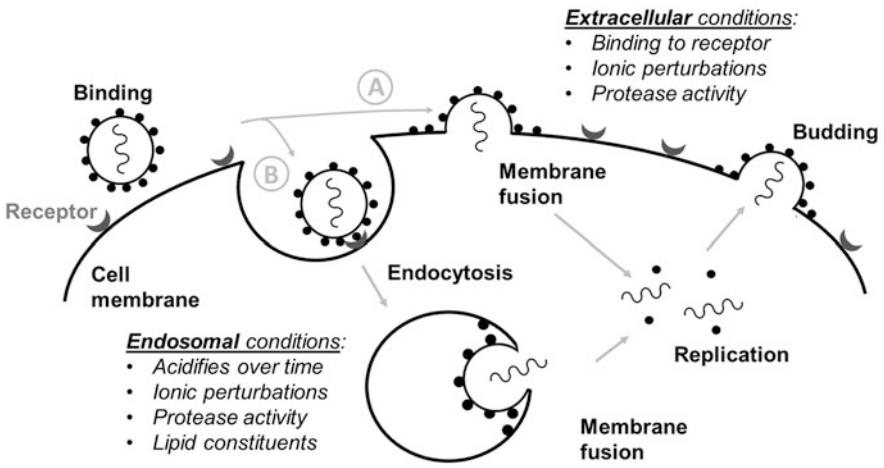

Fig. 2.1 Overview of the life cycle of an enveloped virus. The entry process begins with the virus binding to a receptor on the surface of the cell. This binding may result in (**a**) release of the viral genome via fusion at the plasma membrane or (**b**) uptake by endocytosis or macropinocytosis (not shown) followed by fusion within the endosome. The location and mechanism of fusion can be impacted by environmental conditions, including pH, ions, protease activity, and lipid composition. Once the genome has been released into the cytosol, it can access cellular machinery, leading to replication of the viral genome and synthesis of new viral proteins. Newly synthesized virions can then exit the cell by budding

called spikes. The coat protein of non-enveloped viruses and spike proteins of enveloped viruses facilitate the virus's entry into the cell. These viral proteins engage receptors on host cells to promote attachment to the host cell surface, but after that initial binding event, non-enveloped and enveloped viruses breach host cell membranes through different pathways [1]. Non-enveloped viruses typically enter cells by endocytosis and then either lyse the intracellular compartment, or release genetic material through a pore created in the membrane of the intracellular compartment [2, 3]. Enveloped viruses, on the other hand, must undergo membrane fusion with a cellular membrane to release their genetic material into the host cell (Fig. 2.1).

Some enveloped viruses, like coronaviruses or human immunodeficiency virus (HIV), can undergo fusion at the plasma membrane (A), while others, like influenza, fuse within endosomes (B) [4].

Binding and uncoating of nonenveloped viruses is mediated by the capsid surface or capsid proteins projecting from it. For enveloped viruses, the fusion or spike proteins embedded in the envelope are responsible for both receptor binding and membrane fusion. Membrane fusion proteins can be subdivided into three categories based on their structure [5]. Class I fusion proteins are primarily α-helical, Class II fusion proteins contain mainly β-sheets and β-strands, and Class III fusion proteins contain a mix of both α-helices and β-sheets. Class I and II fusion proteins require a proteolytic priming event to convert them from a fusion-incompetent state to a fusion-competent one. Once the fusion protein is in a fusion-competent state, the structural

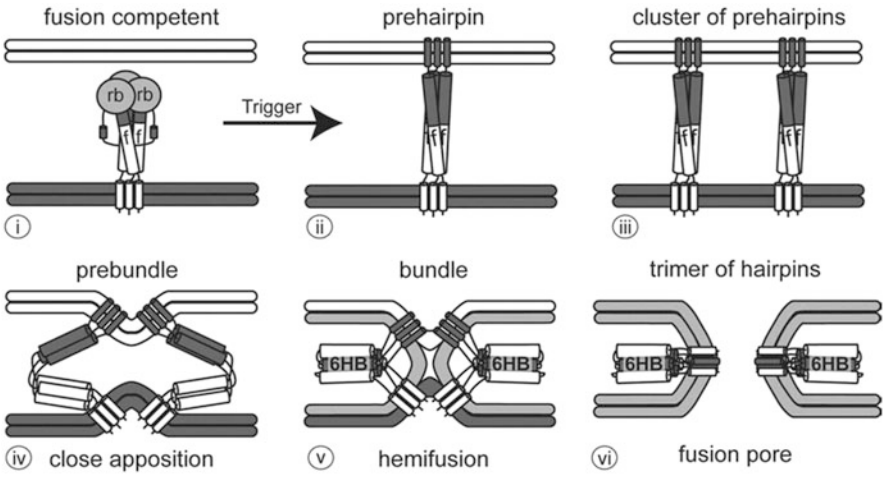

Fig. 2.2 Steps in viral fusion. (**i**) The viral envelope (bottom) approaches the target membrane (top). The viral fusion protein consists of a receptor binding domain (rb) and a fusion domain (f). (**ii**) The prehairpin structure embeds into the target membrane. (**iii**) Several prehairpin trimers cluster together. (**iv**) The prehairpins begin to fold back to form the prebundle state and bring the membranes close together. (**v**) Fusion proteins further fold into a six helix bundle (6HB). Lipids in the outer leaflets of the viral and target bilayers mix during hemifusion. (**vi**) A pore opens between the target membrane and the viral envelope as the fusion proteins become a trimer of hairpins. Source: White et al. [5], Taylor & Francis Ltd., www.tandfonline.com

rearrangement necessary for exposure of the fusion peptide and its burial into the target membrane is often triggered by some change in environmental conditions. Fusion may be triggered by receptor binding itself, lowering of pH, protease action [6], or a combination of these [4, 7]. Viruses that fuse at the plasma membrane may be triggered by receptor binding or protease activation, while those that fuse within the endosome generally require low pH and may require other additional cues, such as changes in other ions than protons, or endosome-specific protease exposure.

Despite the diversity in structure and triggering mechanisms, fusion proteins typically follow a common pathway for merging the viral envelope with the host membrane (Fig. 2.2), as described in White et al. [5] and Harrison [8]. After fusion is triggered, the protein rearranges into a prehairpin intermediate (1) with the fusion peptide inserted into the host membrane. While the fusion protein may be found as dimers or trimers on the surface of the virus (2), the prehairpin intermediate consists of a trimer. It is thought that several prehairpin intermediates cluster together then fold back on themselves to bring the membranes close to each other (3). As the prehairpins fold into a six-helix bundle, the membranes are brought close enough that lipids from their outer leaflets are able to mix, creating a structure often referred to as a "stalk" (4). This step is known as hemifusion. Lastly, a pore forms (5) enabling the viral genome to pass through this opening as the fusion proteins form into a stable trimer of hairpins.

Although all viral fusion proteins studied to date follow this common pathway, much remains unknown about viral entry itself. For example, the dynamics of these fusion steps are not fully understood, the fusion trigger of some viruses remains ambiguous, and developing antivirals to halt virus entry requires further characterization of all of the steps between initial viral contact with the host cell and viral genome release.

Techniques for studying virus entry can be broadly classified as those that examine the entry of a collective group or ensemble of virions and those that track individual virion entry. Ensemble methods provide information on the broader context of entry steps, while single virion imaging provides detailed information on the dynamics of those steps. Ensemble methods include many of the most well-established techniques for studying viral entry and may probe overall infection, receptor binding, fusion, or cargo transfer. Single virion imaging techniques can provide mechanistic detail and kinetics for steps that are masked in ensemble methods. In addition, for HIV [9], influenza [10], and Ebola virus [11], most virions that encounter a cell are not involved in productive entry so the ability of single virion techniques to distinguish entry-competent particles from non-competent ones and characterize their individual behavior provides valuable data on heterogeneity in viral populations and its ultimate impact on infection.

The remaining part of the chapter will focus on single particle tracking microscopy techniques compatible with dynamic/temporal data acquisition, their salient features, and how the data generated complement ensemble methods for studying viral entry processes and their intermediate steps and mechanisms.

2.2 Single Virion Tracking Techniques

2.2.1 Enabling Technologies

Over the past 30 years, microscopy optics, fluorescent labeling strategies, computing power and image processing have enabled the dynamic tracking of individual virions throughout the entry process and the decomposition of their intermediate steps. For some examples, see the following references: [12–18]. In particular, charge coupled device (CCD) cameras combined with advanced microscopy enable single particle resolution [19]. The frame rates of today's cameras dictate temporal resolution of dynamic studies, which can range from a few to hundreds of milliseconds [20, 21]. In the following sections, the main advances enabling single virion tracking techniques are summarized.

2.2.1.1 Microscope Configurations

Three microscopy configurations are commonly employed in virology research: epifluorescence, total internal reflection fluorescence (TIRF), and confocal

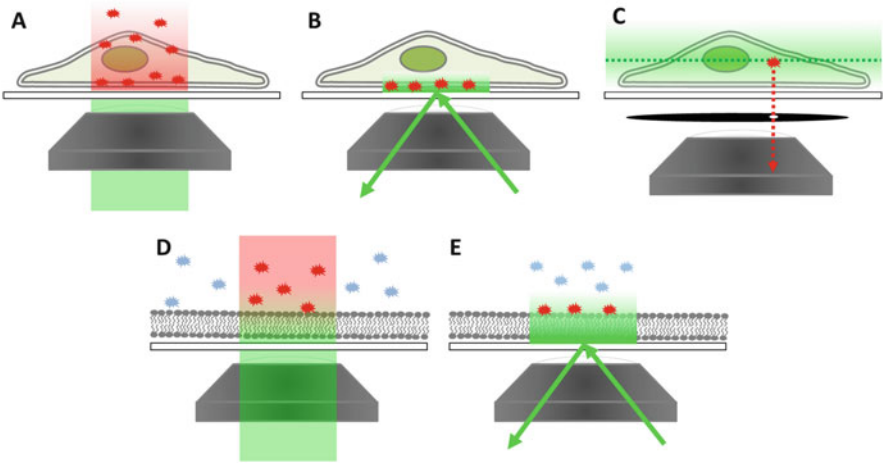

Fig. 2.3 Microscope configurations for viewing virus interactions with cells and biomimetic membrane surfaces. Green color denotes excitation light and red denotes emission light. (**a**) The epifluorescence configuration illuminates an entire light path through the cell and excites any fluorophores within it, making it impossible to track virions in live cells this way due to the overall background signal. (**b**) TIRF microscopy illuminates a thin layer near the interface between the glass microscope slide and buffer solution. Cell membranes residing in this zone with fluorescently labeled virions can be visualized as individuals, provided they are far enough apart from each other. (**c**) Confocal microscopy with a pinhole arrangement can examine specific Z-planes within the cell and block out nearly all background signals from the surrounding media excited by out-of-plane light. Here, the green dashed line denotes the focal plane of excitation, the green gradient denotes out-of-plane light, and the red star and its dashed line arrow indicate only the emission from this fluorophore travel to the camera. (**d**) Epifluorescence illumination in the biomimetic membrane platform suffers the same poor background issue as whole cells when fluorescently labeled virions are in the bulk. (**e**) TIRF microscopy enables individual virion visualization bound to the membrane surface without exciting those in the bulk above it

microscopy [22, 23] as illustrated in Fig. 2.3. The epifluorescence configuration (Fig. 2.3a, d) illuminates everything within the field of view. So, unbound virions in the bulk phase or cells with high background autofluorescence result in high noise that obscures signals from individual virions. As a result, epifluorescence is not typically used for single virion tracking.

In the TIRF configuration (Fig. 2.3b, e), only particles within a shallow field are illuminated, eliminating noise from the bulk solution and thereby enhancing the signal-to-noise. This configuration is achieved by setting the incidence angle of the laser to be higher than the critical angle for total internal reflection of the laser light at the glass/water or glass/cell interface, resulting in an exponentially decaying evanescent field that penetrates roughly 100 nm into the sample [24, 25]. The advantage with this configuration is that a two-dimensional plane can be monitored precisely, enabling the distinction between binding and fusion events of the virions, with appropriate virion labeling (described next). However, no three dimensional tracking information can be obtained; data collection is confined to the interfacial region of

interest. This configuration is most suitable for examination of virus behavior at biomimetic surfaces like supported lipid bilayers or live cell plasma membranes close to the glass surface.

In the confocal microscopy configuration (Fig. 2.3c), a pinhole optic assists in filtering out background noise while scanning across a sample one Z-plane at a time. Cross sections may be stacked to yield a three-dimensional image, making this configuration suitable for imaging live or fixed cells and observing trafficking of viruses in the cytosol. The disadvantage of this configuration is the difficulty in temporally tracking phenomena in real-time, while simultaneously scanning across slices of the sample and reconstructing the image. Furthermore, exposure to strong light can be toxic to living cells [26]. As technology advances, these drawbacks should subside.

2.2.1.2 Virion Labeling

In all of these microscopy techniques, virions must be labeled to visualize them. Virions are commonly labeled by attaching fluorescent proteins to viral proteins, by incorporating chemical dyes into the virion, or by incorporating quantum dots [27–29]. Here, we focus on fluorescent and chemical labels; for a review of quantum dot techniques we refer the reader to Liu et al. [28]. Both fluorescent proteins and chemical labels have been used to label viral coatings as well as contents. Fluorescent viral protein constructs can be prepared for enveloped [30] or non-enveloped viruses [31, 32] and virions are labeled as they are synthesized. Chemical labels, including Alexa dyes, octadecylrhodamine B (R18), and carbocyanine perchlorates (DiD, DiI, or DiO) may be added during virion synthesis or post-production. Some chemical labels, like lipophilic dyes, are only suitable for labeling enveloped viruses while others, like amino-reactive dyes, may be employed with either enveloped or non-enveloped virions [22].

Membrane hemifusion is typically monitored with lipophilic dyes that undergo dequenching when the virion fuses with the target membrane, while pore formation is typically tracked with a dye that can partition into the capsid and then dissipate upon release from the virion [33, 34]. It is also possible to incorporate pH sensors into the envelope of virions to measure the pH of the fusion environment [35]. In all cases, care must be taken to ensure that labeling does not adversely impact viral infectivity. This can be easily assessed by conducting cell infectivity assays with labeled virions. In general, these labeling approaches can be optimized to mitigate any significant negative impact.

2.2.1.3 Image Processing

Once the microscopy configuration and virion labeling method have been chosen, image processing assists in extracting information from the images. Today's fast computers and image processing algorithms assist in noise filtering, virion tracking,

and trajectory mapping, as described in the references that follow. In single virion imaging, noise is always a primary concern, regardless of the microscope configuration. To combat this, several particle detection and image restoration techniques have been developed specifically for single virion tracking [36, 37]. Coordinates of the particles are obtained by scanning filtered images for areas of fluorescence intensity that exceed a certain threshold or fit a particular intensity profile [38, 39]. The next challenge is obtaining accurate virion tracking from one frame to the next (temporal trajectories). Particle trajectories can be calculated from nearest-neighbor associations [21, 40]. Measurements of virion movement and mean squared displacements are then used to determine whether the virions exhibit directed, normal, or anomalous diffusion [41]. The diffusion type can indicate the type of interactions the virion is having with the surface of the cell or extracellular environment. Tracking frame-to-frame is important in measuring binding residence times as well, and by extension, binding strength characteristics [37]. Once bound, the progression of membrane fusion can be tracked from frame-to-frame using strategies like fluorescence dequenching, where the evolution of the fluorescence signal reports on the merging of membranes, the rate of membrane mixing, and the release of viral genome. Finally, obtaining good statistical data from virion tracking experiments requires collecting data on hundreds of individual virions.

2.2.2 Experimental Approach

Single virion tracking may follow virions through the infection process in live cells using confocal microscopy or within an in vitro biomimetic platform using TIRF microscopy. Cell-based virion imaging techniques enable direct visualization of the viral entry pathway and interactions between virions and host cell machinery within the native complexity of the cellular environment. On the other hand, biomimetic platforms utilizing the TIRF configuration enable observation of membrane surface phenomena and can be integrated with tools like microfluidics that allow the user to define and test a tightly controlled environment. This control enables decoupling of factors that may be hard to detangle in vivo. Sections 2.2.2.1 and 2.2.2.2 provide overviews of these two approaches while Sect. 2.3 provides examples of specific implementations of single virion tracking to the investigation of viral entry and contrasts them with ensemble approaches.

2.2.2.1 Live Cell Imaging

In current cell-based fluorescence assays, both virions and cellular components are fluorescently labeled so their interactions can be tracked with multicolor real-time microscopy. Live cell virion tracking can be used to observe cell-cell spread, receptor binding, intracellular trafficking and membrane fusion. Virions may be labeled with fluorescent proteins, chemical dyes, or quantum dots while intracellular

components are typically labeled using fluorescent proteins. Epifluorescence, TIRF, and confocal microscopy have all been used in live cell single virion tracking. Virions may be tracked in two or three dimensions depending on the microscope configuration, as described above. Certain cell types may be easier to image due to autofluorescence of cellular components [11].

As early as the 1980s, fusion of individual virions at the plasma membrane surface was observed. Virions were labeled with R18, which self-quenches at high concentrations, and dequenching of the R18 upon fusion of the virion with a membrane was detected by a simple fluorescence microscope. Early assays monitored fusion at the plasma membrane of erythrocytes, where fusion of influenza could be triggered by lowering the pH [42, 43].

An important aspect of live cell approaches is that it is possible to inhibit cellular machinery by drug treatment or gene knockout. Such cells can be used in combination with live cell imaging to identify key cellular components that are necessary for virus entry. A review of implementations and insights gained from live cell single virion imaging will be provided in Sect. 2.3. We also recommend the reviews by Brandenburg and Zhuang [14], Ewers and Schelhaas [20], Otterstrom and Van Oijen [22], Sun et al. [23], and Wang et al. [29].

2.2.2.2 Biomimetic Platforms

In early work, perhaps the first, observations of membrane fusion of individual virions to biomimetic membranes was monitored with video fluorescence microscopy [44, 45]. In this work, planar bilayers were suspended over a small hole in a Teflon sheet, a so-called black lipid membrane (BLM), to serve as the host cell membrane mimic. However, BLMs are fragile and prone to rupture and continued progress using this approach was slow. In recent years, supported lipid bilayers, which are more robust than BLMs, have become more widely used in in vitro single virion tracking experiments. Because these SLB platforms are becoming the backbone of many types of single virion tracking experiments, it is worth describing them in some detail here.

A supported lipid bilayer is a planar, single bilayer, typically self-assembled by rupturing liposomes at the surface of hydrophilic silica surfaces like glass microscope slides. For reviews of supported lipid bilayer technologies, we encourage the reader to consult Sackmann [46], Tanaka and Sackmann [47], and Castellana and Cremer [48]. These supported lipid bilayers act as mimics for cellular membranes and the compatibility of these bilayers with flat glass surfaces makes them ideal for coupling to microscopy techniques. Additionally, supported bilayers may be assembled within a flow cell or microfluidic device, which enables the exchange of buffers and, consequently, the precise control over the binding and fusion environment during single virion tracking microscopy. The composition of these bilayers is highly tunable, ranging from the simplest lipid components, to recapitulating the complexity of the plasma cell membrane of specific cell types (Fig. 2.4).

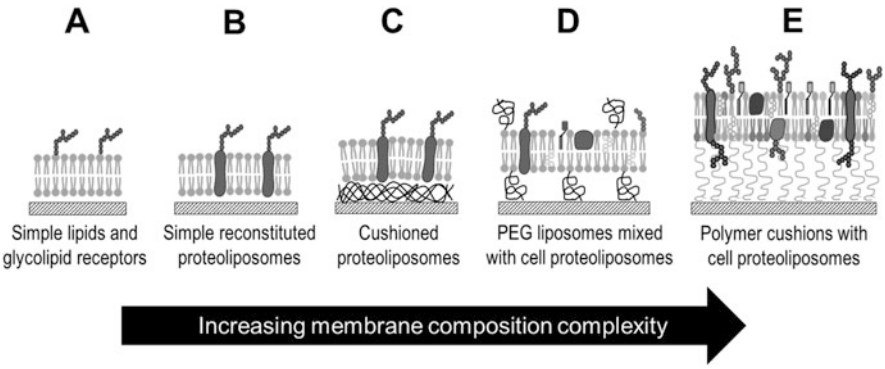

Fig. 2.4 Supported lipid bilayers (SLBs) and their increasing complexity and features. (**a**) A simple SLB with glycolipid receptors. (**b**) A SLB made from reconstituted lipids and protein receptors. (**c**) Cushioned SLB to enhance protein receptor mobility. (**d**) Mixed liposome and cell-derived SLB containing polyethylene glycol cushions. (**e**) Plasma membrane-derived SLB on polymer cushion

Initial studies employed purely lipid bilayers with glycolipid viral receptors [12, 33, 34, 49]. More recent work has used reconstituted proteoliposomes that contain protein receptors [50]. There has also been progress in using composite membranes made from cell-derived membrane components mixed with PEGylated liposomes to engender the SLB with both biologically relevant material (receptors, etc.) and a built-in cushion to maintain constituent mobility [51, 52]. Other work has demonstrated the ability to form bilayers from cell plasma membrane blebs as a way to incorporate transmembrane proteinaceous receptors and complete native cell materials into planar geometries [13, 53, 54]. The incorporation of transmembrane proteins greatly expands the range of viruses that can be studied with single virions tracking techniques [13].

Notably, the simplest lipid-only bilayer on glass is roughly 4 nm thick and sits above a thin layer of water on the order of a nanometer thick [55, 56]. This feature enables the two-dimensional mobility of lipids within the bilayer necessary for membrane fusion, but mobility is also a key property for allowing receptors to rearrange to permit multivalent binding interactions, as they do in live cell membranes. Mobility of protein receptors, particularly those with transmembrane domains, can be a challenge in these platforms if the water gap is insufficient for limiting interaction between the protein and the glass support. To overcome this challenge, various cushions, such as polyethylene glycol (PEG) [52], bovine serum albumin, dextran [33, 57], or polyelectrolyte brushes [54], have been placed between the bilayer and the supporting surface to improve protein mobility [58].

It is also possible to form supported lipid bilayers that mimic the *viral membrane* instead of the host membrane and conduct experiments in the opposite configuration. Here, binding and fusion is studied by monitoring liposomes decorated with host cell receptors interacting with the planar virus-like bilayer containing embedded viral proteins [59–61]. Such an arrangement could be used for screening applications of antivirals that target entry processes, without the need for live virus or pseudotyped particles.

In summary, biomimetic platforms enable a level of environmental control that cannot be attained in live cell particle tracking techniques. First, there is a degree of control over the host cell membrane mimic's composition that is difficult to alter in live cells. Second, in these platforms, the buffers in contact with the virus can have a defined composition and the experimenter controls the timing and order of exposure to proteases, pH, or any other component of interest to the virus. But perhaps the most salient feature of this experimental approach is that these platforms allow detailed examination of the binding and membrane fusion process and gathering of dynamic data from these processes. However, the two-dimensional, in vitro nature of these platforms make them unsuitable for measuring cytoskeletal involvement in entry. Thus, to obtain the most complete information about the infection process, combining data from complementary approaches using live cells and biomimetic platforms is an excellent strategy.

2.3 Applications of Single Virion Tracking and Complementary Ensemble Approaches

In the following sections we describe how single virion tracking has been applied to investigate different steps in virus entry. We also include overviews of a selection of ensemble methods to appreciate the synergy between the data collected by the different techniques in providing a complete description of virus entry. Table 2.1 provides a quick reference of techniques and the data that can be obtained in each approach for each entry stage.

2.3.1 Tracking Extracellular Movement of Virions

There are two scales of transport to be observed during virus spread and infection. On the larger scale is the transport and spread of virions between neighboring cells. Also of interest is the smaller-scale tracking of an individual virion on a cell plasma surface before it is internalized by that particular cell. In the following sections, experiments at each scale will be described with selected examples and references.

2.3.1.1 Tracking Virion Movement Between Cells

Tracking virion movement in the in vivo environment has revealed various avenues of virus spread to surrounding cells. The predominant transport mechanisms of virus spread between cells are: (1) virions freely diffusing through the extracellular environment to neighboring cell surfaces, or (2) spreading to neighboring cells through direct transmission across adjoining membranes. For the first mechanism,

Table 2.1 Comparison of single virion and ensemble methods for studying particular viral entry steps, including key features of each method

Virus entry step	Single virion tracking		Ensemble methods
	Live cell	Biomimetic	
Extracellular transport	• Direct cell-cell spread • Extracellular diffusion	• Movement through mucosa	
Cell-surface trafficking	• Cytoskeletal interaction • Movement toward entry site	• Diffusion, rolling, and rocking along surface • Bilayer composition • Bilayer fluidity	
Binding	• Colocalization with receptor	• Attachment/detachment rates • Bilayer composition • Bilayer fluidity • Receptor mobility • Adhesion-strengthening	QCMD Coflotation ELISA SPR TEM
Internalization	• Clathrin dependence/independence • Internalization timescale • Cytoskeletal interaction	n/a	IFA TEM
Fusion	• Differentiate plasma membrane fusion from endosomal fusion • Escape from early vs. late endosomes	• Bilayer composition • Bilayer fluidity • Viral fusion environment • Timing/sequence of fusion triggers • Hemifusion and pore formation rate constants • Number of rate-limiting fusion steps • Acid stability	TEM Syncytia formation Bulk solution fluorescence Infectivity BlaM release
Intracellular trafficking	• Cytoskeletal interaction • Extra- and intra-nuclear movement	n/a	IFA

Acronyms: *QCMD* Quartz crystal microbalance with dissipation, *ELISA* Enzyme-linked immunosorbent assay, *SPR* Surface plasmon resonance, *TEM* Transmission electron microscopy, *IFA* immunofluoresence assay, *BlaM* Beta lactamase

the mean-squared displacement of virions over time is used to classify their motion as diffusive or sub-diffusive through the extracellular environment. For example, live cell single virion tracking of adeno-associated viruses [17] and simian virus 40 virus-like particles [62] indicates that particles undergo normal diffusion in the extracellular environment. Adeno-associated viruses slow down when in the vicinity of a cell, and touch the cell membrane multiple times before penetrating the cell [17]. In contrast, HIV follows the second mechanism and preferentially transmits directly from one neighboring cell to another through virological synapses rather than transmission by extracellular diffusion [63–65] Some viruses exploit cytoskeletal components to facilitate transport from one cell to another. Vaccinia virus, for

example, induces the formation of actin protrusions from the cell surface and is transported along these to spread from cell to cell [66]. Looking at viral transport over a longer distance scale, single virion imaging has shown that pseudorabies virus is able to spread from the site of infection to the peripheral nervous system ganglia for replication then back along axons to reseed the initial infection site [67]. In vitro experiments have been used to study how respiratory mucosa hinders the ability of pseudorabies virus to cross into the epithelium, revealing that both size and charge interactions are important [68].

2.3.1.2 Tracking Virion Movement on Live Cell Plasma Membranes

There are multiple strategies for observing lateral viral movement along the plasma membrane of a live cell. One method is labeling the core of virions and cellular actin (to delineate the border of cells) and track virion movement along the periphery of the cell [69]. Another method is to label the viral membrane and look at diffusion on top of membrane until the virion overlaps with an endocytosis site [70]. A few examples of virion movement that have been studied this way are as follows. Simian virus 40 undergoes actin independent diffusive movement on the cell membrane until it reaches caveolae [71]. Dengue virus similarly freely diffuses on the membrane until it reaches an existing clathrin-coated pit [70]. Murine polyoma virus-like particles also freely diffuse at first, then become confined and follow actin-directed trajectories afterwards [72]. Vaccinia bound to filopodia have been observed to move towards the cell body along the plasma membrane [73].

Some viruses employ a mix of two mechanisms, free diffusion and directed motion. Some examples of this type of movement are as follows. After binding to filopodia, murine leukemia virus, avian leucosis virus, vesicular stomatitis virus, and rabies virus appear to "surf" on top of the membrane via actin and myosin II driven transport towards entry sites [69, 74]. Similarly, adenovirus binds its receptor then drifts along the cell surface with the assistance of actin and myosin II [75, 76]. Coxsackievirus has been shown to bind on the apical surface of epithelia, which then triggers cytoskeletal rearrangement that transports the virus to the site of viral entry, the tight junctions [77]. Finally, influenza virus appears to undergo actin-directed motion in the area near its initial binding site on the cell surface [10, 78].

2.3.1.3 Tracking Virion Movement on Biomimetic Cell Surfaces

In the in vitro environment of supported lipid bilayer platforms, virions diffusing along the bilayer follow a continuous trajectory, whereas those that bind, detach, and rebind elsewhere on the surface "appear" and "disappear" under TIRF microscopy. These modes of transport are easily distinguished from each other using this microscopy approach [79]. Supported lipid bilayers have an advantage over live cells for certain types of studies because of the ability to tightly control composition, receptor density and mobility, and surface geometry and heterogeneity. For example,

supported lipid bilayers have been used to observe sliding and tumbling of quantum dot–labeled simian virus 40 virus-like particles on bilayers containing low concentrations of GM1 and back-and-forth rocking at high receptor concentrations [36]. However, because lipid bilayers do not contain the full cytoskeletal network of cells, it is possible that virion motion in these platforms could be different from their motion in vivo.

2.3.2 Binding

Studies of virus binding kinetics and determination of binding strength are often carried out in in vitro assays, either by monitoring many single virion events or following ensemble behavior of a population. In this section, we describe these approaches and highlight some selected studies that illustrate their utility.

2.3.2.1 Single Virion Tracking of Binding

Direct observation of many individual virion interactions with supported lipid bilayers can be used to measure receptor binding and detachment rates, multivalent avidity characteristics, and equilibrium binding constants. TIRF microscopy is the most common method used in monitoring individual virions binding to biomimetic membranes because it clearly distinguishes labeled virions that are bound to the lipid bilayer from unbound virions in the bulk solution (Fig. 2.5). In this experimental approach, the residence time of bound virions can be collected for each individual

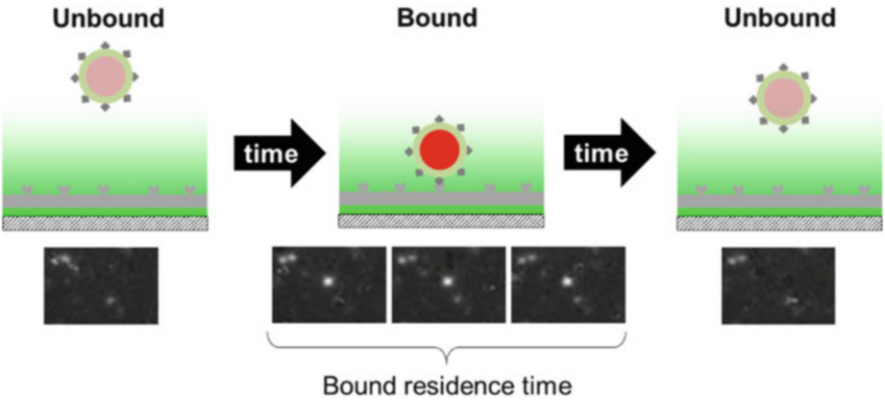

Fig. 2.5 TIRF microscopy visualizes virions bound on the membrane surface (gray) within a 100 nm deep evanescent wave (green). Fluorophores in unbound virions are not excited by the evanescent wave, while virions bound to the bilayer are illuminated, denoted here by the bright red color in the center cartoon. Residence times can be determined by the number of frames the virion remains observable, as shown in the images below the cartoons, before the virion unbinds

virion. As experimental conditions change, shifts in residence times can be monitored. From this data, binding characteristics can be quantified.

Initial work monitoring nanoparticle binding to supported bilayers and surface-tethered vesicles demonstrated the advantage of using TIRF microscopy in this application. Here, a useful approach, equilibrium-fluctuation-analysis, was developed to quantify apparent kinetic rate constants of carbohydrate-bearing particles with carbohydrate presenting SLBs [80]. This analysis was then extended to studies of virus-like particles [49, 81] and live virions [81] interacting with glycosylated bilayers to provide new insight into virus attachment to cell surfaces and applications in biosensing [82]. The kinetics of particle detachment [83] can also be studied in these platforms, as can multivalent binding behavior [62, 84]. Such studies can reveal changes in binding behavior that promote viral attachment. For example, both influenza and canine parvovirus undergo "adhesion-strengthening" where the longer a virion is bound, the more strongly it adheres to the bilayer [37, 85]. Overall, these platforms are convenient for gathering insight on this critical virus entry step and how it depends on the host cell surface.

One advantage of this platform is the tunability of the bilayer compositions and heterogeneity. For example, single particle binding studies have revealed the importance of microdomains in binding of norovirus-like particles, which preferentially bind the edges of glycosphingolipid-enriched domains [49]. Later it was also shown that HIV particles prefer to bind at the edges of cholesterol-rich lipid domains that were reconstituted in supported bilayers [86, 87]; however, observing this preference in live cells due to the small scale and dynamism of lipid rafts is difficult, illustrating the power of using an in vitro system for such studies. Focusing further on the receptors themselves, TIRF microscopy has also been used to measure the affinity of HIV glycoprotein 120 for the glycosphingolipids galactosyl ceramide, glucosylceramide, lactosylceramide and α-hydroxy glucosylceramide in SLBs [88, 89]. The affinity of glycoprotein 120 for these lipids is roughly 5 times lower than its affinity for CD4 [90].

The importance of studying the binding step is that the tropism of a virus is strongly tied to its ability to bind various receptors. A nice example, illustrating the power of combining single virion binding measurements with cell infectivity studies, clearly showed that a single mutation in the canine parvovirus capsid is able to alter binding to dog and raccoon transferrin receptors and completely change the tropism of the virus [85].

2.3.2.2 Ensemble-Based Approaches for Studying Virion Binding

Binding can be monitored using ensemble approaches that monitor the overall change in an aggregate signal from many virions interacting with a target surface. The simplest manner to measure virion binding to a particular host cell receptor is the cofloatation assay. In these assays, viral particles or purified fusion proteins are labeled with a probe and mixed with liposomes containing the receptor for the virus. After the virus has bound, the mixture can then be added to a sucrose gradient and

fractionated. The fractions are analyzed with PAGE or Western Blot to determine under which conditions the virus and liposomes comigrate or cofloat [91, 92]. Altering the composition of the liposomes can be used to determine what lipids and proteins the virus binds to. This assay is able to probe virus-receptor interactions but does not provide information on binding kinetics. An additional limitation is that it may be difficult to purify or prepare liposomes containing the receptor, particularly if it is a transmembrane protein.

Some ensemble viral binding assays, like enzyme-linked immunosorbent assay (ELISA) or glycan arrays, immobilize proteins, carbohydrates, or glycans on a rigid surface. These arrays do not preserve the structure, complexity, or two-dimensional fluidity of cellular membranes, which may limit accurate assessment of binding avidity. However, they can be useful for rapidly identifying binding partners in screening, for example, potential tropism changes [93].

Measurements of real-time binding and desorption can be assessed using techniques like surface plasmon resonance (SPR) [94] and quartz crystal microbalance with dissipation (QCM-D) [49, 95]. SPR uses changes in refractive index to report the binding behavior, while QCM-D uses a shift in resonance frequency to report virus interaction. In both approaches, biomimetic membranes can be used to preserve many properties of the host cell surface, including integration of the receptor. Kinetic analysis of binding with these techniques requires two experimental phases to decouple binding and unbinding of virions. In the first phase, virions are added to a biomimetic surface and bind to the receptors. In this way, an "on" rate can be obtained. In the second phase, a virus-free buffer is added and the dissociation of the virus from the receptor is monitored. In this arrangement, an "off" rate can be obtained.

It should be noted that averaged data from many single virion tracking binding/unbinding events should match the ensemble results generated with SPR or QCM-D. However, direct imaging with single virion tracking allows collection of a richer set of data for on and off rates simultaneously because each particle trajectory is captured [37]. Furthermore, by having the signature of each individual virion's binding behavior, heterogeneities in the virus population or membrane surface can be identified, which can then be compared to infection trends to understand how population dispersity impacts infection [96].

2.3.3 Internalization

Internalization, or the uptake of the virus particle into the cytosol, can be assessed either with live cell imaging or in fixed cells through immunofluorescence imaging.

2.3.3.1 Live Cell Imaging

In live cell virion tracking, cellular components, like clathrin and caveolin, can be fluorescently labeled and colocalization of these components with virions enables determination of whether the primary means of viral entry is through clathrin-dependent endocytosis, caveolin-dependent endocytosis, or a clathrin/caveolin independent uptake mechanism. When tracking labeled virions on live cells, rapid unidirectional motion indicates that particles have been internalized [70, 78, 97].

Live-cell tracking has revealed myriad information about virus internalization, including identifying viral dependence on clathrin or caveolin for uptake as well as the ability of viruses to promote their own uptake. For example, Reovirus induces the formation of clathrin-coated pits for uptake [97]. Simian virus 40 has the ability to induce actin rearrangement to further promote its own internalization whereas echovirus 1 does not [71, 98]. Clathrin-mediated endocytosis is utilized for the uptake of many viruses including Australian bat lyssavirus [99], HIV [100], infectious hematopoietic necrosis virus [101], and rabiesvirus [74]. Other viruses are caveolin-independent or use macropinocytosis. For example, mouse polyomavirus is also delivered to early endosomes by a caveolin independent pathway [102]. Adenovirus 2 enters the cell viaboth clathrin dependent and independent endocytosis and triggers macropinocytosis [103–106]. Still other viruses have been shown to be agile in their internalization route, for example, in the absence of caveolin, simian virus 40 can exploit a clathrin/caveolin independent pathway [107]. Studies have shown that bound influenza virions have the ability to induce the formation of clathrin-coated pits, but can also enter in a clathrin/caveolin independent manner [78]. Influenza is then preferentially sorted into a population of early endosomes that quickly matures [108].

2.3.3.2 Immunofluorescence Imaging

To monitor virus entry without live cell particle tracking, infected cells can be fixed and imaged with an immunofluorescence assay. Permeablized cells can be probed with antibodies against viral proteins, and cytoskeletal elements, or endocytosis markers. Colocalization of viral particles and cellular components can then reveal the general entry pathway of the virus [109–111]. Cells can be fixed at various time points after infection to determine the general time course of entry [112, 113]. This method provides snapshots of the viral entry process because the cells are fixed before imaging, but it requires less specialized microscopes and cameras than live-cell imaging.

2.3.4 Intracellular Trafficking

For viruses that are internalized, live-cell fluorescent imaging can provide insight into how viruses use cellular machinery, such as the cytoskeleton or microtubules, to propel their movement within the cell. One common approach to determining if cytoskeletal elements are involved is to compare the speed and shape of virion trajectories in the presence and absence of cytoskeletal inhibitors such as nocodazole, and cytochalasin D [114]. This strategy has been employed to determine that reovirus movement after endocytosis is microtubule-directed [114]. Microtubules are involved in the cytosolic movement of Adeno-associated virus type 2 [115], HIV [30, 116] infectious hematopoietic necrosis virus [101], rabies virus [74], In contrast, polio movement inside cells is actin dependent, but microtubule independent [117]. Adenovirus interacts with minus-end dynein and a plus-end directed factor to traffic along cytoplasmic microtubules [118]. Influenza in endosomes undergoes unidirectional dynein-directed translocation to the perinuclear region followed by intermittent back-and-forth microtubule-dependent motion within the perinuclear region prior to virion fusion with endosomes [10].

In addition to investigating movement towards the nucleus, live-cell single virion tracking has been used to monitor movement within the nuclear region. Adenovirus utilizes microtubules for movement within the cell, but detaches from them when the virions reach close proximity to the nucleus [119]. HIV cores move toward the nucleus with a microtuble- and actin-dependent motion; within the nucleus, the motion is slow and diffuse [100, 116, 120]. HIV RNA alone moves through the cytoplasm by diffusion [121]. After reaching the nucleus, HIV pre-integration complexes target areas of decondensed chromatin [122]. For influenza, genes are transported to and within the nucleus by diffusion [123].

Intracellular movement of virions is not necessarily mediated by spike or capsid proteins alone; for herpes simplex virus, the inner tegument proteins promote movement along microtubules and are necessary for movement away from the cell body along axons [124–126]. An alternative method is to use immunofluorescence assays of fixed cells to obtain snapshots of intracellular virion trafficking, including what cytoskeletal components are involved [127, 128]. These do not allow for the tracking of individual virion trajectories and are more limited in temporal resolution than live cell virion tracking, but require less specialized equipment.

2.3.5 Fusion

Membrane enveloped viruses must fuse their membrane with the host membrane to deliver their genome to the cytosol for replication. Fusion can occur either at the plasma membrane surface or in endosomes after the virion is internalized. Fusion can be monitored in both live cells and in in vitro platforms. Each approach has

advantages and disadvantages, and some examples of how these experiments are conducted follow next.

2.3.5.1 Tracking Fusion in Live Cells

Viral fusion at the plasma membrane can be differentiated from fusion within endosomes in live cells. To do so, the viral contents can be labeled with a diffusible content marker while the envelope is labeled with an acid-stable lipophilic dye. If fusion occurs at the plasma membrane, both fluorescent markers will seem to disappear because they will be diluted into the plasma membrane and cytosol. If fusion occurs within an endosome, the viral content marker will disappear as it is released into the cytosol and diluted, but the lipid marker will continue to appear bright as the dye mixes into the relatively small endosomal membrane [129]. This approach has been used to show that HIV can undergo full fusion inside endosomes while fusion at plasma membrane is halted at the lipid mixing step. However, this may be cell-type dependent; HIV content release from plasma membrane fusion was observed for U87 cells but not JC5.3 or HOS cells [130]. The ability to detect viral fusion in live cells within the endocytic pathway often relies on labeling virions with quenched amounts of dye. Colocalization of dequenching virions with labeled cellular components, such as clathrin or Rab proteins, can reveal whether fusion occurs in early or late stage endosomes. This approach has been employed in the study of influenza virus, which fuses in early endosomes, revealing that the virus is able to enter a clathrin-dependent manner as well as a clathrin and caveolin independent fashion, and viral fusion can occur in both pathways [78]. In macrophages, HIV undergoes fusion in Rab5A positive endosomes [100]. Fusion of Dengue virus [70] and Ebola virus [11] colocalizes with Rab7, a marker of late stage endosomes. Alternatively, endosomal fusion may be mimicked by binding virions to the plasma membrane then lowering the extracellular pH. This method of acid-induced endosomal bypass has been employed to characterize avian sarcoma and leukosis virus fusion behavior [131].

Viral fusion can also be monitored by observing the release of fluorescent viral cargo. Avian sarcoma and leukosis virions labeled with fluorescent cargo and an envelope pH sensor showed little correlation between endosomal pH and fusion lag time [132]. However fusion lag time and pore size did vary with surface receptor and endosome type, indicating that endosomal composition may modulate fusion [35, 132, 133]. In the case of vesicular stomatitis virus, cytoplasmic nucleocapsid release does not necessarily immediately follow fusion. VSV has been shown to undergo fusion between the early and late endosome stage [134].

2.3.5.2 Tracking Fusion in Biomimetic Platforms

With the lipid bilayer platform, hemifusion and pore formation can be observed within the same particle by dual-labeling the viral envelope and contents with

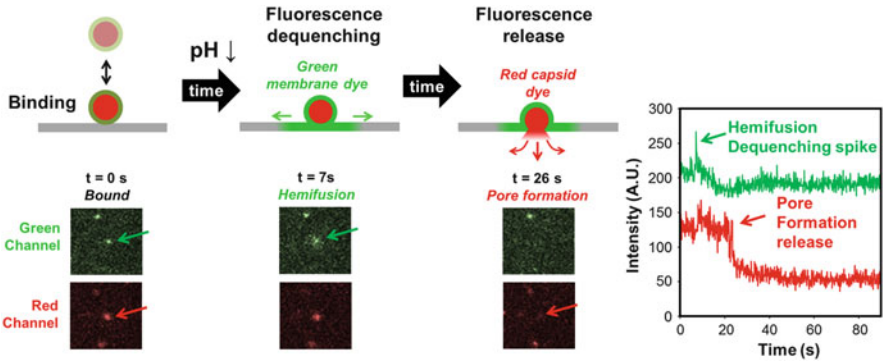

Fig. 2.6 Fusion and intermediate steps can be tracked by a dual-labeling approach. Virions first bind their receptor within the supported lipid bilayer (gray) in the evanescent wave (not shown here) of TIRF. After a trigger (such as a pH drop shown here at $t = 0$) membrane fusion occurs between the virion membrane, labeled with a green fluorophore, and the unlabeled supported bilayer. Fluorescence dequenching during fusion indicates hemifusion. Finally, a fusion pore is formed and the internal capsid fluorophores (red) are expelled across the supported bilayer. The plot to the far right shows the intensity change for the virion highlighted by the arrows in the images to the left

different colors (Fig. 2.6). By using a flow cell or microfluidic device, this platform also enables control over the timing of fusion trigger(s) or other environmental changes within the viral environment.

A common fusion trigger is a drop in pH. To trigger fusion, acidic buffer can be passed over the bilayer inside a microfluidic device. Incorporation of pH sensitive dye into the bilayer enables detection of the time at which bound virions encounter the acid [33]. Alternatively, ultraviolet light can be used to "uncage" protons from *o*-nitrobenzaldehyde in solution to rapidly acidify the bilayer and virions [12]. Both of these methods enable measurement of the lag time between exposure to a fusion trigger and the onset of hemifusion. By analyzing this lag time for hundreds of individual fusion events, the rate constants of hemifusion can be calculated. Pore formation can be monitored by particles also containing internal capsid dyes. Monitoring the drop in signal of this co-localized fluorophore reports the opening of the fusion pore.

If there is a single rate liming step, the distribution of lag times will follow a simple exponential decay, with the decay constant corresponding to the rate constant of that limiting step. If there are multiple rate liming steps, the lag time distribution will rise and decay [135]. A simple approach to quantifying the kinetics of hemifusion and pore formation is fitting the cumulative distribution of fusion events to a convolution of Poisson processes with the equation:

$$P = \int_0^t \frac{k^N t^{N-1}}{\Gamma(t)} e^{-kt} dt$$

where P is the probability of a virion being in that state (hemifused or pore forming) at time t after the fusion trigger has been added and $\Gamma(t)$ is the gamma distribution function. This fit yields k, the rate constant of that step, and N, the number of stochastic rate limiting events governing the kinetics of that step [33]. If there is only one rate-limiting step ($N = 1$), the above equation simplifies to a single exponential decay. As the number of rate-limiting steps increases, more events must be observed to accurately calculate N. For processes with three steps or fewer, 50 events is sufficient to calculate N with a standard deviation of 1 [15]. There are other more complex methods for fitting lag time distributions that may capture more of the details of hemifusion [136].

Viruses with Class I, Class II and Class III fusion proteins have been studied at the single virion level with SLBs. The kinetic analysis described here has indicated that influenza virus hemifusion is controlled by three rate-limiting steps while the kinetics of pore formation is governed by a single step [33]. Chikungunya virus also has three-rate limiting steps governing hemifusion [137]. For West Nile virus, hemifusion has one or two rate-limiting steps, depending on the pH [138]. Vesicular stomatitis virus hemifusion also has multiple rate-limiting steps at higher pH and a single rate-limiting step at low pH [139].

While it cannot be assumed that the kinetics obtained from this method reflect the actual reaction rates within a cell, comparison of these rates under different conditions, such as different bilayer compositions, pH, or viral strains, can yield valuable insight. The ability to manipulate the composition of supported lipid bilayers has been used to determine that anionic lipids are essential for vesicular stomatitis virus fusion and that the lag between hemifusion and pore formation is shortened in the presence of bis(monoacylglycero)phosphate, a lipid found in late endosomes [57]. Precisely controlling the triggering pH has revealed that influenza virus requires a lower pH to trigger fusion than Sindbis virus [34], suggesting that it fuses later in the endocytic pathway. While the rate of influenza X-31 virus hemifusion increases at lower pH [33], the rate of Brisbane is much less pH dependent [140]. The rate of pore formation for influenza virus is pH independent. Multiple influenza hemagglutinin trimers are involved in fusion [141], although not all are active participants [142, 143]. This platform is able to detect differences in the acid stability and fusion behavior of different strains and reassortants of influenza, which is tied to their tropism [140, 144]. This platform can also be used to measure the number of antibodies required to neutralize fusion of a single virion [145]. Figure 2.7 provides a summary of the flexibility, the biomimetic fusion assay and the kinds of insight that has been gained from these tunable assays. With the advances in supported bilayer complexity and fabrication, these platforms can also be used to study viruses that bind proteinaceous receptors, such as feline coronavirus [13].

Finally, given the highly-defined nature of these platforms, viruses that do not have a known fusion trigger or receptor might be difficult to study, because each component must be intentionally added to the platform. However, because SLBs can be formed in a microfluidic device, it should be possible to formulate a high-

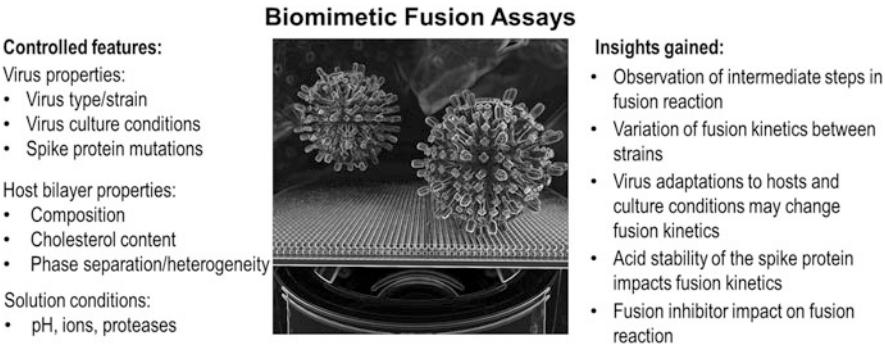

Fig. 2.7 Features that can be easily controlled in biomimetic fusion assays. In combination with a high throughput approach, these conditions (left) can be evaluated to provide new insight into virus fusion. (Right) Examples of the kinds of insight that can be gained with a biomimetic assay that isolates the fusion reaction from other virus entry steps

throughput screen for possible fusion triggers or binding partners with this configuration.

2.3.5.3 Ensemble Approaches for Studies of Fusion

A common method to study fusion behavior is cell-cell fusion assays, where fusion between target cells expressing the receptor for the virus and effector cells expressing the viral fusion protein is monitored. When the viral fusion protein is triggered, for example by lowering the pH, the cells fuse to each other, leading to clusters of multiple nuclei surrounded by a single cell membrane [146]. These clusters are known as syncytia. Lipophilic and aqueous dyes can be used to label the membrane and contents of the effector cell, providing readouts for lipid mixing or pore formation. To isolate the hemifusion step, fusion can be triggered then arrested by quickly cooling the cells to 4 °C [147, 148]. This rapid-cooling approach has been used to determine that hemifusion of avian sarcoma and leukosis virus requires low pH, but expansion of the fusion pore does not [148]. As an alternative to monitoring pore formation by observing the transfer of intracellular fluorescent cargo from effector cells to target cells [149], whole cell patch-clamp electrical measurements can be used [150]. In this configuration, a pipette connected to an electrode and amplifier pierces the membrane of the effector cell. The voltage across the membrane can be manipulated and the resulting current measured. During cell-cell fusion, the cell surface area increases as the membranes merge, resulting in an increase in membrane capacitance. Such measurements can also allow for estimation of fusion pore size [151].

While syncytia assays do not require viral particles or specialized equipment, making them easy to carry out, there are some limitations. Syncytia form over the course of hours, so this technique is not suitable for obtaining kinetic data

[152]. Furthermore, the extracellular environment can differ substantially from the endosomal environment, which may create artifacts when using this technique to study viruses that typically fuse within the endocytic pathway. In this approach, any impact of the virion size or shape on fusion is not captured.

In bulk fusion assays, viral particles are fluorescently labeled, then they are mixed with liposomes in a cuvette and the fluorescent signal of the solution is measured by fluorimetry as fusion triggers are added. In one labeling approach, particles and/or liposome membranes can be labeled with fluorescence energy resonance transfer (FRET) pairs. If fusion occurs, FRET will stop as the pairs become separated, and the fluorescence signal will change accordingly [153]. In the second labeling approach, particle membranes are labeled with a single quenched fluorescent marker [154]. Upon fusion with a liposome, the quenched fluorophores will become diluted and dequench, causing a marked increase in fluorescence.

In a third approach, the release of viral cargo can be detected by measuring β-lactamase (BlaM) activity. In this type of assay, target cells are loaded with a dye containing a β-lactam ring and a FRET pair. Chimeras of viral core proteins and BlaM are incorporated into virions. If virions are able to release their cargo during infection, BlaM will cleave the lactam ring, interrupting FRET and causing the cells to fluoresce a different color [155]. Infected and uninfected cells can then be sorted by flow cytometry for further analysis. This technique requires the ability to make chimeric proteins but otherwise does not require specialized equipment. BlaM activity assays have been combined with single virion imaging to indicate that HIV releases cargo by fusion inside endosomes and not fusion at the plasma membrane surface [156].

Bulk fusion provides information on the kinetics of the fusion of the overall population in the solution, including the lag time between when the viruses are exposed to a fusion trigger and when dequenching begins, with a resolution of less than a second [157]. Varying the composition of the liposomes can reveal how lipids impact viral fusion [158]. However, liposomes containing the viral receptor may be hard to prepare if the receptor is a transmembrane protein. These assays cannot resolve intermediate steps like hemifusion, or resolve fusion of individual virions, but can be used to determine conditions interesting for further investigation with single virion tracking with SLBs [137].

It is worth noting that single virion fusion tracking experiments agree with data obtained from bulk fusion experiments. In a study directly comparing the two methods a combination of bulk fusion and single virion tracking showed that cholesterol enhances the extent of Sindbis virus fusion, but increases the lag between binding and fusion at pH less than 5, revealing a complicated relationship between lipids and viral fusion proteins in binding and fusion [34].

2.4 Conclusion

Methods for studying viral entry vary widely in functional characterization, and structural and temporal resolution. No single technique is sufficient to determine all the steps or details of viral entry. Single virion tracking techniques can bridge the gap between detailed structural information and overall infection measurements to inform our understanding of the structure-function relationship of viral fusion proteins. The development of single virion tracking techniques has been dependent on advances in viral labeling, microscopy, and image analysis. These single virion techniques can be applied to study the progression of infection in live cells as well as used in a tightly-controlled biomimetic platform. Top-down cell culture approaches where inhibition or knockout of cellular components reveals their role in viral entry complement bottom-up biomimetic methods where components of interest are methodically added to the experimental platform. Combining information from these different techniques illuminates the framework of steps involved in viral entry and clarifies the mechanisms underlying each step.

References

1. Marsh M, Helenius A (2006) Virus entry: open sesame. Cell 124:729–740
2. Flint SJ, Enquist LW, Racaniello VR, Skalka AM (2009) Principles of virology, volume I: molecular biology, 3rd edn. ASM Press, Washington DC
3. Suomalainen M, Greber UF (2013) Uncoating of non-enveloped viruses. Curr Opin Virol 3:27–33. https://doi.org/10.1016/j.coviro.2012.12.004
4. White JM, Whittaker GR (2016) Fusion of enveloped viruses in endosomes. Traffic 17:593–614
5. White JM, Delos SE, Brecher M, Schornberg K (2008) Structures and mechanisms of viral membrane fusion proteins: multiple variations on a common theme. Crit Rev Biochem Mol Biol 43:189–219. https://doi.org/10.1080/10409230802058320
6. Matsuyama S, Ujike M, Morikawa S et al (2005) Protease-mediated enhancement of severe acute respiratory syndrome coronavirus infection. Proc Natl Acad Sci USA 102:12543–12547. https://doi.org/10.1073/pnas.0503203102
7. Yamauchi Y, Greber UF (2016) Principles of virus uncoating: cues and the snooker ball. Traffic 17:569–592. https://doi.org/10.1111/tra.12387
8. Harrison SC (2015) Viral membrane fusion. Virology 479–480:498–507. https://doi.org/10.1016/J.VIROL.2015.03.043
9. Ma Y, He Z, Tan T et al (2016) Real-time imaging of single HIV-1 disassembly with multicolor viral particles. ACS Nano 10:6273–6282. https://doi.org/10.1021/acsnano.6b02462
10. Lakadamyali M, Rust MJ, Babcock HP, Zhuang X (2003) Visualizing infection of individual influenza viruses. Proc Natl Acad Sci USA 100:9280–9285. https://doi.org/10.1073/pnas.0832269100
11. Spence JS, Krause TB, Mittler E et al (2016) Direct visualization of Ebola virus fusion triggering in the endocytic pathway. MBio 7:e01857–e01815. https://doi.org/10.1128/mBio.01857-15
12. Costello DA, Lee DW, Drewes J et al (2012) Influenza virus-membrane fusion triggered by proton uncaging for single particle studies of fusion kinetics. Anal Chem 84:8480–8489. https://doi.org/10.1021/ac3006473

13. Costello DA, Millet JK, Hsia CY et al (2013b) Single particle assay of coronavirus membrane fusion with proteinaceous receptor-embedded supported bilayers. Biomaterials 34:7895–7904. https://doi.org/10.1016/j.biomaterials.2013.06.034
14. Ewers H, Schelhaas M (2012) Analysis of virus entry and cellular membrane dynamics by single particle tracking. Methods Enzymol 506:63–80. https://doi.org/10.1016/B978-0-12-391856-7.00028-7
15. Floyd DL, Harrison SC, Van Oijen AM (2010) Analysis of kinetic intermediates in single-particle dwell-time distributions. Biophys J 99:360–366. https://doi.org/10.1016/j.bpj.2010.04.049
16. Helenius A, Kartenbeck J, Simons K, Fries E (1980) On the entry of Semliki forest virus into BHK-21 cells. J Cell Biol 84:404–420. https://doi.org/10.1083/JCB.84.2.404
17. Seisenberger G, Ried MU, Endress T et al (2001) Real-time single-molecule imaging of the infection pathway of an adeno-associated virus. Science 294:1929–1932. https://doi.org/10.1126/science.1064103
18. Suomalainen M, Nakano MY, Keller S et al (1999) Microtubule-dependent plus- and minus end-directed motilities are competing processes for nuclear targeting of adenovirus. J Cell Biol 144:657–672. https://doi.org/10.1083/JCB.144.4.657
19. Michalet X, Siegmund OHW, Vallerga JV et al (2007) Detectors for single-molecule fluorescence imaging and spectroscopy. J Mod Opt 54:239. https://doi.org/10.1080/09500340600769067
20. Otterstrom J, Van Oijen AM (2013) Visualization of membrane fusion, one particle at a time. Biochemistry 52:1654–1668. https://doi.org/10.1021/bi301573w
21. Shen H, Tauzin LJ, Baiyasi R et al (2017) Single particle tracking: from theory to biophysical applications. Chem Rev 117:7331–7376
22. Brandenburg B, Zhuang X (2007) Virus trafficking—learning from single-virus tracking. Nat Rev Microbiol 5:197–208. https://doi.org/10.1038/nrmicro1615
23. Wang I-H, Burckhardt C, Yakimovich A, Greber U (2018) Imaging, tracking and computational analyses of virus entry and egress with the cytoskeleton. Viruses 10:166. https://doi.org/10.3390/v10040166
24. Axelrod D (2003) Total internal reflection fluorescence microscopy in cell biology. Methods Enzymol 361:1–33. https://doi.org/10.1016/S0076-6879(03)61003-7
25. Mattheyses AL, Simon SM, Rappoport JZ (2010) Imaging with total internal reflection fluorescence microscopy for the cell biologist. J Cell Sci 123:3621–3628. https://doi.org/10.1242/jcs.056218
26. Icha J, Weber M, Waters JC, Norden C (2017) Phototoxicity in live fluorescence microscopy, and how to avoid it. BioEssays 39:1700003. https://doi.org/10.1002/bies.201700003
27. Huang L-L, Xie H-Y (2014) Progress on the labeling and single-particle tracking technologies of viruses. Analyst 139:3336–3346. https://doi.org/10.1039/C4AN00038B
28. Liu S-L, Wang Z-G, Zhang Z-L, Pang D-W (2016) Tracking single viruses infecting their host cells using quantum dots. Chem Soc Rev 45:1211–1224. https://doi.org/10.1039/C5CS00657K
29. Sun E, He J, Zhuang X (2013) Live cell imaging of viral entry. Curr Opin Virol 3:34–43. https://doi.org/10.1016/j.coviro.2013.01.005
30. McDonald D, Vodicka MA, Lucero G et al (2002) Visualization of the intracellular behavior of HIV in living cells. J Cell Biol 159:441–452. https://doi.org/10.1083/jcb.200203150
31. Charpilienne A, Nejmeddine M, Berois M et al (2001) Individual rotavirus-like particles containing 120 molecules of fluorescent protein are visible in living cells. J Biol Chem 276:29361–29367. https://doi.org/10.1074/jbc.M101935200
32. Desai P, Person S (1998) Incorporation of the green fluorescent protein into the herpes simplex virus type 1 capsid. J Virol 72:7563–7568
33. Floyd DL, Ragains JR, Skehel JJ et al (2008) Single-particle kinetics of influenza virus membrane fusion. Proc Natl Acad Sci USA 105:15382–15387. https://doi.org/10.1073/pnas.0807771105

34. Wessels L, Elting MW, Scimeca D, Weninger K (2007) Rapid membrane fusion of individual virus particles with supported lipid bilayers. Biophys J 93:526–538. https://doi.org/10.1529/biophysj.106.097485
35. Padilla-Parra S, Matos PM, Kondo N et al (2012b) Quantitative imaging of endosome acidification and single retrovirus fusion with distinct pools of early endosomes. Proc Natl Acad Sci USA 109:17627–17632. https://doi.org/10.1073/pnas.1211714109
36. Kukura P, Ewers H, Müller C et al (2009) High-speed nanoscopic tracking of the position and orientation of a single virus. Nat Methods 6:923–927. https://doi.org/10.1038/nmeth.1395
37. Lee DW, Hsu H-L, Bacon KB, Daniel S (2016b) Image restoration and analysis of influenza virions binding to membrane receptors reveal adhesion-strengthening kinetics. PLoS One 11: e0163437. https://doi.org/10.1371/journal.pone.0163437
38. Carter BC, Shubeita GT, Gross SP (2005) Tracking single particles: a user-friendly quantitative evaluation. Phys Biol 2:60–72. https://doi.org/10.1088/1478-3967/2/1/008
39. Meijering E, Dzyubachyk O, Smal I, van Cappellen WA (2009) Tracking in cell and developmental biology. Semin Cell Dev Biol 20:894–902
40. Sbalzarini IF, Koumoutsakos P (2005) Feature point tracking and trajectory analysis for video imaging in cell biology. J Struct Biol 151:182–195. https://doi.org/10.1016/j.jsb.2005.06.002
41. Ruthardt N, Lamb DC, Bräuchle C (2011) Single-particle tracking as a quantitative microscopy-based approach to unravel cell entry mechanisms of viruses and pharmaceutical nanoparticles. Mol Ther 19:1199–1211. https://doi.org/10.1038/mt.2011.102
42. Georgiou GN, Morrison IEG, Cherry RJ (1989) Digital fluorescence imaging of fusion of influenza virus with erythrocytes. FEBS Lett 250:487–492. https://doi.org/10.1016/0014-5793(89)80782-3
43. Lowy RJ, Sarkar DP, Chen Y, Blumenthal R (1990) Observation of single influenza virus-cell fusion and measurement by fluorescence video microscopy. Proc Natl Acad Sci USA 87:1850–1854
44. Niles WD, Cohen FS (1991a) Fusion of influenza virions with a planar lipid membrane detected by video fluorescence microscopy. J Gen Physiol 97:1101–1119. https://doi.org/10.1085/JGP.97.6.1101
45. Niles WD, Cohen FS (1991b) The role of N-acetylneuraminic (sialic) acid in the pH dependence of influenza virion fusion with planar phospholipid membranes. J Gen Physiol 97:1121–1140. https://doi.org/10.1085/JGP.97.6.1121
46. Sackmann E (1996) Supported membranes: scientific and practical applications. Science 271:43–48. https://doi.org/10.1126/SCIENCE.271.5245.43
47. Tanaka M, Sackmann E (2005) Polymer-supported membranes as models of the cell surface. Nature 437:656–663. https://doi.org/10.1038/nature04164
48. Castellana ET, Cremer PS (2006) Solid supported lipid bilayers: from biophysical studies to sensor design. Surf Sci Rep 61:429–444. https://doi.org/10.1016/J.SURFREP.2006.06.001
49. Bally M, Rydell GE, Zahn R et al (2012) Norovirus GII.4 virus-like particles recognize galactosylceramides in domains of planar supported lipid bilayers. Angew Chemie Int Ed 51:12020–12024. https://doi.org/10.1002/anie.201205972
50. van der Borg G, Braddock S, Blijleven JS et al (2018) Single-particle fusion of influenza viruses reveals complex interactions with target membranes. J Phys Condens Matter 30:204005. https://doi.org/10.1088/1361-648X/aabc21
51. Pace H, Simonsson Nyström L, Gunnarsson A et al (2015) Preserved transmembrane protein mobility in polymer-supported lipid bilayers derived from cell membranes. Anal Chem 87:9194–9203. https://doi.org/10.1021/acs.analchem.5b01449
52. Richards MJ, Hsia C-Y, Singh RR et al (2016) Membrane protein mobility and orientation preserved in supported bilayers created directly from cell plasma membrane blebs. Langmuir 32:2963–2974. https://doi.org/10.1021/acs.langmuir.5b03415
53. Costello DA, Daniel S (2015) Single particle tracking assay to study coronavirus membrane fusion. Methods Mol Biol 1282:183–194. https://doi.org/10.1007/978-1-4939-2438-7_16

54. Liu H-Y, Chen W-L, Ober CK, Daniel S (2017) Biologically complex planar cell plasma membranes supported on polyelectrolyte cushions enhance transmembrane protein mobility and retain native orientation. Langmuir. https://doi.org/10.1021/acs.langmuir.7b02945
55. Bayerl TM, Bloom M (1990) Physical properties of single phospholipid bilayers adsorbed to micro glass beads. A new vesicular model system studied by 2H-nuclear magnetic resonance. Biophys J 58:357–362. https://doi.org/10.1016/S0006-3495(90)82382-1
56. Johnson SJ, Bayerl TM, McDermott DC et al (1991) Structure of an adsorbed dimyristoylphosphatidylcholine bilayer measured with specular reflection of neutrons. Biophys J 59:289–294. https://doi.org/10.1016/S0006-3495(91)82222-6
57. Matos PM, Marin M, Ahn B et al (2013) Anionic lipids are required for vesicular stomatitis virus G protein-mediated single particle fusion with supported lipid bilayers. J Biol Chem 288:12416–12425. https://doi.org/10.1074/jbc.M113.462028
58. Hsia C-Y, Richards MJ, Daniel S (2015) A review of traditional and emerging methods to characterize lipid–protein interactions in biological membranes. Anal Methods 7:7076–7094. https://doi.org/10.1039/C5AY00599J
59. Costello DA, Hsia CY, Millet JK et al (2013a) Membrane fusion-competent virus-like proteoliposomes and proteinaceous supported bilayers made directly from cell plasma membranes. Langmuir 29:6409–6419. https://doi.org/10.1021/la400861u
60. Hinterdorfer P, Baber G, Tamm LK (1994) Reconstitution of membrane fusion sites. J Biol Chem 269:20360–20368
61. Tatulian SA, Hinterdorfer ' P, Baber G, Tamm LK (1995) Influenza hemagglutinin assumes a tilted conformation during membrane fusion as determined by attenuated total reflection FTIR spectroscopy. EMBO J 14:5514–5523
62. Szklarczyk OM, González-Segredo N, Kukura P et al (2013) Receptor concentration and diffusivity control multivalent binding of Sv40 to membrane bilayers. PLoS Comput Biol 9: e1003310. https://doi.org/10.1371/journal.pcbi.1003310
63. Dale BM, McNerney GP, Thompson DL et al (2011) Cell-to-cell transfer of HIV-1 via virological synapses leads to endosomal virion maturation that activates viral membrane fusion. Cell Host Microbe 10:551–562. https://doi.org/10.1016/J.CHOM.2011.10.015
64. Felts RL, Narayan K, Estes JD et al (2010) 3D visualization of HIV transfer at the virological synapse between dendritic cells and T cells. Proc Natl Acad Sci USA 107:13336–13341. https://doi.org/10.1073/pnas.1003040107
65. Hubner W, McNerney GP, Chen P et al (2009) Quantitative 3D video microscopy of HIV transfer across T cell virological synapses. Science 323:1743–1747. https://doi.org/10.1126/science.1167525
66. Cudmore S, Cossart P, Griffiths G, Way M (1995) Actin-based motility of vaccinia virus. Nature 378:636–638. https://doi.org/10.1038/378636a0
67. Granstedt AE, Brunton BW, Enquist LW (2013) Imaging the transport dynamics of single alphaherpesvirus particles in intact peripheral nervous system explants from infected mice. MBio 4:e00358–e00313. https://doi.org/10.1128/mBio.00358-13
68. Yang X, Forier K, Steukers L et al (2012) Immobilization of pseudorabies virus in porcine tracheal respiratory mucus revealed by single particle tracking. PLoS One 7:e51054. https://doi.org/10.1371/journal.pone.0051054
69. Lehmann MJ, Sherer NM, Marks CB et al (2005) Actin- and myosin-driven movement of viruses along filopodia precedes their entry into cells. J Cell Biol 170:317–325. https://doi.org/10.1083/jcb.200503059
70. van der Schaar HM, Rust MJ, Chen C et al (2008) Dissecting the cell entry pathway of dengue virus by single-particle tracking in living cells. PLoS Pathog 4:e1000244. https://doi.org/10.1371/journal.ppat.1000244
71. Pelkmans L, Püntener D, Helenius A (2002) Local actin polymerization and dynamin recruitment in SV40-induced internalization of caveolae. Science 296:535–539. https://doi.org/10.1126/science.1069784

72. Ewers H, Smith AE, Sbalzarini IF et al (2005) Single-particle tracking of murine polyoma virus-like particles on live cells and artificial membranes. Proc Natl Acad Sci 102:15110–15115. https://doi.org/10.1073/pnas.0504407102
73. Mercer J, Helenius A (2008) Vaccinia virus uses macropinocytosis and apoptotic mimicry to enter host cells. Science 320:531–535. https://doi.org/10.1126/science.1155164
74. Xu H, Hao X, Wang S et al (2015) Real-time imaging of rabies virus entry into living vero cells. Sci Rep 5:11753. https://doi.org/10.1038/srep11753
75. Burckhardt CJ, Suomalainen M, Schoenenberger P et al (2011a) Drifting motions of the adenovirus receptor CAR and immobile integrins initiate virus uncoating and membrane lytic protein exposure. Cell Host Microbe 10:105–117. https://doi.org/10.1016/J.CHOM.2011.07.006
76. Helmuth JA, Burckhardt CJ, Koumoutsakos P et al (2007) A novel supervised trajectory segmentation algorithm identifies distinct types of human adenovirus motion in host cells. J Struct Biol 159:347–358. https://doi.org/10.1016/J.JSB.2007.04.003
77. Coyne CB, Bergelson JM (2006) Virus-induced Abl and Fyn kinase signals permit coxsackievirus entry through epithelial tight junctions. Cell 124:119–131. https://doi.org/10.1016/j.cell.2005.10.035
78. Rust MJ, Lakadamyali M, Zhang F, Zhuang X (2004) Assembly of endocytic machinery around individual influenza viruses during viral entry. Nat Struct Mol Biol 11:567–573. https://doi.org/10.1038/nsmb769
79. Peerboom N, Block S, Altgärde N et al (2017) Binding kinetics and lateral mobility of HSV-1 on end-grafted sulfated glycosaminoglycans. Biophys J 113:1223–1234. https://doi.org/10.1016/J.BPJ.2017.06.028
80. Kunze A, Bally M, Höök F, Larson G (2013) Equilibrium-fluctuation-analysis of single liposome binding events reveals how cholesterol and Ca2+ modulate glycosphingolipid trans-interactions. Sci Rep 3:1452. https://doi.org/10.1038/srep01452
81. Bally M, Gunnarsson A, Svensson L et al (2011) Interaction of single viruslike particles with vesicles containing glycosphingolipids. Phys Rev Lett 107:188103. https://doi.org/10.1103/PhysRevLett.107.188103
82. Bally M, Graule M, Parra F et al (2013) A virus biosensor with single virus-particle sensitivity based on fluorescent vesicle labels and equilibrium fluctuation analysis. Biointerphases 8:4. https://doi.org/10.1186/1559-4106-8-4
83. Nasir W, Bally M, Zhdanov VP et al (2015) Interaction of virus-like particles with vesicles containing glycolipids: kinetics of detachment. J Phys Chem B 119:11466–11472. https://doi.org/10.1021/acs.jpcb.5b04160
84. Block S, Zhdanov VP, Höök F (2016) Quantification of multivalent interactions by tracking single biological nanoparticle mobility on a lipid membrane. Nano Lett 16:4382–4390. https://doi.org/10.1021/acs.nanolett.6b01511
85. Lee D, Allison A, Bacon K et al (2016a) Single-particle tracking shows that a point mutation in the carnivore parvovirus capsid switches binding between host-specific transferrin receptors. J Virol 90:4849–4853. https://doi.org/10.1128/JVI.03204-15
86. Yang S-T, Kiessling V, Simmons JA et al (2015) HIV gp41–mediated membrane fusion occurs at edges of cholesterol-rich lipid domains. Nat Chem Biol 11:424–431. https://doi.org/10.1038/nchembio.1800
87. Yang S-T, Kreutzberger AJB, Kiessling V et al (2017) HIV virions sense plasma membrane heterogeneity for cell entry. Sci Adv 3:e1700338. https://doi.org/10.1126/sciadv.1700338
88. Conboy JC, McReynolds KD, Gervay-Hague J, Saavedra SS (2000) Gp120 binds cooperatively to several biologically relevant glycosphingolipids: quantitative measurements at equilibrium by total internal reflection fluorescence microscopy. Angew Chemie 39:2882–2884. https://doi.org/10.1002/1521-3773(20000818)39:16<2882::AID-ANIE2882>3.0.CO;2-M
89. Conboy JC, McReynolds KD, Gervay-Hague J, Saavedra SS (2002) Quantitative measurements of recombinant HIV surface glycoprotein 120 binding to several glycosphingolipids expressed in planar supported lipid bilayers. J Am Chem Soc 124:968–977. https://doi.org/10.1021/ja011225s

90. Myszka DG, Sweet RW, Hensley P et al (2000) Energetics of the HIV gp120-CD4 binding reaction. Proc Natl Acad Sci USA 97:9026–9031. https://doi.org/10.1073/PNAS.97.16.9026
91. Kielian MC, Helenius A (1984) Role of cholesterol in fusion of Semliki forest virus with membranes. J Virol 52:281–283
92. Wahlberg JM, Bron R, Wilschut J, Garoff H (1992) Membrane fusion of Semliki forest virus involves homotrimers of the fusion protein. J Virol 66:7309–7318
93. Stevens J, Blixt O, Tumpey TM et al (2006) Structure and receptor specificity of the hemagglutinin from an H5N1 influenza virus. Science 312:404–410. https://doi.org/10.1126/science.1124513
94. Hidari KIPJ, Shimada S, Suzuki Y, Suzuki T (2007) Binding kinetics of influenza viruses to sialic acid-containing carbohydrates. Glycoconj J 24:583–590. https://doi.org/10.1007/s10719-007-9055-y
95. Rydell GE, Dahlin AB, Hook F, Larson G (2009) QCM-D studies of human norovirus VLPs binding to glycosphingolipids in supported lipid bilayers reveal strain-specific characteristics. Glycobiology 19:1176–1184. https://doi.org/10.1093/glycob/cwp103
96. Banerjee S, Maurya S, Roy R (2018) Single-molecule fluorescence imaging: generating insights into molecular interactions in virology. J Biosci:1–22. https://doi.org/10.1007/s12038-018-9769-y
97. Ehrlich M, Boll W, Van Oijen A et al (2004) Endocytosis by random initiation and stabilization of clathrin-coated pits. Cell 118:591–605. https://doi.org/10.1016/j.cell.2004.08.017
98. Pietiäinen V, Marjomäki V, Upla P et al (2004) Echovirus 1 endocytosis into caveosomes requires lipid rafts, dynamin II, and signaling events. Mol Biol Cell 15:4911–4925. https://doi.org/10.1091/mbc.E04-01-0070
99. Weir DL, Laing ED, Smith IL et al (2014) Host cell virus entry mediated by Australian bat lyssavirus G envelope glycoprotein occurs through a clathrin-mediated endocytic pathway that requires actin and Rab5. Virol J 11:40. https://doi.org/10.1186/1743-422X-11-40
100. Li Q, Li W, Yin W et al (2017) Single-particle tracking of human immunodeficiency virus type 1 productive entry into human primary macrophages. ACS Nano 11:3890–3903. https://doi.org/10.1021/acsnano.7b00275
101. Liu H, Liu Y, Liu S et al (2011) Clathrin-mediated endocytosis in living host cells visualized through quantum dot labeling of infectious hematopoietic necrosis virus. J Virol 85:6252–6262. https://doi.org/10.1128/JVI.00109-11
102. Liebl D, Difato F, Horníková L et al (2006) Mouse polyomavirus enters early endosomes, requires their acidic pH for productive infection, and meets transferrin cargo in Rab11-positive endosomes. J Virol 80:4610–4622. https://doi.org/10.1128/JVI.80.9.4610-4622.2006
103. Burckhardt CJ, Suomalainen M, Schoenenberger P et al (2011b) Drifting motions of the adenovirus receptor CAR and immobile integrins initiate virus uncoating and membrane lytic protein exposure. Cell Host Microbe 10:105–117. https://doi.org/10.1016/J.CHOM.2011.07.006
104. Luisoni S, Suomalainen M, Boucke K et al (2015) Co-option of membrane wounding enables virus penetration into cells. Cell Host Microbe 18:75–85. https://doi.org/10.1016/j.chom.2015.06.006
105. Meier O, Boucke K, Hammer SV et al (2002) Adenovirus triggers macropinocytosis and endosomal leakage together with its clathrin-mediated uptake. J Cell Biol 158:1119–1131. https://doi.org/10.1083/jcb.200112067
106. Nakano MY, Boucke K, Suomalainen M et al (2000) The first step of adenovirus type 2 disassembly occurs at the cell surface, independently of endocytosis and escape to the cytosol. J Virol 74:7085–7095
107. Damm E-M, Pelkmans L, Kartenbeck J et al (2005) Clathrin- and caveolin-1–independent endocytosis. J Cell Biol 168:477–488. https://doi.org/10.1083/jcb.200407113
108. Lakadamyali M, Rust MJ, Zhuang X (2006) Ligands for clathrin-mediated endocytosis are differentially sorted into distinct populations of early endosomes. Cell 124:997–1009. https://doi.org/10.1016/j.cell.2005.12.038

109. Elphick GF, Querbes W, Jordan JA et al (2004) The human polyomavirus, JCV, uses serotonin receptors to infect cells. Science 306:1380–1383. https://doi.org/10.1126/science.1103492
110. Iyengar S, Hildreth JE, Schwartz DH (1998) Actin-dependent receptor colocalization required for human immunodeficiency virus entry into host cells. J Virol 72:5251–5255
111. Sieczkarski SB, Brown HA, Whittaker GR (2003) Role of protein kinase C betaII in influenza virus entry via late endosomes. J Virol 77:460–469. https://doi.org/10.1128/JVI.77.1.460-469.2003
112. Nicola AV, Straus SE (2004) Cellular and viral requirements for rapid endocytic entry of herpes simplex virus. J Virol 78:7508–7517. https://doi.org/10.1128/JVI.78.14.7508-7517.2004
113. Vonderheit A, Helenius A (2005) Rab7 associates with early endosomes to mediate sorting and transport of semliki forest virus to late endosomes. PLoS Biol 3:e233. https://doi.org/10.1371/journal.pbio.0030233
114. Georgi A, Mottola-Hartshornt C, Warner A et al (1990) Detection of individual fluorescently labeled reovirions in living cells. Microbiology 87:6579–6583
115. Xiao P-J, Samulski RJ (2012) Cytoplasmic trafficking, endosomal escape, and perinuclear accumulation of adeno-associated virus type 2 particles are facilitated by microtubule network. J Virol 86:10462–10473. https://doi.org/10.1128/JVI.00935-12
116. Arhel N, Genovesio A, Kim K-A et al (2006) Quantitative four-dimensional tracking of cytoplasmic and nuclear HIV-1 complexes. Nat Methods 3:817–824. https://doi.org/10.1038/nmeth928
117. Vaughan JC, Brandenburg B, Hogle JM, Zhuang X (2009) Rapid actin-dependent viral motility in live cells. Biophys J 97:1647–1656. https://doi.org/10.1016/j.bpj.2009.07.011
118. Bremner KH, Scherer J, Yi J et al (2009) Adenovirus transport via direct interaction of cytoplasmic dynein with the viral capsid hexon subunit. Cell Host Microbe 6:523–535. https://doi.org/10.1016/J.CHOM.2009.11.006
119. Wang I-H, Burckhardt CJ, Yakimovich A et al (2017) The nuclear export factor CRM1 controls juxta-nuclear microtubule-dependent virus transport. J Cell Sci 130:2185–2195. https://doi.org/10.1242/jcs.203794
120. Jun S, Ke D, Debiec K et al (2011) Direct visualization of HIV-1 with correlative live-cell microscopy and cryo-electron tomography. Structure 19:1573–1581. https://doi.org/10.1016/J.STR.2011.09.006
121. Chen J, Grunwald D, Sardo L et al (2014) Cytoplasmic HIV-1 RNA is mainly transported by diffusion in the presence or absence of gag protein. Proc Natl Acad Sci USA 111:E5205–E5213. https://doi.org/10.1073/pnas.1413169111
122. Albanese A, Arosio D, Terreni M, Cereseto A (2008) HIV-1 pre-integration complexes selectively target decondensed chromatin in the nuclear periphery. PLoS One 3:e2413. https://doi.org/10.1371/journal.pone.0002413
123. Babcock HP, Chen C, Zhuang X (2004) Using single-particle tracking to study nuclear trafficking of viral genes. Biophys J 87:2749–2758. https://doi.org/10.1529/biophysj.104.042234
124. Antinone SE, Shubeita GT, Coller KE et al (2006) The Herpesvirus capsid surface protein, VP26, and the majority of the tegument proteins are dispensable for capsid transport toward the nucleus. J Virol 80:5494–5498. https://doi.org/10.1128/JVI.00026-06
125. Luxton GWG, Haverlock S, Coller KE et al (2005) Targeting of herpesvirus capsid transport in axons is coupled to association with specific sets of tegument proteins. Proc Natl Acad Sci USA 102:5832–5837. https://doi.org/10.1073/pnas.0500803102
126. Wolfstein A, Nagel C-H, Radtke K et al (2006) The inner tegument promotes herpes simplex virus capsid motility along microtubules in vitro. Traffic 7:227–237. https://doi.org/10.1111/j.1600-0854.2005.00379.x
127. Döhner K, Radtke K, Schmidt S, Sodeik B (2006) Eclipse phase of herpes simplex virus type 1 infection: efficient dynein-mediated capsid transport without the small capsid protein VP26. J Virol 80:8211–8224. https://doi.org/10.1128/JVI.02528-05

128. Strunze S, Trotman LC, Boucke K, Greber UF (2005) Nuclear targeting of adenovirus type 2 requires CRM1-mediated nuclear export. Mol Biol Cell 16:2999–3009. https://doi.org/10.1091/mbc.E05-02-0121
129. Miyauchi K, Kim Y, Latinovic O et al (2009) HIV enters cells via endocytosis and dynamin-dependent fusion with endosomes. Cell 137:433–444. https://doi.org/10.1016/j.cell.2009.02.046
130. Markosyan RM, Cohen FS, Melikyan GB (2005) Time-resolved imaging of HIV-1 Env-mediated lipid and content mixing between a single virion and cell membrane. Mol Biol Cell 16:5502–5513. https://doi.org/10.1091/mbc.e05-06-0496
131. Melikyan GB, Barnard RJO, Abrahamyan LG et al (2005) Imaging individual retroviral fusion events: from hemifusion to pore formation and growth. Proc Natl Acad Sci USA 102:8728–8733. https://doi.org/10.1073/pnas.0501864102
132. Jha NK, Latinovic O, Martin E et al (2011) Imaging single retrovirus entry through alternative receptor isoforms and intermediates of virus-endosome fusion. PLoS Pathog 7:e1001260. https://doi.org/10.1371/journal.ppat.1001260
133. Padilla-Parra S, Marin M, Kondo N, Melikyan GB (2012a) Synchronized retrovirus fusion in cells expressing alternative receptor isoforms releases the viral core into distinct sub-cellular compartments. PLoS Pathog 8:e1002694. https://doi.org/10.1371/journal.ppat.1002694
134. Le Blanc I, Luyet P-P, Pons V et al (2005) Endosome-to-cytosol transport of viral nucleocapsids. Nat Cell Biol 7:653–664. https://doi.org/10.1038/ncb1269
135. Blijleven JS, Boonstra S, Onck PR et al (2016) Mechanisms of influenza viral membrane fusion. Semin Cell Dev Biol 60:78–88
136. Zhang Y, Dudko OK (2015) Statistical mechanics of viral entry. Phys Rev Lett 114:018104. https://doi.org/10.1103/PhysRevLett.114.018104
137. Van Duijl-Richter MKS, Blijleven JS, van Oijen AM, Smit JM (2015) Chikungunya virus fusion properties elucidated by single-particle and bulk approaches. J Gen Virol 96:2122–2132. https://doi.org/10.1099/vir.0.000144
138. Chao LH, Klein DE, Schmidt AG et al (2014) Sequential conformational rearrangements in flavivirus membrane fusion. elife 3:e04389. https://doi.org/10.7554/eLife.04389
139. Kim IS, Jenni S, Stanifer ML et al (2017) Mechanism of membrane fusion induced by vesicular stomatitis virus G protein. Proc Natl Acad Sci USA 114:E28–E36. https://doi.org/10.1073/pnas.1618883114
140. Costello DA, Whittaker GR, Daniel S (2015) Variations in pH sensitivity, acid stability, and fusogenicity of three influenza virus H3 subtypes. J Virol 89:350–360. https://doi.org/10.1128/JVI.01927-14
141. Ivanovic T, Choi JL, Whelan SP et al (2013) Influenza-virus membrane fusion by cooperative fold-back of stochastically induced hemagglutinin intermediates. elife 2013:e00333. https://doi.org/10.7554/eLife.00333
142. Ivanovic T, Harrison SC (2015) Distinct functional determinants of influenza hemagglutinin-mediated membrane fusion. elife 4:e11009. https://doi.org/10.7554/eLife.11009
143. Lee DW, Thapar V, Clancy P, Daniel S (2014) Stochastic fusion simulations and experiments suggest passive and active roles of hemagglutinin during membrane fusion. Biophys J 106:843–854. https://doi.org/10.1016/j.bpj.2013.12.048
144. Hsu H-L, Millet JK, Costello DA et al (2016) Viral fusion efficacy of specific H3N2 influenza virus reassortant combinations at single-particle level. Sci Rep 6:35537. https://doi.org/10.1038/srep35537
145. Otterstrom JJ, Brandenburg B, Koldijk MH et al (2014) Relating influenza virus membrane fusion kinetics to stoichiometry of neutralizing antibodies at the single-particle level. Proc Natl Acad Sci USA 111:E5143–E5148. https://doi.org/10.1073/pnas.1411755111
146. White J, Matlin K, Helenius A (1981) Cell fusion by Semliki forest, influenza, and vesicular stomatitis viruses. J Cell Biol 89:674–679. https://doi.org/10.1083/JCB.89.3.674

147. Markosyan RM, Bates P, Cohen FS, Melikyan GB (2004) A study of low pH-induced refolding of Env of avian sarcoma and leukosis virus into a six-helix bundle. Biophys J 87:3291–3298. https://doi.org/10.1529/biophysj.104.047696
148. Melikyan GB, Barnard RJO, Markosyan RM et al (2004) Low pH is required for avian sarcoma and leukosis virus Env-induced hemifusion and fusion pore formation but not for pore growth. J Virol 78:3753–3762. https://doi.org/10.1128/JVI.78.7.3753-3762.2004
149. Blumenthal R, Sarkar DP, Durell S et al (1996) Dilation of the influenza hemagglutinin fusion pore revealed by the kinetics of individual cell-cell fusion events. J Cell Biol 135:63–71. https://doi.org/10.1083/JCB.135.1.63
150. Spruce AE, Iwata A, White JM, Almers W (1989) Patch clamp studies of single cell-fusion events mediated by a viral fusion protein. Nature 342:555–558. https://doi.org/10.1038/342555a0
151. Spruce AE, Iwata A, Almers W (1991) The first milliseconds of the pore formed by a fusogenic viral envelope protein during membrane fusion. Proc Natl Acad Sci USA 88:3623–3627. https://doi.org/10.1073/pnas.88.9.3623
152. Cohen FS, Melikyan GB (1998) Methodologies in the study of cell-cell fusion. Methods 16:215–226. https://doi.org/10.1006/meth.1998.0670
153. Struck DK, Hoekstra D, Pagano RE (1981) Use of resonance energy transfer to monitor membrane fusion. Biochemistry 20:4093–4099. https://doi.org/10.1021/bi00517a023
154. Hoekstra D, De Boer T, Klappe K, Wilschut J (1984) Fluorescence method for measuring the kinetics of fusion between biological membranes. Biochemistry 23:5675–5681. https://doi.org/10.1021/bi00319a002
155. Cavrois M, de Noronha C, Greene WC (2002) A sensitive and specific enzyme-based assay detecting HIV-1 virion fusion in primary T lymphocytes. Nat Biotechnol 20:1151–1154. https://doi.org/10.1038/nbt745
156. de la Vega M, Marin M, Kondo N et al (2011) Inhibition of HIV-1 endocytosis allows lipid mixing at the plasma membrane, but not complete fusion. Retrovirology 8:99. https://doi.org/10.1186/1742-4690-8-99
157. Clague MJ, Schoch C, Blumenthal R (1991) Delay time for influenza virus hemagglutinin-induced membrane fusion depends on hemagglutinin surface density. J Virol 65:2402–2407
158. Nieva JL, Bron R, Corver J, Wilschut J (1994) Membrane fusion of Semliki Forest virus requires sphingolipids in the target membrane. EMBO J 13:2797–2804

Chapter 3
Structural Insights into Rotavirus Entry

Javier M. Rodríguez and Daniel Luque

Abstract To initiate infection, non-enveloped viruses must recognize a target cell and penetrate the cell membrane by pore formation or membrane lysis. Rotaviruses are non-enveloped dsRNA viruses that infect the mature intestinal epithelium. They are major etiologic agents of diarrheal disease in human infants, as well as in young individuals of various avian and mammalian species. Rotavirus entry into the cell is a complex multistep process initiated by the interaction of the tip of the viral spike with glycan ligands at the cell surface, and driven by conformational changes of the proteins present in the outer protein capsid, the viral machinery for entry. This review feeds on the abundant structural information produced for rotavirus during the past 30 years and focuses on the structure and the dynamics of the rotavirus entry machinery. We survey the current models for rotavirus entry into cells.

Keywords Structural virology · Viral receptor · Non-enveloped virus · Rotavirus entry · Structural changes · Multi-layered particle · Entry

Abbreviations

cryoEM	cryo-Electron microscopy
DLP	Double-layered particle
dsRNA	Double-stranded RNA
HBGA	Histo-blood group antigens
Hsc70	Heat shock cognate protein 70
ORF	Open reading frame
RdRp	RNA-dependent RNA polymerase
RV	Rotavirus
SA	Sialic acid
SLP	Single-layered particle

J. M. Rodríguez (✉) · D. Luque (✉)
Centro Nacional de Microbiología/ISCIII, Madrid, Spain
e-mail: j.rodriguez@isciii.es; dluque@isciii.es

U. F. Greber (ed.), *Physical Virology*, Advances in Experimental Medicine and Biology 1140, https://doi.org/10.1007/978-3-030-14741-9_3

ssRNA	Single-stranded RNA
TLP	Triple-layered particle
TR	Trypsinized

3.1 Introduction

The first challenge that a viral particle faces to generate a productive infection is to recognize the target host cell and overcome the barriers that surround it. These steps are basic to define the virulence and host range of the virus [1–3]. To initiate the infection, virion must recognize and bind to the cell surface. Usually, this process implies two different kinds of surface structures. Initially, attachment factors, such as heparan sulfate, sialic acids (SA), or other carbohydrate structures are bound with relatively low specificity in order to concentrate virions on the cell surface [2, 3]. Then, virus receptors are recognized, usually with high specificity, and viral entry occurs [1–3]. Entry into the cell may occur through the cellular membrane or by promoting endocytic internalization of the particle. Independently of the path used, the nature of the viral particle defines the membrane penetrating mechanism. While for enveloped viruses penetration involves membrane fusion, for non-enveloped viruses it is mediated by pore formation or membrane lysis [4–7]. Although different structural studies have provided us with a relatively fine knowledge of the membrane fusion mechanisms [8–10], the penetration mechanisms of non-enveloped viruses are less well understood [11].

The segmented double-stranded (ds) RNA viruses of the *Reoviridae* family have non-enveloped multi-layered icosahedral capsids [12]. These viruses present a replication cycle that is regulated through an ordered, stepwise disassembly and assembly of the viral particle layers. In this context, the outer shell of the virions is responsible for orchestrating the entry into the host cell [13, 14]. This process has been structurally and functionally well characterized for Rotavirus (RV), an important human and animal gastrointestinal pathogen [15]. In the past years, a number of studies using NMR, X-ray crystallography, and cryo-electron microscopy (cryoEM) have resolved the structure of the RV virion, its subviral particles, and individual proteins of the RV entry machinery alone, or complexed with different ligands [16–28]. In this review, we explore the current RV entry model, the virion structures, and the biochemical and molecular biology studies underlying these models.

3.2 Rotavirus Structure

RV is the main causative agent of infectious gastroenteritis in infants and young children in developed and developing countries [29]. Due to its clinical relevance, together with bluetongue virus [30] and mammalian orthoreovirus [31], RV is a major model for the *Reoviridae* family [32]. RV has a ~18,500 bp segmented genome with 11 double-stranded (ds) RNA molecules that encode six structural

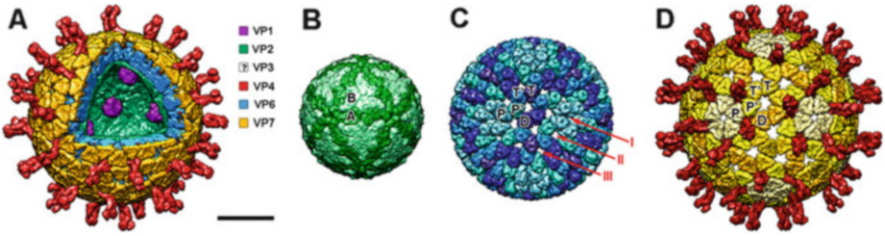

Fig. 3.1 Structure of the rotavirus particle. (**a**) Overview of the TLP structure in a hybrid model built from the atomic model of the RpRd VP1 attached to the inner core [PDB 4AU6, [34]] and the TLP cryoEM structure [PDB 4V7Q, [26]]. Color code is indicated except for the capping enzyme VP3, which is not localized in the model. Scale corresponds to 25 nm. (**b**) Structure of the VP2 T = 1 inner shell. The two types of VP2 conformers (VP2-A and VP2-B) are indicated and colored with different levels of green. (**c**) Structure of the intermediate VP6 T = 13 capsid. The 13 VP6 monomers of the asymmetric unit are arranged into five types of trimeric capsomers colored with different levels of blue and indicated as: P, closest to the fivefold axis; P′, adjacent to P; T, on the threefold; T′, adjacent to T; D, closest to the twofold. The three types of depressions/channels in the shell (I, II and III) are indicated in red. (**d**) Structure of the outer layer. The VP7 glycoprotein trimers are localized in phase with the VP6 trimers in a T = 13 architecture. The five types of trimeric capsomers are indicated with the same nomenclature as that of the underlying VP6 trimers (P, P′, T, T′, and D) and colored with different levels of yellow. The 60 protruding trimeric VP4 spikes are colored in red

proteins (VP1, VP2, VP3, VP4, VP6, and VP7) and six nonstructural proteins (NSP1 to NSP6). All segments are monocistronic with the exception of segment 11 that in some strains has two overlapping open reading frames (ORFs) encoding NSP5 and NSP6 [15, 33]. The infectious entity is a non-enveloped icosahedral triple-layered particle (TLP) with ~100 nm in diameter (Fig. 3.1a) that resembles a wheel (*lat. rota*) when observed by electron microscopy [25, 26, 35].

The inner shell is formed by 60 dimers of the 94 kDa VP2 protein organized in a T = 1 lattice (Fig. 3.1b), which is an architecture present in most dsRNA viruses and that, once assembled, will never be disassembled during the viral cycle [12, 32]. This is a common strategy to isolate the dsRNA molecules of the viral genome from the host sentinels to avoid the induction of the innate antiviral response [12, 36]. Each asymmetric unit of this spherical shell (~55 nm in diameter) is formed of two comma-like shaped VP2 subunits (Fig. 3.1b). Five copies of the VP2-A conformer are forming a star-like complex around the icosahedral fivefold axis, while the VP2-B conformers are located in the gaps between the points of the star [24, 33]. The continuous shell is built by the VP2 subunits and presents pores at the fivefold axes. These channels are relatively small and harbor positively charged residues on their outer face. It has been suggested that a flexion of the loops on the inner face of this pore would be needed to allow the RNA transcripts to pass through during genome transcription [24].

Inside the VP2 shell, each of the 11 dsRNA segments of the viral genome is associated with one copy of the RNA-dependent RNA polymerase (RdRp) VP1 (125 kDa) and the RNA capping enzyme VP3 (88 kDa) [37, 38]. VP1 is located on the inside surface of the pentameric positions (Fig. 3.1a) by contacts with the VP2 N

termini [34]. This VP1–VP2 interaction not only stabilizes the RdRp on the inner shell surface but it is also important for activation of polymerase activity [39]. The structure formed by the viral genome, the VP1/VP3 complex, and the VP2 shell is known as the single-layered particle (SLP) or viral core.

The SLP is surrounded by a ~15 nm thick T = 13 capsid built of 260 pear-shaped VP6 (44 kDa) trimers arranged in five different conformations to form a 70 nm double-layered particle or DLP (Fig. 3.1c) [24, 28]. In contrast to the smooth surface of the core, the DLP shows an uneven surface with depressions at the center of pentamers and hexamers where the VP2 surface is accessible. This DLP is the RV transcriptional machinery and produces capped, non-polyadenylated, positive single-stranded (ss) RNA capable to effectively initiate an infection when the DLP is released into the host cell cytoplasm [40]. VP6 shares structural similarity with the μ1 membrane penetration proteins from aquareovirus and orthoreovirus [41–43]. However, the RV VP6 does not have membrane penetration activity.

Instead, RV uses the outer capsid proteins, the machinery for attachment and entry into the host cell (Fig. 3.1d). This machinery is formed by VP4 (88 kDa) and VP7 (37 kDa). Three copies of VP4 form each of the viral spikes that are anchored at the depressions formed in the center of the pentamer-contacting hexamers built by the D, P, and P′ VP6 trimers (Fig. 3.1c–d, channel II; Fig. 3.2). Finally, the VP7 glycoprotein forms 260 calcium-stabilized trimers that sit atop of each VP6 trimer with the same T = 13 architecture as the VP6 shell (Figs. 3.1d and 3.2) [16, 18, 44]. These VP7 trimers make an ~3 nm thick shell from which the VP4 spikes protrude ~15 nm, creating the TLP, which is the infectious form of the virion.

If added to cells, DLP are non-infective [45, 46]. They are, however, capable of producing an infection when transfected into the cytoplasm [40]. Thus, they have the resources needed to initiate a successful infection but are unable to bind productively and to penetrate into the target cell. Indeed, when DLP are recoated with VP4 and VP7 they gain infectivity by 10^7 fold, reaching a specific infectivity similar to that of virions purified from infected cells [46]. As indicated, the outermost layer of the RV TLP is built by the VP7 T = 13 shell and the VP4 spikes. It constitutes the viral machinery for host cell recognition, attachment, and entry. Additionally, it coordinates these functions and is robust enough to withstand the extracellular conditions that the virions encounter. The VP4 spikes are located at the 60 channel II depressions (Fig. 3.1c) that surround the pentameric positions with their feet sandwiched between the VP6 and VP7 shells (Fig. 3.2) [26]. Biochemical and structural studies [46–48] indicated that not all the positions are necessarily occupied by spikes in an infectious particle. One VP7 trimer sits above each of the 260 VP6 trimers of the DLP to build a continuous T = 13 shell with holes that are contiguous with the channels of the underlying DLP (Figs. 3.1d and 3.2) [18, 26, 49]. Due to antigenic relevance and the key role in infectivity of proteins VP7 and VP4, RV strains are often classified using a G*x*P*y* system [50] similar to the H*x*N*y* one used for influenza virus classification. VP7 defines the G (glycosylated) genotype and VP4 establishes the P (protease sensitive).

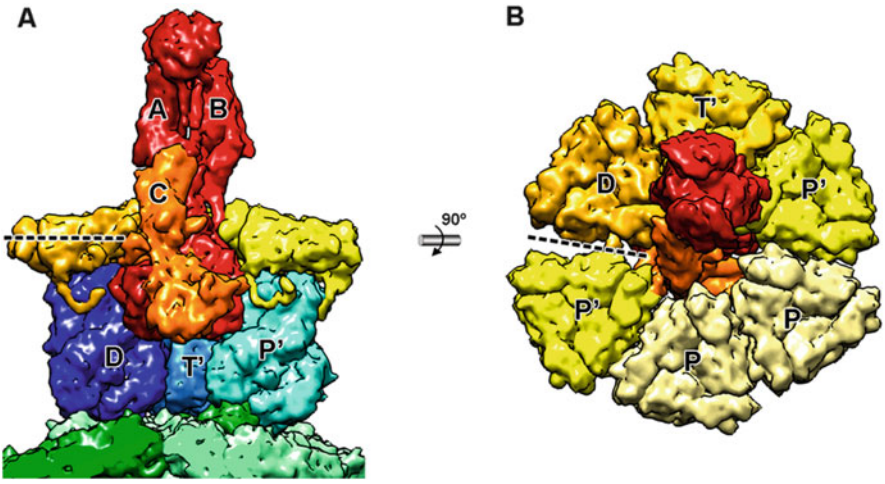

Fig. 3.2 Rotavirus entry machinery interactions. Side (**a**) and Top (**b**) views of the pentamer-contacting hexamers where the spike is located. VP2 is represented in different levels of green, VP6 in blue, VP7 in yellow, and VP4 in red. The VP4 conformers (A, B, C) and the VP6/VP7 trimeric capsomers (P, P′, D, T′) are indicated. For the side view (**a**) only the back VP6 and VP7 trimeric capsomers (D, T′, P′) are shown. Several pear-shaped VP6 trimers contact with each VP2 molecule forming large depressions at the center of pentamers and hexamers. The VP6 trimers in the pentamer-contacting hexamers present a marked gap between the D and P′ trimers (dashed line) where their packaging deviates from the local sixfold symmetry. The VP4 spike foot is anchored to the VP6 lattice through contacts with all the surrounding trimers but the P′ located just aside the gap. A VP7 trimer caps each VP6 trimer and the VP4 C subunit (stalk) is interacting with the D and P′ VP7 trimers that flank the gap

3.2.1 Structure and Functions of VP7

VP7 is a glycoprotein that localizes to the endoplasmatic reticulum (ER). In an unusual pathway for a non-enveloped virus, it is incorporated into the maturing particle, inside the ER, in a not very well-understood process that includes the acquisition and loss of a transient membrane [15]. Its first 50 residues correspond to a signal peptide that is cleaved in the mature form of the protein. The mature VP7 is folded in two compact domains: a Rossman-fold (domain I) with a β-barrel (domain II) inserted in one of its loops (Fig. 3.3a, b). VP7 assembles into trimers that are stabilized by two calcium ions bound at the interface between subunits, accounting for six ions per trimer (Fig. 3.3b, magenta) [16]. While the N- and C-terminal extensions are disordered in the crystallographic structure of the VP7 trimer (and presumably in free VP7), the cryoEM structures of the VP7 recoated DLP and the TLP show that the N-terminal residues are organized as an arm that grips the VP6 beneath it [18, 26]. Each of the three arms of the VP7 trimer forms a β-strand (residues 58–62) that extend the β-sheet of the VP6 jelly roll domain under it (Fig. 3.3c, inset).

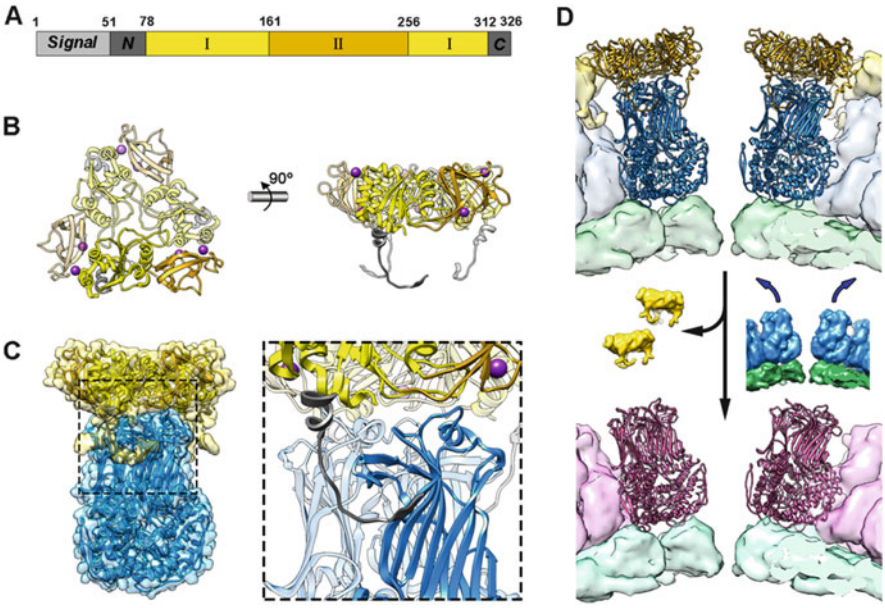

Fig. 3.3 Structure of the Rotavirus glycoprotein VP7. (**a**) Diagram of the VP7 primary structure and domain organization: signal peptide (light gray), N- and C-terminal extensions (dark gray), Rossmann-fold domain I (light yellow), and β-barrel domain II (dark yellow). (**b**) Ribbon representation of top (left) and side (right) views of the atomic structure of the VP7 trimer (PDB 3GZT) color coded as in **a**) with one subunit highlighted. Two calcium ions (magenta) are bound at the interface between VP7 subunits. (**c**) Interaction between VP6 and VP7 trimers. VP7 trimer occupies a position directly on top of the VP6 trimer with minimal contacts in this interface. The contact between them is mediated by the three VP7 N-terminal arms that grip the VP6 trimer beneath it forming an additional β-strand that augments the VP6 jelly roll (inset). (**d**) Conformational differences in the TLP > DLP transition. Side view of the central channel on the icosahedral pentameric positions (Fig. 3.1, channel I) for the models of the TLP (top, PDBs 3GZU, and 3GZT) and DLP (bottom, PDB 3KZ4). An outward movement of the VP2 and VP6 layers is promoted when VP7 is released

Despite the fact that each VP7 trimer caps a VP6 trimer, there are minimal contacts at this interface, and the attachment of VP7 to VP6 is almost exclusively mediated by the N-terminal arm. This region not only grasps the underlying VP6 but its most N-terminal residues (51–57) seem to interact with the neighboring VP7 trimers to form a network of interactions that stabilizes the outer RV shell.

Due to the calcium dependence of VP7 to trimerize, virions and VP7-recoated DLP are effectively uncoated by chelating agents [44, 45, 51]. Calcium depletion not only destroys the virion infectivity but also activates the polymerase transcriptional activity [45]. The structures of the particle with and without VP7 [18, 24] show an upwards and outwards movement of the VP2 and VP6 layers (Fig. 3.3d) that must occur when the VP7 layer dissociates during viral entry and the DLP is released into the host cell cytoplasm. This movement results in an expansion of the pentameric type I channels and would allow the extrusion of newly synthetized positive-sense

ssRNA transcripts. The VP7 layer structurally reinforces the infectious particle integrity and is key to regulate the calcium-dependent outer layer uncoating that delivers a transcriptionally active DLP into the cytoplasm. Additionally, VP7 has been implicated in the binding to integrins as post-attachment receptors [52–56] and in membrane penetration [57, 58].

3.2.2 *Rotavirus Spike Structure*

Once assembled, RV virions are not yet fully infectious. Full infectivity is achieved by limited proteolysis of the spike protein VP4 into N-terminal VP8* (28 kDa) and C-terminal VP5* (60 kDa) fragments by trypsin-like proteases of the intestinal lumen of the host [59–61] (Fig. 3.4). Different cryoEM analysis of trypsinized (TR-) TLP [25, 26, 62] has allowed to understand how the three VP4 subunits

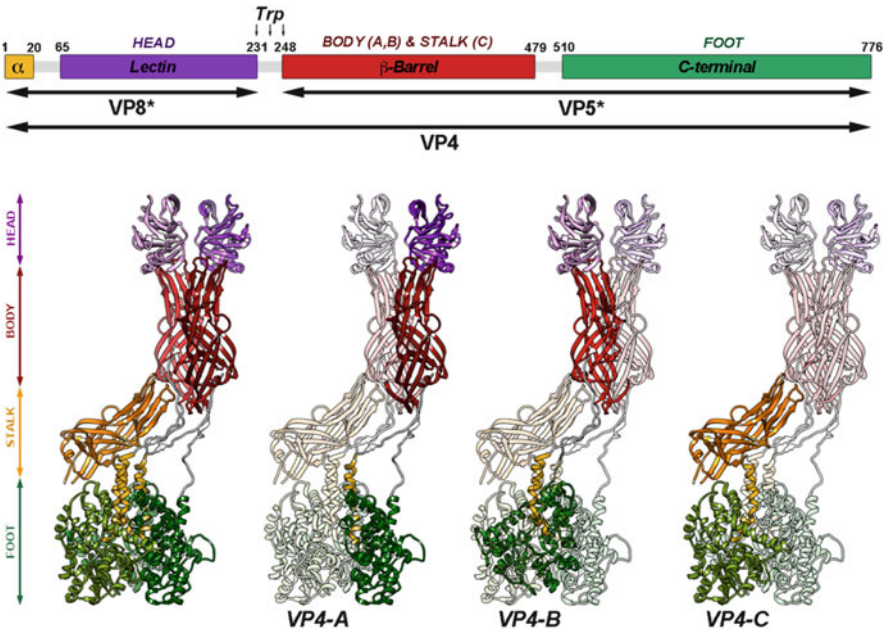

Fig. 3.4 Atomic structure of the Rotavirus VP4 spike. Diagram of the VP4 primary structure and domain organization (bottom): α (yellow), lectin (magenta), β-barrel (red) and C-terminal (green) domains. Residues delimiting domains and trypsin cleavage sites are indicated. Ribbon representation of the atomic model (PDB 4VZQ) of the trypsinized RV spike. Each domain is represented with a different level of the same color in each subunit: foot (green), stalk (red), body (red) and head (purple). At the right, each of the VP4 subunits (VP4-A, -B and -C) is shown highlighted. The N- and C-terminal domains of the three subunits contribute to the foot. The β-barrel domain of the C subunit forms the stalk while the VP4-A and -B built the spike body. The head is constructed by the lectin domains of VP4-A and -B. The VP4-C lectin domain is not present in the structure

(A, B, C) assemble into a spike. The spike is an extreme example of structural polymorphism with trimeric, dimeric and asymmetric elements (Fig. 3.4).

The C-terminal domains of the three VP5* subunits interact to form a trimeric foot that is sandwiched between the VP6 and the VP7 layers (Figs. 3.2 and 3.4). The analysis of the six-coordinated cavity, in which the foot is anchored, shows that while each of the A and C subunits present equivalent interactions with two neighbor VP6 trimers, the B subunit interacts with just one VP6 trimer because its other neighbor is out of contact range (Fig. 3.2). Although the contacts between the spike foot and VP7 are relatively tenuous (mediated by the VP7 N-terminal arms), the assembly of the VP7 trimeric caps onto VP6 locks the spikes by constricting the diameter of the cavity above the spike base [26, 46]. The region that protrudes out of the VP7 layer does not maintain the local trimeric symmetry observed in the foot. The VP5*-C β-barrel forms the spike stalk (Fig. 3.4) and inserts one tip in the gap between the D and P′ VP7 trimers interacting with the subunits to either side (Fig. 3.2).

The β-barrels of the A and B subunits build the dimeric spike body that extends away from the particle surface and is capped by the VP8*-A and -B lectin domains. The remaining VP8*-C lectin domain has not been detected in any TR-TLP reconstruction [25, 26, 62]. It is presumed to dissociate from the particle after proteolytic activation. The distal ends of the VP5* β-barrel domains present a hydrophobic patch formed by three loops that have been implicated in membrane interaction and permeabilization. Indeed, one of them has sequence similarity with an alphavirus fusion loop, and mutations in any of them reduces viral infectivity up to 10,000 times [19, 63–65]. For the VP5*-A and -B subunits, these loops are embedded into the above VP8* spike lobes (Fig. 3.5a), but in the case of the VP5*-C β-barrel, the hydrophobic patch sits on the base of the spike body (Fig. 3.5b).

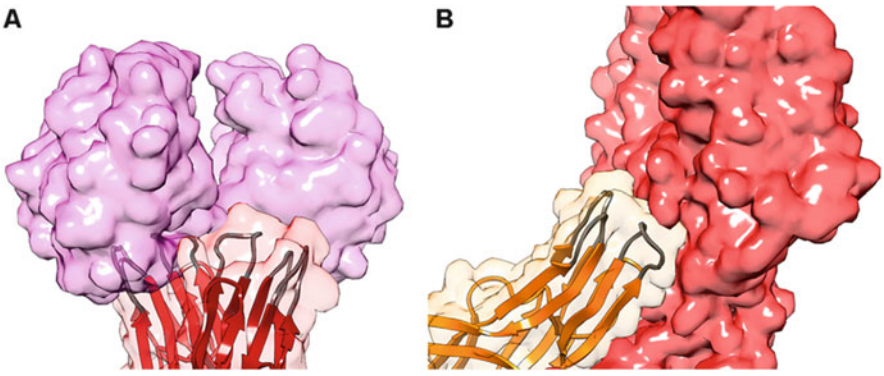

Fig. 3.5 VP5* Hydrophobic loops. Ribbon representation of the (**a**) A-, B- and (**b**) C-VP5* subunits within the spike surface. Ribbon and surfaces of VP5*-A and -B are colored in red, VP5*-C in orange and VP8* in magenta. The three VP5* hydrophobic loops (B′C′, D′E′ and F′G) that form the hydrophobic patch at one tip of the β-barrel domain are colored in gray. The VP5*-A and -B loops are capped by the VP8* spike lobes (**a**), while the VP5*-C hydrophobic patch lies on the spike body base (**b**)

3.3 Trypsin Activation of Rotavirus: Structural Implications

As indicated previously (Fig. 3.4), infection strictly depends on protease digestion of the VP4 spike protein, which occurs after virus release from the infected cell to the lumen of the small intestine [59–61], where there is an abundant supply of trypsin-like proteases. The protein is proteolyzed at three defined sites (Arg231, Arg241 and Arg247) through an ordered cleavage cascade that culminates in scission at Arg247. Cleavage after this residue is essential for membrane permeabilization and infectivity [66, 67]. Interestingly, when cleavage was modified to a furin-sensitive form that is proteolyzed intracellularly, impairment on virus replication was observed, attributed to a premature activation of the viral entry machinery [68].

CryoEM single particle analysis of non-trypsinized (NTR) and TR-TLP of the SA11-4F reassortant strain showed that while TR-TLP spikes were well resolved, no electron-density was identified for the spikes in uncleaved particles [69], leading to the conclusion that trypsin activation triggers large conformational changes in the VP4 domains that give rise to a rigid, entry-competent spike. However, using two unrelated non-reassortant model rotavirus strains, the simian SA11 and the porcine OSU, it was recently found that the cryoEM 3D reconstructions of the uncleaved virions (Fig. 3.6a) show spikes with a structure compatible with the atomic model of the cleaved spike, and indistinguishable from that of digested particles [48]. These results suggest that activation does not entail large conformational changes. Rather, the proteolytic processing has a limited effect on spike structure but allows each of the VP4 domains to move independently during the large conformational changes needed for virus entry (see below, Fig. 3.9). Cryo-electron tomography and subvolume averaging allowed the characterization of the mobility of the different domains for the digested and undigested spike, providing the structure of the complete NTR spike including the lectin domain of the VP4-C subunit (Fig. 3.6b–c).

VP4 shows a striking similarity to membrane fusion proteins of enveloped viruses [19, 70], which depend on proteolytic activation and exhibit characteristic conformational movements during viral entry (see below). Precursors of the class 1 viral fusion glycoproteins require protease activation for virus infectivity [10, 71], a step that results in little structural rearrangement in case of influenza virus [72, 73] or in parainfluenza virus 5 [74], akin to rotavirus VP4.

Trypsin has been shown to be tightly associated with the outer TLP protein layer of RV grown in trypsin-containing medium. The activity of the enzyme is inhibited in the virions but activated when the outer protein layer of the TLP is solubilized by Ca^{++} chelation. Interestingly, when the activity of this virus-associated trypsin is inhibited by protease inhibitors added to the cell culture medium, primary transcription is reduced as well as virus replication. A role for this virus-associated trypsin has been suggested for virus entry, where after TLP dissociation by a drop in Ca^{++} concentration, the activation of this trypsin-associated enzyme would digest VP7 and give rise to trypsin fragments that have been shown to possess membrane permeabilization activity [57].

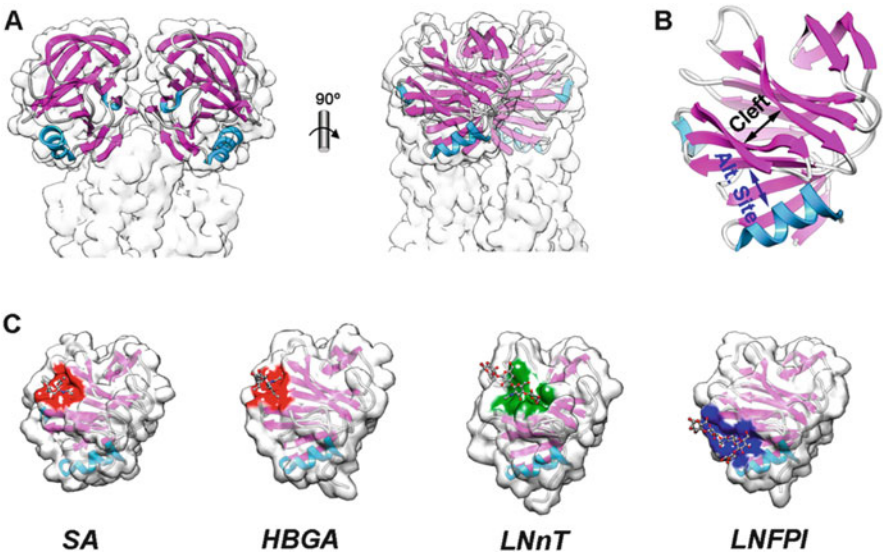

Fig. 3.6 Three-dimensional structures of NTR- and TR-TLP. (**a**) Single particle cryoEM icosahedrally averaged 3D reconstruction of NTR- (left half, EMD-2573) and TR-TLP (right half, EMD-2574) radially color-coded to represent VP4 or VP8*/VP5* spikes, (red), VP7 (yellow) and VP6 (blue). (**b**, **c**) Cryoelectron tomography averaged subvolumes of the (**b**) NTR (EMD-2579) and (**c**) TR (EMD-2580) spikes fitted with the VP4 and VP7 atomic models (PDB 4V7Q). For the NTR spike (**b**) an additional single VP8* lectin domain is superimposed on the extra density at the base of the stalk

Binding to the target cell membrane occurs independently of the activation state of the viral particle. However, the internalization of the undigested particles, which do not result in infection [75], is considerably slower, with a half-life of 30–50 min compared with 3–5 min for the activated virus [75, 76].

3.4 Rotavirus Cell Attachment

RV entry into the host cell is a multistep process that implicates the sequential interaction of the VP4-derived peptides (VP5* and VP8*) and VP7 with different cell surface molecules [77–80]. VP8* has been implicated in the initial attachment to the host cell through the interaction with glycans, whereas VP5* and VP7 have been associated in post-attachment interactions (Table 3.1).

Proposed non-glycan RV co-receptors include integrins αvβ3 and αxβ2 for VP7 and α2β1 for VP5* [53, 54, 81]. Additionally, heat shock cognate protein 70 (Hsc70) has been implicated as a putative co-receptor recognized by VP5* [82]. It has been shown that VP7 interacts with αvβ3 through a GPR motif and to αxβ2 through CNP motif [53, 83]. As it has been previously indicated [16, 18, 76], in the TLP both

Table 3.1 Cellular attachment and post-attachment requirements for different rotavirus strains

Strain	Origin	Sialidase-sensitive	Genotype	Glycan	Post-attachment factors
SA11	Simian	Yes	P[2]	SA (GM2, GM3, GD1a)	Integrins (α2β1, αxβ2 and αvβ3), Hsc70
RRV	Simian	Yes	P[3]	SA (GM3, GM1)	Integrins (α2β1, αxβ2 and αvβ3), Hsc70
DS-1	Human	No	P[4]	A-, H-type I, Le HBGA	?
UK	Bovine	No	P[5]	SA (GM1, GM2)	?
RV-3	Human	No	P[6]	SA (GM1), A-, type-I, Le HBGA	?
CRW-8	Porcine	Yes	P[7]	SA (GM3, GD1a)	?
K8	Human	No	P[8]	A-HBGA, LacNAc	?
Wa	Human	No	P[8]	SA (GM1) A-, H-type I, Le HBGA	Integrins (α2β1, αxβ2 and αvβ3)
N1509	Human	No	P[11]	LacNAc	?
N155	Human	No	P[11]	Type I and type II	?
B223	Bovine	No	P[11]	Type II	?
HAL1166	Human	No	P[14]	A-HBGA	?
NIV929893	Porcine	No	P[19]	Type I HBGA, mucin core	?

motifs are found in regions buried at the VP6–VP7 contact interface (Fig. 3.7, dark blue and green). Thus, contact between VP7 and these integrins could only occur at a post-uncoating step. In addition, VP5* interacts with the α-subunit of α2β1 using a DGE sequence [53, 84]. Analysis of the structure of the spike shows that while in the VP5*-C subunit the DGE motif is localized at the stalk tip close to the VP7 shell, the motifs in the VP5*-A and -B subunits protrude out of the VP7 shell (Fig. 3.7, light blue). However, their position (close to the VP7 shell surface) and the orientation of the lateral chains of the Asp and Glu residues in the DGE motif (facing away from the subunit surface) would require a conformational change to bind to α2β1 [26, 76]. Finally, the interaction of VP5* with Hsc70 has been described as a possible post-attachment step for rotavirus entry [79, 82]. This interaction with Hsc70 is mediated by a region [79, 85] located at the spike foot, as seen in the atomic structure of the TLP (Fig. 3.7, gray). Thus, it is only accessible after the uncoating of the particle.

There is a consensus that the initial virus attachment occurs through the interaction of the two VP8* domains of VP4 with glycans. Although the sequence of the VP8* domain is the most variable among the structural proteins and the major contributor to a phylogeny with 40 P genotypes, its structure is conserved. VP8* genotype-dependent variations in glycan specificity are important for RV interspecies transmission, host range restriction, and tissue tropism [77, 86, 87]. VP8* presents a galectin-like fold with a twisted anti-parallel β-sandwich formed by two

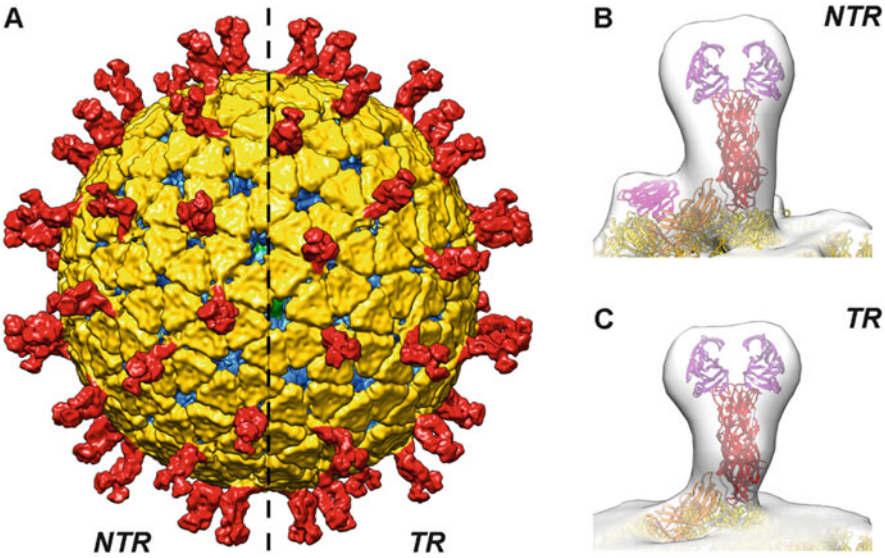

Fig. 3.7 VP4 and VP7 receptor binding sites. (**a**–**c**) Binding sites for the different described RV cellular receptors mapped on the surface of the atomic structure of a VP7 trimer (**b**) and a VP4 spike (**c**). Color code is shown in (**a**). Top (**d**) and side (**e**) views of the spike in the context of a VP6–VP7 type II hexamer (see Fig. 3.1). Notice that when VP7 and VP4 are assembled, just α2β1 sites on VP5*-A and -B seem to be accessible from the outer surface of the viral particle

β-sheets that are separated by a shallow cleft [17, 20–23] (Fig. 3.8a–c). Although the galectin fold is conserved among the different VP8* structures analyzed, the cleft width and the residues exposed in it vary between them and play an important role in the glycan binding specificity of different RV strains [87].

Traditionally, SA has been considered the cellular binding partner for rotavirus VP8*. SA is a generic term for a family of monosaccharides ubiquitously expressed in higher vertebrates and typically found in the terminal branches of N-glycans, O-glycans, and glycosphingolipids (gangliosides) [88]. The susceptibility of the infectivity of some rotavirus strains to the treatment of the target cells with sialidases (neuraminidases) led to the description of sialidase-sensitive and -insensitive strains [89]. Animal rotaviruses are usually sialidase-sensitive, as they interact with terminal sialic acid residues (Table 3.1). The structural basis of this interaction is well documented through a series of crystallographic analysis [17, 20, 90, 91]. The VP8* SA binding site is located in the narrow cleft between the β-sheets (Fig. 3.8b–c, red) in a site distinct from the carbohydrate binding site in galectins [20]. With the exception of the strain HCR3a, the human strains are insensitive to sialidases [92]. However, most sialidases are not able to digest internal (branched) SA residues. Accordingly, it has been shown for the sialidase-insensitive strain Wa by NMR spectroscopy and molecular modeling of the VP8* domain that it binds to gangliosides using internal sialic residues [93] on the same cleft site (Fig. 3.8c, red). Importantly, the structure of the

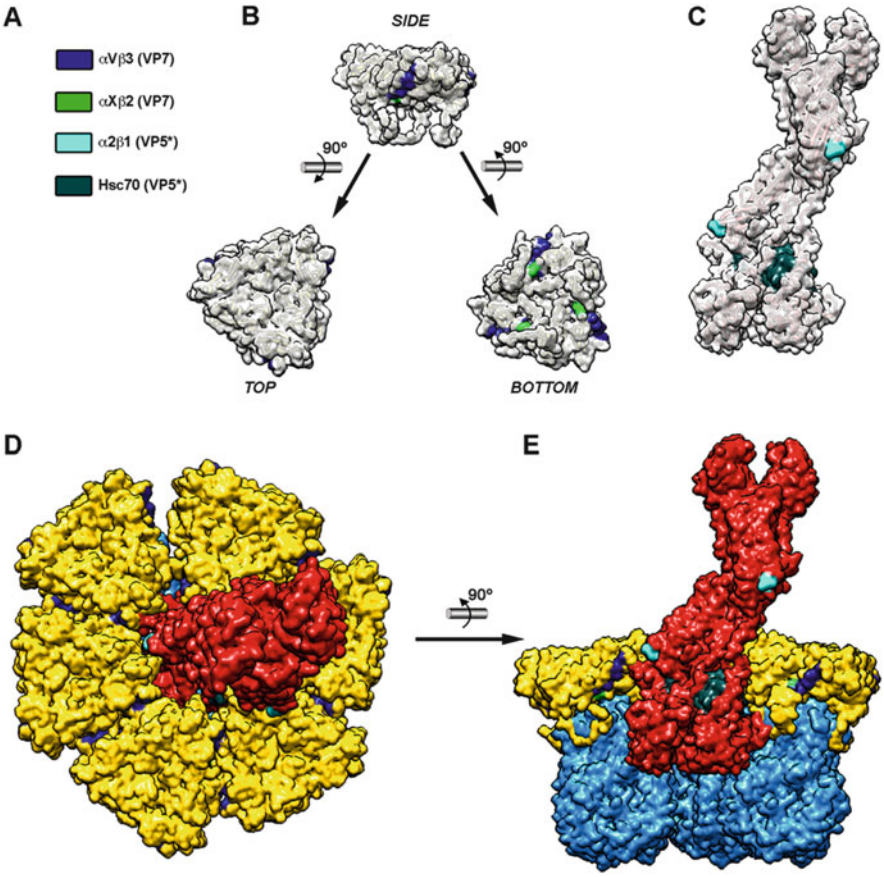

Fig. 3.8 VP8* atomic structure. (**a**) Front and side views (rotation is indicated) of the VP8* atomic structure within the spike surface (PDB 4V7Q). (**b**) Ribbon representation of VP8* colored by its secondary structure: α-helix, blue; β-strand, magenta; loop, gray. The cleft between the twisted β-sheets and an alternative binding site behind it are indicated. (**c**, **d**, **e**) VP8* binding sites. Atomic structures of VP8* complexed with SA (PDB 1KQR, P[3] strain RRV), type A-HBGA (PDB 4DRV, P[14] strain HAL1166), the type II precursor LNnT (PDB 4YG0, P[11] strain N155) and the type I HBGA lacto-N-fucopentaose I (LNFPI, PDB 5VKS, P[19] strain 210). The two different described binding sites on the cleft are colored in red and green [20–22], while a recently described alternative binding site is blue colored [23]

VP8* domain of the most prevalent human strains (P[4] and P[8]) show a considerable wider cleft, which probably allows for the binding to internal sialic acids.

Recently it has been shown that the VP8* of some human rotavirus strains (Table 3.1) binds to histo-blood group antigens (HBGA) [21, 22, 94–99]. HBGA are non-sialylated glycoconjugates expressed on the surface of red blood cells, epithelial cells, and in mucosal secretions [100]. The X-ray crystallographic structure of the VP8* of the P[14] strain HAL1166 shows that its cleft is similar to the characteristic

narrow cleft of the SA binding animal strains. Structural studies show that the binding of this strain to A-type HBGA (Fig. 3.8c, HBGA, red) occurs in an equivalent position to that of the terminal SA in the RRV VP8* (Fig. 3.8c, SA, red). Binding to A-type HBGA was shown for P[14], P[9], and P[25] to be biologically significant [21, 97]. Thus, binding to SA and to the A-type HBGA essentially occurs in the same VP8* cleft region. This is possible, with the level of sequence identity observed, because VP8* can experience significant structural rearrangements upon ligand binding [101], which is likely important during host adaptation.

The VP8* of human P[11] rotaviruses recognizes type I and type II glycans, precursors of HBGA. Interestingly, it has been hypothesized that the binding of P [11] VP8* to precursor glycans and the probable developmental regulation of the expression of the precursors could be linked to the preference of these strains for newborns [96, 98]. The crystal structures of the VP8* of the P[11] strain N155 in complex with the type I tetrasaccharide lacto-N-tetraose (LNT) and type II tetrasaccharide lacto-N-neotetraose (LNnT) [22] show that the binding occurs in the cleft in a different binding site to that where type I and II precursor glycans are recognized (Fig. 3.8c, green, LNnT). Additionally, recent studies demonstrate that some strains could use a novel binding site outside of the cleft that is capable of interacting with a type I HBGA, or a mucin core [23] (Fig. 3.8c, LNFPI, blue).

3.5 Rotavirus Entry Models

After initial binding to the cell by the attachment of the viral VP8* to the corresponding cellular glycan, several sequential interactions have been proposed to occur [80]. Apart from integrins and Hsc70, which have been discussed elsewhere on this review, gangliosides, JAM-A, occludin, and ZO-1 [102, 103] have been proposed to have a role in these post-attachment interactions. However, blocking the interaction of RV with each of the proposed co-receptors or receptors with proteases, antibodies, peptides, or siRNA resulted in a reduction of less than 1 log unit of the virus infectivity. These findings have been interpreted to reflect a high degree of plasticity on the viral entry pathways, the possible existence of several alternative entry routes, the presence of a high redundancy of entry factors, or the existence of a yet undescribed, highly relevant entry factor [77].

RV were initially proposed to enter the cell via direct penetration of the cell membrane, but recent findings indicate that the virus enters the cells by endocytosis, and that membrane disruption occurs in an endocytic compartment, the nature of which depends on the strain. The majority of animal or human RV strains appear to enter cells by clathrin-mediated endocytosis [104, 105], which in MA104 requires cholesterol and dynamin [105]. The simian strain RRV follows a different endocytic pathway that is independent of clathrin and caveolin, but that requires also cholesterol and dynamin [106, 107]. Remarkably, a single amino acid change in VP8* (K187R)

is able to alter the pathway of entry of this strain to a clathrin-dependent pathway [108, 109]. The RRV strain with this mutation, nar3, also changes from a sialidase-sensitive phenotype to a sialidase-insensitive pathway, and interacts with integrin α2β1 [79]. Recently, it has been shown that debrin, an actin binding-protein that is able to bind VP4, restricts rotavirus entry by inhibiting dynamin-mediated endocytosis via interaction with cortactin [110]. Downstream of the formation of the primary endosome, all the strains appear to converge to early endosomes as indicated by their dependence on Rab5 and EEA1 [104, 107, 111]. Also, a functional ESCRT system is essential for RV infection [107].

After reaching the maturing endosome, exit routes to the cytoplasm vary between strains. Their independence of Rab7 suggests that RRV and SA11-4S exit from the maturing endosomes [104, 107], whereas the RRV point mutant nar3 exits from late endosomes. Rab7-dependent viruses behave as late-penetration viruses, while simian RRV and SA11-4S can be considered early-penetration viruses [1]. It has been recently shown that the RV strains that reach the late endosomes require a functional Rab9a, and, with the exception of nar3, all of them depend on the activity of the cation-dependent mannose-6-phosphate receptor and cathepsins B, L, and S [104]. Little is known about the mechanisms used by RV to exit from the endosomal compartments. However, it has been shown that late penetration viruses activate the cellular PI3K, Akt, and ERK pathways, early during infection, to allow for the V-ATPase-dependent endosomal acidification required for their uncoating [112].

A model for the interaction and entry of RRV in BSC-1 cells has been proposed which does not involve the association of the incoming particles with clathrin adaptors or with dynamin, and where the association with Rab5-containing endosomes appears to be unproductive [76]. The experiments leading to this model use recoated TLP with each of the outer proteins, as well as the DLP, labeled with a different fluorophore, without compromising the infectivity. Using live cell imaging, the fate of each of the labeled components is followed for each individual incoming particle. The combination of these data with structural analysis by electron microscopy and electron tomography allows the proposal of a model for the interaction and entry of the RRV TLP, which encompasses previous molecular models, and where VP4 plays a similar role to the fusion proteins of enveloped virus, since its conformational changes provide the energy necessary for membrane disruption [19, 63, 70, 113, 114].

Initial interaction with the cell membrane occurs very rapidly, although some particles have a short period of lateral movement (<1 min). This period increases when the hydrophobic loops of VP5* are mutated, which suggests that lateral movement concludes when the hydrophobic loops are inserted in the membrane. Binding and attachment take place through the interaction of the distal lectin domains of the two VP8* molecules of chains A and B (Fig. 3.9). The progressive saturation of the interactions of all the VP8* domains of the TLP leads to the engulfment of the particle in a tight-fitting membrane. The calculated distance of interaction in the engulfed particle agrees with an interaction of VP8* with a

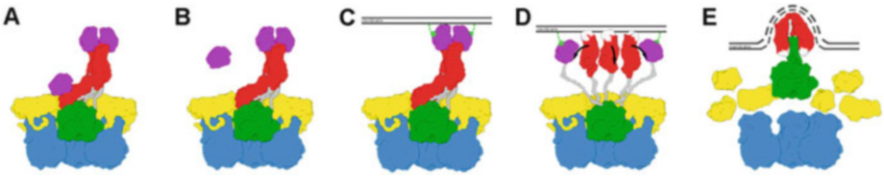

Fig. 3.9 Structural transitions during RV entry. Schematic representation of the current proposed conformational changes of the RV spike during RV membrane penetration. VP6 is colored in blue, VP7 in yellow, VP4/VP5* foot in green, VP4/VP5* β-barrel in red, VP4/VP8* lectin domain in magenta, and loops in gray. (**a**) The three unprocessed VP4 subunits are assembled as an asymmetric trimer in the TLP with two VP4 subunits building the spike body and head, while the β-barrel and the lectin domains of the third subunit are located in the spike stalk. (**b**) Trypsin activation cleaves VP4 into VP5* and VP8* peptides priming the spike for further conformational changes. The lectin domain located at the spike stalk is dissociated after the proteolytic processing. (**c**) Initial attachment to the host cell through the interaction of the VP8* lectin domains with surface glycans (light green). This interaction is necessary for a first conformational change (**d**) in which the lectin domains dissociate from the spike and expose the VP5* hydrophobic patches (white) that interact with the membrane. (**e**) The decrease of calcium concentration promotes the disassembly of the VP7 shell and the release of VP5*, which is now able to fold back to a stable less energetic conformation. Driven by the VP5* fold back, the hydrophobic loops inserted in the membrane produce the membrane distortion and rupture (dashed)

sialidated ganglioside. Within 5 min of attachment, the particles have been completely enveloped, being inaccessible to external agents. Within 3–5 min the engulfed particles release the DLP to the cell cytoplasm. Thin-section electron microscopy confirms the presence of the three proposed stages of TLP—bound to the plasma membrane, enveloped, and compartmentalized. Whole-cell cryo-electron tomography of surface bound rotavirus particles showed that the particles maintain two different distances from the membrane. A longer distance, similar to that of the spikes of normal TLP, which is interpreted as the VP8* domains interacting with the attachment factors, and a shorter distance that would imply a conformational change in the structure of the spike. In the TR-TLP, VP8* domains are anchored to the foot domain by a long, flexible N-terminal loop, that could allow the lateral movement of the two VP8* domains exposing the VP5* hydrophobic loops (Fig. 3.9d). The short distance observed fits very well with the calculated distance when the hydrophobic loops are inserted in the membrane. This corresponds with the proposed extended intermediate, in which the hydrophobic loops of the three VP5* β-barrels, previously covered by the lectin domains (chains A and B) or by the spike body (chain C), are inserted into the target cell membrane [70] (Fig. 3.9d).

The observation that the DLP is released from a vesicle with a tight-fitting membrane is key to link the molecular movements of the VP5* with DLP release. It has been previously proposed that the transition from this extended intermediate to a folded-back structure, in which the hydrophobic loops now point toward the virus particle, releases the free energy that rotavirus uses to disrupt the cell membrane [19, 65]. In this model, transitions are coupled to membrane movements by

the insertion of the hydrophobic loops. Each spike attempting to acquire a folded back structure will produce an expansion of its local bubble (Fig. 3.9e) and, even if only a modest fraction of the 60 spikes successfully folds-back, a tight fitting membrane will likely burst. Importantly, bursting will occur even if the spikes are no longer attached to the DLP because the changes, which are local to each spike, are transmitted through the membrane. This is crucial since VP7 must be depolymerized, likely by the leakage of Ca^{++} ions during the insertion of the hydrophobic loops, to allow for the fold back to occur [114]. This model is the first to link the molecular movements proposed for the spike protein VP5* with a verifiable mechanism for DLP entry. Although several aspects of this model await confirmation, release of the DLP from a tight-fitting membrane driven by VP5* conformational changes is an attractive option irrespective of the nature of the endosomal compartment from where the virus is released.

3.6 Concluding Remarks

Although there is extensive knowledge about the mature RV TLP, important questions about the RV TLP structure remain to be addressed. Knowledge about the structure of the minor protein VP3 and the nature of its complex with VP1 will improve our understanding of the mechanics of viral transcription. Also, there is little information regarding the structure of the 11 dsRNA segments and their dynamics during transcription. Importantly, the rotavirus genus encompasses several species (A to J). Our structural knowledge is largely limited to the species A. There are almost no data available regarding the structural variability in the rotavirus genus.

Regarding the RV entry process, although we are closer to an understanding of the exact role of trypsin activation for rotavirus infectivity, the effect that proteolytic processing has on the structure and location of the VP4 connecting loops remains to be shown. It would be desirable to test if trypsin digestion liberates VP4 from a blockage to fold back. Additionally, the current models for rotavirus entry (Fig. 3.10) are likely complementary to some degree, if the release of the DLP to the cytosol occurs by a mechanism depicted in the model, and as suggested by the Harrison lab [76], even if the particle is released from endocytic compartments. Finally, the discovery of the plasticity of VP8* and the role of new glycan molecules in rotavirus interaction with the target cell have revolutionized our understanding of rotavirus host restriction and the role of the host genetics on the susceptibility to different strains. These are exciting findings with tremendous potential for the next years.

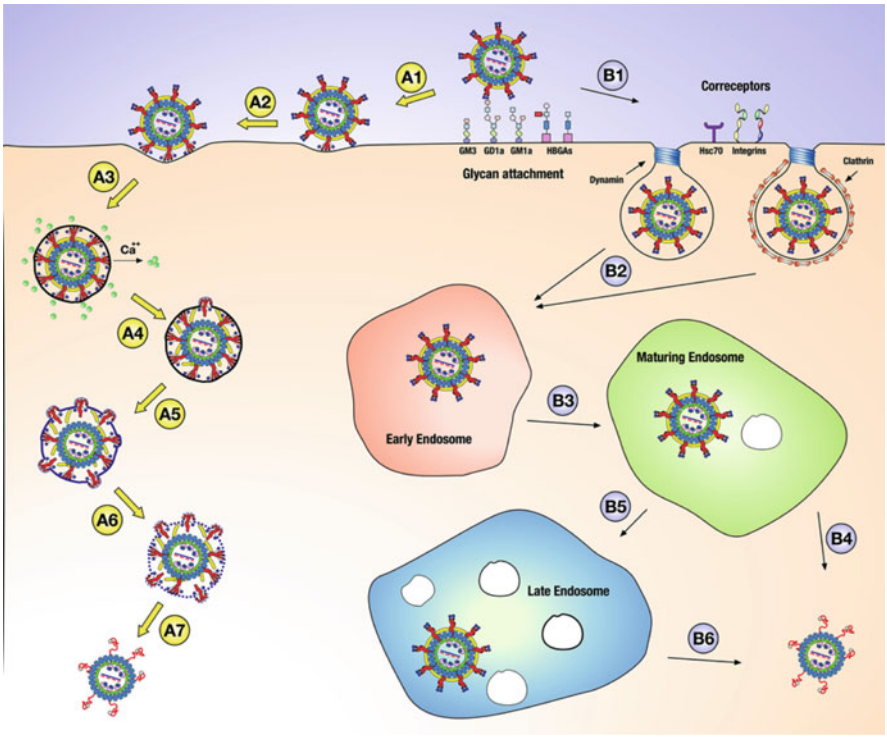

Fig. 3.10 Two models for RV entry. RV entry starts in both models with the interaction of the infectious particle with a glycan attachment molecule. In model A [76], this short initial period of interaction allows lateral movements of the particle, which is immobilized by the insertion of the hydrophobic loops of the VP4 molecule (A1), initiating the engulfment of the virus in a tight-fitting membrane (A2). In this model, virus components direct this engulfment (A3). Probably due to the destabilizing effect on the membrane of the inserted loops, calcium ions leach from the vesicle to the cytoplasm producing a progressive diminution of the calcium concentration which ultimately leads to the disassembling of the VP7 layer (A4). Without de VP7 layer, the VP4 spike is able to perform the fold back transition (A4). The movement of the hydrophobic loops during this conformational change impels the membrane to increase its area, leading to the generation of a local bubble. Ultimately, this strain is shared among the vesicle membrane which accumulates the distortion (A5). When, due to the progressive fold back of VP4 spikes, the accumulated stress surpasses the bursting point of the bilayer the vesicle bursts (A6) and the DLP is released to the cellular cytoplasm, initiating transcription (A7). In model B [77], after interaction with the glycan attachment molecule, the incoming particle is internalized by clathrin-dependent, or -independent endocytosis, depending on the virus strain (B1). Regardless of the endocytic pathway, the particles reach an early endosome (B2) and progress to maturing endosomes (B3) from which some strains (termed early-penetration strains) are able to be released to the cell cytoplasm and initiate transcription (B4). Late-penetration strains must reach late endosomes (B5) before they are released to initiate a productive infection (B6)

References

1. Lozach PY, Huotari J, Helenius A (2011) Late-penetrating viruses. Curr Opin Virol 1 (1):35–43. https://doi.org/10.1016/j.coviro.2011.05.004
2. Marsh M, Helenius A (2006) Virus entry: open sesame. Cell 124(4):729–740
3. Yamauchi Y, Greber UF (2016) Principles of virus uncoating: cues and the snooker ball. Traffic 17(6):569–592. https://doi.org/10.1111/tra.12387
4. Burckhardt CJ, Greber UF (2009) Virus movements on the plasma membrane support infection and transmission between cells. PLoS Pathog 5(11):e1000621. https://doi.org/10.1371/journal.ppat.1000621
5. Greber UF (2002) Signalling in viral entry. Cell Mol Life Sci 59(4):608–626
6. Luisoni S, Greber UF (2016) Biology of adenovirus cell entry – receptors, pathways, mechanism. In: Curiel D (ed) Adenoviral vectors for gene therapy, 2nd edn. Academic, London, pp 27–58
7. Sieczkarski SB, Whittaker GR (2005) Viral entry. Curr Top Microbiol Immunol 285:1–23
8. Harrison SC (2005) Mechanism of membrane fusion by viral envelope proteins. Adv Virus Res 64:231–261. https://doi.org/10.1016/S0065-3527(05)64007-9
9. Kielian M, Rey FA (2006) Virus membrane-fusion proteins: more than one way to make a hairpin. Nat Rev Microbiol 4(1):67–76. https://doi.org/10.1038/nrmicro1326
10. Mas V, Melero JA (2013) Entry of enveloped viruses into host cells: membrane fusion. Subcell Biochem 68:467–487
11. Suomalainen M, Greber UF (2013) Uncoating of non-enveloped viruses. Curr Opin Virol 3 (1):27–33. https://doi.org/10.1016/j.coviro.2012.12.004
12. Mertens P (2004) The dsRNA viruses. Virus Res 101(1):3–13
13. Desselberger U (2014) Rotaviruses. Virus Res 190:75–96. https://doi.org/10.1016/j.virusres.2014.06.016
14. Trask SD, McDonald SM, Patton JT (2012) Structural insights into the coupling of virion assembly and rotavirus replication. Nat Rev Microbiol 10(3):165–177. https://doi.org/10.1038/nrmicro2673. nrmicro2673 [pii]
15. Estes MK, Greenberg HB (2013) Rotaviruses. In: Knipe DM, Howley PM, Cohen JI et al (eds) Fields virology, 6th edn. Lippincott Williams & Wilkins, Philadelphia, p 1
16. Aoki ST, Settembre EC, Trask SD, Greenberg HB, Harrison SC, Dormitzer PR (2009) Structure of rotavirus outer-layer protein VP7 bound with a neutralizing Fab. Science 324 (5933):1444–1447
17. Blanchard H, Yu X, Coulson BS, von Itzstein M (2007) Insight into host cell carbohydrate-recognition by human and porcine rotavirus from crystal structures of the virion spike associated carbohydrate-binding domain (VP8*). J Mol Biol 367(4):1215–1226. https://doi.org/10.1016/j.jmb.2007.01.028
18. Chen JZ, Settembre EC, Aoki ST, Zhang X, Bellamy AR, Dormitzer PR, Harrison SC, Grigorieff N (2009) Molecular interactions in rotavirus assembly and uncoating seen by high-resolution cryo-EM. Proc Natl Acad Sci USA 106(26):10644–10648
19. Dormitzer PR, Nason EB, Prasad BV, Harrison SC (2004) Structural rearrangements in the membrane penetration protein of a non-enveloped virus. Nature 430(7003):1053–1058
20. Dormitzer PR, Sun ZY, Wagner G, Harrison SC (2002) The rhesus rotavirus VP4 sialic acid binding domain has a galectin fold with a novel carbohydrate binding site. EMBO J 21 (5):885–897
21. Hu L, Crawford SE, Czako R, Cortes-Penfield NW, Smith DF, Le Pendu J, Estes MK, Prasad BV (2012) Cell attachment protein VP8* of a human rotavirus specifically interacts with A-type histo-blood group antigen. Nature 485(7397):256–259. https://doi.org/10.1038/nature10996
22. Hu L, Ramani S, Czako R, Sankaran B, Yu Y, Smith DF, Cummings RD, Estes MK, Venkataram Prasad BV (2015) Structural basis of glycan specificity in neonate-specific bovine-human reassortant rotavirus. Nat Commun 6:8346. https://doi.org/10.1038/ncomms9346

23. Liu Y, Xu S, Woodruff AL, Xia M, Tan M, Kennedy MA, Jiang X (2017) Structural basis of glycan specificity of P[19] VP8*: implications for rotavirus zoonosis and evolution. PLoS Pathog 13(11):e1006707. https://doi.org/10.1371/journal.ppat.1006707
24. McClain B, Settembre E, Temple BR, Bellamy AR, Harrison SC (2010) X-ray crystal structure of the rotavirus inner capsid particle at 3.8 A resolution. J Mol Biol 397(2):587–599. https://doi.org/10.1016/j.jmb.2010.01.055. S0022-2836(10)00110-5 [pii]
25. Prasad BV, Wang GJ, Clerx JP, Chiu W (1988) Three-dimensional structure of rotavirus. J Mol Biol 199(2):269–275
26. Settembre EC, Chen JZ, Dormitzer PR, Grigorieff N, Harrison SC (2011) Atomic model of an infectious rotavirus particle. EMBO J 30(2):408–416. https://doi.org/10.1038/emboj.2010.322. emboj2010322 [pii]
27. Yeager M, Dryden K, Olson N, Greenberg H, Baker T (1990) Three-dimensional structure of rhesus rotavirus by cryoelectron microscopy and image reconstruction. J Cell Biol 110 (6):2133–2144
28. Zhang X, Settembre E, Xu C, Dormitzer PR, Bellamy R, Harrison SC, Grigorieff N (2008) Near-atomic resolution using electron cryomicroscopy and single-particle reconstruction. Proc Natl Acad Sci USA 105(6):1867–1872. https://doi.org/10.1073/pnas.0711623105. 0711623105 [pii]
29. Collaborators GBDDD (2017) Estimates of global, regional, and national morbidity, mortality, and aetiologies of diarrhoeal diseases: a systematic analysis for the Global Burden of Disease Study 2015. Lancet Infect Dis 17(9):909–948. https://doi.org/10.1016/S1473-3099(17)30276-1
30. Roy P (2013) Orbiviruses. In: Knipe DM, Howley PM, Cohen JI et al (eds) Fields virology, 6th edn. Lippincott Williams & Wilkins, Philadelphia, p 1
31. Dermody TS, Parker JS, Sherry B (2013) Orthoreoviruses. In: Knipe DM, Howley PM, Cohen JI et al (eds) Fields virology, 6th edn. Lippincott Williams & Wilkins, Philadelphia, p 1
32. King A, Lefkowitz EJ, Adams MJ, Carstens EB (eds) (2011) Virus taxonomy. Ninth report of the International Committee on Taxonomy of Viruses. Academic, San Diego
33. Pesavento JB, Crawford SE, Estes MK, Prasad BV (2006) Rotavirus proteins: structure and assembly. Curr Top Microbiol Immunol 309:189–219
34. Estrozi LF, Settembre EC, Goret G, McClain B, Zhang X, Chen JZ, Grigorieff N, Harrison SC (2013) Location of the dsRNA-dependent polymerase, VP1, in rotavirus particles. J Mol Biol 425(1):124–132
35. Flewett TH, Bryden AS, Davies H, Woode GN, Bridger JC, Derrick JM (1974) Relation between viruses from acute gastroenteritis of children and newborn calves. Lancet 2 (7872):61–63
36. Arnold MM, Sen A, Greenberg HB, Patton JT (2013) The battle between rotavirus and its host for control of the interferon signaling pathway. PLoS Pathog 9(1):e1003064. https://doi.org/10.1371/journal.ppat.1003064
37. Patton JT, Chen D (1999) RNA-binding and capping activities of proteins in rotavirus open cores. J Virol 73(2):1382–1391
38. Periz J, Celma C, Jing B, Pinkney JN, Roy P, Kapanidis AN (2013) Rotavirus mRNAS are released by transcript-specific channels in the double-layered viral capsid. Proc Natl Acad Sci USA 110(29):12042–12047
39. McDonald SM, Patton JT (2011) Rotavirus VP2 core shell regions critical for viral polymerase activation. J Virol 85(7):3095–3105. https://doi.org/10.1128/JVI.02360-10
40. Bass DM, Baylor MR, Chen C, Mackow EM, Bremont M, Greenberg HB (1992) Liposome-mediated transfection of intact viral particles reveals that plasma membrane penetration determines permissivity of tissue culture cells to rotavirus. J Clin Invest 90(6):2313–2320
41. Liemann S, Chandran K, Baker TS, Nibert ML, Harrison SC (2002) Structure of the reovirus membrane-penetration protein, Mu1, in a complex with is protector protein, Sigma3. Cell 108 (2):283–295

42. Mathieu M, Petitpas I, Navaza J, Lepault J, Kohli E, Pothier P, Prasad BV, Cohen J, Rey FA (2001) Atomic structure of the major capsid protein of rotavirus: implications for the architecture of the virion. EMBO J 20(7):1485–1497
43. Zhang X, Jin L, Fang Q, Hui WH, Zhou ZH (2010) 3.3 A cryo-EM structure of a nonenveloped virus reveals a priming mechanism for cell entry. Cell 141(3):472–482. https://doi.org/10.1016/j.cell.2010.03.041. S0092-8674(10)00360-0 [pii]
44. Dormitzer PR, Greenberg HB, Harrison SC (2000) Purified recombinant rotavirus VP7 forms soluble, calcium-dependent trimers. Virology 277(2):420–428
45. Cohen J, Laporte J, Charpilienne A, Scherrer R (1979) Activation of rotavirus RNA polymerase by calcium chelation. Arch Virol 60(3–4):177–186
46. Trask SD, Dormitzer PR (2006) Assembly of highly infectious rotavirus particles recoated with recombinant outer capsid proteins. J Virol 80(22):11293–11304
47. Chen DY, Ramig RF (1992) Determinants of rotavirus stability and density during CsCl purification. Virology 186(1):228–237
48. Rodriguez JM, Chichon FJ, Martin-Forero E, Gonzalez-Camacho F, Carrascosa JL, Caston JR, Luque D (2014) New insights into rotavirus entry machinery: stabilization of rotavirus spike conformation is independent of trypsin cleavage. PLoS Pathog 10(5):e1004157. https://doi.org/10.1371/journal.ppat.1004157
49. Prasad BV, Chiu W (1994) Structure of rotavirus. Curr Top Microbiol Immunol 185:9–29
50. Matthijnssens J, Ciarlet M, Rahman M, Attoui H, Banyai K, Estes MK, Gentsch JR, Iturriza-Gomara M, Kirkwood CD, Martella V, Mertens PP, Nakagomi O, Patton JT, Ruggeri FM, Saif LJ, Santos N, Steyer A, Taniguchi K, Desselberger U, Van Ranst M (2008) Recommendations for the classification of group A rotaviruses using all 11 genomic RNA segments. Arch Virol 153(8):1621–1629. https://doi.org/10.1007/s00705-008-0155-1
51. Dormitzer PR, Greenberg HB (1992) Calcium chelation induces a conformational change in recombinant herpes simplex virus-1-expressed rotavirus VP7. Virology 189(2):828–832
52. Coulson BS, Londrigan SL, Lee DJ (1997) Rotavirus contains integrin ligand sequences and a disintegrin-like domain that are implicated in virus entry into cells. Proc Natl Acad Sci USA 94 (10):5389–5394
53. Graham KL, Halasz P, Tan Y, Hewish MJ, Takada Y, Mackow ER, Robinson MK, Coulson BS (2003) Integrin-using rotaviruses bind alpha2beta1 integrin alpha2 I domain via VP4 DGE sequence and recognize alphaXbeta2 and alphaVbeta3 by using VP7 during cell entry. J Virol 77(18):9969–9978
54. Guerrero CA, Mendez E, Zarate S, Isa P, Lopez S, Arias CF (2000) Integrin alpha(v)beta (3) mediates rotavirus cell entry. Proc Natl Acad Sci USA 97(26):14644–14649. https://doi.org/10.1073/pnas.250299897
55. Hewish MJ, Takada Y, Coulson BS (2000) Integrins alpha2beta1 and alpha4beta1 can mediate SA11 rotavirus attachment and entry into cells. J Virol 74(1):228–236
56. Ludert JE, Ruiz MC, Hidalgo C, Liprandi F (2002) Antibodies to rotavirus outer capsid glycoprotein VP7 neutralize infectivity by inhibiting virion decapsidation. J Virol 76 (13):6643–6651
57. Charpilienne A, Abad MJ, Michelangeli F, Alvarado F, Vasseur M, Cohen J, Ruiz MC (1997) Solubilized and cleaved VP7, the outer glycoprotein of rotavirus, induces permeabilization of cell membrane vesicles. J Gen Virol 78(Pt 6):1367–1371. https://doi.org/10.1099/0022-1317-78-6-1367
58. Elaid S, Libersou S, Ouldali M, Morellet N, Desbat B, Alves ID, Lepault J, Bouaziz S (2014) A peptide derived from the rotavirus outer capsid protein VP7 permeabilizes artificial membranes. Biochim Biophys Acta 1838(8):2026–2035. https://doi.org/10.1016/j.bbamem.2014.04.005
59. Clark SM, Roth JR, Clark ML, Barnett BB, Spendlove RS (1981) Trypsin enhancement of rotavirus infectivity: mechanism of enhancement. J Virol 39(3):816–822
60. Estes MK, Graham DY, Mason BB (1981) Proteolytic enhancement of rotavirus infectivity: molecular mechanisms. J Virol 39(3):879–888

61. Ludert JE, Krishnaney AA, Burns JW, Vo PT, Greenberg HB (1996) Cleavage of rotavirus VP4 in vivo. J Gen Virol 77(Pt 3):391–395. https://doi.org/10.1099/0022-1317-77-3-391
62. Li Z, Baker ML, Jiang W, Estes MK, Prasad BV (2009) Rotavirus architecture at subnanometer resolution. J Virol 83(4):1754–1766. https://doi.org/10.1128/JVI.01855-08. JVI.01855-08 [pii]
63. Kim IS, Trask SD, Babyonyshev M, Dormitzer PR, Harrison SC (2010) Effect of mutations in VP5 hydrophobic loops on rotavirus cell entry. J Virol 84(12):6200–6207
64. Tihova M, Dryden KA, Bellamy AR, Greenberg HB, Yeager M (2001) Localization of membrane permeabilization and receptor binding sites on the VP4 hemagglutinin of rotavirus: implications for cell entry. J Mol Biol 314(5):985–992. https://doi.org/10.1006/jmbi.2000.5238
65. Yoder JD, Dormitzer PR (2006) Alternative intermolecular contacts underlie the rotavirus VP5* two- to three-fold rearrangement. EMBO J 25(7):1559–1568. https://doi.org/10.1038/sj.emboj.7601034
66. Arias CF, Romero P, Alvarez V, Lopez S (1996) Trypsin activation pathway of rotavirus infectivity. J Virol 70(9):5832–5839
67. Gilbert JM, Greenberg HB (1998) Cleavage of rhesus rotavirus VP4 after arginine 247 is essential for rotavirus-like particle-induced fusion from without. J Virol 72(6):5323–5327
68. Komoto S, Wakuda M, Ide T, Niimi G, Maeno Y, Higo-Moriguchi K, Taniguchi K (2011) Modification of the trypsin cleavage site of rotavirus VP4 to a furin-sensitive form does not enhance replication efficiency. J Gen Virol 92(Pt 12):2914–2921
69. Crawford SE, Mukherjee SK, Estes MK, Lawton JA, Shaw AL, Ramig RF, Prasad BV (2001) Trypsin cleavage stabilizes the rotavirus VP4 spike. J Virol 75(13):6052–6061
70. Trask SD, Kim IS, Harrison SC, Dormitzer PR (2010) A rotavirus spike protein conformational intermediate binds lipid bilayers. J Virol 84(4):1764–1770
71. Harrison SC (2008) Viral membrane fusion. Nat Struct Mol Biol 15(7):690–698
72. Chen J, Lee KH, Steinhauer DA, Stevens DJ, Skehel JJ, Wiley DC (1998) Structure of the hemagglutinin precursor cleavage site, a determinant of influenza pathogenicity and the origin of the labile conformation. Cell 95(3):409–417
73. Wilson IA, Skehel JJ, Wiley DC (1981) Structure of the haemagglutinin membrane glycoprotein of influenza virus at 3 A resolution. Nature 289(5796):366–373
74. Welch BD, Liu Y, Kors CA, Leser GP, Jardetzky TS, Lamb RA (2012) Structure of the cleavage-activated prefusion form of the parainfluenza virus 5 fusion protein. Proc Natl Acad Sci USA 109(41):16672–16677
75. Kaljot KT, Shaw RD, Rubin DH, Greenberg HB (1988) Infectious rotavirus enters cells by direct cell membrane penetration, not by endocytosis. J Virol 62(4):1136–1144
76. Abdelhakim AH, Salgado EN, Fu X, Pasham M, Nicastro D, Kirchhausen T, Harrison SC (2014) Structural correlates of rotavirus cell entry. PLoS Pathog 10(9):e1004355. https://doi.org/10.1371/journal.ppat.1004355
77. Arias CF, Silva-Ayala D, Lopez S (2015) Rotavirus entry: a deep journey into the cell with several exits. J Virol 89(2):890–893. https://doi.org/10.1128/JVI.01787-14
78. Baker M, Prasad BV (2010) Rotavirus cell entry. Curr Top Microbiol Immunol 343:121–148. https://doi.org/10.1007/82_2010_34
79. Lopez S, Arias CF (2004) Multistep entry of rotavirus into cells: a Versaillesque dance. Trends Microbiol 12(6):271–278
80. Lopez S, Arias CF (2006) Early steps in rotavirus cell entry. Curr Top Microbiol Immunol 309:39–66
81. Zarate S, Espinosa R, Romero P, Guerrero CA, Arias CF, Lopez S (2000) Integrin alpha2beta1 mediates the cell attachment of the rotavirus neuraminidase-resistant variant nar3. Virology 278(1):50–54. https://doi.org/10.1006/viro.2000.0660
82. Guerrero CA, Bouyssounade D, Zarate S, Isa P, Lopez T, Espinosa R, Romero P, Mendez E, Lopez S, Arias CF (2002) Heat shock cognate protein 70 is involved in rotavirus cell entry. J Virol 76(8):4096–4102

83. Zarate S, Romero P, Espinosa R, Arias CF, Lopez S (2004) VP7 mediates the interaction of rotaviruses with integrin alphavbeta3 through a novel integrin-binding site. J Virol 78 (20):10839–10847. https://doi.org/10.1128/JVI.78.20.10839-10847.2004
84. Fleming FE, Graham KL, Takada Y, Coulson BS (2011) Determinants of the specificity of rotavirus interactions with the alpha2beta1 integrin. J Biol Chem 286(8):6165–6174. https://doi.org/10.1074/jbc.M110.142992
85. Jolly CL, Huang JA, Holmes IH (2001) Selection of rotavirus VP4 cell receptor binding domains for MA104 cells using a phage display library. J Virol Methods 98(1):41–51
86. Ramani S, Hu L, Venkataram Prasad BV, Estes MK (2016) Diversity in rotavirus-host glycan interactions: a "sweet" spectrum. Cell Mol Gastroenterol Hepatol 2(3):263–273. https://doi.org/10.1016/j.jcmgh.2016.03.002
87. Venkataram Prasad BV, Shanker S, Hu L, Choi JM, Crawford SE, Ramani S, Czako R, Atmar RL, Estes MK (2014) Structural basis of glycan interaction in gastroenteric viral pathogens. Curr Opin Virol 7:119–127. https://doi.org/10.1016/j.coviro.2014.05.008
88. Varki A, Schnaar RL, Schauer R (2015) Sialic acids and other nonulosonic acids. In: rd VA, Cummings RD et al (eds) Essentials of glycobiology. Cold Spring Harbor Laboratory Press, Cold Spring Harbor, pp 179–195. https://doi.org/10.1101/glycobiology.3e.015
89. Ciarlet M, Estes MK (1999) Human and most animal rotavirus strains do not require the presence of sialic acid on the cell surface for efficient infectivity. J Gen Virol 80 (Pt 4):943–948. https://doi.org/10.1099/0022-1317-80-4-943
90. Kraschnefski MJ, Scott SA, Holloway G, Coulson BS, von Itzstein M, Blanchard H (2005) Cloning, expression, purification, crystallization and preliminary X-ray diffraction analysis of the VP8* carbohydrate-binding protein of the human rotavirus strain Wa. Acta Crystallogr Sect F Struct Biol Cryst Commun 61(11):989–993. https://doi.org/10.1107/S1744309105032999
91. Yu X, Guillon A, Szyczew AJ, Kiefel MJ, Coulson BS, von Itzstein M, Blanchard H (2008) Crystallization and preliminary X-ray diffraction analysis of the carbohydrate-recognizing domain (VP8*) of bovine rotavirus strain NCDV. Acta Crystallogr Sect F Struct Biol Cryst Commun 64(6):509–511. https://doi.org/10.1107/S1744309108011949
92. Ciarlet M, Ludert JE, Iturriza-Gomara M, Liprandi F, Gray JJ, Desselberger U, Estes MK (2002) Initial interaction of rotavirus strains with N-acetylneuraminic (sialic) acid residues on the cell surface correlates with VP4 genotype, not species of origin. J Virol 76(8):4087–4095
93. Haselhorst T, Fleming FE, Dyason JC, Hartnell RD, Yu X, Holloway G, Santegoets K, Kiefel MJ, Blanchard H, Coulson BS, von Itzstein M (2009) Sialic acid dependence in rotavirus host cell invasion. Nat Chem Biol 5(2):91–93. https://doi.org/10.1038/nchembio.134
94. Bohm R, Fleming FE, Maggioni A, Dang VT, Holloway G, Coulson BS, von Itzstein M, Haselhorst T (2015) Revisiting the role of histo-blood group antigens in rotavirus host-cell invasion. Nat Commun 6:5907. https://doi.org/10.1038/ncomms6907
95. Huang P, Xia M, Tan M, Zhong W, Wei C, Wang L, Morrow A, Jiang X (2012) Spike protein VP8* of human rotavirus recognizes histo-blood group antigens in a type-specific manner. J Virol 86(9):4833–4843. https://doi.org/10.1128/JVI.05507-11
96. Liu Y, Huang P, Jiang B, Tan M, Morrow AL, Jiang X (2013) Poly-LacNAc as an age-specific ligand for rotavirus P[11] in neonates and infants. PLoS One 8(11):e78113. https://doi.org/10.1371/journal.pone.0078113
97. Liu Y, Huang P, Tan M, Liu Y, Biesiada J, Meller J, Castello AA, Jiang B, Jiang X (2012) Rotavirus VP8*: phylogeny, host range, and interaction with histo-blood group antigens. J Virol 86(18):9899–9910. https://doi.org/10.1128/JVI.00979-12
98. Ramani S, Cortes-Penfield NW, Hu L, Crawford SE, Czako R, Smith DF, Kang G, Ramig RF, Le Pendu J, Prasad BV, Estes MK (2013) The VP8* domain of neonatal rotavirus strain G10P [11] binds to type II precursor glycans. J Virol 87(13):7255–7264. https://doi.org/10.1128/JVI.03518-12
99. Yu Y, Lasanajak Y, Song X, Hu L, Ramani S, Mickum ML, Ashline DJ, Prasad BV, Estes MK, Reinhold VN, Cummings RD, Smith DF (2014) Human milk contains novel glycans that are potential decoy receptors for neonatal rotaviruses. Mol Cell Proteomics 13 (11):2944–2960. https://doi.org/10.1074/mcp.M114.039875

100. Marionneau S, Cailleau-Thomas A, Rocher J, Le Moullac-Vaidye B, Ruvoen N, Clement M, Le Pendu J (2001) ABH and Lewis histo-blood group antigens, a model for the meaning of oligosaccharide diversity in the face of a changing world. Biochimie 83(7):565–573
101. Yu X, Mishra R, Holloway G, von Itzstein M, Coulson BS, Blanchard H (2015) Substantial receptor-induced structural rearrangement of rotavirus VP8*: potential implications for cross-species infection. Chembiochem 16(15):2176–2181. https://doi.org/10.1002/cbic.201500360
102. Martinez MA, Lopez S, Arias CF, Isa P (2013) Gangliosides have a functional role during rotavirus cell entry. J Virol 87(2):1115–1122. https://doi.org/10.1128/JVI.01964-12
103. Torres-Flores JM, Silva-Ayala D, Espinoza MA, Lopez S, Arias CF (2015) The tight junction protein JAM-A functions as coreceptor for rotavirus entry into MA104 cells. Virology 475:172–178. https://doi.org/10.1016/j.virol.2014.11.016
104. Diaz-Salinas MA, Silva-Ayala D, Lopez S, Arias CF (2014) Rotaviruses reach late endosomes and require the cation-dependent mannose-6-phosphate receptor and the activity of cathepsin proteases to enter the cell. J Virol 88(8):4389–4402. https://doi.org/10.1128/JVI.03457-13
105. Gutierrez M, Isa P, Sanchez-San Martin C, Perez-Vargas J, Espinosa R, Arias CF, Lopez S (2010) Different rotavirus strains enter MA104 cells through different endocytic pathways: the role of clathrin-mediated endocytosis. J Virol 84(18):9161–9169. https://doi.org/10.1128/JVI.00731-10
106. Sanchez-San Martin C, Lopez T, Arias CF, Lopez S (2004) Characterization of rotavirus cell entry. J Virol 78(5):2310–2318
107. Silva-Ayala D, Lopez T, Gutierrez M, Perrimon N, Lopez S, Arias CF (2013) Genome-wide RNAi screen reveals a role for the ESCRT complex in rotavirus cell entry. Proc Natl Acad Sci USA 110(25):10270–10275. https://doi.org/10.1073/pnas.1304932110
108. Diaz-Salinas MA, Romero P, Espinosa R, Hoshino Y, Lopez S, Arias CF (2013) The spike protein VP4 defines the endocytic pathway used by rotavirus to enter MA104 cells. J Virol 87(3):1658–1663. https://doi.org/10.1128/JVI.02086-12
109. Fleming FE, Bohm R, Dang VT, Holloway G, Haselhorst T, Madge PD, Deveryshetty J, Yu X, Blanchard H, von Itzstein M, Coulson BS (2014) Relative roles of GM1 ganglioside, N-acylneuraminic acids, and alpha2beta1 integrin in mediating rotavirus infection. J Virol 88(8):4558–4571. https://doi.org/10.1128/JVI.03431-13
110. Li B, Ding S, Feng N, Mooney N, Ooi YS, Ren L, Diep J, Kelly MR, Yasukawa LL, Patton JT, Yamazaki H, Shirao T, Jackson PK, Greenberg HB (2017) Drebrin restricts rotavirus entry by inhibiting dynamin-mediated endocytosis. Proc Natl Acad Sci USA 114(18):E3642–E3651. https://doi.org/10.1073/pnas.1619266114
111. Wolf M, Deal EM, Greenberg HB (2012) Rhesus rotavirus trafficking during entry into MA104 cells is restricted to the early endosome compartment. J Virol 86(7):4009–4013. https://doi.org/10.1128/JVI.06667-11
112. Soliman M, Seo JY, Kim DS, Kim JY, Park JG, Alfajaro MM, Baek YB, Cho EH, Kwon J, Choi JS, Kang MI, Park SI, Cho KO (2018) Activation of PI3K, Akt, and ERK during early rotavirus infection leads to V-ATPase-dependent endosomal acidification required for uncoating. PLoS Pathog 14(1):e1006820. https://doi.org/10.1371/journal.ppat.1006820
113. Wolf M, Vo PT, Greenberg HB (2011) Rhesus rotavirus entry into a polarized epithelium is endocytosis dependent and involves sequential VP4 conformational changes. J Virol 85(6):2492–2503
114. Yoder JD, Trask SD, Vo TP, Binka M, Feng N, Harrison SC, Greenberg HB, Dormitzer PR (2009) VP5* rearranges when rotavirus uncoats. J Virol 83(21):11372–11377. https://doi.org/10.1128/JVI.01228-09

Chapter 4
The HIV-1 Capsid: More than Just a Delivery Package

Leo C. James

Abstract Productive HIV infection requires integration of viral genes into the host genome. But how viral DNA gets to the nucleus in the first place remains one of the most controversial yet deceptively simple questions in HIV post-entry biology. This is illustrated in cartoons of viral entry, which often depict the entry process as an 'explosion' of the HIV capsid in the cytosol and independent movement of viral DNA through nuclear pores and into the nucleus. HIV enters the cell cytosol with two encapsidated RNA strands and must undergo reverse transcription (RT) to synthesise DNA. Even here there is no consensus for where, when or how RT happens. HIV must get into the nucleus, which in a non-dividing cell requires transport through the nuclear pore. Finally, the virus must 'uncoat': shed its protein capsid to allow its DNA to be spliced with that of the host. Where the virus uncoats and whether this is a single or multi-step process are similarly hotly debated. Understanding these processes is further complicated by three broad factors. First, that there are inter-relationships between these processes that may ensure HIV undergoes the right step at the right place at the right time. Second, the host has cofactors which the virus is dependent upon and must recruit but also immune factors that can sense and inhibit virus and so must be avoided. Third, HIV post-entry biology is cell-type dependent—meaning that factors which are essential in one cell type can be redundant in another.

Keywords HIV · Capsid · Pore · Reverse transcription · Uncoating · Entry · Nucleotide · Non-membranous compartment · Sequestration · Nuclear pore complex · Host factors · Infection · Nuclear import · DNA

L. C. James (✉)
Medical Research Council Laboratory of Molecular Biology, Cambridge, UK
e-mail: lcj@mrc-lmb.cam.ac.uk

U. F. Greber (ed.), *Physical Virology*, Advances in Experimental Medicine and Biology 1140, https://doi.org/10.1007/978-3-030-14741-9_4

4.1 Introduction

Recent research has highlighted that the viral capsid is the principle coordinator of HIV post-entry events. Once thought to be simply an inert shell, we now know that the capsid interacts with multiple cellular cofactors required for infection. These include nuclear pore and cargo proteins Nup153, Nup358 and CPSF6 and the chaperone CypA. The capsid is also the newest target of antiretrovirals and has been actively pursued by multiple pharmaceutical companies including Pfizer, Boehringer-Ingelheim and Gilead. This review will focus on the cofactors and ligands that interact with the HIV capsid and attempt to illustrate how a basic understanding of the structure and function of these interactions is helping us unpick the mystery of HIV post-entry biology. Key to recent discoveries has been structure–function analysis of the HIV capsid hexamer. The hexamer is the primary constituent of the capsid, which also contains exactly 12 pentamers. The hexamer is made up of monomers comprised of two domains—an N-terminal domain (NTD) and a C-terminal domain (CTD) (Fig. 4.1a). All of the cofactors discussed in this review concern the hexamer as shown.

4.2 Cyclophilin A

The first, and for a long time only, cofactor that was identified as a ligand for the HIV capsid was Cyclophilin A (CypA) [1]. CypA is a cis–trans prolyl isomerase, which catalyses the interconversion between cis and trans forms of proline imide bonds. CypA is a ubiquitous enzyme, whose activity and mechanism have been extensively characterised but whose function and cellular importance remain ambiguous. It is generally considered to be a chaperone, which assists in protein folding by catalysing the otherwise slow and potentially rate-limiting step of proline isomerisation [2]. If so, this function is a nonessential one as its removal from yeast, even simultaneous with other Cyp homologs, is non-lethal [3]. Within the HIV capsid, CypA binds to the CypA-loop, an extended and flexible motif in the NTD that projects from the capsid surface (Fig. 4.1a, b). CypA specifically binds to a glycine–proline (GP) motif at the centre of this loop, near its apex. While six molecules could potentially bind the six loops in an assembled hexamer, the packing between hexamers in a complete virion would preclude this. Thus, in a complete HIV capsid core, it is likely that a maximum of only three CypA molecules per hexamer are possible. The CypA loop is nevertheless highly accessible and readily available for binding to CypA in the cytosol. CypA is packaged into virions, despite the fact that the mature hexamer assembles only after budding [4, 5]. However, it is CypA in the target cell rather than the producer cell that is most crucial to virus infection and infection phenotypes can be generated when perturbing CypA through siRNA depletion, capsid mutation or using small molecule inhibitors [6].

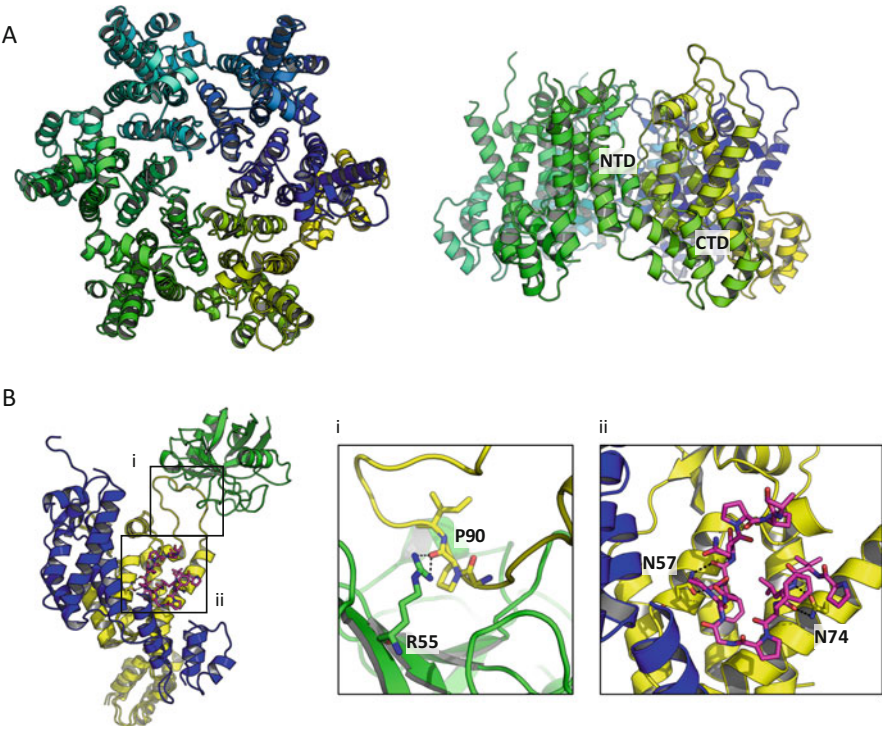

Fig. 4.1 HIV-1 capsid hexamer. (**a**) Views down the sixfold axis of the hexamer and from the side. The N-terminal domain (NTD) and C-terminal domain (CTD) are indicated. (**b**) Two monomers of the hexamer are shown in yellow and blue. Two interaction motifs are boxed as 'i' and 'ii'. The first (i) shows the CypA binding loop and its interaction with CypA (shown in green). The key 'catalytic' residue R55 is shown, together with the substrate proline P90 in the capsid. The second interaction interface (ii) shows binding to the cofactor CPSF6 (pink). Key binding residues N74 and N57 are shown

The CypA binding loop is one of the most prominent distinguishing features between lentiviruses like HIV and other retroviruses like the gammaretrovirus MLV. It is highly conserved in lentiviruses and only strong selection pressure results in its loss, as exemplified by SIVmac (see below). An illustration of this is that the sequences of ancient endogenised lentiviruses, such as RELIK (from rabbits) and PSIV (from lemurs), all preserve CypA binding suggesting that this interaction has been conserved for at least 10 million years [7]. Despite this, the function of CypA in HIV biology remains enigmatic, and it has been variously described as stabilising or destabilising the viral capsid during its journey through the cytosol. It has even been hypothesised to do both depending on CypA concentration [8]. Inhibition of CypA binding using cyclosporine blocks infection at the level of reverse transcription [4, 5]. However, the structural consequences of CypA binding are not clear—despite much detailed analysis by NMR, crystallography and Cryo-EM. The HIV capsid is a

substrate for CypA isomerisation and this has been measured by NMR exchange spectroscopy [9]. Whether isomerisation or binding alone is sufficient for CypA to promote infection is not clear, partly because it has not been possible to separate binding from catalysis. Arguments against isomerisation being important are that capsid structures have been solved in complex with CypA with both cis and trans forms of the target proline, P90 [10]. However, this is probably only reflective of the fact that catalysis can occur in both directions; activity may be linked to a downstream event which is preferentially triggered by one specific state. Reconstituted systems have failed to provide evidence for CypA-induced uncoating of in vitro assembled HIV-1 capsid tubes [11]. Other suggested roles for CypA in HIV infection include that it may protect the virus from host cell recognition, for example by blocking the interaction of anti-capsid restriction factors such as TRIM5 [8]. Such a hypothesis is supported by data showing that mutation of the isomerised proline, P90, causes HIV-1 M to be sensed in primary human macrophages, resulting in an interferon response that blocks infection [12]. However, care should be taken to link these two phenomenon directly; it could equally be the case that by failing to interact with CypA, HIV-1 simply fails to use its normal transport and nuclear entry pathway resulting in premature uncoating or extended persistence in the cytosol. Just as with cell line experiments, there is variation in the importance of CypA between different primary cells. Deletion of CypA from CD4+ T cells reduces but does not prevent HIV-1 replication [13]. The role of CypA in dendritic cells is even more complex, with reports that it is required for activation and infection of HIV-2 but not HIV-1—something in complete contradiction to the known binding properties of CypA [14].

One of the most widely used tools to study CypA dependence in HIV infection is the immunosuppressive drug cyclosporine. Cyclosporine A (CsA) is a naturally occurring, fungal cyclic nonribosomal peptide. It binds to CypA to generate a composite interface that binds and inhibits the calcium-dependent phosphatase calcineurin, blocking signal transduction in activated T cells [15]. Why a fungal peptide has evolved to block T cell signalling in mammalian cells is just one of many unanswered questions in the CypA story. Cyclosporine inhibits HIV infection, but if forcibly passaged in HeLa cells, then the virus acquires one of two CA mutations (A92E or G94D) and is then able to replicate as normal—however, the mutant virus is now both resistant to and dependent on CsA [16]. The defect of these CsA-acquired mutants is potentiated by arresting cell division and this has been interpreted as further evidence of the link between CypA uncoating and infection [17]. One inference being that the CsA escape mutations stabilise capsid in the absence of CypA but in its presence have difficulties uncoating. In this respect, it is noteworthy that both A92E and G94D can still bind CypA [17].

An interesting paradox in the CypA story is that whilst almost all lentiviruses preserve a CypA-binding loop not all bind CypA [1] or require it for infection. For instance, HIV-2 neither packages CypA [18], is inhibited by cyclosporine [19] or interacts with it (at least with low μM affinity) [20]. Similarly, some HIV-1 O group viruses do not require CypA for replication, although they still incorporate CypA [21]. Despite this, mutation of the conserved GP motif in both HIV-1 and HIV-2

results in a decrease in infectivity [13]. This data suggests that conservation of the CypA-loop and a CypA requirement are separable. This interpretation is further highlighted by the fact that pseudotyping HIV-1 with VSV-G rescues HIV-1 from sensitivity to CsA but does not recover the infectivity of viruses with mutations in the GP motif [22]. One explanation for this paradox is that CypA is a highly duplicated domain, copies of which have been incorporated into numerous multidomain proteins. The conservation of the GP motif and the CypA-binding loop within lentiviral capsids could be to preserve interaction with any of these related gene duplicates. An example of one such duplication is within the nuclear pore protein Nup358 or RanBP2, which is a very large protein with many domains including a CypA-like domain at its extreme N-terminus. Nup358 is one of a number of nuclear pore proteins that was identified as an HIV-1 cofactor during siRNA screens [23, 24]. Structural and biophysical characterisation of Nup358 has revealed that not only HIV-1 but also the CypA non-binding virus HIV-2 both avidly bind to the CypA-like domain of Nup358 [25]. Importantly, CsA does not inhibit Nup358 CypA. Furthermore, Nup358 Cyp is capable of isomerising the HIV capsid as well as its CypA parent. The results of these experiments highlight that the CypA-binding loop might not be conserved solely to bind CypA. For instance, it might be preserved to promote docking of the virus at the nuclear pore. If true, this has implications for viral entry models: it would require the viral capsid to be intact at least up until it reaches the nucleus.

From the host perspective, the direct binding of CypA to the HIV capsid and its conservation throughout lentiviruses make CypA an ideal targeting domain for a restriction factor. Soon after the discovery of the restriction factor TRIM5 in primates, it was found that old world owl monkeys lacked the gene. Remarkably, they instead expressed a fusion protein called TRIM5-Cyp that arose following retrotransposition of yet another CypA gene copy, this time between the introns of exons 7 and 8 in the TRIM5 locus [26]. TRIM5-Cyp potently blocks HIV infection and reverse transcription and illustrates the powerful selection pressure viruses exert on their host. A further twist to this story came 4 years later when it was discovered that new world macaque species also express a TRIM5-Cyp and that, incredibly, this gene has arisen independently from the owl monkey version. In macaque's, a copy of CypA is located after exon 8 and is spliced into the TRIM5 mRNA as a result of a skipping mutation in exon 6 [27]. Curiously, the macaque TRIM5 originally identified was incapable of restricting HIV-1 but potently blocked HIV-2 infection. This was unexpected given that HIV-2 does not bind CypA or appear to use it as a cofactor (see above). Analysis of the duplicated CypA gene in macaque TRIM5-Cyp revealed two coding mutations—D66N and R69H. Surprisingly, these two relatively conservative mutations have caused a complete remodelling of the active site loop of CypA, allowing it to bind the different CypA-loop conformation found in HIV-2. Further investigation revealed that instead of simply adopting a new static conformation, macaque TRIM-Cyp had become conformationally dynamic and was now sampling multiple alternative states [20, 28]. As well as binding and restricting HIV-2, macaque TRIM-Cyp can also restrict HIV-1 O group viruses. Macaque TRIM5-Cyp is not capable of restricting all HIV viruses however and intriguingly

has lost the ability to restrict M group viruses, the specificity encoded by its parent CypA gene.

The example of TRIM5-Cyp serves as an elegant demonstration of the Red Queen host–pathogen evolution hypothesis. A reference to Lewis Carrol's 'Alice through the looking glass', in which the Red Queen explains to Alice that it 'takes all the running. . . to keep in the same place', it postulates that host and pathogen are in a continuous evolutionary arms race neither can ultimately win. In this case, lentiviruses have evolved to exploit the host factor CypA, resulting in cofactor dependence. This dependence has in turn been exploited by the host to evolve TRIM5-Cyp proteins that restrict lentiviral infection. Evolutionary signatures that this is an ongoing arms race can be detected in the phylogenetics of macaque speciation. Following retrotransposition of ancestral CypA into the TRIM5 locus, a single mutation, R66H, occurred early in macaque evolution [29]. This mutation broadens TRIM5-Cyp specificity at the cost of potency. As macaques diverged, further mutations were acquired in certain species that re-specified TRIM5-Cyp to increase its potency against particular lentiviral stains. In rhesus macaques, where the fusion was originally discovered, a second mutation D66N improves activity to HIV-2 at the cost of HIV-1 M specificity. Meanwhile, in some species of fascicularis, a second mutation E143K has resulted in the loss of HIV-2 restriction but enhances HIV-1 M activity. This ongoing variation is likely the result of different viral strains being endemic in distinct populations. The selective pressure that may have been exerted by TRIM5-Cyp back onto lentiviruses is not clear. However, it is probable that the expression of this protein explains the curious properties of SIVmac. SIVmac was produced following force-passage in macaques and has lost the GP motif responsible for CypA binding. As a result, SIVmac does not interact with or use CypA. The reason for this adaptation is likely because it allowed the virus to escape from TRIM5-Cyp restriction in the passaged macaques.

4.3 CPSF6

Cleavage and polyadenylation splicing factor 6 (CPSF6) was first identified as a possible HIV cofactor as a result of screening HIV against a mouse cDNA expression library [30]. A truncated region of CPSF6 was found to limit HIV infection, in essence functioning as a restriction factor. CPSF6 itself is involved in pre-mRNA splicing but this is not thought to be relevant to its potential role in HIV infection. CPSF6 is normally imported into the nucleus as a result of its C-terminal RS domain, which recruits karyopherins such as Transportin SR2/TNPO3. The CPSF6 fragment identified in the original screen lacks this nuclear localisation domain, explaining its cytosolic expression, and comprises the N-terminal RNA-recognition motif and half of the proline-rich domain. The truncated CPSF6 blocks HIV infection before nuclear entry but after reverse transcription. Curiously, the equivalent human fragment of CPSF6 does block reverse transcription. This was subsequently attributed to exon6, which was missing in the original mouse fragment [31]. While the molecular

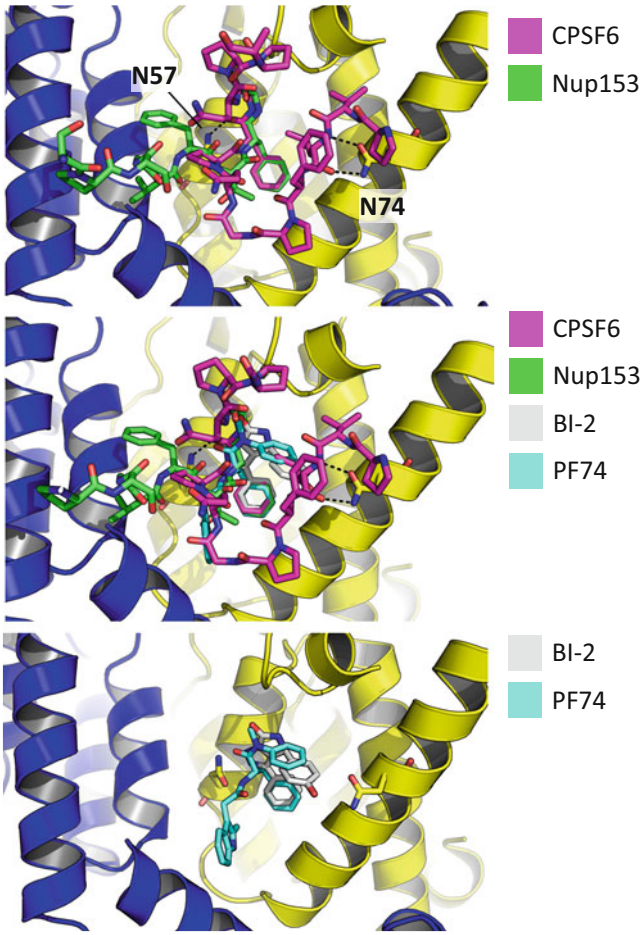

Fig. 4.2 HIV-1 capsid contains a conserved hot-spot for protein–protein interactions. Cofactors CPSF6 and Nup153 bind the same interface in capsid, located between two monomers. They share a key FG motif that anchors each cofactor epitope in exactly equivalent positions. However, the conformation of each cofactor epitope is different and each makes unique interactions with the capsid. In the case of CPSF6 this is N74. The middle panel shows both protein and pharmacological ligands (BI-2 and PF74). Note that all four ligands contain a phenyl ring that superposes exactly. The bottom panel shows only the small molecule ligands. PF74 contains a second indole moiety with which it contacts the second monomer, an interaction lacking in BI-2

basis for this difference has not been determined, the different fragments suggest that binding per se does not prevent HIV DNA synthesis but it is sufficient to block infection. Subsequent biophysical work showed that CPSF6 binds directly to the HIV-1 capsid hexamer (Figs. 4.1b and 4.2) [32]. The discovery of this binding site was in itself highly important as previously it had been thought that the HIV capsid had no protein:protein interfaces with the exception of the CypA-binding loop.

Whether CPSF6 is a cofactor at all is not entirely clear. Depletion of CPSF6 does not inhibit HIV infection in cell lines [30]. Passaging virus in the presence of truncated CPSF6 selects for a point mutation, N74D, in the capsid NTD (Fig. 4.1b). N74D is comparable to wild type in its infectivity of cell lines but in primary human macrophages, N74D cannot replicate. This loss of function is attributable to the fact that N74D induces an interferon response; if interferon receptor-blocking antibodies are added, then N74D can replicate [12]. This phenotype is similar to that of CypA mutant P90A, which also triggers an immune block to replication in macrophages. There are, however, some clues to a potential cellular function. While N74D is still infective, it drastically alters the integration pattern of HIV-1 [33]. Normally HIV-1 targets relatively gene rich regions that are actively transcribing. In contrast, N74D integrates at random, typically ending up in regions that are transcriptionally quiet. Even more intriguingly, N74D rescues HIV-1 from depletion of other cofactors—most notably TNPO3. TNPO3 was one of many hits identified in the same large siRNA screens against HIV that identified nuclear protein cofactors [23]. HIV-1 infection but not reverse transcription is inhibited upon TNP03 depletion, suggesting that the virus might hijack CPSF6 to assist in nuclear entry. Depletion of TNPO3 results in an integration site defect that mirrors that induced by N74D [34]. An attractive hypothesis therefore is that CPSF6 binds directly to the viral capsid and recruits TNPO3, facilitating nuclear import. Under this hypothesis, mutant N74D, which no longer binds CPSF6, is unaffected by TNPO3 depletion because the karyopherin can no longer be recruited anyway. In support of this hypothesis, not only is N74D unaffected by depletion of TNPO3 but mutations in TNPO3 that are selectively impaired for CPSF6 binding do not support HIV-1 infection [35]. However, a problem with the model of CPSF6 recruitment of TNPO3 is why CPSF6 depletion has no phenotype but TNPO3 depletion does. Some current models of HIV infection therefore propose that there are multiple routes of infection, at least in permissive cell lines. It is proposed that viruses that cannot bind CPSF6 (e.g. N74D) utilise an alternative entry route whereas those that bind CPSF6 are committed to a cofactor-dependent pathway. This potentially explains why TNPO3 depletion reduces infection, because it inhibits viruses committed to the pathway by CPSF6 binding.

4.4 Nup153

Nup153 was first identified as a potential HIV cofactor in the same siRNA screens that identified TNPO3 and Nup358. Depletion of Nup153 inhibits HIV-1 infection but not reverse transcription, while a modest reduction in 2-LTR circles suggests that the cofactor has a role in nuclear entry [36]. Nup153 is core component of the nuclear pore and forms a gel-like matrix that controls transport into the nucleus [37]. This matrix is formed by the C-terminus of Nup153, which contains many phenylalanine-glycine (FG) motif repeats (29 in humans) [38]. Curiously, it is an FG motif that is crucial for binding of CPSF6 to the HIV-1 capsid, with mutation of the

phenylalanine abolishing binding [32]. Biochemical experiments revealed that it is also an FG repeat in Nup153 that determines its interaction with capsid [39]. However, mutation N74D that prevents interaction with CPSF6 does not prevent binding to Nup153 [39]. Whilst this is consistent with Nup153 depletion reducing infection but N74D having wild-type infectivity, it illustrates that the two proteins must make different specific interactions.

4.5 Structural Basis for CPSF6 and Nup153 Interaction with the HIV-1 Capsid

The mystery of the shared but distinct binding of CPSF6 and Nup153 to the HIV capsid was solved when structures of the binding epitopes of each cofactor was determined in complex with capsid hexamers [40]. As can be seen in Fig. 4.2, both proteins broadly target the same region within hexamer. The CPSF6/Nup153 binding site has several noteworthy features. First, it is formed at the interface between two monomers within the hexamer. Interaction principally involves residues in the NTD of one monomer and residues in the CTD of the adjacent monomer. The significance of this is that the binding site is lost when the capsid dissociates. This can be seen in binding experiments; CPSF6 binds more tightly to capsid hexamer than to monomer, while Nup153 loses binding entirely upon hexamer dissociation [40]. The implication of this is that the capsid must be to some extent intact if these cofactors are to bind and be used by HIV. Given that Nup153 is located at the nuclear pore, it is strongly suggestive that capsid uncoating does not take place prior to pore docking. This in turn argues against an early uncoating model of HIV infection. A second important feature that the structures reveal is the importance of the shared FG repeat between CPSF6 and Nup153. The phenylalanine residues of each cofactor superpose almost exactly and positions the main-chain to hydrogen bond with capsid residue N57 (Fig. 4.2). The importance of this interaction for cofactor binding helps explain the phenotype of capsid mutant N57A, which reduces HIV infection by inhibiting nuclear entry [39]. Tellingly, the infectivity defect of N57A is increased during cell cycle arrest. In a nondividing cell the nuclear envelope is intact, meaning that access to the host genome can only be achieved by passing through the pore. In contrast, in a dividing cell, viruses can potentially infect simply when the envelope is dissolved during prophase. The fact that N57A prevents HIV capsid binding to Nup153 and is concomitantly cell cycle dependent is further evidence that Nup153 is involved in nuclear entry. A third important finding made when comparing the Nup153 and CPSF6 structures was that while they share a core binding motif, they also make key specific interactions. In CPSF6 this involves hydrogen binding to capsid residue N74. The fact that this interaction is absent in Nup153 explains why N74D prevents CPSF6 binding and not Nup153 and why the mutation does not reduce infectivity in cell lines. In contrast, Nup153 makes much more extensive

interactions with the CTD of the second monomer than does CPSF6. This in turn explains why Nup153 is more sensitive to the assembly state of the capsid hexamer.

4.6 HIV-1 Capsid Is an Important Drug Target

Discovery of the CPSF6/Nup153 binding site also solved a further mystery, involving the action of anti-capsid drugs that had been developed against HIV. Pfizer and Boehringer-Ingelheim had independently identified small molecule inhibitors of HIV infection but their mechanism of action had remained obscure [41, 42]. As it turned out, both drugs, PF74 and BI-2, targeted the CPSF6/Nup153 binding site [40]. Remarkably, the shared phenyl ring in PF74 and BI-2 superposes exactly with the phenylalanine in the FG repeat in the two cofactors (Fig. 4.2). This finding revealed that one reason why the drugs inhibit infection is because they are competitive inhibitors of these HIV cofactors. Comparison of all four complexed structures—the two cofactors and two pharmacological ligands—also explained the puzzle of why PF74 was significantly more potent than BI-2 despite their reported affinities to capsid NTD being almost identical. The BI-2 drug makes contacts only within the NTD half of the binding site, whereas PF74 also makes contact with the CTD half (Fig. 4.2; bottom panel). Comparing interaction with monomer and hexamer has confirmed that the additional contacts PF74 makes across the hexamer interface allow it to bind capsid much more strongly than BI-2 [40]. A further important finding of this study was to explain the biphasic inhibition profile of PF74. At low doses where the occupancy of PF74 to the HIV capsid is sub-stoichiometric, infection but not reverse transcription is blocked consistently with the importance of the CPSF6/Nup153 interface in nuclear entry. Mutations such as N74D that prevent CPSF6 binding and render HIV insensitive to Nup153 depletion are resistant to this low dose PF74 inhibition. Importantly, N74D is still capable of binding PF74, confirming that the drug must act as a competitive inhibitor at this dose rather than exerting a direct effect on the capsid. Moreover, a low dose of PF74 loses inhibition in cells depleted of Nup153 [39]. Curiously, just after the low dose inhibition titration profile has plateaued, a second inhibition curve begins that corresponds to drug concentrations approaching complete saturation of all binding sites in the HIV capsid. Notably, this second inhibitory effect occurs concomitantly with a reduction in measured reverse transcription products. Furthermore, it cannot be rescued by N74D mutation or depletion of either Nup153 or TNPO3 [39, 43]. These findings suggest that at sub-stoichiometric occupancy PF74 inhibits by preventing cofactor interaction, but that at stoichiometric concentrations it has a direct effect on the capsid that occurs early enough to inhibit DNA synthesis. The likelihood is that the high dose of PF74 causes catastrophic capsid uncoating. This model is supported by the fact that while low dose inhibition is reversible, i.e. the drug can be washed out of cells and infection restored, high dose inhibition is irreversible and infection remains blocked even when PF74 is removed [40].

4.7 HIV Capsids Are Semi-Permeable with an Electrostatic Pore

The most recent revelation concerning the HIV capsid has been the discovery that at the centre of every capsid hexamer is a dynamic electrostatic pore [44]. By capturing the hexamer in different conformational states it was revealed that the β-hairpin at the N-terminus is dynamic and can populate at least two states. These two states termed 'open' and 'closed' alternately reveal and hide a pore at the centre of each hexamer (Fig. 4.3a). The interactions determining these states are located at the base of the hairpin and involve a hydrogen bond network mediated by H12 and residues P1, T48, Q50 and D51. Switching between a direct and water-mediated interaction results in a hinge-like motion of the β-hairpin. In the context of the hexamer this causes an iris-like opening of a pore. Remarkably, this pore controls access to a hidden chamber at the centre of the hexamer that culminates in a ring of arginine residues provided by R18 (Fig. 4.3a). This strongly negatively charged ring allows binding of dNTPs to the capsid with high affinity. Sequential mutation of R18 to glycine results in a decline in dNTP affinity [44]. In the context of viral infection, the same mutation gives a concomitant decrease in infectivity and reverse transcription [44].

These findings provide a potential explanation to an otherwise tricky problem in viral uncoating. While encapsidated, HIV can protect its genome from nucleases or sensors that would trigger an antiviral state. However, the virus must also copy its RNA genome into DNA prior to integration in the nucleus. While reverse

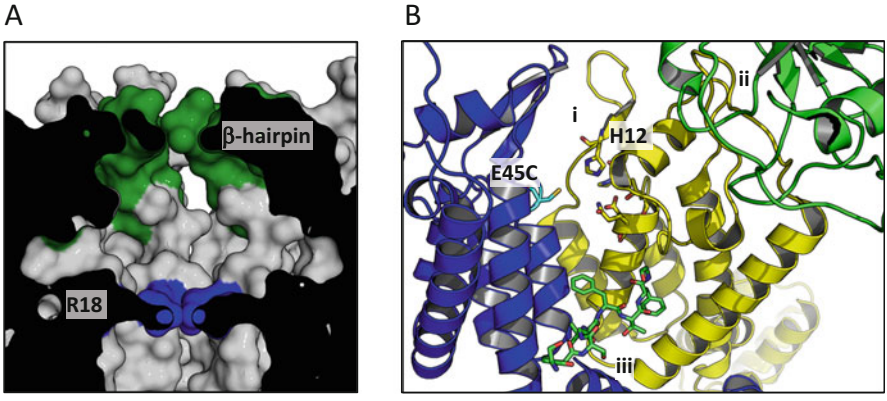

Fig. 4.3 HIV-1 has an electrostatic pore located near both the CypA-binding loop and CPSF6/Nup153 binding site. (**a**) A cut-away view of a surface representation of the core of the hexamer. HIV-1 capsid hexamers are hollow, with a large chamber that can be accessed only when the β-hairpin (green) adopts an 'open' conformation. At the bottom of the chamber is a ring of arginine residues (R18; shown in blue). (**b**) Two adjacent capsid monomers are shown in yellow and blue, with CypA in green. The locations of three functional sites in the capsid are labelled to indicate their proximity: (i) the β-hairpin, (ii) the CypA-binding loop and (iii) the CPSF6/Nup153 binding site

transcription inside the capsid is physically possible, at least initially, the fuel needed for DNA synthesis, namely dNTPs, is located outside. The existence of a highly electropositive channel at the centre of each hexamer potentially provides hundreds of portals through which to recruit nucleotides. The physicochemical properties of these pores ensure that large molecules such as proteins are excluded while the positive charge is ideal for the recruitment of highly negatively charged ligands. The binding kinetics of dNTPs to the capsid are also ideal for a recruitment mechanism. The on-rate is extremely fast (indeed is diffusion limited), but the off-rate is also quick ensuring that recruited dNTPs are rapidly released to allow movement into the capsid interior [44]. This mechanism would not provide directionality but the consumption of dNTPs by reverse transcriptase inside the capsid would ensure a favourable concentration gradient for entry of dNTPs attracted to the pore.

Nucleotide triphosphates are not the only polyanion in the cell nor the most abundant. One of the most highly negatively charged cellular polyanions, which is also present at high concentration, is the inositol phosphate IP6. Indeed, IP6 also binds to the R18 pore and its addition to intact HIV capsids in vitro greatly potentiates the accumulation of encapsidated viral DNA synthesised during reverse transcription [45]. This effect is likely due to IP6 stabilisation of the capsid. IP6 coordinates all six arginines in the pore simultaneously, increasing hexamer thermostability by ~10 °C. Remarkably, single molecule measurements of individual HIV virions demonstrate that IP6 increases the half-life of capsid uncoating from ~7 min to >10 h [45]. The dramatic effect of IP6 on HIV capsid uncoating suggests it may play an analogous role to pocket factors in picornavirus capsid biology. Picornavirus pocket factors impart a property of metastability; they greatly stabilise the capsid until environmental cues trigger their release, at which point uncoating can occur. IP6 may be an HIV pocket factor that functions in a similar manner. In this respect, an important finding is that HIV selectively packages IP6 when it buds from the cell, and in sufficient numbers for at least one IP6 molecule for every mature hexamer in the capsid [45]. However, as the mature hexamer only forms after budding it cannot be the R18 pore that is responsible for IP6 recruitment during budding. Intriguingly, the immature hexamers that comprise the immature lattice formed during budding contain two lysine rings (K158 and K227) that are structurally reminiscent of the R18 ring. Furthermore, these lysine rings can bind IP6 in a similar manner [46]. It is likely that IP6 is recruited by these lysine rings during HIV budding, where it assists in the assembly of the immature lattice. This would explain previous data that IP6 added in vitro catalyses lattice assembly [47]. Capsid maturation is triggered by proteolytic cleavage and one of the protease sites is within the six helix bundle where K227 is located. Cleavage may cause disassembly of the immature lattice concomitantly with IP6 release. Released IP6 would then be available to catalyse assembly of the mature lattice via stabilisation and coordination of the R18 pore. Moreover, the resulting viral capsid would be pre-bound and pre-stabilised by IP6, ready for its journey through the cytosol.

4.8 Conclusion

This review has attempted to highlight the considerable progress that has been made in our understanding of the HIV capsid. Once thought to be important primarily as a delivery capsule that is discarded soon after cell entry, it has become increasingly clear that the capsid is in fact the critical viral protein for determining productive infection. We now know that the capsid has at least three functional interfaces—the CypA binding site, the CPSF6/Nup153 interface and the R18 pore (Fig. 4.3b). These features can themselves be further subdivided, for instance considering the R18 pore as distinct from the β-hairpin that controls access to the R18 ring and chamber within the hexamer. The next phase of capsid research will undoubtedly address the relationships that exist between these different features. While there is little existing structural evidence for allostery between the various interfaces, they are located in clear proximity to each other (Fig. 4.3b). It would therefore be astonishing if structural allostery did not exist. Moreover, the existence of distinct motifs within the capsid allow for complex mechanisms that could exert precise spatiotemporal control over where and when the capsid uncoats. For instance, cofactor binding to the CypA-binding loop or CPSF6/Nup153 interface could influence whether the nearby β-hairpin is open or closed and therefore whether IP6 is released or dNTPs recruited. While such hypotheses remain to be tested there is already tantalising functional and phenotypic data to indicate that the three sites influence each other. For instance, there is clearly functional allostery between the CypA-binding loop and the CPSF6/Nup153 interface. This is highlighted by the fact that mutations G89V and P90A rescue low dose PF74 inhibition in the same way as N74D and Nup153 depletion [48]. Curiously, while CsA also rescues this is far less effective than the mutations—yet further evidence that conservation of the CypA-loop may not be solely to do with CypA itself. Indeed, the CypA-loop appears to be the most upstream determinant of the HIV nuclear import pathway as G89V and P90A mutations rescue from most post-entry perturbations, including TNPO3 and Nup153 depletion [33]. Relationships between the R18 pore and the other interfaces are less clear. However, E45A, a mutation that escapes PF74 inhibition, is noteworthy in its proximity to H12 and the pivotal hydrogen bond network made around this side chain to determine whether the β-hairpin is open or closed (Fig. 4.3b). Unravelling the precise allosteric mechanisms and interdependencies between the various capsid interfaces may hold the key to many of the remaining fundamental questions in HIV-1 biology, including the contentious issue of uncoating and precisely where, when and how this occurs.

References

1. Luban J, Bossolt KL et al (1993) Human immunodeficiency virus type 1 Gag protein binds to cyclophilins A and B. Cell 73(6):1067–1078
2. Lang K, Schmid FX et al (1987) Catalysis of protein folding by prolyl isomerase. Nature 329 (6136):268–270

3. Dolinski K, Muir S et al (1997) All cyclophilins and FK506 binding proteins are, individually and collectively, dispensable for viability in *Saccharomyces cerevisiae*. Proc Natl Acad Sci USA 94(24):13093–13098
4. Braaten D, Franke EK et al (1996a) Cyclophilin A is required for an early step in the life cycle of human immunodeficiency virus type 1 before the initiation of reverse transcription. J Virol 70 (6):3551–3560
5. Braaten D, Franke EK et al (1996b) Cyclophilin A is required for the replication of group M human immunodeficiency virus type 1 (HIV-1) and simian immunodeficiency virus SIV(CPZ) GAB but not group O HIV-1 or other primate immunodeficiency viruses. J Virol 70 (7):4220–4227
6. Sokolskaja E, Sayah DM et al (2004) Target cell cyclophilin A modulates human immunodeficiency virus type 1 infectivity. J Virol 78(23):12800–12808
7. Goldstone DC, Yap MW et al (2010) Structural and functional analysis of prehistoric lentiviruses uncovers an ancient molecular interface. Cell Host Microbe 8(3):248–259
8. Li Y, Kar AK et al (2009) Target cell type-dependent modulation of human immunodeficiency virus type 1 capsid disassembly by cyclophilin A. J Virol 83(21):10951–10962
9. Bosco DA, Eisenmesser EZ et al (2002) Catalysis of cis/trans isomerization in native HIV-1 capsid by human cyclophilin A. Proc Natl Acad Sci USA 99(8):5247–5252
10. Lammers M, Neumann H et al (2010) Acetylation regulates Cyclophilin A catalysis, immunosuppression and HIV isomerization. Nat Chem Biol 6:331–337
11. Grattinger M, Hohenberg H et al (1999) In vitro assembly properties of wild-type and cyclophilin-binding defective human immunodeficiency virus capsid proteins in the presence and absence of cyclophilin A. Virology 257(1):247–260
12. Rasaiyaah J, Tan CP et al (2013) HIV-1 evades innate immune recognition through specific cofactor recruitment. Nature 503(7476):402–405
13. Braaten D, Luban J (2001) Cyclophilin A regulates HIV-1 infectivity, as demonstrated by gene targeting in human T cells. EMBO J 20(6):1300–1309
14. Manel N, Hogstad B et al (2010) A cryptic sensor for HIV-1 activates antiviral innate immunity in dendritic cells. Nature 467(7312):214–217
15. Schreiber SL, Crabtree GR (1992) The mechanism of action of cyclosporin A and FK506. Immunol Today 13(4):136–142
16. Aberham C, Weber S et al (1996) Spontaneous mutations in the human immunodeficiency virus type 1 gag gene that affect viral replication in the presence of cyclosporins. J Virol 70 (6):3536–3544
17. Ylinen LM, Schaller T et al (2009) Cyclophilin A levels dictate infection efficiency of human immunodeficiency virus type 1 capsid escape mutants A92E and G94D. J Virol 83 (4):2044–2047
18. Franke EK, Yuan HE et al (1994) Specific incorporation of cyclophilin A into HIV-1 virions. Nature 372(6504):359–362
19. Billich A, Hammerschmid F et al (1995) Mode of action of SDZ NIM 811, a nonimmunosuppressive cyclosporin A analog with activity against human immunodeficiency virus (HIV) type 1: interference with HIV protein-cyclophilin A interactions. J Virol 69 (4):2451–2461
20. Price AJ, Marzetta F et al (2009) Active site remodeling switches HIV specificity of antiretroviral TRIMCyp. Nat Struct Mol Biol 16(10):1036–1042
21. Wiegers K, Krausslich HG (2002) Differential dependence of the infectivity of HIV-1 group O isolates on the cellular protein cyclophilin A. Virology 294(2):289–295
22. Aiken C (1997) Pseudotyping human immunodeficiency virus type 1 (HIV-1) by the glycoprotein of vesicular stomatitis virus targets HIV-1 entry to an endocytic pathway and suppresses both the requirement for Nef and the sensitivity to cyclosporin A. J Virol 71(8):5871–5877
23. Brass AL, Dykxhoorn DM et al (2008) Identification of host proteins required for HIV infection through a functional genomic screen. Science 319(5865):921–926
24. Konig R, Zhou Y et al (2008) Global analysis of host-pathogen interactions that regulate early-stage HIV-1 replication. Cell 135(1):49–60

25. Bichel K, Price AJ et al (2013) HIV-1 capsid undergoes coupled binding and isomerization by the nuclear pore protein NUP358. Retrovirology 10(1):81
26. Sayah DM, Sokolskaja E et al (2004) Cyclophilin A retrotransposition into TRIM5 explains owl monkey resistance to HIV-1. Nature 430(6999):569–573
27. Wilson SJ, Webb BL et al (2008) Independent evolution of an antiviral TRIMCyp in rhesus macaques. Proc Natl Acad Sci USA 105(9):3557–3562
28. Caines ME, Bichel K et al (2012) Diverse HIV viruses are targeted by a conformationally dynamic antiviral. Nat Struct Mol Biol 19(4):411–416
29. Ylinen LM, Price AJ et al (2010) Conformational adaptation of Asian macaque TRIMCyp directs lineage specific antiviral activity. PLoS Pathog 6(8):e1001062
30. Lee K, Ambrose Z et al (2010) Flexible use of nuclear import pathways by HIV-1. Cell Host Microbe 7(3):221–233
31. Hori T, Takeuchi H et al (2013) A carboxy-terminally truncated human CPSF6 lacking residues encoded by exon 6 inhibits HIV-1 cDNA synthesis and promotes capsid disassembly. J Virol 87 (13):7726–7736
32. Price AJ, Fletcher AJ et al (2012) CPSF6 defines a conserved capsid interface that modulates HIV-1 replication. PLoS Pathog 8(8):e1002896
33. Schaller T, Ocwieja KE et al (2011) HIV-1 capsid-cyclophilin interactions determine nuclear import pathway, integration targeting and replication efficiency. PLoS Pathog 7(12):e1002439
34. Ocwieja KE, Brady TL et al (2011) HIV integration targeting: a pathway involving transportin-3 and the nuclear pore protein RanBP2. PLoS Pathog 7(3):e1001313
35. Maertens GN, Cook NJ et al (2014) Structural basis for nuclear import of splicing factors by human Transportin 3. Proc Natl Acad Sci USA 111(7):2728–2733
36. Matreyek KA, Engelman A (2011) The requirement for nucleoporin NUP153 during human immunodeficiency virus type 1 infection is determined by the viral capsid. J Virol 85 (15):7818–7827
37. Cardarelli F, Lanzano L et al (2012) Capturing directed molecular motion in the nuclear pore complex of live cells. Proc Natl Acad Sci USA 109(25):9863–9868
38. Bastos R, Lin A et al (1996) Targeting and function in mRNA export of nuclear pore complex protein Nup153. J Cell Biol 134(5):1141–1156
39. Matreyek KA, Yucel SS et al (2013) Nucleoporin NUP153 phenylalanine-glycine motifs engage a common binding pocket within the HIV-1 capsid protein to mediate lentiviral infectivity. PLoS Pathog 9(10):e1003693
40. Price AJ, Jacques DA et al (2014) Host cofactors and pharmacologic ligands share an essential interface in HIV-1 capsid that is lost upon disassembly. PLoS Pathog 10(10):e1004459
41. Blair WS, Pickford C et al (2010) HIV capsid is a tractable target for small molecule therapeutic intervention. PLoS Pathog 6(12):e1001220
42. Lamorte L, Titolo S et al (2013) Discovery of novel small-molecule HIV-1 replication inhibitors that stabilize capsid complexes. Antimicrob Agents Chemother 57(10):4622–4631
43. Shah VB, Shi J et al (2013) The host proteins transportin SR2/TNPO3 and cyclophilin A exert opposing effects on HIV-1 uncoating. J Virol 87(1):422–432
44. Jacques DA, McEwan WA et al (2016) HIV-1 uses dynamic capsid pores to import nucleotides and fuel encapsidated DNA synthesis. Nature 536(7616):349–353
45. Mallery DL, Márquez CL et al (2018) IP6 is an HIV pocket factor that prevents capsid collapse and promotes DNA synthesis. eLife. pii: e35335. https://doi.org/10.7554/eLife.35335
46. Dick RA, Zadrozny KK, Xu C, Schur FKM, Lyddon TD, Ricana CL, Wagner JM, Perilla JR, Ganser-Pornillos BK, Johnson MC, Pornillos O, Vogt VM (2018) Inositol phosphates are assembly co-factors for HIV-1. Nature. https://doi.org/10.1038/s41586-018-0396-4. [Epub ahead of print]
47. Campbell S, Fisher RJ et al (2001) Modulation of HIV-like particle assembly in vitro by inositol phosphates. Proc Natl Acad Sci USA 98(19):10875–10879
48. Saito A, Ferhadian D et al (2016) Roles of capsid-interacting host factors in multimodal inhibition of HIV-1 by PF74. J Virol 90(12):5808–5823

Chapter 5
Membrane-Containing Icosahedral Bacteriophage PRD1: The Dawn of Viral Lineages

Hanna M. Oksanen and Nicola G. A. Abrescia

Abstract Membrane-containing enterobacterial phage PRD1 was isolated from sewage more than 40 years ago. At that time none would have expected the impact that unravelling its biology would have on modern virology and on the way we understand virus assembly, evolution and classification today. PRD1 structural analyses have provided a framework for understanding some aspects of virus evolution—introducing the concept of "viral lineages"—where the three-dimensional structures of virus capsids represent the fingerprint for evolutionary relationship which cannot be traced from the sequence data. In this review we summarise those findings that have led to the notion of viral lineages and the multidisciplinary efforts made in elucidating PRD1 life cycle. These studies have rendered PRD1 a model system not only for the family *Tectiviridae* to which it belongs, but more generally to complex DNA viruses enclosing a membrane vesicle beneath the capsid shell.

Keywords Viral lineage · PRD1 · Adenovirus · 3D structure · Bacteriophage · *Tectiviridae* · Assembly · Packaging · DNA ejection · Uncoating

H. M. Oksanen (✉)
Faculty of Biological and Environmental Sciences, Molecular and Integrative Biosciences Research Programme, University of Helsinki, Helsinki, Finland
e-mail: hanna.oksanen@helsinki.fi

N. G. A. Abrescia (✉)
Molecular Recognition and Host-Pathogen Interactions Programme, CIC bioGUNE, CIBERehd, Derio, Spain

IKERBASQUE, Basque Foundation for Science, Bilbao, Spain
e-mail: nabrescia@cicbiogune.es

U. F. Greber (ed.), *Physical Virology*, Advances in Experimental Medicine and Biology 1140, https://doi.org/10.1007/978-3-030-14741-9_5

5.1 Introduction

The first identification of a bacteriophage that contains lipids was made by Espejo and Canelo 50 years ago [1]. They were inspired by a previous work by Spencer [2], which reported that two bacteriophages active against marine pseudomonads were inactivated by organic solvents. Espejo and Canelo motivated by this work isolated several strains of marine pseudomonads from the Pacific Ocean off the coast of Chile (Viña del Mar; Fig. 5.1a). A bacteriophage that grew on one of the strains was found in the same water and was named PM2. PM2 resulted to be sensitive to ether, chloroform and 0.05% Sarkosyl. Chemical analysis demonstrated that virions possessed DNA containing phosphorus, as well as another phosphorus-containing component that could be extracted with chloroform–methanol [1]. This material proved to be phospholipid based on thin-layer chromatography.

Fifty years after its discovery, bacteriophage PM2, which infects marine gram-negative *Pseudoalteromonas* strains, is still the only member of the family *Corticoviridae*, although sequences related to PM2 are widespread in the genomes of aquatic proteobacteria [6]. Very recently phage Cr39582 was induced from *Pseudoalteromonas* sp. isolated from the gut of marine invertebrate *Ciona robusta* [7]. Cr39582 shows significant sequence similarity and gene synteny to PM2 proposing that Cr39582 could be the second member of the family *Corticoviridae* [7]. PM2 is a virulent phage with a supercoiled circular double-stranded (ds) DNA genome of ~10 kb that is enclosed by the internal membrane vesicle located underneath the icosahedral protein coat [4, 8] (Fig. 5.1a, inset).

Discovery of the marine bacteriophage PM2 opened up a new research field and more membrane-containing phages were isolated in the early 1970s. One such phage was PRD1, isolated from Kalamazoo (Michigan, USA) sewage, which is the representative member of the family *Tectiviridae* [9–11]. The current understanding of PRD1 is shown schematically in Fig. 5.1b. It infects gram-negative bacteria such as *Salmonella enterica*, *Pseudomonas aeruginosa* and *Escherichia coli* that contain a conjugative plasmid belonging to the incompatibility (Inc) group IncP, IncN or IncW. The plasmid is essential for the phage as it codes for the receptor [9]. Tectiviruses have a tail-less, icosahedrally symmetric capsid approximately 65 nm in diameter, surrounding a protein enriched membrane vesicle which in turn encapsulates the linear, dsDNA genome of approximately 15 kb [10]. Viruses of this morphology also infect gram-positive bacteria, e.g. among the *Bacillus cereus* group, and this group of tectiviruses is genetically more diverse than the tectiviruses of gram-negative hosts [12]. Recently, tectiviruses were split into two genera *Alphatectivirus* and *Betatectivirus* where virulent PRD1-like tectiviruses belong to the genus *Alphatectivirus*.

Two primary features of PRD1 draw considerable interest for elevating it as a model system. Firstly, the PRD1 genome is replicated by a protein-primed, sliding-back mechanism [13]. The inverted terminal repeats on the genome and a covalently bound terminal protein at the 5′ ends play a significant role in the replication of the linear dsDNA molecule [14, 15]. Secondly, the presence of the lipidic vesicle beneath the proteinaceous capsid that allows studying the function and structure of the membrane during the virus life cycle [5, 11, 16–19]. The well-defined genetic

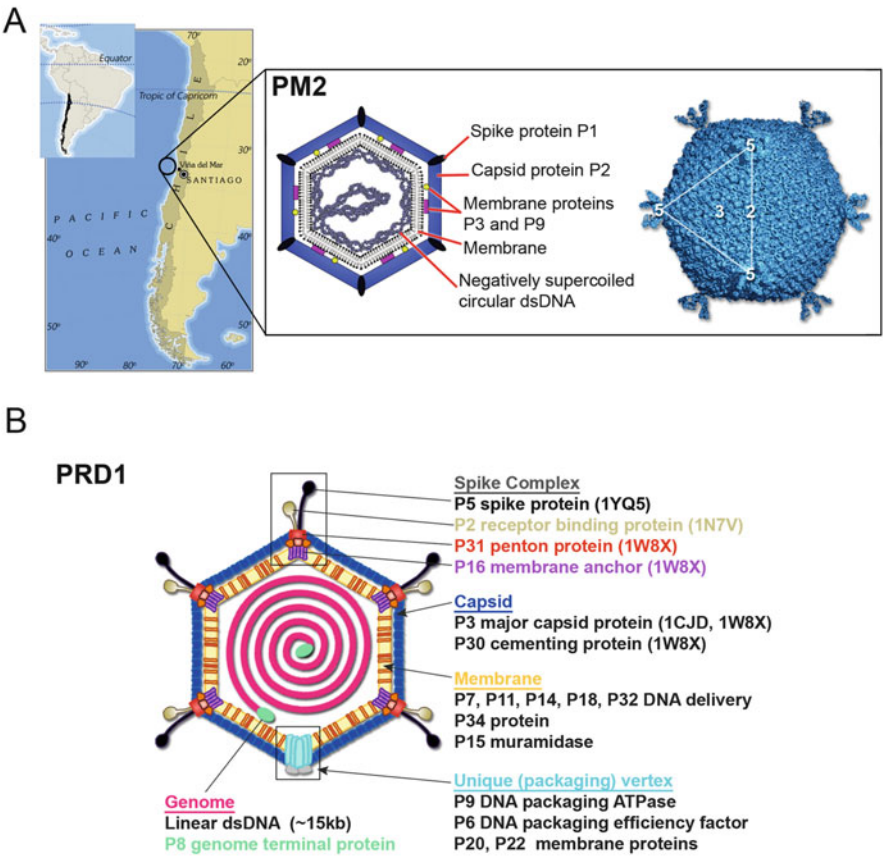

Fig. 5.1 First membrane-containing viruses studied. (**a**) Location where the first membrane-containing bacteriophage PM2 was identified and that paved the way to further studies on this type of viruses (Map: J. Oksanen). Inset: left, schematic representation of PM2 with its architectural components [3]; right, PM2 electron density map (blue) displayed at 1σ determined by X-ray crystallography at 7 Å resolution [4]. The white triangle marks a virus facet, and the numbers define the icosahedral symmetry axes. (**b**) Schematic representation of membrane-containing bacteriophage PRD1 (numbers in parentheses identify the corresponding protein structures in the Protein Data Bank) adapted from Peralta et al. [5]; reproduced under the terms of Creative Commons Attribution

background, where PRD1 grows, e.g. *E. coli* and *S. enterica*, together with a wide range of tools and the library of PRD1 mutants with optimised virus production and purification protocols [20–23] have also contributed to make PRD1 one of the most used membrane-containing virus models. In addition, the extensively studied assembly of PRD1, utilising pre-formed procapsids, provides a framework for genome packaging and assembly of other large, complex icosahedral viruses with an internal membrane [5, 11, 16, 17, 24, 25] (Fig. 5.1b).

A significant step was taken in 1999, when the PRD1 major capsid protein (MCP) structure was determined and soon after that the shared conservation in the capsid structures between the phage PRD1 and human pathogenic adenovirus was recognised [26] (Fig. 5.2a). It was later realised that the MCP fold of PRD1

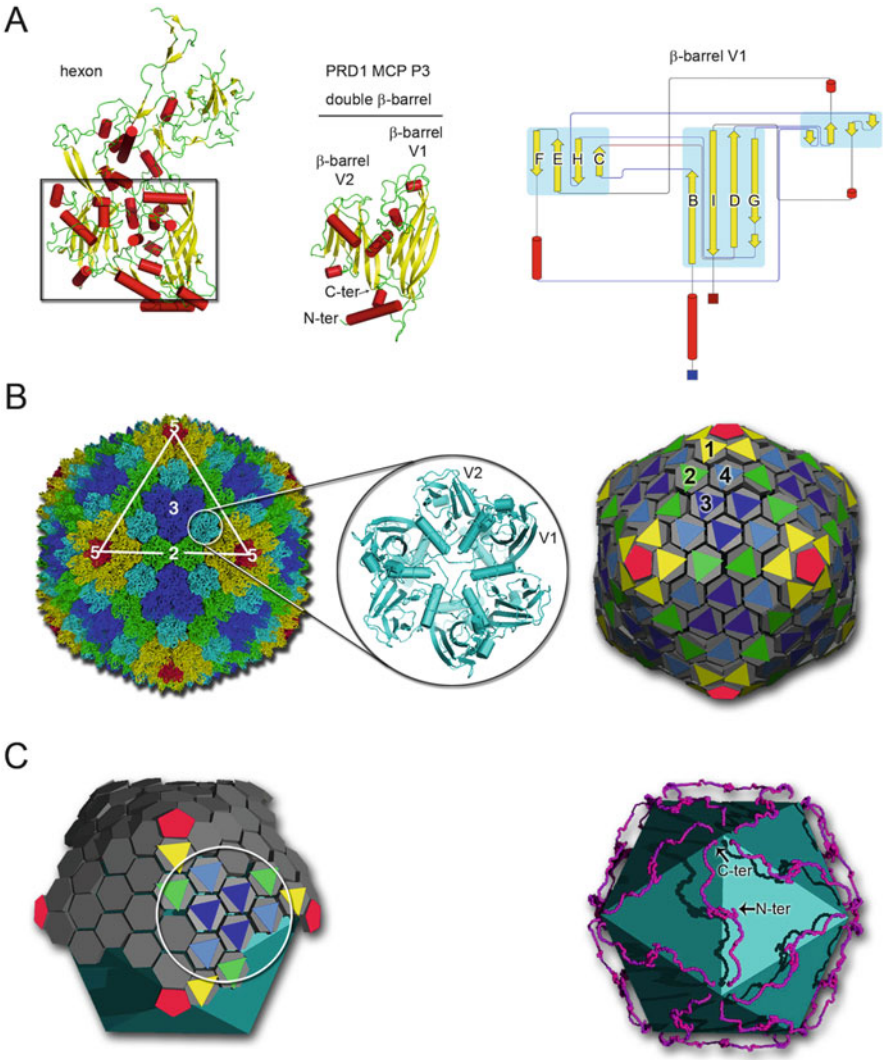

Fig. 5.2 PRD1 structure and assembly. (**a**) Side-by-side comparison of the MCP hexon in adenovirus (PDB ID 1P2Z) (left) with the MCP P3 in PRD1 (PDB ID 1CJD) (right) displayed in cartoon with α-helices represented as red cylinders and the conserved core double β-barrel as strands in yellow; the black rectangle on the hexon marks the double β-barrel. V1 (residues 15–245) and V2 (residues 246–383) define the individual β-barrel in P3; at the far right, the topological drawing of the V1 barrel (strands labelled as BIDG/CHEF) with the dark-blue and red squares being respectively the N-terminus and C-terminus of V1 (http://munk.csse.unimelb.edu.au/pro-origami/). (**b**) Left PRD1 atomic model as derived by crystallographic studies and showing the capsid organisation represented with each of the four P3 MCPs trimers composing the icosahedral asymmetric unit (IAU) in ribbon and coloured in green, cyan, blue and yellow; in red is the vertex penton protein P31 and the white triangle indicates a virus facet with numbers 2, 3 and 5 labelling the icosahedral symmetry axes (PDB ID 1W8X) [10]; adapted from Peralta et al. [5]. The inset shows the "cyan" P3 trimer as cartoon forming the capsomers viewed along the pseudo threefold axis. Right, geometric representation of PRD1 derived from the coordinates of the atomic model

resembles that found in MCPs of certain other viruses infecting eukaryotes and archaea, possibly signifying descent from a common ancestor. Together with earlier observations, the structure-based virus phylogeny found on the conservation of the MCP folds was formulated and nowadays can be applied to a number of viruses irrespective of the virus family they represent [26–32].

Here, we summarise those findings on PRD1 that have led to the concept of viral lineages and the most recent results that allow a deeper understanding of PRD1 life cycle.

5.2 Assembly of PRD1 and the Tape Measure P30

Over the years the optimised protocols in production and purification of PRD1, and derived particles (e.g. mutant particles or subviral complexes) together with the advances in cryo-electron microscopy (cryo-EM), crystallization and X-ray diffraction techniques made possible its structural investigation. In 1995, the first three-dimensional (3D) visualisation of the whole PRD1 particle was obtained by cryo-EM at 28 Å resolution [33]. This structure illustrated the position of the MCPs P3 and hinted at the importance of the interactions between the membrane vesicle and the capsid layer. Importantly, it was only after the crystal structure of P3 at 1.85 Å was resolved some years later in 1999 that the comparison was done with the crystal structure of adenovirus type 2 hexon [26, 34]; the unexpected finding that both MCP possessed a similar fold prompted further cryo-EM analyses. A quasi-atomic model of PRD1 was achieved by fitting the P3 crystal structure into improved cryo-EM maps of PRD1 which lead to new information about the contacts across the MCPs building the virus facet and the membrane vesicle underneath [26, 35]. In 2002 the PRD1 architecture was analysed using difference imaging between several cryo-EM reconstructions (at ~13 Å resolution) and their quasi-atomic models [36]. Integration of functional studies with analysis of the viral mutant particles and difference maps identified not only small proteins at the capsid edges and how the peripentonal P3 MCPs connect to the vertex complex, but also the contacts across the capsid and linking it to the membrane.

Fig. 5.2 (continued) with solid hexagons (grey) to represent the pseudo-hexameric geometry adopted by the capsomers—the building blocks of the protein shell—which in turn are P3 trimers whose oligomerisation is represented by flat triangles coloured as (**b**); numbers 1–4 label the four independent capsomers of the IAU. (**c**) Left, as (**b**) right, but rotated 90° clockwise along the icosahedral 2-fold axis with the bottom half of the capsomers removed showing the membrane underneath as light-cyan icosahedron and with a white circle defining the group-of-nine (GON) capsomers composing the planar virus facet as in adenovirus. Right, all capsomers have been removed so the tape measure P30 protein (83 residues) is visible (magenta); P30 stretches linearly from the N-terminus located at the icosahedral twofold to the C-terminus located at the icosahedral fivefold and it dimerises at twofold, so two P30 molecules cement the edge of a triangular virus facet

Despite the advances in the understanding of the PRD1 structure it was not until its X-ray structure was determined at 4.2 Å resolution that the full network of protein interactions and the principles governing the PRD1 assembly became clear [11, 16]. PRD1 was the first—and it remains still today the only—virus with an internal membrane to have been studied by X-ray crystallography and solved at high resolution. The crystal structure of PRD1 revealed the molecular contacts that hold together the 720 copies of the MCP P3 on the membrane vesicle and the membrane structure with its interactions with viral proteins and the dsDNA (Fig. 5.2b). Four P3 trimers (capsomers) compose the viral icosahedral asymmetric unit (Nos 1–4 in Fig. 5.2b). Capsomers 2–4 arrange in the so-called group of nine (GON), as originally defined for the hexons in adenovirus and studied by negative stain EM, laying out the virus central facet with a strikingly similar architecture to adenovirus (both viruses possess the same triangulation number, pseudo $T = 25$) (Fig. 5.2b and c, left) [11, 37].

PRD1 scaffolding protein P30, stretching linearly, cements the edges of the icosahedron through interactions with the C termini of P3 subunits and sizes the virion (Fig. 5.2c, right). Eleven of twelve vertices are capped by peripentonal P3 trimers and by spike complexes composed of vertex-stabilising membrane protein P16, penton protein P31, spike protein P5 and receptor-binding protein P2 [38–40] (Figs. 5.1b and 5.2b, left and centre). The internal membrane enclosing the densely packaged dsDNA—up to four spooled layers are visible—is composed of phosphatidylethanolamine (PE) and phosphatidylglycerol (PG) lipids and membrane proteins at roughly equal mass [16]. The two lipid species are asymmetrically distributed across the membrane bilayer, with PG enriching the outer leaflet while the PE the inner leaflet [16]. At long last, recent studies (see Sect. 5.4) have structurally identified and elucidated the unique vertex, which is the 12th vertex where the membrane-embedded portal is used for DNA packaging into the procapsid [17, 41, 42]. This unique vertex also serves as a conduit for the DNA ejection through the proteo-lipidic tube formed from the internal protein enriched membrane vesicle [5]. In summary, the elucidation of the principles governing the assembly of PRD1 scalable to other viruses opened the door to a new conceptual framework for virus taxonomy that has allowed to establish viral evolutionary relationships otherwise undetectable.

5.3 The Dawn of Viral Lineages

Sequence homology is easily lost when comparing viral sequences, even across viruses that belong to the same family. The earliest structural analyses of viruses, however, showed that the capsid protein fold and the arrangement of protein subunits can be preserved between viruses that belong to different families and infect divergent hosts. Some of the first plant and animal virus structures (family *Picornaviridae*) revealed prominent similarities in their MCP folds which were assumed as probably demonstrating a descent from a common ancestor regardless of any noticeable sequence similarity [28–30]. These MCPs displayed single

horizontal β-barrels and arranged with the long axis of the β-barrel tangentially to the virus surface. At the time, the paucity of available virus structures hindered the understanding of which similarities were the remains of an ancestral relationship from those that appeared simply because there was no other way of forming a suitable viral capsid. Fifteen years passed before it was shown that the enteric membrane-containing bacteriophage PRD1 and human adenovirus share a common coat protein fold, the so-called double β-barrel (or double jelly-roll) [26, 34] (Fig. 5.2a).

Both PRD1 MCP P3 and adenovirus hexon arranged in similar trimers, with the long axis of the β-barrels orthogonal to the virus surface, to form pseudo-hexagonal capsomer structures, the elemental building blocks of the icosahedral facets from which both of these virions are constructed (Fig. 5.2b, c). This observation led to the proposal that viruses could be grouped in viral lineages using the structural similarity of their MCPs, and precipitated a reanalysis of the low resolution structure of the chlorella virus PBCV-1 (family *Phycodnaviridae*), one of the largest viruses known at the time [27]. A simple and yet perspicacious manual fitting of the four P3 capsomers making up the PRD1 icosahedral asymmetric unit into the 3D PBCV-1 reconstruction supported the hypothesis that it belonged to the same lineage (Fig. 5.3a) [27]. Few months later the crystal structure of PBCV-1 MCP Vp54 determined at 2 Å resolution provided the experimental proof to the groundwork layout by Bamford and colleagues [27, 31].

This knowledge, together with the PRD1 crystal structure that allowed the understanding of its assembly pathway and offered a unique scalable mechanism for determining particle size by using a molecular tape measure, prompted the possibility that many more viruses within the virosphere could belong to the same PRD1-adeno viral lineage [11]. At the time the structural sampling of viral MCPs and/or viruses represented, however (and regardless of all subsequent efforts—still represents), a very small fraction of the enormous amount of viruses, 10^{30}–10^{31}, that have been estimated to permeate the biosphere [46]. Despite this astronomical number, whether viruses could be defined by few structural principles—recapitulating the building of the viral capsid and the encapsidation of the viral genome—came into question. Topological alterations in proteins involved in any of these processes would be disadvantageous as possibly compromising the virus identity—"self"—and/or progeny. Since 2002 several more structures of viral MCPs and viruses have been determined by different laboratories worldwide, thus increasing the conformational sampling of the MCP topology adopted by viruses [4, 47–51]. Viruses (e.g. PBCV-1, STIV and PM2) infecting hosts residing in all three domains of life were identified as possessing a MCP with a double β-barrel fold and expanding the PRD1-adeno lineage (Fig. 5.3b). This structural similarity detected between proteins of viruses infecting their own hosts across all three domains of life suggested that this is a very ancient lineage, whose origins predate the separation of the domains.

In 2012, a systematic structure-based analysis of all available virus coat protein folds provided a new means to classify viruses within the viral universe (virosphere) [45]. Such study shows the existence of four different lineages for icosahedral viruses presently identified (Fig. 5.3c). The PRD1-adenovirus lineage is now

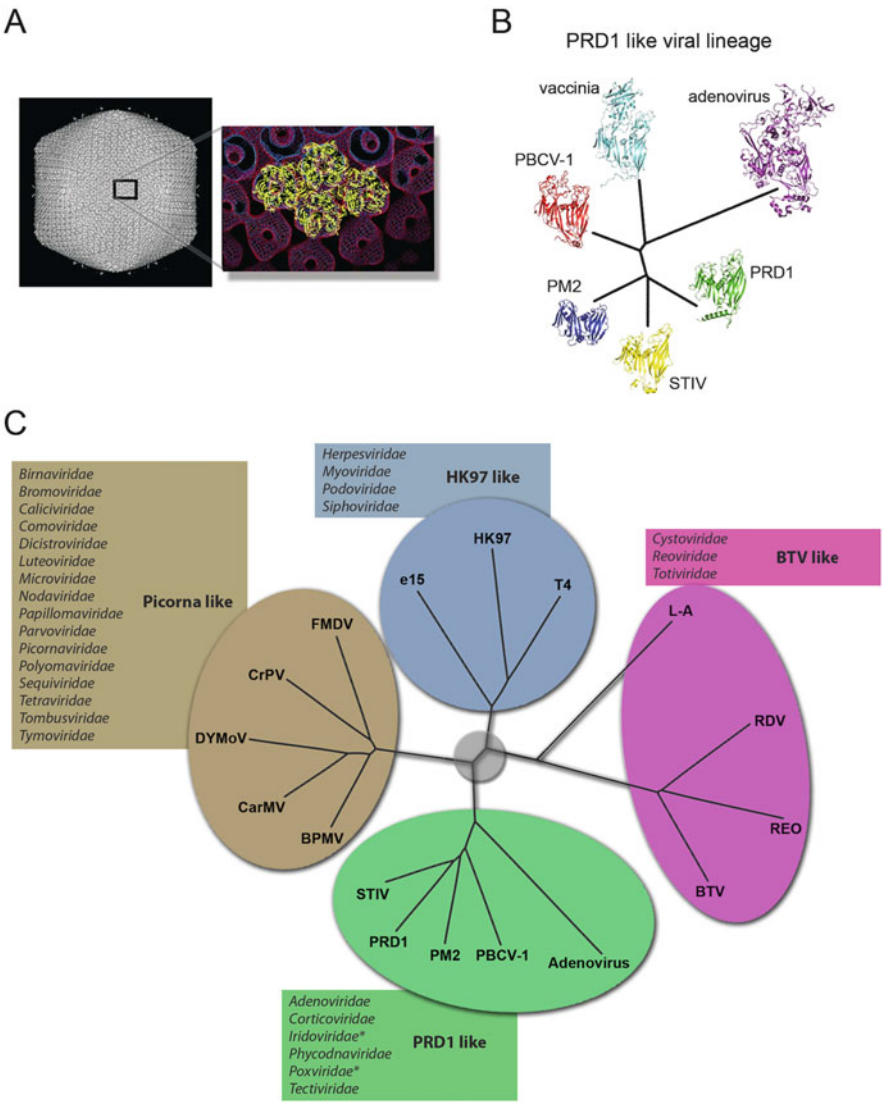

Fig. 5.3 Structure-based viral lineages. (**a**) Surface rendering of the 3D reconstruction of PBCV-1 at ~26 Å resolution [43] with a preliminary fit of the atomic structure of the PRD1 MCPs P3 into the PBCV-1 reconstruction anticipating some of the structural assembly principles of the PRD1-like viral lineage, adapted from Bamford et al. [27]. (**b**) PRD1-adeno structure-based phylogeny tree of the MCPs of vaccinia virus (D13), PBCV-1, adenovirus, STIV, PRD1 and PM2. MCP atomic models are represented in cartoon and differently coloured; reproduced from Bahar et al. [44]. (**c**) Structure-based phylogenetic tree showing the four different lineages identified by structural comparison of viral MCPs. Details of the methods and atomic models used are described in Abrescia et al. [45] from where the panel has been reproduced with permission. The table associated with each clade lists the virus families (left) of the virosphere that can be placed in the corresponding viral lineage (right). The grey circle at the centre of the tree denotes that the lineages should not be intrepreted as sharing a common ancestor (viruses are polyphyletic in origin)

postulated to include six virus families (Fig. 5.3b). Strikingly, pleomorphic vaccinia viruses (family *Poxviridae*), through viral protein D13 possessing the double β-barrel fold, share the pseudo-hexagonal structural building block characteristic of this lineage, albeit D13 is used only transiently as a scaffold during the virion assembly [44].

There is no doubt that only a tiny fraction of viruses have been identified so far and even a smaller number has been structurally analysed. Consequently, new virus coat protein folds will be discovered in the future. Nevertheless the systematic comparison and classification of all currently known virus coat protein folds—and virion architectures when available—represent a powerful means to establish relationships across members of the virosphere apparently not related; and this will remain so at least until the sensitivity of current standard bioinformatics tools for detection of sequence similarity is improved [52].

5.4 PRD1 Genome Packaging and Delivery

The studies on PRD1 assembly fuelled also the investigation of other aspects of the PRD1 lifecycle that remained obscure still. One of the fundamental steps in any virus lifecycle is the packaging of the genome. In icosahedral dsDNA bacteriophages the genome is translocated into preformed procapsids using specific enzymes, terminases or packaging ATPases (see for example [17, 53]). In some bacteriophages the elastic, electrostatic, entropic osmotic, and hydration energetic costs incurred by constraining the dsDNA at very high densities within the fixed volume of the capsids build up a significant internal pressure [54]. This pressure is considered to provide the force initially driving genome injection into the cell, while DNA-binding proteins, DNA condensation or enzymes may help during the final stages of the transfer [55]. In the tailed phages (order *Caudovirales*) the DNA packaging occurs at a unique portal vertex. In the mature virion this special vertex is equipped with a preformed proteinaceous tail which is used as a DNA ejection device during infection. Several bacteriophage portals to which the tail attaches during assembly have been studied. One of the best characterised packaging systems is that of Φ29, a short-tailed icosahedral virus with a prolate capsid containing a linear dsDNA genome, infecting gram-positive bacteria [56, 57]. Enterobacterial phage P22 portal has also been analysed in great biochemical and structural detail recently leading to the elucidation of the mechanism that couples genome packaging with capsid maturation [53]. A portal assembly complex has also been identified in herpes simplex virus type 1 (HSV-1), a eukaryotic enveloped virus whose nucleocapsid forms an icosahedral protein shell. The portal of HSV-1 is located at a single vertex of the nucleocapsid and contains a ring-shaped multimer of the UL6 protein [58, 59].

In the case of tail-less PRD1 several efforts have been made to understand how the dsDNA is packaged and how the dsDNA is ejected into the host-cell at infection owing that it possesses a further architectural element constituted by the protein rich membrane vesicle. Intriguingly, early negative stain 2D images of PRD1 showed the

occasional presence of a tubular appendix protruding from one of the twelve icosahedral vertices; this tubular structure was also observed when the isolated viral membrane vesicles were imaged [60]. The first confirmation of a unique vertex in PRD1 came from immune-gold negative-stain experiments where gold-conjugated antibodies against proteins P6 and P20 were shown to bind to a single vertex of PRD1 [41]. This suggested that at least the minor capsid protein P6, which has no previously appointed function, and the membrane protein P20 are located at a unique vertex. Biochemical and genetic studies were also performed to dissect both the genome packaging and ejection mechanisms [61]. These studies revealed two sets of proteins respectively involved in DNA packaging (or in the stable maintenance of the DNA within the particles) and in the DNA delivery system. The former were small membrane proteins P20, P22, the packaging efficiency factor P6 and the packaging ATPase P9, and the latter ones were proteins P7, P14, P11, P16, P18 and P32 [17, 24, 61, 62]. The packaging ATPase P9 powered by ATP hydrolysis pumps the dsDNA into the empty procapsid; to harness this mechanism an in vitro system for packaging DNA into preformed procapsid was developed [63].

The averaging techniques used to investigate the PRD1 three-dimensional structure while provided exquisite details of icosahedrally ordered protein components, they blurred all those that do not obey icosahedral symmetry. Only when cryo-EM single particle asymmetrical reconstruction was used, the location and the structure of the unique vertex were determined [17]. The special vertex is occupied by several protein components not obeying to the fivefold symmetry (Fig. 5.4a). Ten MCP P3 trimers wrap around the 12-fold symmetrical P9/P6 complex at the unique vertex (Figs. 5.4a inset and b). Such a symmetry mismatch is also a structural hallmark of the tailed dsDNA viruses with a portal complex arranged with 12-fold symmetry [53]. Strikingly, the capsid and the icosahedral internal membrane vesicle interconnect via membrane proteins P20 and P22, organised as sixfold symmetry, to the P9/P6 complex portal, organised as 12-fold symmetry, thus generating a symmetry mismatch (Fig. 5.4b).

Using an integrative approach combining immuno-labelling, cryo-EM and cryo-electron tomography (cryo-ET) techniques, and using mature PRD1, PRD1 procapsid (defective in P9) and in vivo analysis of virus-infected cells, Peralta and colleagues reported a new principle of virus–cell interaction essential for the translocation of the viral genome [5]. The study anticipated that the PRD1 DNA ejection tube captured many years earlier by negative-stain EM techniques, protrudes from the same unique vertex used for DNA packaging and that it is structured (Fig. 5.4c and d). These findings support the direct involvement of self-assembling and lattice forming membrane-associated proteins with likely candidates being P7, P14, P18 and P32 proteins [61]. Importantly, the packaged genome does not have a role in the triggering or in the formation of the tail tube. However, in the procapsid where the membrane vesicle is devoid of the genome, the formation of tail tube fails to make the correct orientation and consequently the tubular structure does not always protrude from the vertex. Moreover, the genome-less membrane vesicle displayed diverse morphologies from stomatocyte-like to discocyte-like revealing not only the elasto-mechanical properties of giant unilamellar (proteo-)vesicles but also the

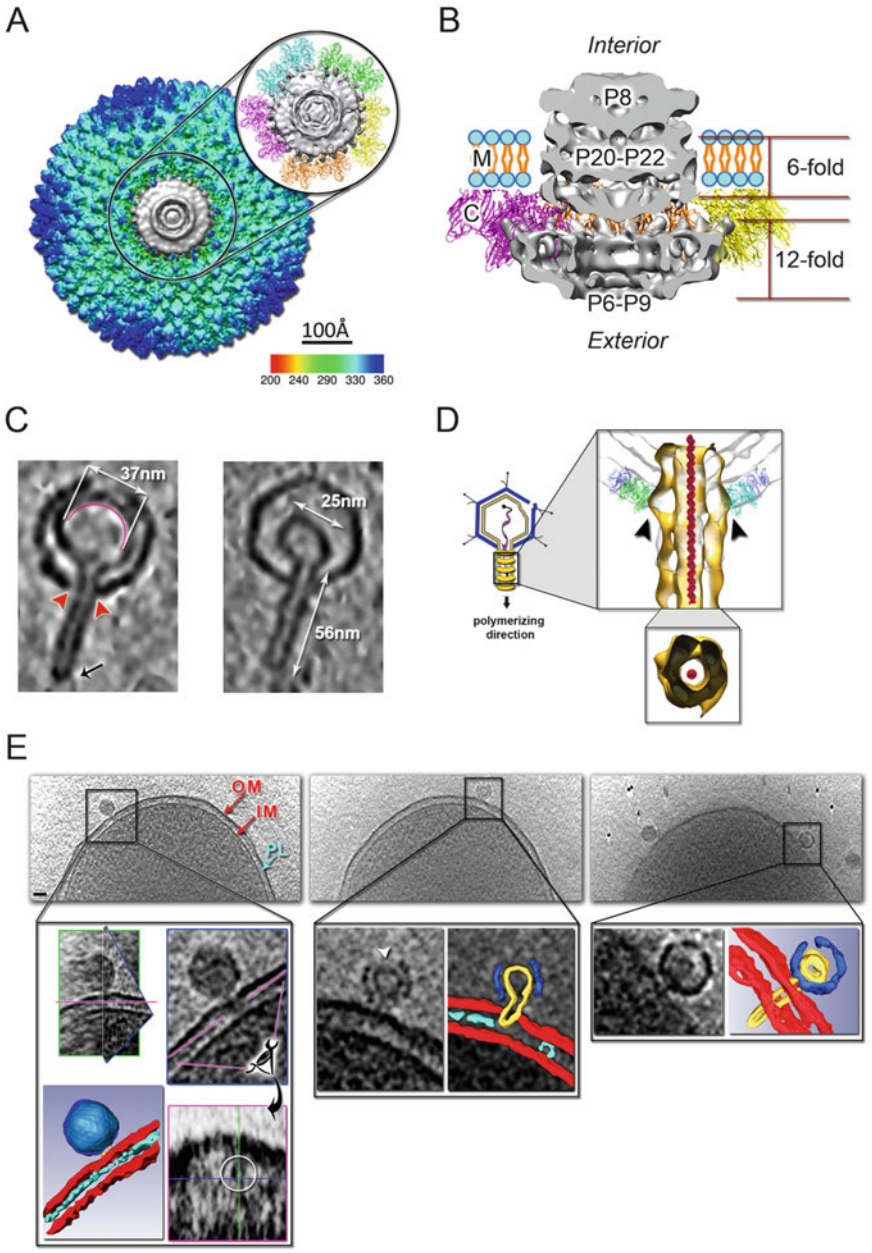

Fig. 5.4 PRD1 unique vertex and DNA ejection mechanism. (**a**) Surface rendering of the asymmetrical 3D reconstructed cryo-map of PRD1 at 12 Å resolution viewed along the symmetry axis of the unique vertex (grey) and coloured by radius (colour bar); right, top inset shows the 10 MCP P3 trimers (represented as cartoon and coloured in green, yellow, orange, magenta and light-blue) wrapping around the 12-fold symmetrical P9/P6 complex at the unique vertex. (**b**) Cross-sectional view of the architecture of the unique vertex coloured as in (**a**), M marks the membrane depicted schematically and C the capsomers surrounding the unique vertex. The unique vertex is modular

triggering factors leading to the remodelling of the membrane into the tail tube [5]. These factors were attributed to the change in structural and environmental and/or osmotic conditions of the internal membrane vesicle upon binding of the phage to the cellular receptor. This event (or multiple events) would initially alter the structure of the vertex complex leading to the de-capping of the vertices, thus exposing the membrane to the extracellular milieu conditions and initiating the remodelling of the membrane vesicle and tube self-assembly process. It has also been postulated that the membrane elastic properties could aid the translocation of the viral genome into the host-cell during the initial stages of infection [19]. Finally, the use of cellular cryo-ET remarkably captured PRD1 infecting a *E. coli* cell in vivo using the tail tube to drill into the bacterial cell envelope, leaving no doubts as to the mechanisms governing the tube self-assembly, the viral DNA ejection apparatus and the cell infection (Fig. 5.4e) [5].

Fig. 5.4 (continued) and composed of the DNA terminal protein P8 of the membrane embedded P20/P22 complex forming the sixfold symmetrical membrane conduit for the portal vertex, and, on the exterior, of proteins P6 and P9 assembling in a 12-fold symmetrical complex. (**a**–**b**) adapted from Hong et al. [17] under the terms of Creative Commons Attribution. (**c**) Left, tomographic central xy section of a PRD1 particle possibly at initial stage of DNA ejection with a tail tube self-assembled and the internal membrane vesicle not yet fully deflated; the semicircular red line within the vesicle marks the possible presence of residual genome whereas the red arrowheads indicate the vertex aperture from where the tube protrudes and the black arrow the conical tip of the tube. Right, same as left but a different PRD1 particle with the tube possibly at the final stages of the DNA ejection with the vesicle showing a "map pin" morphology. (**d**) Schematic of PRD1 with tube with inset showing as cut-through the sub-tomogram averaged tube density (in gold) within the capsid region corresponding to the vertex from where the tube protrudes (semitransparent light-grey); the black arrowheads mark a ring-like structure visible in one of the tube averaged classes and that likely correspond to peripentonal P3 MCPs surrounding the unique vertex [17] (see also **b**); inset below shows an orthogonal view of the tube density, a B-form dsDNA is modelled in the tube channel. (**e**) Cellular tomographic slices of an *E. coli* cell infected by PRD1. Scale bar, 50 nm. Left, full PRD1 particle, outlined by a black square, with forming tube crossing the outer membrane (OM), inner plasma membrane (IM) and peptidoglycan layer (PL) are indicated; the inset below shows on the left-top the particle viewed through three intersecting planes (outlined in green, blue and magenta with corresponding blue and magenta planes on the right while on the left-bottom a segmentation of the particle (dark-blue) is superimposed with the density derived from the atomic model (PDB code 1W8X) in light-blue, in red the outer and inner membranes and cyan the peptidoglycan layer. Centre, semi-full particle, outlined by a black square with below inset showing a tomographic slice (left) with a segmentation of the capsid and cell envelope superimposed (right); the white arrowhead defines additional openings of the capsid. Right, an almost empty particle with the inset below showing a particle with a "map-pin" shape vesicle and full-length tube penetrating the cell envelope (left) and corresponding segmentation (right). (**c**–**e**) reproduced from Peralta et al. [5]

5.5 Mechanical Properties of PRD1

The coupling of the fold of the viral MCPs with the building principles of the virion, and the genome packaging mechanism does not only emerge as signature for detecting virus common ancestry but it is the same quintessential purpose for protection of genome integrity. To secure the genetic cargo outside the cell, viruses have devised different viral protein folds, architecture and material composition (protein or lipids or a mixture of both). Indeed when travelling outside of the host cell, virions may encounter harsh environmental conditions. This combination of materials and architectures provide specific mechanical properties fulfilling the requirement for protection. Single-molecule techniques such as atomic force microscopy (AFM) have been proven to be very useful in unravelling the mechanical properties of viruses [64]. This information is pivotal not only to grasp their biology but also for manipulating and using them as nano-carriers of foreign cargos. AFM studies on viruses have provided unprecedented knowledge of the deformability (stiffness, k), the energy required for mechanical failure (toughness, T), and the limits to fatigue for virions [65]. However, the majority of these studies have been performed on icosahedral viruses with a proteinaceous capsid shell enclosing the genome (DNA or RNA).

Only recently, to the best of our knowledge, the first AFM study on viruses such as PRD1, where an internal membrane vesicle surrounds the densely packaged dsDNA, was performed [66]. The wealth of genetic, biochemical and structural information on PRD1 together with the availability of different particles, [e.g. (1) mature PRD1; (2) procapsid devoid of DNA and packaging ATPase; (3) icosahedral P3-shell composed of MCP P3 and minor protein P30, but lacking the pentons and peripentonal capsomers; and (4) proteo-lipidic membrane vesicle enclosing a complete genome], lend PRD1 an amenable system to AFM examination. The morphology and mechanical responses of these particles were assessed in an aqueous environment and their stiffness and yield behaviour under an applied force analysed (Fig. 5.5a–i).

One of the major findings is that PRD1 displays a similar breaking force whether it is packaged or devoid of DNA, with the presence of the DNA inducing a stiffening of the mature PRD1 over the procapsid [66]. This implies that the mechanical stability of mature PRD1 is independent from the presence of the genome. In contrast, the fragility (brittleness) of the P3-shell particle unequivocally demonstrates the decrease in structural reinforcement of the particle when only interactions across capsomers containing the GON and the cementing protein P30 are considered. The protein-rich membrane vesicle displayed the least stiffness and no clear yield point. Thus the contribution of the membrane to the overall stiffness of mature PRD1 is marginal, mainly transmitting the stiffening due to the DNA pressure to the capsid. Interestingly, when the architecture of PRD1 was modelled as a simplified two-shell composite capsid-membrane system using the experimentally derived mechanical properties, it was confirmed that the presence of the membrane layer contributes less than 10% to the stiffness of the particle [66]. To assess how the

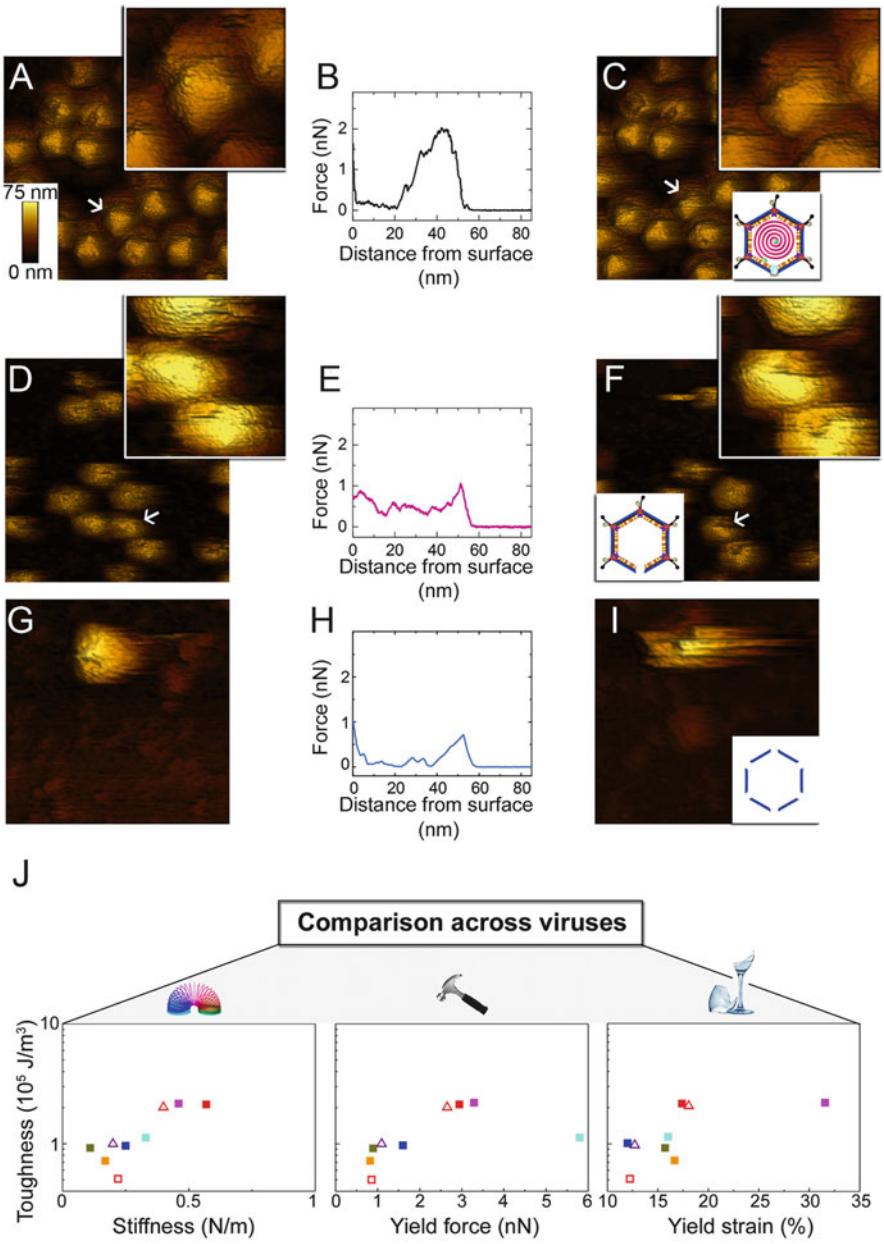

Fig. 5.5 The mechanics of PRD1. Representative topographic consecutive AFM images deriving from nanoindentation studies of the different PRD1 particles with (**a**), (**d**) and (**g**) before and (**c**), (**f**) and (**i**) after nanoindentation with schematics identifying particle types: wt PRD1 (top), Sus1 procapsid (middle) and P3-shell (bottom) (vesicle not shown; vesicles displayed the least stiffness and not defined yield points). Panels (**b**), (**e**) and (**h**) represent a single mechanical indentation, with the corresponding force curve obtained for each particle type. Image size: 500 nm; *z* range (vertical dimension): 0–75 nm, see colour key in (**a**). The white arrows in (**a**), (**c**), (**d**) and (**f**) mark the indented particles with insets showing their view enlarged (image size: 160 nm). (**j**) PRD1's

capsid and membrane vesicle together influence the resilience, the toughness was estimated for each PRD1 derived particles and compared with available dsDNA icosahedral viruses. Surprisingly, the toughness of the mature PRD1 is rivalled only by adenovirus (Fig. 5.5j). Adenovirus does not possess an internal membrane but a relatively large number of cementing proteins (IIIa, V, VI, VIII and IX) that glue together the different hexons making up the capsid shell [37]. Although deconvoluting the individual contribution of the capsid and membrane vesicle to the overall PRD1 toughness is challenging as an intact capsid without the membrane cannot be produced, PRD1 mechanics indicate that the proteinaceous capsid is stiff and brittle, whereas the membrane vesicle is ductile and soft [66]. However, it is only when these two layers and materials are architecturally integrated that PRD1 achieves a high resilience. Thus, the mechanical properties displayed by the mature PRD1 are reminiscent of those of a composite material not man-made but optimised through evolution for the protection of the fragile and precious genome.

5.6 The Appearance of Single Vertical β-Barrel Viruses

In Sect. 5.3 we accounted for the origin of the concept of viral lineages based on structure and the efforts made from thereafter to provide a systematic classification of the virosphere. An increased interest in unexplored extreme ecological niches such as thermophilic and halophilic environments led to the isolation of viruses displaying PRD1-adenovirus type architecture, but with two genes encoding two MCP types, each with a single β-barrel and both composing the lattice. We have called them "vertical single β-barrel viruses". The first isolate was highly halophilic virus SH1 of euryarchaeal host *Haloarcula hispanica* [67]. Other viruses of this group are thermophilic Thermus phages P23-77 and IN93, halophilic Salisaeta phage SSIP-1 and archaeal halophilic viruses HHIV-2, HCIV-1 and PH1 infecting *Haloarcula* species and SNJ1 infecting *Natrinema* species [68–73]. Currently, all such viruses are either bacteriophages or archaeal icosahedral viruses with an internal membrane and thriving in extreme surroundings and classified to the family *Spherolipoviridae* [74]. Only SSIP-1 is currently unclassified. Common to all vertical single β-barrel viruses is that they have a conserved gene that encodes for a putative packaging ATPase similar to those found in the double β-barrel viruses and shown in PRD1 to be the packaging ATPase at the portal vertex [17]. In

Fig. 5.5 (continued) mechanical properties compared to other dsDNA viruses via Ashby plots of toughness (*y*-axis in log scale) versus stiffness, yield force and yield strain (*x*-axis), respectively, with the slinky, hammer and broken glass symbolising the investigated mechanical property. The filled, empty squares and empty triangles identify virions, penton-less particles and procapsids respectively; PRD1 particles in red, bacteriophage λ in blue, HSV-1 in cyan, bacteriophage P22 in purple, adenovirus in magenta, bacteriophage T7 in orange and bacteriophage HK97 in dark-green. Adapted from Azinas (2018)

addition, virus-related, genome-integrated elements resembling the core elements of single β-barrel viruses have been identified in the genomes of bacterial *Meiothermus* and archaeal *Halomicrobium* and *Haladaptus*, *Halociforma* and *Haloarcula* species suggesting that vertical single β-barrel viruses are more common than previously thought [69, 72, 74] (Fig. 5.6a).

Thermus phage P23-77 provided the first example of assembly of an icosahedral capsid lattice made of two MCP types, VP16 and VP17 [71, 76]. Interestingly, the capsid lattice of P23-77 displays the same *T* number as SH1 and HHIV-2 (Fig. 5.6b left), pseudo $T = 28$, which is unique to these viruses [71, 77, 78], whereas Salisaeta phage SSIP-1 capsid is organised on a $T = 49$ icosahedral lattice [68]. The P23-77 capsid consists of pseudo-hexameric capsomers with two-tower morphology (i.e. two out of six subunits have a turret on top of the lattice forming unit) [71]. The capsomers are composed of VP16 homodimers stabilised by strand swapping, and VP17 monomers, both possessing a vertical single β-barrel fold but with VP17 displaying a further small domain as turret (Fig. 5.6c) [76]. Contrary to P23-77, SH1 and HHIV-2 pseudo-hexameric capsomers display two different morphologies: capsomers with either two or three turrets, but both types are composed of MCPs VP4 and VP7 that adopt a vertical single β-barrel topology (Fig. 5.6b) [77].

The observation that P23-77 MCPs VP16 and VP17 adopt a vertical single β-barrel fold places this type of viruses as predating the advent of double β-barrel MCPs and suggests a fusion event between the MCP encoding genes (Fig. 5.6c) [76]. It is worth underlining that the pseudo-hexameric footprint of the capsomers is a unifying feature of the viruses in the PRD1-adeno lineage, and it is not dependent on genome type, capsid assembly mechanism, the number of MCPs or host recognising components. However, while VP16 and VP17 crystal structures demonstrated the β-barrel fold, the principle governing the assembly of these viruses has remained elusive. It has been proposed that the assembly of icosahedral membrane-containing viruses with two single vertical β-barrel MCPs may require further proteins that aid the registering of single β-barrel MCPs into pseudo-hexameric capsomers onto the membrane vesicle [77]. Only very recently this hypothesis was demonstrated using high-resolution cryo-EM of whole virions [79, 80].

5.7 PRD1 in Environmental and Applied Biology

In the biosphere, phages modulate bacterial populations, which in turn influence phage distribution and abundance; in particular dsDNA phages are considered to be the most abundant viruses on Earth with dsDNA tailed phages overshadowing the environmental diversity of viruses [46, 81]. It has been shown that non-tailed dsDNA phages represent a profuse and ecologically important fraction of marine viral communities. Remarkably, a new virus family, termed “Autolykiviridae”, was recently proposed and it contains a group of marine dsDNA viruses displaying morphological and structural features similar to PRD1 and more generally to tectiviruses [82]. The structural homology extends beyond the double β-barrel fold

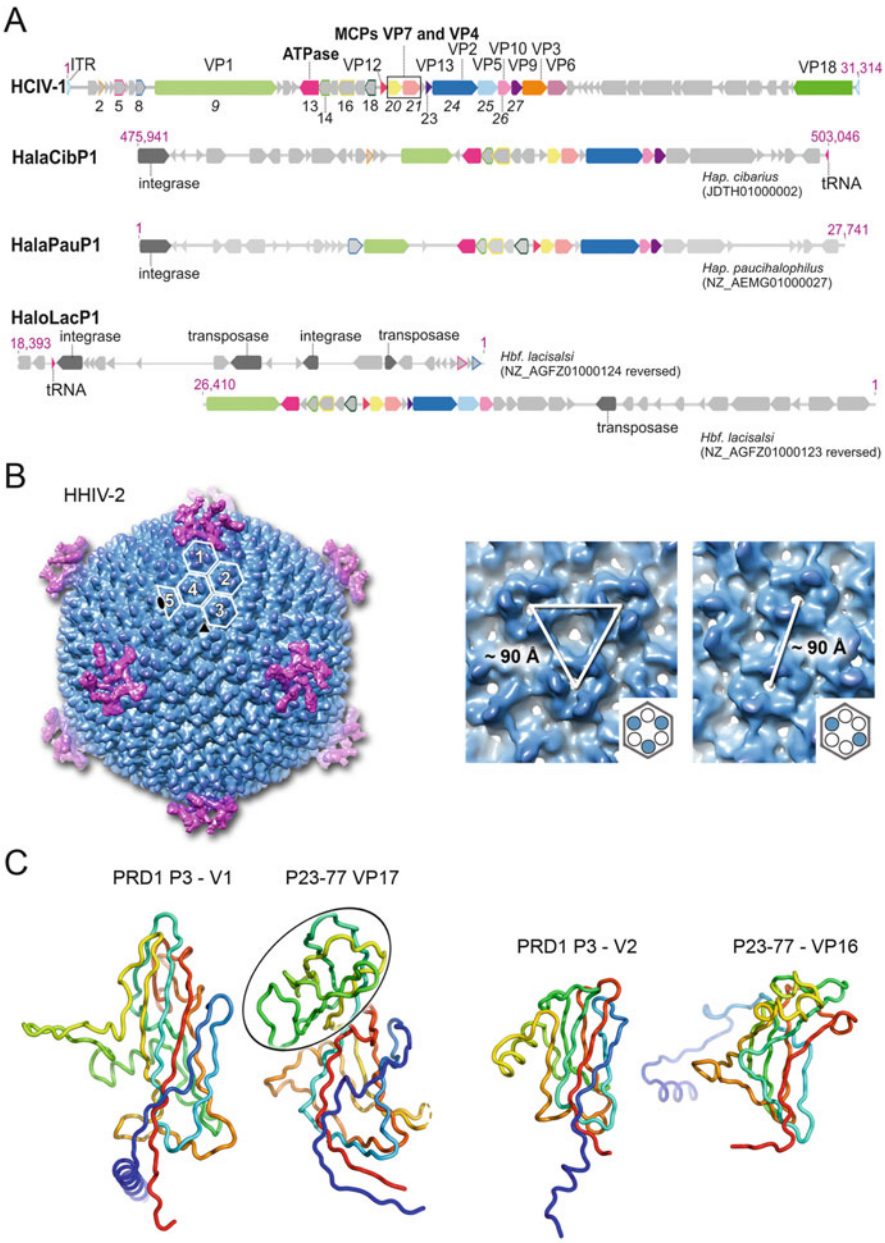

Fig. 5.6 Single vertical jelly roll viruses. (**a**) Spherolipovirus HCIV-1 genome and putative proviral genetic elements (HalaCibP1, HalaPauP1 and HaloLacP1) identified in euryarchaeal chromosomes based on sequence similarity as examples for spherolipovirus-like proviruses [75]. Grey arrows indicate open reading frames (ORFs) or genes. Coloured arrows and arrows with colour frames indicate homologous genes known to encode structural proteins in HCIV-1 or putative homologous proteins. HCIV-1 gene numbers and structural proteins (VP), putative packaging ATPase and the major capsid proteins (MCP) are indicated. Nucleotide coordinates are in purple. Integrase and transposase encoding genes, as well as tRNA genes, are shown in the putative

of the MCP to the infection process. As in PRD1, a tail tube protrudes from one of the icosahedral vertices upon infection in order to penetrate the bacterial cell envelope. These newly discovered phages infecting potential members of *Vibrionaceae* can be considered as efficient killers of marine bacteria due to their wide host spectrum, as opposed to tailed dsDNA phages with a considerably narrower host range. Autolykiviruses demonstrate that the diversity of non-tailed dsDNA viruses of prokaryotic hosts that are represented by the currently recognised families *Tectiviridae*, *Corticoviridae*, *Turriviridae* and *Spherolipoviridae* greatly surpasses the diversity previously observed. This type of virus architecture is not restricted to dsDNA genomes, but can be found from ssDNA phage FLiP of *Flavobacterium*, which has also an internal membrane and icosahedral capsid made of double jelly roll MCPs (recently proposed family of "Finnlakeviridae") [83].

Searching for new viruses from various ecological niches has revealed previously unknown PRD1-like viruses and their new potential for applied science. New likely members of the family *Tectiviridae*, phage Toil and Gluconobacter phage GC1, infect oleaginous bacterium *Rhodococcus opacus* and *Gluconobacter cerinus* respectively. In the former case it has been proposed that phage Toil can be possibly used as an agent to extract biolipids from the host as starting material for biodiesel production [84]. In the latter case, bacteriophage GC1 was isolated while surveying for phages infecting acetic acid bacteria which are spoilage microorganisms during wine making [85]. GC1 is the first example of a temperate tectivirus of gram-negative bacteria and represents a new genus *Gammatectivirus* in the family *Tectiviridae*. On the other hand, the temperate phages GIL01 and GIL16 in their lysogeny growth phase (genus *Betatectivirus*) have been shown to have a significant influence on the bacterial growth, sporulation rate, biofilm formation and swarming motility of *Bacillus thuringiensis*, all of which might be beneficial in the survival and

Fig. 5.6 (continued) proviruses. Modified from Demina et al. [75]. *Hap. cibarius*, *Haladaptatus cibarius*; *Haladaptatus paucihalophilus*; *Hbf. lacisalsi*, *Halobiforma lacisalsi*. (**b**) Left, overall view of cryo-EM map of vertical single β-barrel archaeal virus HHVI-2 (pseudo-$T = 28$) at 13 Å resolution (capsid, light-blue; spike proteins at the fivefold vertices, light magenta). Capsomers composing the IAU are numbered 1–5 with the two-turret capsomers labelled 4 and 5 and three-turret capsomers labelled 1–3; capsomer 5 is located on the twofold icosahedral symmetry axis (black oval) and capsomer 3 is proximal to the threefold axis (black triangle). Right, surface rendering of the three-turret capsomers (left) and two-turret capsomers (right). The distances between the centres of the capsomers are marked (left and right panels are not to scale). Schematic diagrams (bottom right) illustrate the organisation of the pseudo-hexameric capsomers (white circles, VP7; slate-blue circles, VP4). (**c**) Side-by-side comparison of individual β-barrel V1 and V2 of PRD1 MCP P3 and corresponding crystal structures of the two MCPs of Thermus phage P23-77, VP17 (PDB ID 3ZMN) and VP16 (PDB ID 3ZMO) [76]; the black oval marks the turret domain in VP17. Atomic models are similarly oriented, displayed in cartoon tube and coloured from blue to red, from N- to C-terminus

colonisation of bacteria in different environmental habitats indicating that the presence of the tectivirus might give ecological advantage for the cells [12].

As a phage of enterobacteria, PRD1 has also been used for comparative and analytical purposes in environmental studies. It has served with single-stranded RNA bacteriophage MS2 in modelling and estimating the inactivation rates of natural sunlight and artificial light in water with the purpose of tackling other viruses and/or microorganisms [86]. Moreover, PRD1, because of its physicochemical properties and stability, is commonly used as a substitute tracer in subsurface transport and groundwater environment studies, for example to estimate expected virus removal rates occurring during on-land application of sewage during testing of aquifer recharge operations [87]. Tectiviruses have shown their potential also in applied science and have been used as models for viral biosafety level 1 surrogates in water disinfection to facilitate novel strategies in providing safe water, or in Ebola outbreaks to evaluate surface disinfection efficacy, and utilised also for studies on airborne viruses [88, 89]. Finally, emerging interest in human gut microbiota—our internal "biosphera"—has shown evidence of the existence of a human gut "virome" [90]. The composition of this virome includes also tectiviruses of which PRD1 is the representative family member.

Overall, the above described involvement of PRD1 and more generally the presence and usage of PRD1-like viruses in multiple environmental scenarios reiterate the fundamental role that decades of genetic, biochemical and structural studies on PRD1 have also played in contributing to the understanding of current environmental models of bacteria–virus interactions.

5.8 What More Can We Learn from PRD1?

More than 40 years have passed since PRD1 was isolated [9]. During these decades PRD1 has served as a marvellous model system for membrane-containing viruses unravelling fundamental aspects in microbiology, virology, membrane biology, structural biology and recently environmental biology. Importantly, its extensive biochemical and structural studies have led to the formulation of fundamental concepts in viral phylogeny that have revolutionised the way we "look" at viruses and classify them in higher taxonomic ranks, not visible in the nucleotide sequence. Using structure-based viral phylogeny through the systematic structural comparison of the fold of the MCPs, the vast majority of known viruses within the virophere can now be classified [45]. This has also manifested the intricate symbiotic relationships that viruses and their corresponding hosts maintain to survive through evolutionary times.

So, is research on bacteriophage PRD1 coming to a close? Not yet. Fundamental aspects concerning the viral morphogenesis remain unknown—specifically how the membrane vesicle is formed. It is known that PRD1 selects the lipids from the host bacterial cell but the mechanisms behind this selection process and the vesicle assembly are elusive. Unravelling these mechanisms will provide insights into

cellular membrane biology and vesicle biogenesis. The huge advances in electron microscopy favour this type of analysis. Particularly, cellular cryo-ET with implementation of phase-plate technology can help the dissection of this viral vesicle formation.

Moreover, while progress has been made in the understanding of the PRD1 DNA ejection, it remains unclear what triggers the opening of the end tip of the viral tube allowing the DNA to flow inside the cell and importantly whether the tail tube possesses an ordered symmetrical structure possibly similar to the complexity of the tails in tailed phages. In summary, the wealth of information accumulated on membrane-containing bacteriophage PRD1 is a valuable asset to contextualise future insights and illuminate on the biology of this type of viruses that have recently been shown to be abundant in seawater and in the biosphere.

5.9 Conclusion

The discovery of membrane-containing bacteriophage PRD1 has turned out to unravel important viral processes, but more significantly the way we look at and group the virosphere today. While our knowledge of the virus world remains limited, the use of structure-based virus phylogeny has already uncovered unexpected relationships across viruses infecting organisms belonging to the three domains of life. Certainly, challenges still remain in clustering for example enveloped viruses using the "viral lineages" framework but other newly discovered virus families such as the *Spherolipoviridae*, displaying two vertical single β-barrel MCPs, are interpretable as possible predating clade of the PRD1-adeno viral lineage.

The multidisciplinary research efforts and the wealth of information accumulated on PRD1 have, however, elevated this bacteriophage to a unique model system for membrane-containing dsDNA viruses, a type of virus that nowadays seems to rival at least in abundance other bacteriophages in the marine world—the place where life began.

Acknowledgments We are grateful to Stavros Azinas and Ralf Richter for the collaborative work on virus mechanics and Dennis Bamford for insightful comments on the review. We also thank Juliet Cowper for language editing. This study was supported by the Spanish *Ministerio de Economía y Competitividad* (MINECO/FEDER BFU2015-64541-R), by the Basque *Departamento de Desarrollo Económico e Infraestructuras* (Ref: 37-2017-00036) and *Departamento de Educación*, *Política Lingüística y Cultura* (Ref: PRE_2016_2_0151) to N.G.A.A. H.M.O was supported by the University of Helsinki and Academy of Finland funding for Instruct-FI research infrastructure and Biomolecular Complex Purification (BioComplex) core facility. We thank MINECO for the Severo Ochoa Excellence Accreditation to the CIC bioGUNE (SEV-2016-0644).

References

1. Espejo RT, Canelo ES (1968) Properties of bacteriophage PM2: a lipid-containing bacterial virus. Virology 34:738–747
2. Spencer R (1963) Bacterial viruses in the sea. In: Oppenheimer CH (ed) Symposium on marine microbiology. Charles C Thomas, Springfield, pp 350–365
3. Kivelä HM, Kalkkinen N, Bamford DH (2002) Bacteriophage PM2 has a protein capsid surrounding a spherical proteinaceous lipid core. J Virol 76:8169–8178
4. Abrescia NG, Grimes JM, Kivelä HM, Assenberg R, Sutton GC, Butcher SJ, Bamford JK, Bamford DH, Stuart DI (2008) Insights into virus evolution and membrane biogenesis from the structure of the marine lipid-containing bacteriophage PM2. Mol Cell 31:749–761
5. Peralta B, Gil-Carton D, Castaño-Díez D, Bertin A, Boulogne C, Oksanen HM, Bamford DH, Abrescia NG (2013) Mechanism of membranous tunnelling nanotube formation in viral genome delivery. PLoS Biol 11:e1001667
6. Oksanen HM, ICTV Report C (2017) ICTV virus taxonomy profile: *Corticoviridae*. J Gen Virol 98:888–889
7. Leigh B, Breitbart M, Oksanen HM, Bamford DH, Dishaw L (2018) Genome sequence of PM-like phage Cr39582 induced from Pseudoalteromonas sp. isolate from gut of Ciona robusta. Genome Announc 6:e00368-18
8. Kivelä HM, Mannisto RH, Kalkkinen N, Bamford DH (1999) Purification and protein composition of PM2, the first lipid-containing bacterial virus to be isolated. Virology 262:364–374
9. Olsen RH, Siak JS, Gray RH (1974) Characteristics of PRD1, a plasmid-dependent broad host range DNA bacteriophage. J Virol 14:689–699
10. Oksanen HM, Bamford DH (2012) Tectiviridae/PRD1 chapter. In: King MJAAMQ, Carstens EB, Lefkowitz EJ (eds) Virus taxonomy: ninth report of the international committee on taxonomy of viruses. Elsevier, London, pp 317–322
11. Abrescia NG, Cockburn JJ, Grimes JM, Sutton GC, Diprose JM, Butcher SJ, Fuller SD, San Martin C, Burnett RM, Stuart DI et al (2004) Insights into assembly from structural analysis of bacteriophage PRD1. Nature 432:68–74
12. Gillis A, Mahillon J (2014) Prevalence, genetic diversity, and host range of tectiviruses among members of the *Bacillus cereus* group. Appl Environ Microbiol 80:4138–4152
13. Caldentey J, Blanco L, Savilahti H, Bamford DH, Salas M (1992) In vitro replication of bacteriophage PRD1 DNA. Metal activation of protein-primed initiation and DNA elongation. Nucleic Acids Res 20:3971–3976
14. Bamford D, McGraw T, MacKenzie G, Mindich L (1983) Identification of a protein bound to the termini of bacteriophage PRD1 DNA. J Virol 47:311–316
15. Savilahti H, Bamford DH (1993) Protein-primed DNA replication: role of inverted terminal repeats in the *Escherichia coli* bacteriophage PRD1 life cycle. J Virol 67:4696–4703
16. Cockburn JJ, Abrescia NG, Grimes JM, Sutton GC, Diprose JM, Benevides JM, Thomas GJ Jr, Bamford JK, Bamford DH, Stuart DI (2004) Membrane structure and interactions with protein and DNA in bacteriophage PRD1. Nature 432:122–125
17. Hong C, Oksanen HM, Liu X, Jakana J, Bamford DH, Chiu W (2014) A structural model of the genome packaging process in a membrane-containing double stranded DNA virus. PLoS Biol 12:e1002024
18. Laurinavicius S, Bamford DH, Somerharju P (2007) Transbilayer distribution of phospholipids in bacteriophage membranes. Biochim Biophys Acta 1768:2568–2577
19. Santos-Pérez I, Oksanen HM, Bamford DH, Goni FM, Reguera D, Abrescia NGA (2017) Membrane-assisted viral DNA ejection. BBA-Gen Subjects 1861:664–672
20. Bamford JK, Bamford DH (1991) Large-scale purification of membrane-containing bacteriophage PRD1 and its subviral particles. Virology 181:348–352
21. Eskelin K, Lampi M, Meier F, Moldenhauer E, Bamford DH, Oksanen HM (2016) Asymmetric flow field flow fractionation methods for virus purification. J Chromatogr A 1469:108–119

22. Mindich L, Bamford D, Goldthwaite C, Laverty M, Mackenzie G (1982) Isolation of nonsense mutants of lipid-containing bacteriophage PRD1. J Virol 44:1013–1020
23. Oksanen HM, Domanska A, Bamford DH (2012) Monolithic ion exchange chromatographic methods for virus purification. Virology 434:271–277
24. Karhu NJ, Ziedaite G, Bamford DH, Bamford JK (2007) Efficient DNA packaging of bacteriophage PRD1 requires the unique vertex protein P6. J Virol 81:2970–2979
25. Ziedaite G, Kivelä HM, Bamford JK, Bamford DH (2009) Purified membrane-containing procapsids of bacteriophage PRD1 package the viral genome. J Mol Biol 386:637–647
26. Benson SD, Bamford JK, Bamford DH, Burnett RM (1999) Viral evolution revealed by bacteriophage PRD1 and human adenovirus coat protein structures. Cell 98:825–833
27. Bamford DH, Burnett RM, Stuart DI (2002) Evolution of viral structure. Theor Popul Biol 61: 461–470
28. Abad-Zapatero C, Abdel-Meguid SS, Johnson JE, Leslie AGW, Rayment I, Rossmann MG, Suck D, Tsukihara T (1980) Structure of southern bean mosaic virus at 2.8 Å resolution. Nature 286:33–39
29. Hogle JM, Chow M, Filman DJ (1985) Three-dimensional structure of poliovirus at 2.9 Å resolution. Science 229:1358–1365
30. Rossmann MG, Arnold E, Erickson JW, Frankenberger EA, Griffith JP, Hecht HJ, Johnson JE, Kamer G, Luo M, Mosser AG et al (1985) Structure of a human common cold virus and functional relationship to other picornaviruses. Nature 317:145–153
31. Nandhagopal N, Simpson AA, Gurnon JR, Yan X, Baker TS, Graves MV, Van Etten JL, Rossmann MG (2002) The structure and evolution of the major capsid protein of a large, lipid-containing DNA virus. Proc Natl Acad Sci USA 99:14758–14763
32. Rice G, Tang L, Stedman K, Roberto F, Spuhler J, Gillitzer E, Johnson JE, Douglas T, Young M (2004) The structure of a thermophilic archaeal virus shows a double-stranded DNA viral capsid type that spans all domains of life. Proc Natl Acad Sci USA 101:7716–7720
33. Butcher SJ, Bamford DH, Fuller SD (1995) DNA packaging orders the membrane of bacteriophage PRD1. EMBO J 14:6078–6086
34. Athappilly FK, Murali R, Rux JJ, Cai Z, Burnett RM (1994) The refined crystal structure of hexon, the major coat protein of adenovirus type 2, at 2.9 A resolution. J Mol Biol 242:430–455
35. San Martin C, Burnett RM, de Haas F, Heinkel R, Rutten T, Fuller SD, Butcher SJ, Bamford DH (2001) Combined EM/X-ray imaging yields a quasi-atomic model of the adenovirus-related bacteriophage PRD1 and shows key capsid and membrane interactions. Structure 9:917–930
36. San Martin C, Huiskonen JT, Bamford JK, Butcher SJ, Fuller SD, Bamford DH, Burnett RM (2002) Minor proteins, mobile arms and membrane-capsid interactions in the bacteriophage PRD1 capsid. Nat Struct Biol 9:756–763
37. Liu H, Jin L, Koh SB, Atanasov I, Schein S, Wu L, Zhou ZH (2010) Atomic structure of human adenovirus by cryo-EM reveals interactions among protein networks. Science 329:1038–1043
38. Huiskonen JT, Manole V, Butcher SJ (2007) Tale of two spikes in bacteriophage PRD1. Proc Natl Acad Sci USA 104:6666–6671
39. Jaatinen ST, Viitanen SJ, Bamford DH, Bamford JK (2004) Integral membrane protein P16 of bacteriophage PRD1 stabilizes the adsorption vertex structure. J Virol 78:9790–9797
40. Xu L, Benson SD, Butcher SJ, Bamford DH, Burnett RM (2003) The receptor binding protein P2 of PRD1, a virus targeting antibiotic-resistant bacteria, has a novel fold suggesting multiple functions. Structure 11:309–322
41. Gowen B, Bamford JK, Bamford DH, Fuller SD (2003) The tailless icosahedral membrane virus PRD1 localizes the proteins involved in genome packaging and injection at a unique vertex. J Virol 77:7863–7871
42. Strömsten NJ, Bamford DH, Bamford JK (2003) The unique vertex of bacterial virus PRD1 is connected to the viral internal membrane. J Virol 77:6314–6321
43. Yan X, Olson NH, Van Etten JL, Bergoin M, Rossmann MG, Baker TS (2000) Structure and assembly of large lipid-containing dsDNA viruses. Nat Struct Biol 7:101–103

44. Bahar MW, Graham SC, Stuart DI, Grimes JM (2011) Insights into the evolution of a complex virus from the crystal structure of vaccinia virus D13. Structure 19:1011–1020
45. Abrescia NG, Bamford DH, Grimes JM, Stuart DI (2012) Structure unifies the viral universe. Annu Rev Biochem 81:795–822
46. Suttle CA (2007) Marine viruses—major players in the global ecosystem. Nat Rev Microbiol 5:801–812
47. Baker ML, Jiang W, Rixon FJ, Chiu W (2005) Common ancestry of herpesviruses and tailed DNA bacteriophages. J Virol 79:14967–14970
48. Jiang W, Li Z, Zhang Z, Baker ML, Prevelige PE Jr, Chiu W (2003) Coat protein fold and maturation transition of bacteriophage P22 seen at subnanometer resolutions. Nat Struct Biol 10:131–135
49. Khayat R, Tang L, Larson ET, Lawrence CM, Young M, Johnson JE (2005) Structure of an archaeal virus capsid protein reveals a common ancestry to eukaryotic and bacterial viruses. Proc Natl Acad Sci USA 102:18944–18949
50. Yan X, Yu Z, Zhang P, Battisti AJ, Holdaway HA, Chipman PR, Bajaj C, Bergoin M, Rossmann MG, Baker TS (2009) The capsid proteins of a large, icosahedral dsDNA virus. J Mol Biol 385:1287–1299
51. Zhang X, Xiang Y, Dunigan DD, Klose T, Chipman PR, Van Etten JL, Rossmann MG (2011) Three-dimensional structure and function of the *Paramecium bursaria* chlorella virus capsid. Proc Natl Acad Sci USA 108:14837–14842
52. Sinclair RM, Ravantti JJ, Bamford DH (2017) Nucleic and amino acid sequences support structure-based viral classification. J Virol 91:e02275–e02216
53. Lokareddy RK, Sankhala RS, Roy A, Afonine PV, Motwani T, Teschke CM, Parent KN, Cingolani G (2017) Portal protein functions akin to a DNA-sensor that couples genome-packaging to icosahedral capsid maturation. Nat Commun 8:14310
54. Molineux IJ, Panja D (2013) Popping the cork: mechanisms of phage genome ejection. Nat Rev Microbiol 11:194–204
55. Jeembaeva M, Jonsson B, Castelnovo M, Evilevitch A (2010) DNA heats up: energetics of genome ejection from phage revealed by isothermal titration calorimetry. J Mol Biol 395:1079–1087
56. Mao H, Saha M, Reyes-Aldrete E, Sherman MB, Woodson M, Atz R, Grimes S, Jardine PJ, Morais MC (2016) Structural and molecular basis for coordination in a viral DNA packaging motor. Cell Rep 14:2017–2029
57. Simpson AA, Tao Y, Leiman PG, Badasso MO, He Y, Jardine PJ, Olson NH, Morais MC, Grimes S, Anderson DL et al (2000) Structure of the bacteriophage phi29 DNA packaging motor. Nature 408:745–750
58. Cardone G, Winkler DC, Trus BL, Cheng N, Heuser JE, Newcomb WW, Brown JC, Steven AC (2007) Visualization of the herpes simplex virus portal in situ by cryo-electron tomography. Virology 361:426–434
59. Newcomb WW, Juhas RM, Thomsen DR, Homa FL, Burch AD, Weller SK, Brown JC (2001) The UL6 gene product forms the portal for entry of DNA into the herpes simplex virus capsid. J Virol 75:10923–10932
60. Bamford D, Mindich L (1982) Structure of the lipid-containing bacteriophage PRD1: disruption of wild-type and nonsense mutant phage particles with guanidine hydrochloride. J Virol 44: 1031–1038
61. Grahn AM, Daugelavicius R, Bamford DH (2002a) Sequential model of phage PRD1 DNA delivery: active involvement of the viral membrane. Mol Microbiol 46:1199–1209
62. Grahn AM, Daugelavicius R, Bamford DH (2002b) The small viral membrane-associated protein P32 is involved in bacteriophage PRD1 DNA entry. J Virol 76:4866–4872
63. Strömsten NJ, Bamford DH, Bamford JK (2005) In vitro DNA packaging of PRD1: a common mechanism for internal-membrane viruses. J Mol Biol 348:617–629

64. Martin-Gonzalez N, Ortega-Esteban A, Moreno-Madrid F, Llauro A, Hernando-Perez M, de Pablo PJ (2018) Atomic force microscopy of protein shells: virus capsids and beyond. Methods Mol Biol 1665:281–296
65. Llauro A, Schwarz B, Koliyatt R, de Pablo PJ, Douglas T (2016) Tuning viral capsid nanoparticle stability with symmetrical morphogenesis. ACS Nano 10:8465–8473
66. Azinas S, Bano F, Torca I, Bamford DH, Schwartz GA, Esnaola J, Oksanen HM, Richter RP, Abrescia NG (2018) Membrane-containing virus particle exhibits mechanics of a composite material for genome protection. Nanoscale 10:7769–7779
67. Bamford DH, Ravantti JJ, Rönnholm G, Laurinavicius S, Kukkaro P, Dyall-Smith M, Somerharju P, Kalkkinen N, Bamford JK (2005) Constituents of SH1, a novel lipid-containing virus infecting the halophilic euryarchaeon Haloarcula hispanica. J Virol 79:9097–9107
68. Aalto AP, Bitto D, Ravantti JJ, Bamford DH, Huiskonen JT, Oksanen HM (2012) Snapshot of virus evolution in hypersaline environments from the characterization of a membrane-containing Salisaeta icosahedral phage 1. Proc Natl Acad Sci USA 109:7079–7084
69. Demina TA, Pietilä MK, Svirskaite J, Ravantti JJ, Atanasova NS, Bamford DH, Oksanen HM (2016) Archaeal Haloarcula californiae icosahedral virus 1 highlights conserved elements in icosahedral membrane-containing DNA viruses from extreme environments. MBio 7: e00699–e00616
70. Jaakkola ST, Penttinen RK, Vilen ST, Jalasvuori M, Rönnholm G, Bamford JK, Bamford DH, Oksanen HM (2012) Closely related archaeal Haloarcula hispanica icosahedral viruses HHIV-2 and SH1 have nonhomologous genes encoding host recognition functions. J Virol 86: 4734–4742
71. Jaatinen ST, Happonen LJ, Laurinmäki P, Butcher SJ, Bamford DH (2008) Biochemical and structural characterisation of membrane-containing icosahedral dsDNA bacteriophages infecting thermophilic Thermus thermophilus. Virology 379:10–19
72. Porter K, Tang S-L, Chen C-P, Chiang P-W, Hong M-J, Dyall-Smith M (2013) PH1: an archaeovirus of Haloarcula hispanica related to SH1 and HHIV-2. Archaea 2013:456318
73. Zhang Z, Liu Y, Wang S, Yang D, Cheng Y, Hu J, Chen J, Mei Y, Shen P, Bamford DH et al (2012) Temperate membrane-containing halophilic archaeal virus SNJ1 has a circular dsDNA genome identical to that of plasmid pHH205. Virology 434:233–241
74. Pawlowski A, Rissanen I, Bamford JK, Krupovic M, Jalasvuori M (2014) Gammasphaerolipovirus, a newly proposed bacteriophage genus, unifies viruses of halophilic archaea and thermophilic bacteria within the novel family Sphaerolipoviridae. Arch Virol 159:1541–1554
75. Demina TA, Pietilä MK, Svirskaite J, Ravantti JJ, Atanasova NS, Bamford DH, Oksanen HM (2017) HCIV-1 and other tailless icosahedral internal membrane-containing viruses of the family Sphaerolipoviridae. Viruses 9:32
76. Rissanen I, Grimes JM, Pawlowski A, Mantynen S, Harlos K, Bamford JK, Stuart DI (2013) Bacteriophage P23-77 capsid protein structures reveal the archetype of an ancient branch from a major virus lineage. Structure 21:718–726
77. Gil-Carton D, Jaakkola ST, Charro D, Peralta B, Castaño-Díez D, Oksanen HM, Bamford DH, Abrescia NG (2015) Insight into the assembly of viruses with vertical single beta-barrel major capsid proteins. Structure 23:1866–1877
78. Jäälinoja HT, Roine E, Laurinmäki P, Kivelä HM, Bamford DH, Butcher SJ (2008) Structure and host-cell interaction of SH1, a membrane-containing, halophilic euryarchaeal virus. Proc Natl Acad Sci USA 105:8008–8013
79. Santos-Pérez I, Charro D, Gil-Carton D, Azkargorta M, Elortza F, Bamford DH, Oksanen HM, Abrescia NG (2019) Structural basis for assembly of vertical single β-barrel viruses. Nat Commun 10:1184
80. De Colibus L, Roine E, Walter TS, Ilca SL, Wang X, Wang N, Roseman AM, Bamford D, Huiskonen JT, Stuart DI (2019) Assembly of complex viruses exemplified by a halophilic euryarchaeal virus. Nat Commun 10:1456
81. Chibani-Chennoufi S, Bruttin A, Dillmann ML, Brussow H (2004) Phage-host interaction: an ecological perspective. J Bacteriol 186:3677–3686

82. Kauffman KM, Hussain FA, Yang J, Arevalo P, Brown JM, Chang WK, VanInsberghe D, Elsherbini J, Sharma RS, Cutler MB et al (2018) A major lineage of non-tailed dsDNA viruses as unrecognized killers of marine bacteria. Nature 554:118–122
83. Laanto E, Mantynen S, De Colibus L, Marjakangas J, Gillum A, Stuart DI, Ravantti JJ, Huiskonen JT, Sundberg LR (2017) Virus found in a boreal lake links ssDNA and dsDNA viruses. Proc Natl Acad Sci U S A 114 (31):8378–8383. https://doi.org/10.1073/pnas.1703834114
84. Gill JJ, Wang B, Sestak E, Young R, Chu KH (2018) Characterization of a novel tectivirus phage Toil and its potential as an agent for biolipid extraction. Sci Rep 8:1062
85. Philippe C, Krupovic M, Jaomanjaka F, Claisse O, Petrel M, le Marrec C (2018) Bacteriophage GC1, a novel tectivirus infecting Gluconobacter cerinus, an acetic acid bacterium associated with wine-making. Viruses 10:39
86. Fisher MB, Love DC, Schuech R, Nelson KL (2011) Simulated sunlight action spectra for inactivation of MS2 and PRD1 bacteriophages in clear water. Environ Sci Technol 45: 9249–9255
87. Harvey RW, Ryan JN (2004) Use of PRD1 bacteriophage in groundwater viral transport, inactivation, and attachment studies. FEMS Microbiol Ecol 49:3–16
88. Gallandat K, Lantagne D (2017) Selection of a Biosafety Level 1 (BSL-1) surrogate to evaluate surface disinfection efficacy in Ebola outbreaks: comparison of four bacteriophages. PLoS One 12:e0177943
89. Turgeon N, Toulouse MJ, Martel B, Moineau S, Duchaine C (2014) Comparison of five bacteriophages as models for viral aerosol studies. Appl Environ Microbiol 80:4242–4250
90. Scarpellini E, Ianiro G, Attili F, Bassanelli C, De Santis A, Gasbarrini A (2015) The human gut microbiota and virome: potential therapeutic implications. Dig Liver Dis 47:1007–1012

Chapter 6
Structure and Function of Negri Bodies

Jovan Nikolic, Cécile Lagaudrière-Gesbert, Nathalie Scrima, Danielle Blondel, and Yves Gaudin

Abstract Replication and assembly of many viruses occur in viral factories which are specialized intracellular compartments formed during viral infection. For rabies virus, those viral factories are called Negri bodies (NBs). NBs are cytoplasmic inclusion bodies in which viral RNAs (mRNAs as well as genomic and antigenomic RNAs) are synthesized. NBs are spherical, they can fuse together, and can reversibly deform when encountering a physical barrier. All these characteristics are similar to those of eukaryotic membrane-less liquid organelles which contribute to the compartmentalization of the cell interior. Indeed, the liquid nature of NBs has been confirmed by FRAP experiments. The co-expression of rabies virus nucleoprotein N and phosphoprotein P is sufficient to induce the formation of cytoplasmic inclusions recapitulating NBs properties. Remarkably, P and N have features similar to those of cellular proteins involved in liquid organelles formation: N is an RNA-binding protein and P contains intrinsically disordered domains. An overview of the literature indicates that formation of liquid viral factories by phase separation is probably common among Mononegavirales. This allows specific recruitment and concentration of viral proteins. Finally, as virus-associated molecular patterns recognized by cellular sensors of RNA virus replication are probably essentially present in the viral factory, there should be a subtle interplay (which remains to be characterized) between those liquid structures and the cellular proteins which trigger the innate immune response.

Keywords Rabies virus · Viral factory · Negri bodies · Liquid organelles · Phase separation

J. Nikolic · C. Lagaudrière-Gesbert · N. Scrima · D. Blondel (✉) · Y. Gaudin (✉)
Institute for Integrative Biology of the Cell (I2BC), CEA, CNRS, Univ. Paris-Sud, Université Paris-Saclay, Gif-sur-Yvette cedex, France
e-mail: danielle.blondel@i2bc.paris-saclay.fr; yves.gaudin@i2bc.paris-saclay.fr

U. F. Greber (ed.), *Physical Virology*, Advances in Experimental Medicine and Biology 1140, https://doi.org/10.1007/978-3-030-14741-9_6

Abbreviations

aa	Amino acid
BHK21	Baby Hamster Kidney 21 cells
FAK	Focal adhesion kinase
FRAP	Fluorescence recovery after photobleaching
IDD	Intrinsically disordered domain
le	Leader RNA
NB	Negri body
PML	Promyelocytic leukemia protein
RABV	Rabies virus
RdRP	RNA-dependent RNA polymerase
RNP	Ribonucleoprotein
VSV	Vesicular stomatitis virus

6.1 Viral Factories: An Overview

Replication and assembly of many viruses occur in specialized intracellular compartments formed during viral infection. These structures, known as viral factories, viral inclusions, or viroplasms, concentrate viral proteins, nucleic acids, and cellular factors to build a platform facilitating viral replication and protecting the viral genome from cellular defense mechanisms. Such viral factories are widespread in the viral world and have been identified for a variety of non-related viruses [1, 2].

The location and the nature of viral factories are very heterogeneous. The first viral factories which were characterized were those of large DNA viruses such as the Poxviridae, the Iridoviridae, and the Asfaviridae [3–6]. Those factories are devoid of membrane, located in close proximity to the microtubule organizing center. They have several characteristics reminiscent of those of the cellular aggresomes which concentrate misfolded proteins in the cell [7]. They recruit mitochondria, contain molecular chaperones such as HSP proteins, and are surrounded by a vimentin cage. In the case of positive strand RNA viruses, viral factories are associated with rearrangements of membranes from diverse organelles (Mitochondria, ER, etc.) leading to the formation of double-membrane vesicles [8–10]. The inner of these vesicles remain connected to the cytoplasm by channels which allow ribonucleotide import and product RNA export.

Several negative strand RNA viruses also induced the formation of membraneless cytoplasmic inclusions which, in the case of rhabdoviruses [11–13], filoviruses [14], and respiratory syncytial virus [15], have been demonstrated to harbor several viral replication stages. In the case of rabies virus (RABV), those inclusions are called Negri bodies (NBs) [16].

6.2 Rhabdoviruses and Rabies Virus

Rhabdoviruses (order Mononegavirales, MNV) constitute a family of viruses having a particularly broad host range among a great diversity of organisms including plants, insects, fishes, mammals, reptiles, and crustaceans. They are associated with significant pathologies in humans and livestock [17]. The prototypes of this family are vesicular stomatitis virus (VSV), a member of the Vesiculovirus genus, and RABV, a member of the Lyssavirus genus.

RABV is a neurotropic virus that causes acute encephalitis in humans and animals with almost always lethal outcomes. Human rabies is a zoonosis, which still accounts for ~50,000 deaths per year worldwide even though effective vaccines are available. RABV virions have a bullet-like shape which is rounded at one end and flat at the other, with a diameter of ~75 nm and a length of ~180 nm. The genome consists of a negative sense, single-stranded RNA molecule of approximately 12 kb, flanked on both sides by noncoding leader and trailer RNA regions. It comprises only five genes that are common to all members of the family which, starting from the 3′ terminus, encode successively the nucleoprotein (N, 450aa), the phosphoprotein (P, 297aa), the matrix protein (M, 202aa), the glycoprotein (G, 505aa), and the large subunit of the RNA-dependent RNA polymerase—RdRp—(L, 2128aa). The viral RNA is tightly associated with the nucleoprotein (N) to form a helical nucleocapsid. This nucleocapsid interacts with the viral RdRp complex, composed of L and its non-enzymatic cofactor P, to form the ribonucleoprotein (RNP). The RNP is enwrapped by a lipid bilayer which is derived from a host cell membrane during the budding process. The matrix protein (M) is located beneath the viral membrane and bridges the RNP and the lipid bilayer which contains a single transmembrane glycoprotein (G) that is involved in viral entry.

The cellular cycle of rhabdoviruses is entirely cytoplasmic (Fig. 6.1). After binding to a receptor, the viral particle enters the cell via the endocytic pathway [18–20]. Thereafter, the acidic environment within early endosomes induces a conformational change of G that catalyzes fusion of the viral envelope with the endosomal membrane [21]. This results in the cytoplasmic release of the negative-sense RNP which constitutes the template for viral gene expression and replication by the RdRp complex. Transcription begins at the 3′ end of the genome RNA and results in the synthesis of a positive, uncapped, and short leader RNA (le) and five capped and polyadenylated mRNAs encoding the five viral proteins. During this process, the RdRp complex is thought to dissociate from the template at each stop signal and to reinitiate at the next start signal. The process continues until the enzyme reaches the end of the L gene. As some complexes fail to reinitiate transcription of the downstream gene, there is a concentration gradient of the amount of each mRNA depending on the position of the corresponding gene (i.e., [le] > [N mRNA] > [P mRNA] > [M mRNA] > [G mRNA] > [L mRNA]). Viral mRNAs are then translated by the host cell translation machinery providing a source of N protein necessary to encapsidate the nascent RNA. This results in the

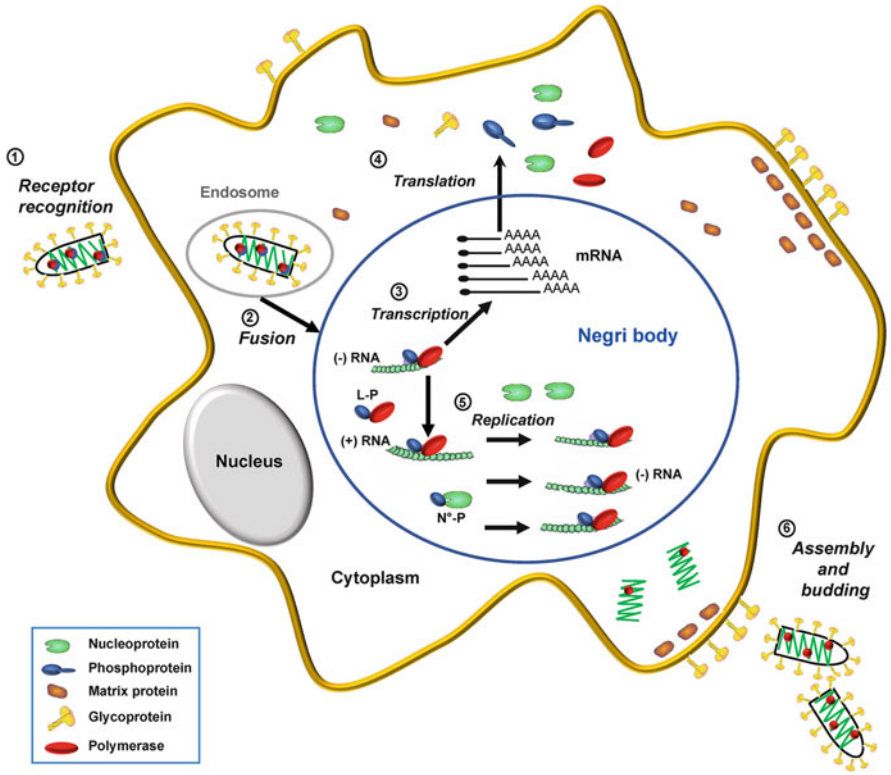

Fig. 6.1 Rabies virus life cycle. Rabies virus replicates in the cytoplasm of the host cell. Several steps can be observed: entry phase involving the binding of viral particles to receptors (step 1), endocytosis followed by membrane fusion and nucleocapsid release (step 2), transcription of mRNA (step 3), translation of the viral mRNAs by the cell machinery (step 4), replication (step 5), and finally virus assembly and progeny virus budding (step 6). Viral transcription and replication take place in Negri bodies

switch of the activity of the RdRp complex from transcription to replication to produce RNPs containing full-length antigenomic RNA (positive sense), which in turn serve as templates for the synthesis of genomic RNA (negative sense) [22]. RABV transcription and replication take place within NBs [12] which constitute the topic of this review.

The neo-synthesized genomic RNPs then serve as templates for additional rounds of transcription and/or replication [22]. They can also be addressed to membranes enriched in both M and G proteins where interactions between RNP, M, and G drive the assembly of viral particles and subsequent budding.

6.3 RABV Transcription and Replication Machinery

In association with the RNA genome, N forms the nucleocapsid, an N-RNA complex which constitutes the template for both transcription and replication and also protects the genome against innate immune receptors and cellular nucleases. Free N protein (N°) plays a crucial role in the switch from transcription to replication as it binds to nascent leader RNA, prevents recognition of termination signals, and leads to the encapsidation of the viral RNA, thus promoting the synthesis of an encapsidated full-length antigenome rather than the production of individual viral mRNAs [23].

The crystal structure of a nucleocapsid-like ring (Fig. 6.2a), formed by an undecamer of N proteins oligomer associated with RNA, has been solved [24]. N is a two domain protein (N-terminal core domain—NTD- and C-terminal core domain—CTD-) associated with nine nucleotides of single-stranded RNA (Fig. 6.2b). The RNA is positioned in a positively charged cleft located between

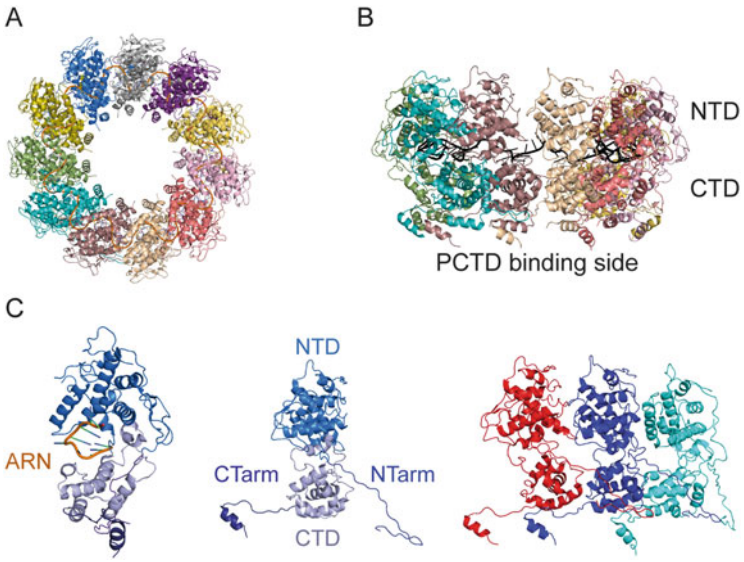

Fig. 6.2 Crystal structure of RABV N protein in association with RNA. Ribbon diagram of a top view of RABV N_{11}-ring in association with RNA (PDB Code 2GTT). The RNA molecule is in orange. All the protomers are colored differently. Lateral view of the ring (from the outside) with the NTD at the top and the CTD at the bottom. The RNA molecule is shown as a ribbon and black sticks. Left panel: side view of an N protomer showing how the RNA molecule (in orange) is positioned in the positively charged cleft located between the NTD and the CTD. Central panel: N protomer viewed from the outside of the ring indicating the position of the N-terminal core—NTD- and C-terminal core—CTD-domains together with the N and C-terminal extensions (NTarm and CTarm). Right panel: ribbon diagram of three consecutive N protomers showing the RNP-stabilizing interactions between the CTD of one protomer (in blue), the NTarm of the previous one (in red), and the CTarm of the next one (in cyan)

the NTD and the CTD (Fig. 6.2c) through interactions with the sugar-phosphate backbone.

There are also two N-terminal and C-terminal extensions (NTarm and CTarm) that only adopt a stable structure in the context of nucleocapsid-like complexes (Fig. 6.2c). There are no significant interactions between the NTDs within the ring structure. The stability of the nucleocapsid-like structure is ensured by the bound RNA and interactions between the CTD of one N protomer and the NTarm of the previous one, and the CTarm of the next one (Fig. 6.2c). The RNA is completely enwrapped in the nucleocapsid-like structure [24]. As a consequence, the RdRp cannot have access to the RNA and a conformational change in N is necessary in order to release the RNA from the nucleocapsid for transcription or replication.

The RdRp complex is made by L associated with its nonenzymatic cofactor P. In addition to its RdRp activity [25], L catalyzes an unusual sequence of mRNA capping reactions [26, 27] and polyadenylates the viral mRNAs [28]. The structure of L protein has been recently determined by electron microscopy [29].

P is a multifunctional protein which is essential in viral transcription and replication. These functions are dependent on sequences which enable the P protein to interact with L and N. Indeed, P is a modular protein (Fig. 6.3a) containing an N-terminal domain (PNTD) which binds the polymerase L and N° (the soluble form

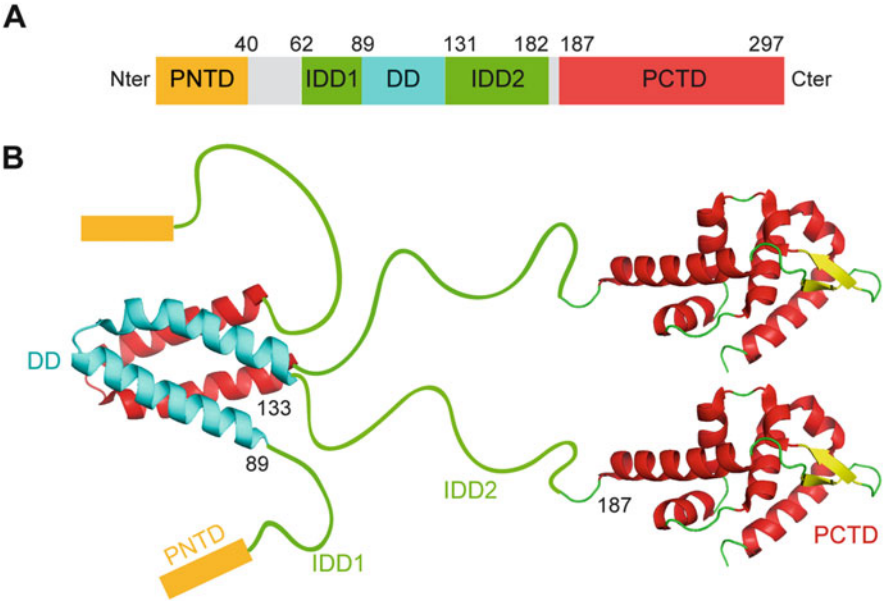

Fig. 6.3 RABV P is a modular protein. (**a**) Domain organization of RABV P polypeptide chain. P contains an N-terminal domain which binds to L and N° (PNTD), two intrinsically disordered domains (IDD1 and IDD2), a dimerization domain (DD), and a C-terminal domain which binds to N-RNA (PCTD). (**b**) Model of RABV P dimer. The X-ray structures of the dimerization domain (DD, PDB Code: 3L32) (one protomer colored in cyan, the other in red) and the C-terminal domain (PCTD: PDB code: 1VYI) are displayed

of N protein devoid of RNA), a C-terminal domain (PCTD) which binds N associated with RNA, and two central intrinsically disordered domains (IDD1 and IDD2) flanking a dimerization domain (DD) [30]. P is also phosphorylated at multiple serine residues by protein kinase-C and another cellular kinase yet unidentified [31]. P phosphorylation is not required for its oligomerization [32] and its role on viral transcription and replication is unknown.

The N-terminal region of RABV P (1–20 residues) associates with L [33, 34] to form the active RdRp, which uses the N-RNA complex rather than the naked RNA as a functional template. The first 40 amino acids are involved in forming the N°P complex. In this complex, in which one molecule of N° binds a dimer of P [35], P acts as a chaperone by binding the N alone in order to keep it from binding nonspecifically to cellular RNA and to prevent N from self-assembling. In the case of VSV, the N° binding domain of P is sufficient for keeping N° in a soluble form preventing its association with RNA and assembly into nucleocapsid by filling the RNA-binding cavity on the side of N that accommodates the 3′-end of the RNA molecule [36]. It is worth noting that when engaged with N°, P cannot bind L. The central domain (residues 91–132) of P is the dimerization domain [30]. For rabies virus the domain consists of two helical hairpins that stick together and are stabilized by extensive hydrophobic contacts [37] (Fig. 6.3b). The role of dimerization in the viral cycle is still not known.

The C-terminal domain of P binds to the nucleocapsid (i.e., N associated with RNA) and attaches the polymerase complex to its template [30, 38, 39]. This domain has the shape of a lengthwise cut pear (Fig. 6.3b). Several charged amino acid residues located on both the round and the flat side of the domain have been shown to be involved in nucleocapsid binding [38, 40]. In complex with the nucleocapsid, P interacts with both L and N, which allows the correct positioning of the RdRp on its template. A crystal structure of a ring of VSV nucleoproteins in complex with the C-terminal domain of P has been determined. In the crystal, P binds primarily to the C-terminal domains of two adjacent N proteins [41].

P is also the major viral counteractant of the innate immunity [42]. Direct interaction of P with STAT1 leads to the inhibition of interferon (IFN) signaling by different processes including sequestration of STAT1 away from the nuclear compartment [43], and inhibition of STAT1-DNA binding [44]. In addition, P interacts with the IFN-induced promyelocytic leukemia (PML) protein, alters PML nuclear bodies by retaining PML in the cytoplasm [45], and consequently is thought to counteract the antiviral effect of isoform PML IV against RABV [46]. Furthermore, P has a critical role in suppression of IFN production through blocking the phosphorylation of the transcription factor interferon regulatory factor 3 (IRF-3) [47].

Finally, P has been shown to interact with several other partners including the dynein light chain (LC8) [48–50], the focal adhesion kinase (FAK) [51], and the nucleolin [52]. Those interactions have been shown to favor viral infection [51, 53], but the molecular basis of their role remains unknown.

6.4 Negri Bodies

NBs are cytoplasmic inclusion bodies having a diameter up to a few μm. They have been discovered by Adelchi Negri in 1903 [16, 54] and are easily observed using Seller's staining (a mixture of saturated solution of basic fuschin and methylene blue dissolved in methanol). These structures are typical of RABV infection of the brain and, as a consequence, have been used as a histological proof of the infection.

Similar structures, which are also referred as NBs, are observed in the cytoplasm of cell culture of both neuronal and non-neuronal origin [12, 13] (Fig. 6.4a). In electron microscopy, they appear as homogeneous dense spherical structures [12, 55] (Fig. 6.4b). At late stage of infections (16 h p.i. and after), they often wrap in a double membrane, most probably derived from rough endoplasmic reticulum [12], and their shape appears to be altered [12, 55]. At 24 h p.i., viral particles are observed budding from NBs into the compartment delimited by the associated double membrane [12, 56].

Confocal microscopy and electron microscopy after immune-gold labeling revealed that N and P proteins selectively partition in NBs [12] which also concentrate L protein [57] together with Hsp 70 [12, 58], FAK [51], chaperonins CCTα and CCTγ [59, 60], endothelial nitric oxide synthase [61], and ubiquitinylated proteins [12].

Some authors have also reported that part of RABV M protein is associated with NBs [62]. Menager et al. [13] have also reported that, after 24 h of infection, Toll-Like Receptor 3 (TLR3) aggregates are detected in some NBs (but not all of them). As TLR3 is a membrane protein, this association is probably a late event when NBs associate with ER-derived membranes. The same authors have also suggested a major role of TLR3 in the formation of NBs based on silencing experiments [13]. However, in those experiments, cells in which TLR3 was silenced did not express N protein (and thus could not form NBs).

Fluorescence in situ hybridization (FISH) experiments indicated that viral mRNAs as well as antigenomic and genomic RNAs accumulate in NBs [12]. Finally, short-term RNA labeling in the presence of BrUTP followed by immunofluorescence staining using anti-BrdU demonstrated that newly synthesized viral RNA are located inside NBs [12]. This proved that NBs are bona fide viral factories.

At early time p.i., there is a limited number (up to 2 per cell) of NBs [12, 55]. Those initial NBs, most probably formed around incoming RNPs, grow with time and eventually exceed 1 μm in diameter at later stages of infection. At that time, they cohabit with intermediate inclusions having from 0.3 to 1 μm in diameter (a few tens per cell), and punctate structures (several hundred per cell) which have been shown to correspond to condensed RNPs [55]. Those newly formed RNPs were ejected out of NBs and transported further away across the cell along microtubules. Then, they can give rise either to new virions upon budding at a cell membrane or to new viral factories which form NBs of intermediate size [55].

As NBs were spherical structures, this suggested that they were liquid organelles formed by phase separation. Eukaryotic cells contain several kind of membrane-less

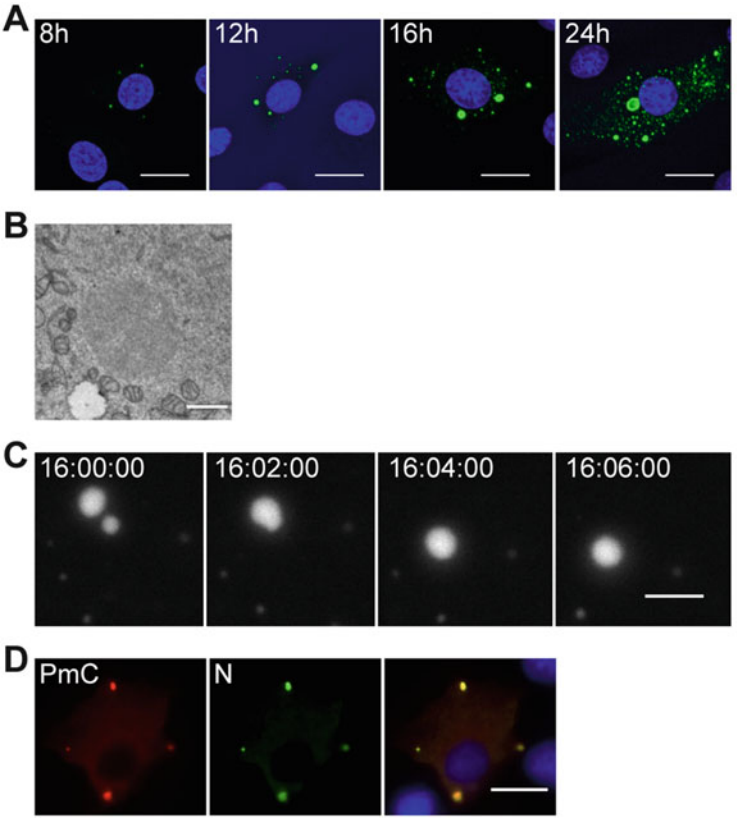

Fig. 6.4 Negri bodies are liquid organelles. (**a**) BSR cells (a clone of BHK21 cells) were infected with CVS strain at a MOI of 0.5 and fixed at different times p.i. (8 h, 12 h, 16 h, 24 h). Confocal analysis was performed after staining with a mouse monoclonal anti-N antibody followed by incubation with Alexa-488 donkey anti-mouse IgG. DAPI was used to stain the nuclei. Scale bars correspond to 15 μm. (**b**) EM characterization of the ultrastructural aspects of NBs displaying an electron dense granular structure. Scale bar: 1 μm. (**c**) NBs can fuse together. BSR cells, infected by a recombinant RABV expressing a P protein fused to mCherry, were imaged at the indicated time. Images are shown at 2 min intervals. Scale bars: 3 μm. (**d**) Co-expression of RABV N and P proteins leads to the formation of inclusion bodies recapitulating NB properties. BSR cells constitutively expressing the T7 RNA polymerase (BSR-T7/5) were co-transfected by plasmids pTit-P and pTit-N [55]. N was revealed with a mouse monoclonal anti-N antibody followed by incubation with Alexa-488 donkey anti-mouse IgG, and P was revealed with a rabbit polyclonal anti-P antibody followed by incubation with Alexa-568 donkey anti-rabbit IgG. DAPI was used to stain the nuclei

liquid organelles which contribute to the compartmentalization of the cell interior [63–66]. These compartments are involved in a wide range of cell processes. In the literature, they are referred as droplet organelles, proteinaceous membrane-less organelles, or biomolecular condensates. They can be located either in the nucleus (which is the case for Cajal Bodies [67], nucleoli [68, 69], and nuclear speckles [70])

or in the cytosol, for example stress granules (SG) [71, 72] and P-bodies [64]. The liquid organelles are highly enriched in some proteins that are much more concentrated in those structures than in the cytosol, as a result of liquid–liquid demixing phase separation [66].

The liquid nature of NBs was confirmed by live cell imaging using a recombinant RABV expressing a P protein C-terminally fused to the mCherry fluorescent protein. First, it was shown that when two NBs contact one another, they readily fuse and round up into a single larger sphere (Fig. 6.4c). Second, it was observed that they reversibly deform when encountering a physical barrier. Finally, FRAP measurement, during which fluorescent P-mCherry located inside NBs was photobleached, definitively demonstrated the liquid nature of NBs and that P, although more concentrated in NBs, is able to shuttle between the cytosol and the viral factories [55].

The liquid properties of NBs explain why in the presence of Nocodazole (NCZ), a drug which depolymerizes microtubules, NBs of intermediate size are absent and a single-large NB is observed which is bigger than those observed in the absence of the drug. In the presence of NCZ, RNPs are still ejected from NBs but cannot be transported further away. As a consequence, the newly formed viral factories remain located in the vicinity of, and rapidly fuse with the initial NB which then becomes much larger [55].

Different kinds of liquid organelles may be simultaneously present in the cell without any mixing of their content. This immiscibility of cellular liquid phases has been demonstrated to underlie the formation of nucleolar subcompartments [69]. Similarly, in the context of RABV infection, it has been shown that NBs and SGs come into close contact but do not fuse together [55]. Nevertheless, transfer of viral mRNAs from NBs to SGs was observed, of which the molecular basis is unknown [72].

Although they differ in size and composition, almost all liquid organelles contain proteins having IDDs and RNA-binding proteins [65, 66, 73]. Recent studies have also pinpointed the role of RNA in their formation and the modulation of their fluidity [74, 75]. In line with those observations, the two major proteins found in NBs are P which contains two intrinsically disordered domains [30] and N which binds RNA [24]. The co-expression of N and P after cell transfection is indeed sufficient to induce the formation of spherical cytoplasmic inclusions having the same liquid properties as NBs (Fig. 6.4d). It is probable that in such N–P inclusions, N is associated with cellular RNAs and forms N-RNA rings and short RNP-like structures [35]. Using this system, it was shown that the central DD, the amino terminal part of IDD2, and the PCTD (which binds to RNA-associated N protein) were required for NB-like structures formation [55]. A schematic model for the phase separated Negri bodies in RABV infected cells is shown in Fig. 6.5.

It has been proposed that the phase separation, leading to the formation of liquid organelles, is driven by weak interactions [66]. They may involve IDDs but may also occur between IDDs and RNA, as RNA, being a highly charged molecule, can contribute to electrostatic interactions with positively charged residues in IDDs [65]. Indeed, in vitro experiments show that phase separation is highly sensitive to

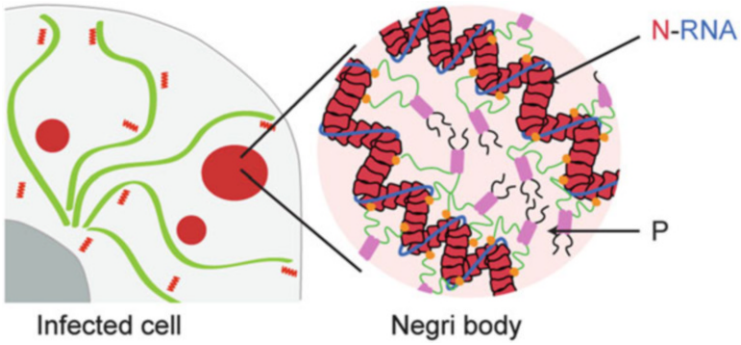

Fig. 6.5 Scheme of Negri body organization. The cohesion of the liquid phase is most probably ensured by weak interactions between P IDDS (and eventually RNA)

salt concentration [75, 76] and in vivo liquid organelles respond rapidly to cellular osmotic shock [76]. In the case of RABV infection, a hypotonic shock resulted in a fast and complete disappearance of NBs followed by their reformation in ~15 min [55].

The sequence of the amino-terminal part of IDD2 is strongly biased toward polar and charged residues which is a common feature of IDDs [66, 77]. However, this sequence is very poorly conserved among lyssavirus genus compared to the rest of P aa sequence [55]. Therefore, the ability of IDD2 to induce phase separation does not rely in its aa sequence but rather in some global physicochemical properties which remain to be characterized.

6.5 Implications of the Liquid Nature of Viral Factories

The literature suggests that, besides RABV, several negative strand RNA viruses form viral factories with properties of liquid organelles. As a non-exhaustive list of examples, we will mention (1) the replication centers of filoviruses that form perinuclear spherical inclusions [14, 78], (2) the N and P proteins of paramyxoviruses which form spherical inclusions during the infection or when co-expressed in the cell [79–81], (3) the Borna virus phosphoprotein which is also found in spherical inclusions in the nucleus of infected cells [82], and (4) the spherical inclusions which concentrate Bunyavirus genome segments [83]. It is highly probable that liquid viral factories will be identified beyond negative strand RNA viruses and probably beyond eukaryotic viruses. Indeed, nucleus-like structures formed upon bacteriophage infection have also characteristics of liquid organelles [84].

The liquid nature of the viral factories is certainly a requirement for optimal transcription and replication. Indeed, it is difficult to imagine the working of the RdRp complex in a solid or in a gel state. Furthermore, liquid–liquid phase

separation is an efficient process to enrich the viral factories in factors which are required for viral transcription or replication. Those factors can be recruited by two different ways. First, their physicochemical properties can induce their preferential partitioning in the NB liquid phase. Second, they may be recruited by a viral or cellular protein which itself preferentially partitions in the NBs. Indeed, several partners of P (which although more concentrated in NBs is able to shuttle between these liquid compartments and the cytosol) are concentrated in NBs [12, 51, 55].

The fact that viral factories are liquid organelles may also lead to some paradigm shift in the field of innate immunity. On one hand, phase separation may exclude proteins with antiviral properties from the viral factories (in which the virus-associated molecular patterns recognized by cellular sensors of RNA virus replication are particularly abundant). On the other hand, the seemingly ubiquitous nature of liquid viral factories among negative strand RNA viruses makes them a signature of infection. It is thus highly probable that the cell has developed mechanisms sensing the presence of such structures. If this is the case, viruses have in turn evolved to increase the furtiveness of their factories. From this point of view, the fact that SGs, which contain virus-associated pattern recognition receptor such as RIG-I [85] and MDA-5 [72], cannot fuse with NBs, but that transfer of viral mRNAs nevertheless occurs from NBs to SGs reveals a subtle interplay between RABV viral factories and innate immunity [72]. It is worth noting that VSV has evolved a different way of dealing with SGs: in this case, infection also induces the formation of SG-like structures which, however, colocalize with viral replication proteins and RNA [86].

At some stage, the virus has to escape from the viral factory. For RABV, two independent phenomena seem to contribute to this process. The first one is the microtubule-independent ejection of RNPs from NBs. Although the molecular basis for this process is unknown, an attractive hypothesis is that a conformational change of RNPs (e.g., their compaction) changes their physicochemical properties and drastically decreases their solubility in the NB liquid phase, which provokes their ejection in the cytoplasm. The second way for the virus to escape from NBs occurs at the latest stages of infection when a double membrane is wrapped around the viral factory, thus allowing direct budding of neo-synthesized virions in intracellular compartments. Here again, the molecular basis of the association between the liquid compartment and the membrane is unknown. Finally, the liquid–liquid phase separation which gives rise to the viral factory ensures that the virus keeps its identity in the cell cytoplasm. Therefore, rabies virus and most probably other negative strand viruses exist under two distinct states: a virion, outside the cell, and a liquid organelle, which is the cellular state of the virus.

Acknowledgments This work was supported by the CNRS and by a grant from the Fondation pour la Recherche Médicale (FRM DEQ20120323711) to Y.G.

References

1. Netherton CL, Wileman T (2011) Virus factories, double membrane vesicles and viroplasm generated in animal cells. Curr Opin Virol 1(5):381–387. https://doi.org/10.1016/j.coviro.2011.09.008
2. Novoa RR, Calderita G, Arranz R, Fontana J, Granzow H, Risco C (2005) Virus factories: associations of cell organelles for viral replication and morphogenesis. Biol Cell 97 (2):147–172. https://doi.org/10.1042/BC20040058
3. Chinchar VG, Hyatt A, Miyazaki T, Williams T (2009) Family Iridoviridae: poor viral relations no longer. Curr Top Microbiol Immunol 328:123–170
4. Risco C, Rodriguez JR, Lopez-Iglesias C, Carrascosa JL, Esteban M, Rodriguez D (2002) Endoplasmic reticulum-Golgi intermediate compartment membranes and vimentin filaments participate in vaccinia virus assembly. J Virol 76(4):1839–1855
5. Rojo G, Garcia-Beato R, Vinuela E, Salas ML, Salas J (1999) Replication of African swine fever virus DNA in infected cells. Virology 257(2):524–536
6. Schramm B, Locker JK (2005) Cytoplasmic organization of POXvirus DNA replication. Traffic 6(10):839–846. https://doi.org/10.1111/j.1600-0854.2005.00324.x
7. Wileman T (2007) Aggresomes and pericentriolar sites of virus assembly: cellular defense or viral design? Annu Rev Microbiol 61:149–167. https://doi.org/10.1146/annurev.micro.57.030502.090836
8. Avila-Perez G, Rejas MT, Rodriguez D (2016) Ultrastructural characterization of membranous torovirus replication factories. Cell Microbiol 18(12):1691–1708. https://doi.org/10.1111/cmi.12620
9. Harak C, Lohmann V (2015) Ultrastructure of the replication sites of positive-strand RNA viruses. Virology 479-480:418–433. https://doi.org/10.1016/j.virol.2015.02.029
10. Kopek BG, Perkins G, Miller DJ, Ellisman MH, Ahlquist P (2007) Three-dimensional analysis of a viral RNA replication complex reveals a virus-induced mini-organelle. PLoS Biol 5(9): e220. https://doi.org/10.1371/journal.pbio.0050220
11. Heinrich BS, Cureton DK, Rahmeh AA, Whelan SP (2010) Protein expression redirects vesicular stomatitis virus RNA synthesis to cytoplasmic inclusions. PLoS Pathog 6(6): e1000958. https://doi.org/10.1371/journal.ppat.1000958
12. Lahaye X, Vidy A, Pomier C, Obiang L, Harper F, Gaudin Y, Blondel D (2009) Functional characterization of Negri bodies (NBs) in rabies virus-infected cells: Evidence that NBs are sites of viral transcription and replication. J Virol 83(16):7948–7958. https://doi.org/10.1128/JVI.00554-09
13. Menager P, Roux P, Megret F, Bourgeois JP, Le Sourd AM, Danckaert A, Lafage M, Prehaud C, Lafon M (2009) Toll-like receptor 3 (TLR3) plays a major role in the formation of rabies virus Negri Bodies. PLoS Pathog 5(2):e1000315. https://doi.org/10.1371/journal.ppat.1000315
14. Hoenen T, Shabman RS, Groseth A, Herwig A, Weber M, Schudt G, Dolnik O, Basler CF, Becker S, Feldmann H (2012) Inclusion bodies are a site of ebolavirus replication. J Virol 86 (21):11779–11788. https://doi.org/10.1128/JVI.01525-12
15. Rincheval V, Lelek M, Gault E, Bouillier C, Sitterlin D, Blouquit-Laye S, Galloux M, Zimmer C, Eleouet JF, Rameix-Welti MA (2017) Functional organization of cytoplasmic inclusion bodies in cells infected by respiratory syncytial virus. Nat Commun 8(1):563. https://doi.org/10.1038/s41467-017-00655-9
16. Negri A (1903) Contributo allo studio dell' eziologia della rabia. Bol Soc Med Chir Pavia 2:88–114
17. Dietzgen RG, Kondo H, Goodin MM, Kurath G, Vasilakis N (2017) The family Rhabdoviridae: mono- and bipartite negative-sense RNA viruses with diverse genome organization and common evolutionary origins. Virus Res 227:158–170. https://doi.org/10.1016/j.virusres.2016.10.010

18. Cureton DK, Massol RH, Saffarian S, Kirchhausen TL, Whelan SP (2009) Vesicular stomatitis virus enters cells through vesicles incompletely coated with clathrin that depend upon actin for internalization. PLoS Pathog 5(4):e1000394
19. Johannsdottir HK, Mancini R, Kartenbeck J, Amato L, Helenius A (2009) Host cell factors and functions involved in vesicular stomatitis virus entry. J Virol 83(1):440–453
20. Piccinotti S, Whelan SP (2016) Rabies internalizes into primary peripheral neurons via clathrin coated pits and requires fusion at the cell body. PLoS Pathog 12(7):e1005753. https://doi.org/10.1371/journal.ppat.1005753
21. Albertini AAV, Baquero E, Ferlin A, Gaudin Y (2012) Molecular and cellular aspects of rhabdovirus entry. Viruses 4(1):117–139
22. Albertini AA, Ruigrok RW, Blondel D (2011) Rabies virus transcription and replication. Adv Virus Res 79:1–22. https://doi.org/10.1016/B978-0-12-387040-7.00001-9
23. Blumberg BM, Leppert M, Kolakofsky D (1981) Interaction of VSV leader RNA and nucleocapsid protein may control VSV genome replication. Cell 23(3):837–845
24. Albertini AA, Wernimont AK, Muziol T, Ravelli RB, Clapier CR, Schoehn G, Weissenhorn W, Ruigrok RW (2006) Crystal structure of the rabies virus nucleoprotein-RNA complex. Science 313(5785):360–363. https://doi.org/10.1126/science.1125280
25. Emerson SU, Wagner RR (1973) L protein requirement for in vitro RNA synthesis by vesicular stomatitis virus. J Virol 12(6):1325–1335
26. Hercyk N, Horikami SM, Moyer SA (1988) The vesicular stomatitis virus L protein possesses the mRNA methyltransferase activities. Virology 163(1):222–225
27. Ogino T, Banerjee AK (2007) Unconventional mechanism of mRNA capping by the RNA-dependent RNA polymerase of vesicular stomatitis virus. Mol Cell 25(1):85–97. https://doi.org/10.1016/j.molcel.2006.11.013
28. Hunt DM, Smith EF, Buckley DW (1984) Aberrant polyadenylation by a vesicular stomatitis virus mutant is due to an altered L protein. J Virol 52(2):515–521
29. Liang B, Li Z, Jenni S, Rahmeh AA, Morin BM, Grant T, Grigorieff N, Harrison SC, Whelan SPJ (2015) Structure of the L protein of vesicular stomatitis virus from electron cryomicroscopy. Cell 162(2):314–327. https://doi.org/10.1016/j.cell.2015.06.018
30. Gerard FC, Ribeiro Ede A Jr, Leyrat C, Ivanov I, Blondel D, Longhi S, Ruigrok RW, Jamin M (2009) Modular organization of rabies virus phosphoprotein. J Mol Biol 388(5):978–996. https://doi.org/10.1016/j.jmb.2009.03.061
31. Gupta AK, Blondel D, Choudhary S, Banerjee AK (2000) The phosphoprotein of rabies virus is phosphorylated by a unique cellular protein kinase and specific isomers of protein kinase C. J Virol 74(1):91–98
32. Gigant B, Iseni F, Gaudin Y, Knossow M, Blondel D (2000) Neither phosphorylation nor the amino-terminal part of rabies virus phosphoprotein is required for its oligomerization. J Gen Virol 81. (Pt 7:1757–1761. https://doi.org/10.1099/0022-1317-81-7-1757
33. Castel G, Chteoui M, Caignard G, Prehaud C, Mehouas S, Real E, Jallet C, Jacob Y, Ruigrok RW, Tordo N (2009) Peptides that mimic the amino-terminal end of the rabies virus phosphoprotein have antiviral activity. J Virol 83(20):10808–10820. https://doi.org/10.1128/JVI.00977-09
34. Chenik M, Schnell M, Conzelmann KK, Blondel D (1998) Mapping the interacting domains between the rabies virus polymerase and phosphoprotein. J Virol 72(3):1925–1930
35. Mavrakis M, Iseni F, Mazza C, Schoehn G, Ebel C, Gentzel M, Franz T, Ruigrok RW (2003) Isolation and characterisation of the rabies virus N degrees-P complex produced in insect cells. Virology 305(2):406–414
36. Leyrat C, Yabukarski F, Tarbouriech N, Ribeiro EA Jr, Jensen MR, Blackledge M, Ruigrok RW, Jamin M (2011) Structure of the vesicular stomatitis virus N(0)-P complex. PLoS Pathog 7(9):e1002248. https://doi.org/10.1371/journal.ppat.1002248
37. Ivanov I, Crépin T, Jamin M, Ruigrok RW (2010) Structure of the dimerization domain of the rabies virus phosphoprotein. J Virol 84(7):3707–3710. https://doi.org/10.1128/JVI.02557-09

38. Mavrakis M, McCarthy AA, Roche S, Blondel D, Ruigrok RW (2004) Structure and function of the C-terminal domain of the polymerase cofactor of rabies virus. J Mol Biol 343(4):819–831. https://doi.org/10.1016/j.jmb.2004.08.071
39. Ribeiro Ede A Jr, Leyrat C, Gerard FC, Albertini AA, Falk C, Ruigrok RW, Jamin M (2009) Binding of rabies virus polymerase cofactor to recombinant circular nucleoprotein-RNA complexes. J Mol Biol 394(3):558–575. https://doi.org/10.1016/j.jmb.2009.09.042
40. Jacob Y, Real E, Tordo N (2001) Functional interaction map of lyssavirus phosphoprotein: identification of the minimal transcription domains. J Virol 75(20):9613–9622. https://doi.org/10.1128/JVI.75.20.9613-9622.2001
41. Green TJ, Luo M (2009) Structure of the vesicular stomatitis virus nucleocapsid in complex with the nucleocapsid-binding domain of the small polymerase cofactor, P. Proc Natl Acad Sci U S A 106(28):11713–11718. https://doi.org/10.1073/pnas.0903228106
42. Chelbi-Alix MK, Vidy A, El Bougrini J, Blondel D (2006) Rabies viral mechanisms to escape the IFN system: the viral protein P interferes with IRF-3, Stat1, and PML nuclear bodies. J Interf Cytokine Res 26(5):271–280. https://doi.org/10.1089/jir.2006.26.271
43. Vidy A, Chelbi-Alix M, Blondel D (2005) Rabies virus P protein interacts with STAT1 and inhibits interferon signal transduction pathways. J Virol 79(22):14411–14420. https://doi.org/10.1128/JVI.79.22.14411-14420.2005
44. Vidy A, El Bougrini J, Chelbi-Alix MK, Blondel D (2007) The nucleocytoplasmic rabies virus P protein counteracts interferon signaling by inhibiting both nuclear accumulation and DNA binding of STAT1. J Virol 81(8):4255–4263. https://doi.org/10.1128/JVI.01930-06
45. Blondel D, Regad T, Poisson N, Pavie B, Harper F, Pandolfi PP, De The H, Chelbi-Alix MK (2002) Rabies virus P and small P products interact directly with PML and reorganize PML nuclear bodies. Oncogene 21(52):7957–7970. https://doi.org/10.1038/sj.onc.1205931
46. Blondel D, Kheddache S, Lahaye X, Dianoux L, Chelbi-Alix MK (2010) Resistance to rabies virus infection conferred by the PMLIV isoform. J Virol 84(20):10719–10726. https://doi.org/10.1128/JVI.01286-10
47. Brzozka K, Finke S, Conzelmann KK (2005) Identification of the rabies virus alpha/beta interferon antagonist: phosphoprotein P interferes with phosphorylation of interferon regulatory factor 3. J Virol 79(12):7673–7681. https://doi.org/10.1128/JVI.79.12.7673-7681.2005
48. Jacob Y, Badrane H, Ceccaldi PE, Tordo N (2000) Cytoplasmic dynein LC8 interacts with lyssavirus phosphoprotein. J Virol 74(21):10217–10222
49. Poisson N, Real E, Gaudin Y, Vaney MC, King S, Jacob Y, Tordo N, Blondel D (2001) Molecular basis for the interaction between rabies virus phosphoprotein P and the dynein light chain LC8: dissociation of dynein-binding properties and transcriptional functionality of P. J Gen Virol 82. (Pt 11:2691–2696. https://doi.org/10.1099/0022-1317-82-11-2691
50. Raux H, Flamand A, Blondel D (2000) Interaction of the rabies virus P protein with the LC8 dynein light chain. J Virol 74(21):10212–10216
51. Fouquet B, Nikolic J, Larrous F, Bourhy H, Wirblich C, Lagaudriere-Gesbert C, Blondel D (2015) Focal adhesion kinase is involved in rabies virus infection through its interaction with viral phosphoprotein P. J Virol 89(3):1640–1651. https://doi.org/10.1128/JVI.02602-14
52. Oksayan S, Nikolic J, David CT, Blondel D, Jans DA, Moseley GW (2015) Identification of a role for nucleolin in rabies virus infection. J Virol 89(3):1939–1943. https://doi.org/10.1128/JVI.03320-14
53. Tan GS, Preuss MA, Williams JC, Schnell MJ (2007) The dynein light chain 8 binding motif of rabies virus phosphoprotein promotes efficient viral transcription. Proc Natl Acad Sci U S A 104(17):7229–7234. https://doi.org/10.1073/pnas.0701397104
54. Kristensson K, Dastur DK, Manghani DK, Tsiang H, Bentivoglio M (1996) Rabies: interactions between neurons and viruses. A review of the history of Negri inclusion bodies. Neuropathol Appl Neurobiol 22(3):179–187
55. Nikolic J, Le Bars R, Lama Z, Scrima N, Lagaudriere-Gesbert C, Gaudin Y, Blondel D (2017) Negri bodies are viral factories with properties of liquid organelles. Nat Commun 8(1):58. https://doi.org/10.1038/s41467-017-00102-9

56. Matsumoto S, Schneider LG, Kawai A, Yonezawa T (1974) Further studies on the replication of rabies and rabies-like viruses in organized cultures of mammalian neural tissues. J Virol 14 (4):981–996
57. Finke S, Brzozka K, Conzelmann KK (2004) Tracking fluorescence-labeled rabies virus: enhanced green fluorescent protein-tagged phosphoprotein P supports virus gene expression and formation of infectious particles. J Virol 78(22):12333–12343. https://doi.org/10.1128/JVI.78.22.12333-12343.2004
58. Lahaye X, Vidy A, Fouquet B, Blondel D (2012) Hsp70 protein positively regulates rabies virus infection. J Virol 86(9):4743–4751. https://doi.org/10.1128/JVI.06501-11
59. Zhang J, Wu X, Zan J, Wu Y, Ye C, Ruan X, Zhou J (2013a) Cellular chaperonin CCTgamma contributes to rabies virus replication during infection. J Virol 87(13):7608–7621. https://doi.org/10.1128/JVI.03186-12
60. Zhang J, Ye C, Ruan X, Zan J, Xu Y, Liao M, Zhou J (2014) The chaperonin CCTalpha is required for efficient transcription and replication of rabies virus. Microbiol Immunol 58 (10):590–599. https://doi.org/10.1111/1348-0421.12186
61. Shin T, Weinstock D, Castro MD, Hamir AN, Wampler T, Walter M, Kim HY, Acland H (2004) Immunohistochemical localization of endothelial and inducible nitric oxide synthase within neurons of cattle with rabies. J Vet Med Sci 66(5):539–541
62. Pollin R, Granzow H, Kollner B, Conzelmann KK, Finke S (2013) Membrane and inclusion body targeting of lyssavirus matrix proteins. Cell Microbiol 15(2):200–212. https://doi.org/10.1111/cmi.12037
63. Banani SF, Lee HO, Hyman AA, Rosen MK (2017) Biomolecular condensates: organizers of cellular biochemistry. Nat Rev Mol Cell Biol 18(5):285–298. https://doi.org/10.1038/nrm.2017.7
64. Brangwynne CP, Eckmann CR, Courson DS, Rybarska A, Hoege C, Gharakhani J, Julicher F, Hyman AA (2009) Germline P granules are liquid droplets that localize by controlled dissolution/condensation. Science 324(5935):1729–1732. https://doi.org/10.1126/science.1172046
65. Courchaine EM, Lu A, Neugebauer KM (2016) Droplet organelles? EMBO J 35 (15):1603–1612. https://doi.org/10.15252/embj.201593517
66. Uversky VN (2017) Intrinsically disordered proteins in overcrowded milieu: membrane-less organelles, phase separation, and intrinsic disorder. Curr Opin Struct Biol 44:18–30. https://doi.org/10.1016/j.sbi.2016.10.015
67. Handwerger KE, Cordero JA, Gall JG (2005) Cajal bodies, nucleoli, and speckles in the Xenopus oocyte nucleus have a low-density, sponge-like structure. Mol Biol Cell 16 (1):202–211. https://doi.org/10.1091/mbc.E04-08-0742
68. Brangwynne CP, Mitchison TJ, Hyman AA (2011) Active liquid-like behavior of nucleoli determines their size and shape in *Xenopus laevis* oocytes. Proc Natl Acad Sci U S A 108 (11):4334–4339. https://doi.org/10.1073/pnas.1017150108
69. Feric M, Vaidya N, Harmon TS, Mitrea DM, Zhu L, Richardson TM, Kriwacki RW, Pappu RV, Brangwynne CP (2016) Coexisting liquid phases underlie nucleolar subcompartments. Cell 165 (7):1686–1697. https://doi.org/10.1016/j.cell.2016.04.047
70. Marzahn MR, Marada S, Lee J, Nourse A, Kenrick S, Zhao H, Ben-Nissan G, Kolaitis RM, Peters JL, Pounds S, Errington WJ, Prive GG, Taylor JP, Sharon M, Schuck P, Ogden SK, Mittag T (2016) Higher-order oligomerization promotes localization of SPOP to liquid nuclear speckles. EMBO J 35(12):1254–1275. https://doi.org/10.15252/embj.201593169
71. Jain S, Wheeler JR, Walters RW, Agrawal A, Barsic A, Parker R (2016) ATPase-modulated stress granules contain a diverse proteome and substructure. Cell 164(3):487–498. https://doi.org/10.1016/j.cell.2015.12.038
72. Nikolic J, Civas A, Lama Z, Lagaudriere-Gesbert C, Blondel D (2016) Rabies virus infection induces the formation of stress granules closely connected to the viral factories. PLoS Pathog 12 (10):e1005942. https://doi.org/10.1371/journal.ppat.1005942
73. Nielsen FC, Hansen HT, Christiansen J (2016) RNA assemblages orchestrate complex cellular processes. BioEssays 38(7):674–681. https://doi.org/10.1002/bies.201500175

74. Berry J, Weber SC, Vaidya N, Haataja M, Brangwynne CP (2015) RNA transcription modulates phase transition-driven nuclear body assembly. Proc Natl Acad Sci U S A 112(38):E5237–E5245. https://doi.org/10.1073/pnas.1509317112
75. Elbaum-Garfinkle S, Kim Y, Szczepaniak K, Chen CC, Eckmann CR, Myong S, Brangwynne CP (2015) The disordered P granule protein LAF-1 drives phase separation into droplets with tunable viscosity and dynamics. Proc Natl Acad Sci U S A 112(23):7189–7194. https://doi.org/10.1073/pnas.1504822112
76. Nott TJ, Petsalaki E, Farber P, Jervis D, Fussner E, Plochowietz A, Craggs TD, Bazett-Jones DP, Pawson T, Forman-Kay JD, Baldwin AJ (2015) Phase transition of a disordered nuage protein generates environmentally responsive membraneless organelles. Mol Cell 57 (5):936–947. https://doi.org/10.1016/j.molcel.2015.01.013
77. Tompa P, Fuxreiter M (2008) Fuzzy complexes: polymorphism and structural disorder in protein-protein interactions. Trends Biochem Sci 33(1):2–8. https://doi.org/10.1016/j.tibs.2007.10.003
78. Schudt G, Kolesnikova L, Dolnik O, Sodeik B, Becker S (2013) Live-cell imaging of Marburg virus-infected cells uncovers actin-dependent transport of nucleocapsids over long distances. Proc Natl Acad Sci U S A 110(35):14402–14407. https://doi.org/10.1073/pnas.1307681110
79. Derdowski A, Peters TR, Glover N, Qian R, Utley TJ, Burnett A, Williams JV, Spearman P, Crowe JE Jr (2008) Human metapneumovirus nucleoprotein and phosphoprotein interact and provide the minimal requirements for inclusion body formation. J Gen Virol 89 (Pt 11):2698–2708. https://doi.org/10.1099/vir.0.2008/004051-0
80. Fearns R, Young DF, Randall RE (1994) Evidence that the paramyxovirus simian virus 5 can establish quiescent infections by remaining inactive in cytoplasmic inclusion bodies. J Gen Virol 75. (Pt 12:3525–3539. https://doi.org/10.1099/0022-1317-75-12-3525
81. Zhang S, Chen L, Zhang G, Yan Q, Yang X, Ding B, Tang Q, Sun S, Hu Z, Chen M (2013b) An amino acid of human parainfluenza virus type 3 nucleoprotein is critical for template function and cytoplasmic inclusion body formation. J Virol 87(22):12457–12470. https://doi.org/10.1128/JVI.01565-13
82. Charlier CM, Wu YJ, Allart S, Malnou CE, Schwemmle M, Gonzalez-Dunia D (2013) Analysis of borna disease virus trafficking in live infected cells by using a virus encoding a tetracysteine-tagged p protein. J Virol 87(22):12339–12348. https://doi.org/10.1128/JVI.01127-13
83. Wichgers Schreur PJ, Kortekaas J (2016) Single-molecule FISH reveals non-selective packaging of rift valley fever virus genome segments. PLoS Pathog 12(8):e1005800. https://doi.org/10.1371/journal.ppat.1005800
84. Chaikeeratisak V, Nguyen K, Khanna K, Brilot AF, Erb ML, Coker JK, Vavilina A, Newton GL, Buschauer R, Pogliano K, Villa E, Agard DA, Pogliano J (2017) Assembly of a nucleus-like structure during viral replication in bacteria. Science 355(6321):194–197. https://doi.org/10.1126/science.aal2130
85. Oh SW, Onomoto K, Wakimoto M, Onoguchi K, Ishidate F, Fujiwara T, Yoneyama M, Kato H, Fujita T (2016) Leader-containing uncapped viral transcript activates RIG-I in antiviral stress granules. PLoS Pathog 12(2):e1005444. https://doi.org/10.1371/journal.ppat.1005444
86. Dinh PX, Beura LK, Das PB, Panda D, Das A, Pattnaik AK (2013) Induction of stress granule-like structures in vesicular stomatitis virus-infected cells. J Virol 87(1):372–383. https://doi.org/10.1128/JVI.02305-12

Chapter 7
Virus Maturation

Carmen San Martín

Abstract A virus particle consists of a genome contained within a protein shell. This shell (the capsid) plays multiple roles throughout the infectious cycle, from genome protection to host recognition to successful genome delivery. When capsids first assemble in the cell, most often an initial product is obtained that has not achieved its fully infectious form. To do so, it must undergo a final process called maturation. Virus maturation entails conformational and stability changes. These changes are often driven by proteolytic cleavages, and their main purpose is to ensure successful delivery of the virus genome to a new host cell. Recent advances in molecular, structural, and physical virology techniques are providing a wealth of detailed information and new points of view to understand the principles of virus maturation. Evidence showing that viral capsids are built with a limited set of structural solutions has prompted a new virus classification in structural lineages deriving from a few initial ancestors. This chapter summarizes the current knowledge on maturation for the main virus structural lineages, as well as for other relevant viruses not assigned to any particular lineage yet.

Keywords Virus structure · Virus assembly · Capsid · Scaffold · Maturation · Stability · Uncoating · Virus proteases

Abbreviations

AdV	Adenovirus
AFM	Atomic force microscopy
AVP	Adenovirus protease
BTV	Bluetongue virus

C. San Martín (✉)
Department of Macromolecular Structure, Centro Nacional de Biotecnología (CNB-CSIC), Madrid, Spain
e-mail: carmen@cnb.csic.es

U. F. Greber (ed.), *Physical Virology*, Advances in Experimental Medicine and Biology 1140, https://doi.org/10.1007/978-3-030-14741-9_7

cryo-EM	Cryo-electron microscopy
EMD	Electron microscopy data bank
ER	Endoplasmic reticulum
FHV	Flock House virus
HIV	Human immunodeficiency virus
IBDV	Infectious bursal disease virus
ICTV	International Committee on Taxonomy of Viruses
MCP	Major coat protein
MS	Mass spectrometry
NCLDV	Nucleo-cytoplasmic large DNA viruses
PC	Bacteriophage Φ6 polymerase complex (PC)
PDB	Protein data bank
STED	Stimulated emission depletion

7.1 Introduction

Viruses are obligate parasites, unable to self-replicate unless inside the cells of a host organism [1]. In the host cell, the viral genome directs the production of progeny infectious virus particles, also known as virions. Virions are the vehicle for transmission of the viral genome to the next host, to initiate a new round of infection. Formation of viral particles starts with the synthesis of their components (proteins and genomes). Capsid proteins are assembled together to form a protective shell, into which the genome is encapsidated for its safe transport to a new host. Two morphogenetic pathways are possible: sequential, where the genome is injected into a preformed capsid using a motor complex, or concurrent, where the capsid is assembled around the genome. However, in most known viruses morphogenesis is not completed after synthesis, assembly, and packaging. A last step, called maturation, is required for the particle to achieve its fully infectious potential. Maturation induces structural and physical changes in the viral particle that enable it to deal with conflicting stability requirements throughout the infectious cycle, and prepare it for correct genome delivery to restart the cycle in a new host cell [2, 3].

On one hand, viral particles must be stable enough to survive deleterious environmental conditions such as extremes of temperature, osmotic shock, or dehydration. On the other hand, they must be able to disassemble at the correct time and place to successfully deliver their genome into the host cell. This conflict between stability and instability is overcome in many viruses by assembling metastable particles. Conformational rearrangements undergone during maturation are often the trigger to achieve a metastable state, primed to start the uncoating cascade upon receiving the appropriate cellular (e.g., receptor binding) or environmental (e.g., pH change) cue [4, 5]. These conformational rearrangements often involve cleavage by virus coded protease activities, which are incorporated into the viral particle and must be tightly regulated to avoid unspecific, untimely protein degradation.

Proteolytic cleavage is an irreversible process which, apart from structural rearrangements, may cause the removal of no longer needed elements such as scaffolding proteins, or the generation of lytic peptides. These are particularly important in non-enveloped viruses, which need to disrupt cellular membranes in their trafficking to and from the assembly site [6]. Morphological or physical changes induced by maturation ensure that these internal lytic peptides are released from the metastable capsid at the appropriate time and place. In enveloped viruses, cell proteases also play a role in maturation to prime the particle for membrane fusion, required for correct trafficking during entry in the new host cell. Posttranslational modifications such as myristoylations also play a role in preparing viruses for achieving their full infectious potential.

Recent methodological advances are helping us to understand new aspects on virus assembly and dynamics, including maturation. Biophysics techniques such as fluorescence or calorimetry, as well as structural biology methods, have been used to investigate the molecular basis of viral capsid maturation and stability. Among the latter, X-ray crystallography has been instrumental to provide high resolution structural insights, for those cases in which the specimen was amenable to crystallization [7]. Most viruses, however, are hardly compliant with the stringent requirements of highly ordered, large 3D crystal growth. In the past few years, cryo-electron microscopy (cryo-EM) methods have dramatically improved, so much so that at present, the resolution achievable by cryo-EM single particle averaging has converged with that obtained by X-ray crystallography of viral capsids [8, 9]. Unlike crystallography, cryo-EM can address the structural characterization of transient or fragile assembly or disassembly intermediates, provided that structurally homogeneous preparations can be obtained or extracted from heterogeneous datasets by image classification. In an alternative approach, cryo-electron tomography is also providing highly detailed structural information on the components of non-symmetrical viruses in their biological context [10].

In the last decade, the importance of understanding the physical properties of viral capsids has been recognized, not only from the nanoengineering point of view, but also for the biological relevance of these previously overlooked aspects [11]. On one hand, the fact that viral particles can fulfill the conflicting stability needs along the infectious cycle tells about their remarkable mechanical properties. On the other hand, a growing number of studies indicate that mechanical stress plays a significant role not only as a deleterious factor during the virus extracellular existence, but also as a determinant of infectious cycle processes such as cell entry [12]. Physical properties of virus particles are starting to be understood, thanks to the advances in single molecule techniques. A successful technique in this category is atomic force microscopy (AFM), which can be used not only to image the capsid surface, but also to interact with the specimen, applying and detecting forces in individual virus particles [13]. AFM allows measuring magnitudes such as stiffness or surface charge density, helping to relate structure to physical properties in single viral particles. Specifically devised, non-destructive imaging modes minimize sample damage and allow repeated data collection on the same viral particle in near physiological conditions [14, 15].

Other analytical techniques are being incorporated into the toolbox for large macromolecular complex characterization, and applied to the study of virus maturation. Advances in fluorescence-based methodologies offer the possibility to discern protein rearrangements in individual viral particles, or to sort them according to their maturation state [16, 17]. Mass spectrometry (MS) can nowadays address additional questions apart from the standard determination of viral particle composition by in-gel digestion or liquid chromatography followed by peptide identification. H/D exchange or cross-linking, followed by MS analyses, yield residue neighborhood information that helps interpret structural data or understand conformational changes. Native and ion-mobility MS can provide estimations on the stoichiometry of the viral particle, as well as its assembly or disassembly intermediates [18].

As structural studies keep revealing new details on the architecture of viruses, it is becoming clear that viruses that infect hosts far apart in evolution share common structural solutions to build their coats [19]. A virus classification based on similarity between coat protein structures (rather than sequence, genome type or host) has been proposed as an alternative to the classical Baltimore or ICTV classifications [19]. Adenoviruses (AdV), which infect vertebrates, share common structural features with viruses infecting organisms across the evolutionary tree, from bacteriophages and archaeal viruses to the nucleo-cytoplasmic large DNA viruses (NCLDV) such as asfarvirus, iridoviruses, mimivirus, and its virophages [20]. All these viruses form the PRD1-AdV (or PRD1-like) lineage, named after its two first identified members, AdV and the tectivirus PRD1, a tail-less, membrane containing bacteriophage [21–23]. Herpesviruses, which infect all sorts of animal organisms, share many structural characteristics with tailed bacteriophages. They follow a similar assembly pathway, and their major capsid protein folds with a topology very similar to that of the HK97 phage family. Herpesviruses and tailed phages are therefore considered to form a second structural lineage. The third lineage includes the dsRNA cystoviruses (bacteriophages, representative Φ6) together with eukaryotic dsRNA viruses such as reo- or totiviruses. Finally, the fourth lineage encompasses picorna-like viruses, with coat proteins folding as a β-barrel lying parallel to the capsid surface. At the time this classification was proposed, almost half of the ICTV virus families could be placed in one of these four structural lineages. Some notable, well-studied virus families have not been assigned to a particular structural lineage yet, but they show notable maturation pathways that will also be addressed in this chapter.

7.2 Maturation in the RNA Virus Lineages

7.2.1 Picorna-Like Viruses

More than 15 virus families have been assigned to the picorna-like lineage based on major coat protein (MCP) structural similarity [19]. These include viruses as

different as the small, ssRNA picornaviruses (*pseudoT* = 3, 30 nm diameter) [24], the ssDNA parvoviruses (*pseudoT* = 3, 25 nm) [25], and even the large, dsRNA birnaviruses (*T* = 13, 65 nm) [26]. Members of the picorna-like lineage have simple capsid compositions, facilitating the study of their assembly and maturation process in vitro. Their structural signature is a MCP folded as a single β-barrel (jelly roll) lying tangential to the capsid surface. Autoproteolytic processing of the MCP is a common theme in maturation of picorna-like viruses.

The ssRNA noda- and tetravirus capsids are built from a single protein component, facilitating the extensive characterization of the changes undergone during maturation [3]. The best studied nodavirus is Flock House virus (FHV), with an icosahedral *T* = 3, 320 Å diameter capsid, and three gene products encoded from two RNA molecules [27]. The coat protein is synthesized as a 407 amino acid long polypeptide designated as α. After assembly of the provirion (noninfectious particle), autocatalytic cleavage generates the β (residues 1–363) and γ (364–407) peptides. This cleavage does not result in any detectable morphological change in the particles, but it makes them more stable and is required for FHV to become infectious [28, 29]. The γ peptide remains inside the mature particle, as shown by the observation of its first 25 residues forming an amphipathic helix beneath each β monomer (Fig. 7.1a) [30]. This peptide has membrane lytic activity, and is therefore thought to play a role in helping FHV release from endosomes. The cleavage at Asn363 is catalyzed by Asp75 in the same polypeptide chain. Only after provirion assembly has placed these residues in close proximity can the cleavage take place. In this way, untimely reactions that would be deleterious for the virus are avoided [31].

A very similar autocatalytic cleavage mechanism is responsible for the maturation of the ssRNA, *T* = 4 tetraviruses, as revealed mainly by studies on *Nudaurelia capensis* omega virus (NωV) [34]. Unlike nodaviruses, tetravirus capsids undergo remarkable conformational rearrangements associated with maturation, which have been characterized by a combination of crystallography and cryo-EM. A spherical, unstable procapsid of 480 Å diameter is assembled at neutral pH, and matures by acidification during apoptosis to result in the infectious, faceted 410 Å mature particle [35]. This shell shrinking is driven by the protonation at low pH of acidic residues causing repulsion at the subunit interfaces. Only when the particle reaches its smaller conformation does proteolytic cleavage of the capsid protein take place, suggesting that in the swollen form the catalytic residues are not correctly positioned for cleavage. Once the autocatalytic process has started, the particle can no longer swell, even if the pH is raised to neutral values. The γ peptides act as a molecular switch between subunits, adopting different conformations depending on their position in the four *quasi* equivalent positions in the asymmetric unit. As a result of the proteolytic cleavage, these γ peptides go from a mobile to a more ordered state, therefore stabilizing the particle [36, 37].

Maturation in the archetypal virus family in this lineage, the picornaviruses (as exemplified by poliovirus), follows a similar mechanism to the one described above, except that the *pseudoT* = 3 capsid is built from three different polypeptides (VP0, VP1, and VP3), all of them having originated from previous cleavage from the single, long polypeptide translated from the viral mRNA. After assembly of the

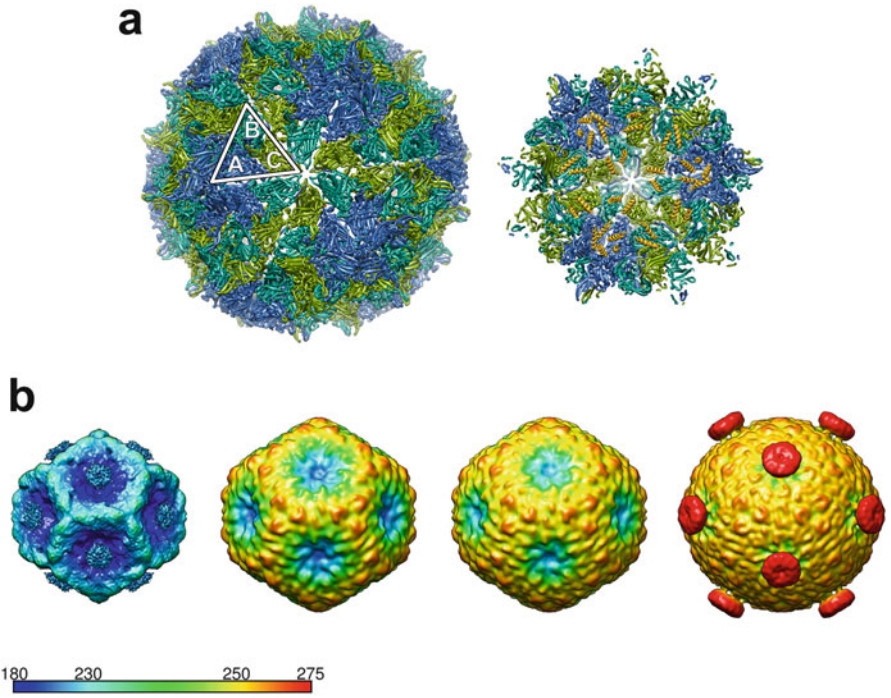

Fig. 7.1 Maturation in the RNA lineages. (**a**) A view of the FHV capsid (PDB ID 4FTB) from outside (left), and a facet from inside (right) to show the position of the lytic γ peptide (orange). An asymmetric unit is delineated by a white triangle. The three independent copies of the MCP are colored in blue, turquoise, and lime, and labeled A–C. The view is along a three-fold symmetry axis. (**b**) Bacteriophage Φ6 capsid expansion. Two expansion intermediates (center left and right, EMD-5355 and 5356) have been detected by in vitro treatments on the genome-less (left, EMD-1500) or fully packaged (right, EMD-5358) polymerase complex, and proposed to correspond to the sequential expansion stages occurring upon packaging the first and the second RNA genomic segments [32]. The maps are colored by radius (Å), as indicated by the color bar at the bottom. Unless otherwise indicated, all ribbon and surface structure representations in this chapter were prepared using UCSF Chimera [33]

provirion and in the presence of the viral genome, an autocatalytic reaction cleaves the N terminal region of VP0 to produce VP4, a 68 residue dynamic peptide similar to the γ peptides in noda- and tetraviruses. In poliovirus, maturation also requires a posttranslational modification of VP4, namely addition of a fatty acid (myristate). Myristoylation of VP4 appears to play a double role: during assembly, it mediates interactions between VP4 and the rest of the icosahedral shell; during entry, it helps to open pores in the host membranes when it is exposed as a result of conformational changes undergone by the particle upon receptor binding [38–43].

The most unexpected member of the picorna-like virus lineage was found when the capsid structure of the infectious bursal disease virus (IBDV) was solved. This structure showed that the birnavirus large capsid (65 nm diameter) turned out to use the same building block as the small, simple picorna-like viruses, instead of a

BTV-like fold as would have been expected from the genome type (dsRNA) and capsid geometry ($T = 13$) similarities [26]. Birnavirus maturation also holds similarities with the maturation of the smaller members of the lineage described above. The birnavirus MCP is synthesized as a precursor (pVP2, 512 residues) which undergoes sequential cleavages (both autocatalytic and viral protease driven) at its C-terminal region to produce the final form VP2 (441 residues) [44]. The pVP2 C-terminal peptide is a key player in IBDV assembly, acting as a transient, flexible molecular switch to allow the different interactions between identical MCP monomers required to form the large capsid. Different conformations, or degrees of proteolytic processing, in this region determine whether a hexamer or a pentamer of the MCP is formed. After assembly, the switch is removed, eliminating this flexibility to render the assembly reaction irreversible. Part of the conformational switching role of the pVP2 C-terminal region is based on its ability to interact with a multifunctional viral protein, VP3, which may act as a scaffold, indicating that the birnavirus capsid follows a more complex morphogenetic pathway than the smaller members of the picorna-like lineage [45, 46].

7.2.2 BTV-Like Viruses

This lineage is named after the bluetongue virus (BTV), a reovirus and the first dsRNA virus for which a high resolution structure was obtained [47]. Apart from reoviruses, recognized members of the BTV-like lineage are fungal pathogens such as the totiviruses and chrysoviruses, and the cystovirus phages such as Φ6 [48–50]. BTV-like viruses encapsidate dsRNA genomes that can be segmented in as many as 12 different linear molecules. Some members of the BTV-like lineage have multilayered capsids while others are single layered, but in most of them the innermost layer (or core shell) is formed by 120 copies of the core protein. Because of the number of protein monomers in this shell, it is described as having a $T = 2$ triangulation number, a conformation not allowed in the Caspar and Klug formalism [51]. In fact, the core protein monomers adopt two different conformations to yield a $T = 1$ icosahedron of asymmetric dimers, with the only known exception of *Penicillium chrysogenum* virus, where instead of a dimer the icosahedral asymmetric unit is formed by a single, large protein formed by two structurally similar domains [52]. dsRNA viruses need to keep their genome confined within the core shell at all times during infection, to protect it from aggressions by cellular nucleases, and to prevent antiviral reactions triggered by accumulation of dsRNA. The external layers (in case they exist) carry the viral components in charge of initial interaction with the host: recognition, attachment, and entry. Fungal viruses, which have no extracellular part of the infectious cycle, are single layered [49].

Given their relevance in animal and human health, the triple layered reoviruses, particularly BTV and rotavirus, are the most studied members in this lineage [53–55]. Assembly of reovirus particles is coupled with replication of the segmented dsRNA genome, by the action of the viral polymerase that synthesizes dsRNA

molecules from the (+)ssRNA transcripts stored in cytoplasmic structures called viroplasms. Polymerase-(+)RNA complexes are activated by interaction with the core shell protein, producing early subviral particles where synthesis of the complementary RNA strand will happen. Once the genome is replicated, these particles will recruit the two $T = 13$ outer layers. A double layered particle (DLP) is first assembled in the viroplasm, and may traffic to a different location (for example, endoplasmic reticulum for rotavirus) where the third layer will be acquired to complete the ~80 nm diameter virion. Since the DLP is not infectious, acquisition of this third layer is usually considered the maturation step in reovirus assembly. In rotaviruses, an additional maturation step consisting in cleavage of surface spikes by trypsin-like proteases from the intestinal lumen after cell exit is required for infectivity.

There are no detailed structural studies on the early, single layered reovirus assembly products. Subviral particles competent for dsRNA synthesis extracted from rotavirus infected cells are fragile, and present a variety of sizes between 30 and 70 nm. These characteristics make them unsuitable for structural studies, while suggesting the possibility of stability and architectural changes (expansion) associated with genome packaging [56]. However, more data are required to understand these changes, if they exist. Conversely, remarkable structural changes associated with genome packaging have been observed in the bacterial members of the BTV-like lineage: the cystoviruses.

Cystoviruses are the only known dsRNA viruses infecting bacteria. The best characterized member of the family, bacteriophage Φ6, has a triple layered particle formed by the "$T = 2$" core (46 nm), a $T = 13$ shell (58 nm), and a membrane envelope studded with viral proteins. Twelve hexamers of the packaging motor protrude from the core vertices [57, 58]. Bacteriophage Φ6 is one of the most complex viruses for which infectious particles can be produced in vitro, starting from purified components [59]. Unlike reoviruses, Φ6 assembles complete shells prior to RNA packaging. These shells are formed by the structural protein P1 (with two copies, P1A and P1B, forming the asymmetric unit of the "$T = 2$" shell), the packaging NTPase, the viral polymerase, and an accessory protein. These particles, also termed polymerase complex (PC), are active in packaging the three viral (+) ssRNA segments, synthesizing the complementary strands, and transcribing new (+) ssRNA strands. Prior to packaging, the PC is a dodecahedral cage where the center of each pentagonal facet is deeply recessed towards the particle center. Packaging of the three (+)ssRNA is thought to proceed in a sequential way, causing three successive capsid expansion transitions to end with a spherical, mature particle (Fig. 7.1b). Only after the three segments have been packaged is synthesis of the complementary strands initiated. In this sense, expansion of the PC is considered a maturation process required to activate the particle functionality for virus propagation. During Φ6 PC expansion, the five-fold vertices are pushed out; the five-fold radius doubles (from ~12 to ~22 nm) and the inner capsid volume increases by a factor of 2.4 [32, 60, 61]. This large conformational change is driven by large rotations of the P1 monomers and hinging domain movements that alter the intersubunit contacts. As a consequence, the angle between neighboring P1B

subunits changes from 98° to 148°, and the buried surfaces increase by 50% for P1B and 16% for P1A [62].

7.3 Maturation in the dsDNA Virus Lineages

7.3.1 HK97-Like Viruses

Tailed phages constitute ~96% of all the known bacteriophages, and as such are among the most abundant entities in the biosphere [63, 64]. Although their capsids vary in size and some morphological features, all of them seem to use similar morphogenetic pathways, which are also shared by the animal infecting herpesviruses [63, 65]. In dsDNA bacteriophages, maturation encompasses large structural changes and capsid protein rearrangements, concomitant with scaffold removal and genome packaging. The capsid changes from a weak, labile object to a highly stable shell, ready to withstand the high internal pressure imposed by the tightly packed DNA inside [66, 67]. These changes have been studied in great detail for a variety of viruses, particularly for bacteriophage HK97, the first tailed phage for which high resolution structural data were obtained [68]. The structural hallmark of the HK97-like lineage is a MCP with a mixture of α and β secondary structure elements. The monomer is L shaped, and usually described as divided into two domains, each one corresponding to one arm of the L. In the $T = 7$ HK97 particle, the axial (A) domain is located near the icosahedral five-fold and quasi-six-fold axes, while the peripheral (P) domain occupies the region between three-fold axes. The P domain, in turn, includes a long α-helix designated as the spine helix, a mobile loop (E-loop), and a long N-terminal arm (Fig. 7.2a) [68].

In tailed bacteriophages, morphogenesis starts by MCP monomers being organized into hexameric and pentameric capsomers in a spherical procapsid, with the help of the portal and scaffolding elements that act as nucleating seeds and modulators of capsid assembly elongation [69]. Scaffolding elements can be independent proteins, as in phages P22 and Φ29, or be part of other capsid components (e.g., the MCP), as in HK97 [70]. The HK97 procapsid, also termed Prohead-I, is built from 60 hexamers and 11 pentamers of the MCP in its precursor form. This form contains a scaffold domain fused at the N-term (residues 2–103), which is absolutely required for assembly [71]. The 12th vertex of the procapsid contains the packaging motor. In HK97, a maturation protease is also present in the immature procapsid [72]. Other phages such as P22, Φ29, or T7 do not require a maturation protease. In Prohead-I, the long arm of the L-shaped MCP monomers (containing the P domain) is positioned in a roughly radial orientation, and the hexameric capsomers present a pronounced skewed shape: they do not display six-fold, but rather two-fold local symmetry. This distorted shape is due to a bending of the spine helix induced by the presence of the scaffolding domains. The 56 nm particle is very fragile because a large part of the contacts between capsomers established by a small loop in the P

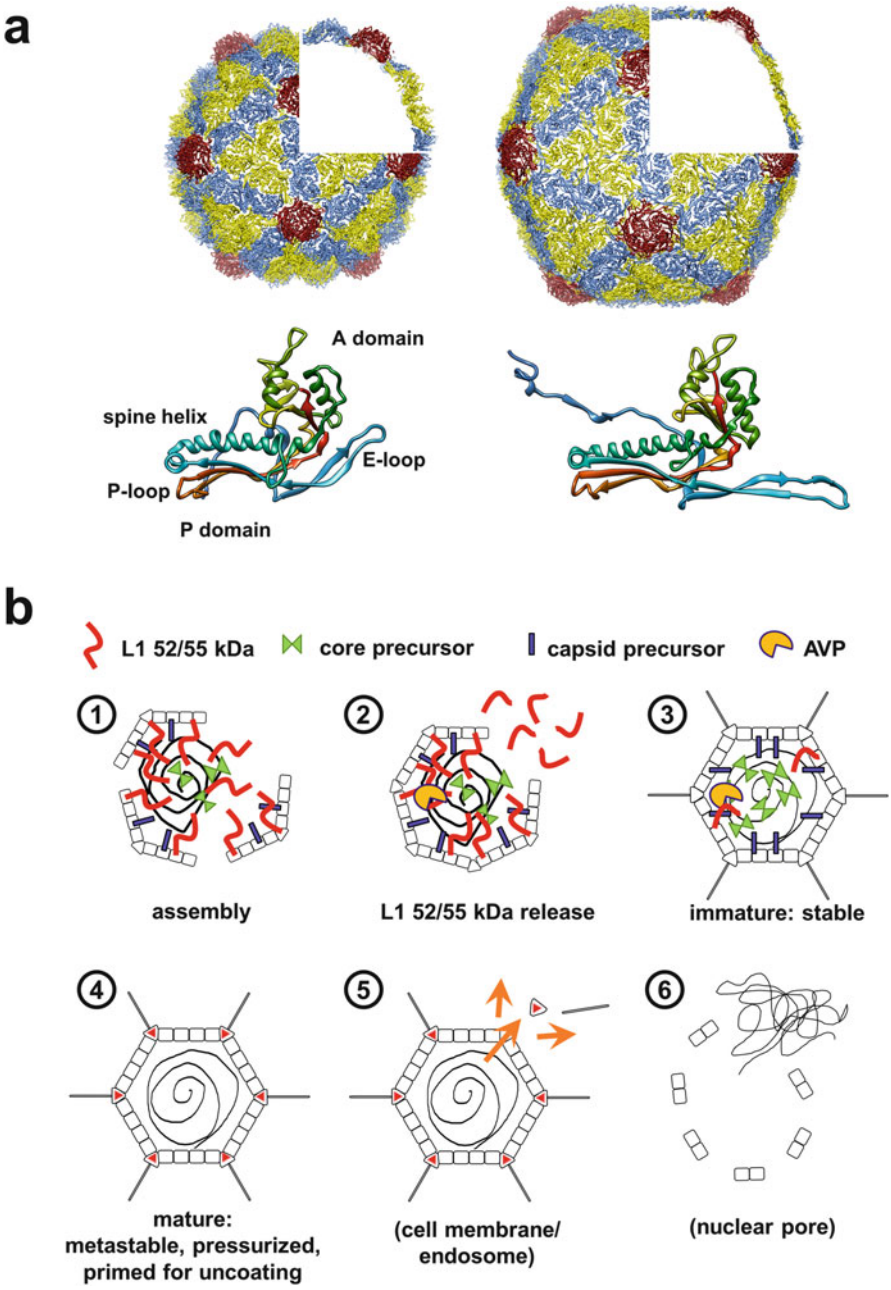

Fig. 7.2 Maturation in the dsDNA lineages. (**a**) Maturation of bacteriophage HK97. The immature (left) and mature (right) capsids are shown with the pentamers colored in red, and the hexamers in yellow and cyan. One quarter of each capsid has been removed and substituted by a slice across the particle, to illustrate the thickness change in the protein shell. The view is along a two-fold

domain (the P-loop) at three-fold symmetry axes are not formed, due to constraints imposed by the presence of the scaffolding domain [73].

The HK97 maturation protease is tethered to the scaffolding domains [74]. Upon Prohead-I assembly, the protease becomes active, cleaves the scaffolding domains, and autocleaves itself, producing small peptides that can diffuse out of the particle. The result of these cleavages is another morphogenetic intermediate called Prohead-II. While assembly of Prohead-I is a reversible reaction, cleavage of scaffolding elements defines the irreversibility of the HK97 morphogenetic pathway. In Prohead-II, the scaffolding domains are no longer constraining the P-loop interactions between capsomers, and therefore the contacts at three-fold axes are stronger. The particle is metastable, primed to jump to a lower energy state in the next stage of assembly. Phages lacking a maturation protease, such as P22 or Φ29, assemble directly a Prohead-II particle.

In the next morphogenetic step, the dsDNA genome is translocated into the empty shell by the action of the packaging motor, which converts chemical energy (ATP hydrolysis) into mechanical work. This work has to fight against the increasing internal pressure generated by the electrostatic repulsion and decreasing entropy of the tightly packed DNA strands [66, 75]. DNA packaging triggers the actual maturation reaction, taking the particle from the metastable state to a much more stable one. In phages lacking a maturation protease, start of DNA packaging causes the release of scaffolding proteins using large pores present in the immature capsid. In HK97, DNA packaging causes the particle to transition into a first expansion intermediate (EI-I), 15% larger in diameter and with a shell thinner than the prohead. In EI-I, the hexameric capsomers are no longer skewed. Then (EI-II), in a remarkable cross-linking mechanism, isopeptide bonds start forming between the E-loop of one subunit and the P-domain of the neighboring one. As early as 1995, MS was instrumental in determining the exact location and chemical characteristics of the cross-link [76]. As cross-linking propagates across the hexameric capsomers, the particle expands by another 9% (balloon state, EI-IV). Finally, pentamers are also cross-linked to the adjacent hexamers, to produce the mature particle (Head-II) where all protein subunits are covalently cross-linked to other subunits [77, 78]. Head-II has a clearly faceted icosahedral shape, a diameter of ~66 nm, symmetrical hexamers, and a 1.8 nm thick shell formed by MCP molecules positioned tangential to the capsid surface (Fig. 7.2a). A combination of crystallography with H/D exchange assays showed that contacts established by the P-loops after cleavage of the scaffolding domain remain unchanged during head expansion, and serve as pivot points for the large capsid rearrangements that involve domain twisting of the MCP (between 20 and 40 degrees, depending on the capsomer

Fig. 7.2 (continued) icosahedral axis. The bottom panel shows the structure of the HK97 MCP in the immature (Prohead-II, PDB ID 3E8K, left) and mature (right, PDB ID 1OHG) capsids. (**b**) Cartoon summarizing the AdV maturation pathway and its effects in priming for uncoating (see main text for details)

position in the $T = 7$ asymmetric unit). To accommodate these substantial rotations of domain A over domain P, the spine helix unbends and adopts a more canonical helix structure than in the prohead (Fig. 7.2a) [73, 79, 80]. The completely cross-linked particle resembles a knight chainmail, with covalently bonded protein circles interlocking at the icosahedral and local three-fold axes [68]. The chainmail structure provides the necessary stability to the HK97 virion to withstand deleterious environmental conditions, as well as the internal pressure generated by the packed genome [81, 82]. Stabilization by cross-linking relates to the HK97 capsid mechanical properties in a complex way. Full cross-linking is not required to make the particle resilient against large capsid deformations, but it is determinant in producing a structure that can withstand material fatigue [83]. A cross-linked chainmail is not the only way to build stable mature capsids. Alternative stabilization strategies are used by other bacteriophages, such as cementing by additional proteins (e.g., gpD in phage λ) or MCP domains (phage P22) which interlock several capsomers from the outer capsid surface [84, 85].

Although they present a larger particle complexity, with extra layers formed by the tegument and the glycoprotein-containing envelope [86], herpesviruses share many structural characteristics with tailed bacteriophages [87]. The large nucleocapsid ($T = 16$, 125 nm diameter) is assembled from MCP capsomers sharing the basic HK97 fold [65, 88]; it contains a packaging portal at a single vertex that works against high internal pressure [89–91]; assembles with the help of a scaffolding protein later removed by the maturation protease action [92, 93]; and transitions from an immature state with skewed hexamers to a mature state where hexamers are symmetric [94, 95]. AFM studies on the herpesvirus mechanical properties suggest that removal of the scaffold also plays a role in capsid stabilization [96]. Unlike HK97, the herpesvirus capsid is not stabilized by cross-linking, but by cementing proteins [95].

7.3.2 PRD1-Like Viruses

The PRD1-like lineage was founded when crystallographic studies showed that the MCP of PRD1, a dsDNA tail-less, lipid containing bacteriophage, had the same fold as the MCP of the vertebrate-infecting adenoviruses (AdV) [22, 97]. After this discovery, which prompted the classification of viruses in structural lineages, more members of the PRD1-like family have been described or predicted, and the lineage now extends from viruses infecting bacteria or archaea to the nucleo-cytoplasmic large DNA viruses such as phycodnaviruses, asfarvirus, iridoviruses, and the giant mimivirus [20]. MCPs in most members of the PRD1-AdV lineage are built from a double eight-stranded β-barrel (also called double jelly roll) orthogonal to the capsid surface, forming pseudo-hexagonal capsomers. Exceptions are some members of the lineage infecting bacteria or archaea, which possess two genes encoding two MCPs, each with a single β-barrel (see, for example, [98]). PRD1-like viruses also have a single orthogonal jelly roll protein (different from the MCP) forming the vertex

capsomers. Members of this lineage have complex capsid compositions and large triangulation numbers, ranging between $T = 21$ [99] and $T = 499$ [100], and reaching up to $972 < T < 1200$ for mimivirus [101]. Remarkably, even a scaffold protein of the non-icosahedral poxviruses (vaccinia virus D13 protein) folds as a double β-barrel pseudo-hexamer [102]. Other common traits in the lineage are the protein-primed initiation of genome replication, and the presence of an ATPase presumed to be involved in DNA translocation for genome packaging [103]. Most PRD1-like viruses possess an internal lipid membrane intercalated between the genome and the icosahedral capsid. Exceptions are AdV and the virophages, satellites of the giant viruses [104].

An intriguing evolutionary connection has been found between PRD1-like viruses and large (15–20 kbp) eukaryotic dsDNA transposons called Polintons [105]. Polintons are so named because they all encode a protein-primed DNA polymerase (to sustain self-replication, POL) and a retroviral-like integrase (INT). Most of them also include genes for a DNA-packaging ATPase and a maturation protease similar to that found in AdV. Exhaustive sequence analyses revealed that these transposable elements also encode genes that could translate into double or single jelly roll proteins, suggesting that at some point in time, or in certain conditions, they could form icosahedral capsids. These observations prompted the hypothesis that Polintons may have evolved from a tectivirus-like ancestor (encoding the capsid proteins, POL, and packaging ATPase), which entered a proto-eukaryotic host with a bacterial endosymbiont (mitochondria) and acquired the maturation protease and integrase genes by recombination with a eukaryotic DNA transposon [103]. Subsequent evolution would have resulted in the "polintovirus" elements splitting into two different ways of life: the transposable, capsid-less integrating elements, and the bona fide viruses like AdV.

The assembly pathway of the complex PRD1-like viruses is known at a much lower level of detail than in herpesvirus and tailed bacteriophages. Capsids in the PRD1/AdV lineage do not seem to undergo extensive conformational changes upon genome packaging [23, 106]. In PRD1, it is at the internal membrane where significant conformational changes related to genome packaging and release have been observed. The membrane expands upon genome packaging to follow the icosahedral contours of the inner capsid surface [23, 107, 108], and forms a tubular device to penetrate the host cell wall for genome delivery [109, 110]. Even within the same lineage, there seem to be fundamental differences in the packaging mechanism (sequential or concurrent with assembly) that may depend on the particular genome type (linear or circular dsDNA, protein bound or not) [99, 111, 112]. As the maturation protease is only found in members of the lineage infecting eukaryotic organisms, it is surmised that the prokaryotic members do not undergo proteolytic maturation.

For historical reasons and because of its importance in medicine as a pathogen and vector, AdV (in particular human AdV type 5, Ad5) is the most extensively studied PRD1-like virus. The Ad5 virion is composed of more than ten different proteins in various copy numbers, plus the 35 kbp dsDNA genome, totaling a mass of 150 MDa for the 95 nm, $pseudoT = 25$ icosahedral virion [113, 114]. Each capsid

facet has 12 trimers of the MCP, hexon. A pentamer of penton base protein sits at each vertex, in complex with a trimer of the projecting fiber. In addition, Ad5 assembly requires four different minor coat proteins: IIIa (60 copies), VI (360), VIII (120), and IX (240). Particle size and composition represent a challenge for structural biology techniques, so much so that Ad5 capsid architecture remained controversial even after the structure was solved at near atomic resolution (~3.6 Å) by both protein crystallography and cryo-EM [115–119]. Recent reports have solved the controversy [120, 121].

The icosahedral Ad5 shell encloses a non-icosahedral core with the genome tightly packed together with positively charged, virus-encoded proteins: core polypeptides V (150 copies), VII (500), and μ (300); the terminal protein (TP); and the maturation protease (AdV protease, AVP). There are no structural data on any of the core proteins, and the core architecture cannot be analyzed by structural methods that make use of icosahedral symmetry or averaging. It is not known how the 12 μm long molecule of dsDNA, bound to ~25 MDa of protein, fits into the ~0.1 μm diameter capsid. A combination of cryo-electron tomography and statistical analyses has provided the first images of the AdV "mini-chromosome" in its physiological environment, as well as a model for the interactions present within the confined core [122]. The AdV genome and bound proteins are organized in approximately 230 subunits (*adenosomes*) per virion, behaving as a fluid of soft repulsive particles. This soft repulsion is consistent with the lack of enough protein positive charges to compensate for all the dsDNA negative charges.

AVP, the main actor in Ad5 maturation, cleaves internal coat proteins IIIa, VI, and VIII, and core proteins VII and μ, as well as the replication priming TP. Immature virions contain the precursor versions of all the AVP targets and the fully packaged genome, but they are not infectious [123]. AVP is packaged together with the viral genome and uses a peptide (pVIc) cleaved from one of its substrates (protein VI) to slide on the dsDNA and reach all its other substrates, in a unique one-dimensional chemistry mechanism [124–127]. AdV maturation is tightly linked to uncoating. Immature virions are defective in the initial stages of uncoating: they do not release fibers upon receptor binding at the cell membrane, nor the lytic, internal protein VI in the early endosome. Consequently, they become trapped in the endocytic pathway, and are finally destroyed in lysosomes, thereby aborting infection [128–132].

Recent biochemical, cryo-EM, and AFM studies have shown how maturation cleavages disrupt interactions in both capsid and core that stabilize immature Ad5 (Fig. 7.2b, step 3). Upon maturation, the particle becomes metastable (Fig. 7.2b, step 4), in contrast to the stability changes in bacteriophage, where the mature capsid is more stable than the immature intermediates [133–135]. This difference is likely related to the different mode of infection of the two types of viruses. Instead of ejecting its genome across the plasma membrane leaving the capsid behind, AdV is internalized in the cell, and must be disassembled within in a concerted fashion to ensure exposure of the genome at the appropriate place and time for successful replication. Maturation prepares AdV to start the programmed uncoating sequence

upon reception of the appropriate signal, for example, attachment to the receptor, or pH changes along the endocytic pathway [130, 132, 136–139].

AdV priming for uncoating consists in facilitating vertex release, as well as loosening the condensed genome and its attachment to the icosahedral shell [133–135, 140, 141]. AFM probing of the mechanical properties of mature and immature Ad5 capsids and cores revealed that core protein maturation results in internal pressurization of the Ad5 virion, providing a physical mechanism to facilitate penton loss in the initial stages of uncoating (Fig. 7.2b, steps 4 and 5), therefore opening an exit channel for the membrane lytic protein VI [132, 142]. This work represented the first indication of internal pressure in a dsDNA virus packaging charge neutralizing, DNA condensing proteins. Cleavage of protein VI seems to weaken its binding to the inner capsid surfaces, and is required for extrusion of its mature form [134, 141, 143]. Protein L1 52/55k, one of the four viral proteins required for packaging [144–147], is also a substrate for AVP [148]. L1 52/55k can form homooligomers and interact with both capsid and core components, acting as a "Velcro" tether during assembly (Fig. 7.2b, step 1). Proteolytic cleavages by AVP disrupt interactions between L1 52/55k and other virion components, facilitating its removal during maturation (similarly to scaffolds in bacteriophage) (Fig. 7.2b, step 2), as well as separation of the genome from capsid fragments in the final stages of uncoating (Fig. 7.2b, step 6) [106, 148–152].

The complex, brick-shaped poxviruses also encode an AdV-like protease whose action is required to remove the double jelly roll scaffolding protein in the transition from mature to immature particles [153]. Apart from sharing the MCP fold and the protease, another common trait in PRD1-like eukaryotic viruses is the presence of virus encoded, positively charged proteins bound to the packed dsDNA. Proteolytic maturation of core proteins in poxviruses is also a requisite for infectivity [154]. The evidence collected for AdV, together with molecular dynamics modeling, suggests that the major role of core proteins is modulating internal capsid pressure [155]. Details on physical changes in these large viruses are scarce, but it is intriguing to consider that they may also undergo pressure changes associated with maturation. These hypothetical pressure changes may be related to sequential uncoating within the cell as in AdV, or to bacteriophage-like genome ejection across cell walls in the case of algae infecting viruses [156].

7.4 Maturation in Viruses Not Assigned to a Structural Lineage

7.4.1 Enveloped Icosahedral Viruses: Alpha- and Flaviviruses

The ssRNA *flavivirus* and *alphavirus* families include many human and animal pathogens such as dengue, hepatitis C, West Nile, Venezuelan equine encephalitis, Zika or Semliki forest viruses [157, 158]. While for some of them (e.g., hepatitis C)

there are little structural data, others have been extensively studied and their maturation process is understood in considerable detail [3, 159, 160]. Although there are structural similarities between the alphavirus and flavivirus glycoproteins, evidence for a common ancestry of these families is not considered enough to define their belonging to a structural lineage [19]. Maturation in alpha- and flaviviruses involves proteolytic processing of the external glycoproteins orchestrated with virus egress along the secretory pathway, to expose the fusion peptide that will enable the virus to enter a new host cell.

Sindbis virus and Semliki forest virus, the most studied cases of alphavirus maturation, have a $T = 4$ icosahedral core (40 nm diameter) formed by protein C, containing the ssRNA genome. This core is enveloped by a membrane covered by glycoproteins (E1 and E2), also arranged in a $T = 4$ icosahedral lattice, to form the ~70 nm diameter particle. A total of 240 copies each of E1 and E2 are arranged in trimeric heterodimers, resulting in 80 three-petal spikes on the virus surface [161–165]. Protein C is a protease that cleaves itself from the polyprotein product that contains all structural components. Both E1 and E2 are anchored to the virus membrane, but in two different ways. While E2 is oriented perpendicular to the membrane and interacts with the core protein C, E1 lays on the membrane surface. E2 is the receptor binding protein, while E1 carries the fusion peptide. The immature particle carries a precursor version of E2 (preE2). The N-terminal region of preE2 hides the E1 fusion peptide while the virus transits across the Golgi. Later on, this region is cleaved by furin-like cell proteases, and the E1–E2 heterodimer changes conformation to expose the fusion peptide which, after being endocytosed, will allow the genome-containing core to escape the endosome. Cryo-EM studies on Semliki forest virus, and more recently on Chikungunya virus, have shown that these conformation changes are subtle, and involve a compaction of the spikes and decompaction of the core [161, 166]. In alphaviruses, large conformational changes do not occur during maturation, but later on during membrane fusion, when the E1–E2 dimer will dissociate to give rise to a postfusion E1 homotrimer [167].

The composition of flavivirus particles is similar to that of alphaviruses, with three structural proteins: protein C located inside the membrane envelope together with the RNA genome, and proteins M and E anchored to the membrane and covering its outer surface. Unlike alphaviruses, flaviviruses do not have an ordered icosahedral core beneath the membrane [168, 169]. This lack of order is probably a consequence of the C protein being much shorter (99 residues in dengue virus vs. 264 in Sindbis virus) and its lack of direct interactions with M and E.

Proteins E and M stage a complicated ballet during maturation of dengue virus, one of the best studied flaviviruses (Fig. 7.3a). In the immature particle, 180 heterodimers composed by the glycoprotein E and the precursor version of M (prM) form 60 trimeric spikes protruding from the particle surface. The C-terminal domain of prM is inserted in the membrane, while the N-terminal domain (termed "pr") occupies the outermost part of the spike, hiding the fusion peptide in E, similarly to preE2 in alphaviruses [169–172]. When this particle (assembled in the ER lumen) is exposed to low pH in the trans Golgi network, the trimers dissociate, and protein E forms homodimers that lie flat on the membrane surface, giving the particle a smooth aspect and decreasing its total diameter from 60 to 50 nm. In the

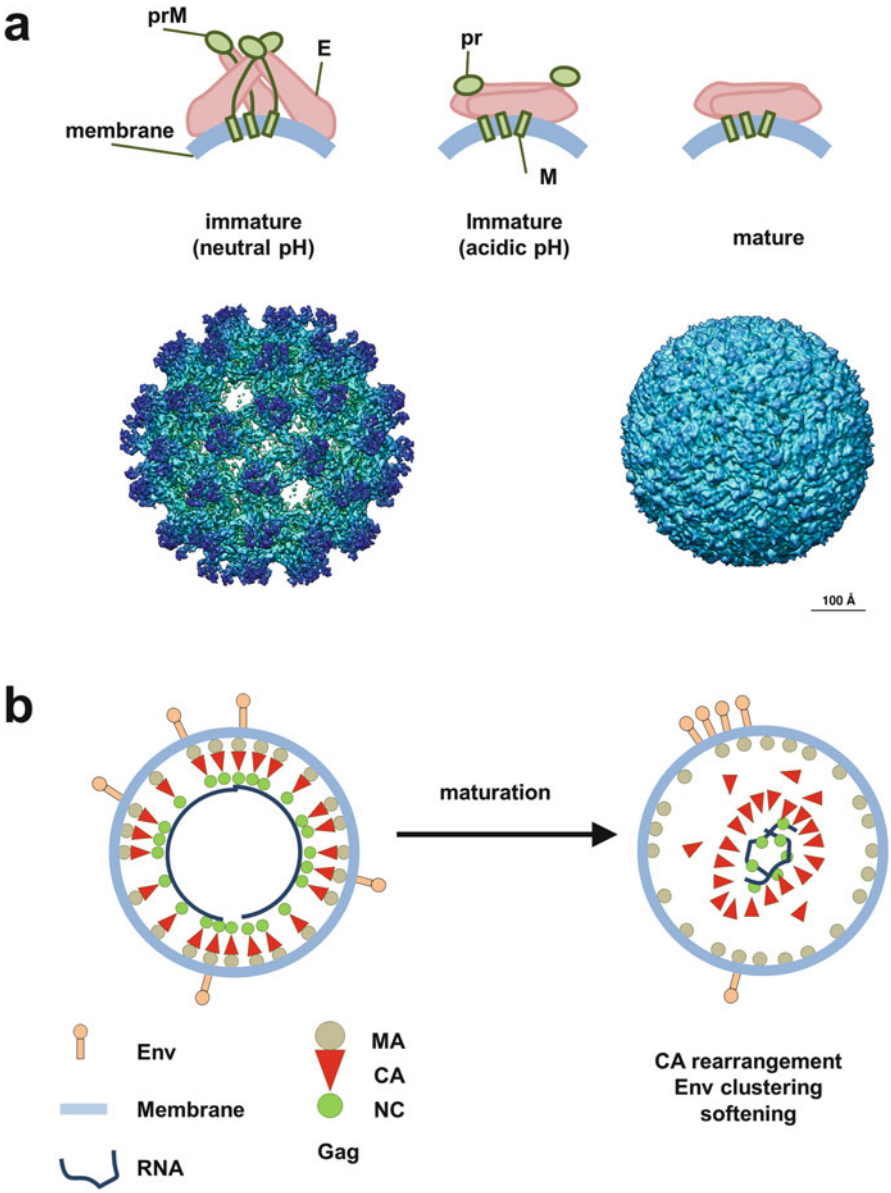

Fig. 7.3 Maturation in viruses not assigned to a structural lineage. (**a**) Schematics of the dengue virus maturation pathway. The bottom panel shows surface rendering representations of the immature (left, EMD-2141) and mature (right, EMD-5520) capsids, colored according to radius. The view is along a two-fold icosahedral axis. (**b**) Cartoon summarizing the HIV maturation pathway

mature dengue virus capsid, 90 dimers of glycoprotein E are arranged in a herringbone pattern. There are three E monomers per icosahedral asymmetric unit, but they do not have quasiequivalent symmetric environments, and therefore the particle geometry does not conform to the Caspar and Klug theory [51, 173, 174]. In spite of the large reorganization undergone by the E protein monomers, their transmembrane domains conserve their positions in the icosahedral asymmetric unit [170]. Concomitant with spike dissociation, a furin target motif in the long linker region between the pr and transmembrane domains of prM is exposed, facilitating its cleavage by this cellular protease. The cleaved peptide (pr) that covers the fusion peptide in protein E remains associated with the particle at acidic pH, but is released when the viral particle encounters neutral pH upon cell exit. The particle is now in a metastable state, prepared for successful entry into the next host, where acidic endosomal pH will trigger a new change and organize the E monomers into the homotrimers required for membrane fusion. Partially mature particles composed by a mosaic of spiky and smooth protomers have been found in dengue virus preparations, suggesting that the structural reorganizations during maturation are not synchronized throughout the whole particle [175]. The heterogeneity on dengue virus maturation has recently been quantitated by fluorescence-based sorting ("flow virometry"), showing that only half of the particles in a viral preparation are in fully mature state [176].

7.4.2 Retroviruses

Retroviruses [177] have pleomorphic capsids that may adopt a range of sizes, shapes, and composition from particle to particle, making each virion unique. Because of this intrinsic variability, their organization cannot be deduced from structural biology techniques based on averaging data from many identical virions, such as X-ray crystallography or cryo-EM single particle averaging. Although the structure of isolated components of the retroviral particle could be solved to high resolution by crystallography, it was not straightforward to deduce their interactions in the context of the actual particle, or how these changed during maturation. The advent of cryo-electron tomography to visualize individual virus particles in 3D, together with subtomogram averaging to reinforce the signal of identical, but not symmetrically ordered, structural subunits, has been crucial to reveal the architectural details of these viruses [10]. Among retroviruses, the most studied because of its clinical relevance is HIV [178].

The main structural component of the HIV particle is the 55 kDa polyprotein Gag, composed by three major domains connected by flexible linkers: matrix (MA), capsid (CA), and nucleocapsid (NC). Gag molecules bound to the viral genome via the NC domain are recruited to patches of cell membrane carrying the virus glycoproteins gp120 and gp41 (cleavage products of the viral envelope protein, Env). Gag recruitment to the membrane induces budding and release of the immature, noninfectious HIV particle. Several thousand copies (~5000) of Gag arrange

radially to form a roughly spherical, incomplete shell, with the MA domain in the outermost region, anchored to the viral envelope, and the NC domain in the innermost, in contact with two copies of the ssRNA genome (Fig. 7.3b). Gag monomers oligomerize via CA–CA interactions to form a discontinuous hexameric lattice. In the immature HIV particle, the critical interactions for assembly of this lattice seem to be provided by the C-terminal region of the CA domain. Contacts involving the CA N-terminal domain vary between different retroviruses [179–181].

Immature HIV particles also contain the GagPol polyprotein, which comprises three enzymes critical for the infectious cycle: integrase, reverse transcriptase, and protease. Upon budding and release from the cell, the viral protease sequentially cleaves Gag and GagPol into the individual polypeptides, triggering a remarkable cascade of conformational changes to produce the mature virion, competent for entry into a new host cell (Fig. 7.3b) [182]. The mechanism of protease activation is not clear yet, but its activity kinetics are important and must be tightly regulated for successful production of mature particles [183]. Processing of Gag results in detachment of the MA, CA, and NC proteins. MA remains anchored to the membrane, and NC remains bound to the RNA inside a shell formed by CA, together with the integrase and reverse transcriptase. Certain integrase inhibitors or mutations in the integrase gene produce particles where the NC-RNA complex localizes outside the mature capsid, suggesting a role for integrase in correct genome encapsidation [184]. CA can assemble into either hexamers or pentamers, in much the same way as capsid proteins of icosahedral viruses. Recombinant CA forms only hexamers in certain conditions, giving rise to tubular oligomers or flat, ordered sheets; while when pentameric oligomerization is enforced, $T = 1$ icosahedral particles are formed [185–188]. When CA hexamers and pentamers associate to form the mature capsid, they do it in such manner that the pentamers are not distributed regularly within the hexamer lattice. The asymmetry of their distribution results in asymmetrical structures that can adopt shapes ranging from roughly spherical to roughly conical, and can be modeled using the geometrical principles governing fullerene cones [189].

Upon maturation, CA–CA interactions change, resulting in an increase of the space between CA hexamers from 8 to 9.6 nm, and the appearance of the pentamers that induce the higher curvature of the fullerene cone [179, 190]. MS combined with H/D exchange was used to reveal contacts between the N-terminal domain of CA in the mature virion that were absent in the immature particle [191]. Cross-linking followed by MS also detected an interaction between the N- and C-terminal domains of adjacent CA monomers that appears upon maturation [192, 193]. All-atom molecular dynamics was used to produce a model of the mature core, starting from the crystal structures of CA domains and cryo-EM structures of tubular CA assemblies [188]. Cryo-electron tomography and subtomogram averaging has finally produced the first subnanometer resolution image of hexamers and pentamers within the intact mature virion [190]. Mature CA forms 100–120 nm long fullerene cones with ~1100–1330 copies of CA and 12 pentamers. Remarkably, only ~1/3 of the CA molecules present in the immature particle form the mature capsid [179]. The different curvatures required to make the cone are facilitated by the flexible linker between the CA N-terminal and C-terminal domains. In the virion, CA–CA

pentameric interfaces differ from those observed in crystallographic structures of the isolated protein. The position of pentamers in the conical capsid does not seem to correlate with the gaps in the immature Gag lattice. The current evidence favors a model where the immature CA hexameric lattice completely disassembles and reforms de novo to produce the mature capsid, but little is known about how this de novo formation would take place [182]. A recent study has shown that it is possible to follow the CA reorganization in real time by super-resolution STED microscopy in particles carrying fluorescently labeled Gag and a photodestructible protease inhibitor to synchronize the reaction. This kind of analyses holds the promise to obtain more detailed insights on the in situ HIV maturation dynamics in the near future [194].

The dramatic conformational changes undergone by Gag inside the viral envelope during HIV maturation are reflected in the particle physical properties and the localization of Env proteins on its outer surface (Fig. 7.3b). AFM nanoindentation studies have shown that immature HIV particles are 14 times stiffer than mature virions. This stiffness change is mediated by the cytoplasmic tail of the viral envelope (Env) protein. Deletion of the Env tail made immature particles as soft as the mature ones, and restored their ability to enter the cell, suggesting a critical role of the particle physical properties in modulating its biological cycle. The excessive stiffness imposed by the Gag shell on the membrane of the immature particle might impair the ability of the viral envelope to fuse with the cell membrane for entry [195–198]. HIV particles carry only a few copies (7–14) of Env proteins, responsible for cell binding and membrane fusion during entry. STED analyses have shown that maturation induces clustering of Env. This clustering is facilitated by an increase in Env mobility that depends on the Env tail (possibly via its interactions with Gag across the membrane), but not on the lipid order. The entry efficiency of HIV-1 is directly correlated to its capacity to form Env clusters, possibly to mediate efficient receptor binding [199, 200]. The long tail (151 residues) and scarce copy number of Env is a particular feature of HIV, suggesting that their role in infectivity must be played by other actors in other retroviruses.

7.5 Conclusion

Virus maturation involves structural, chemical, and physical changes required for a newly assembled particle to achieve its full infectious potential. A common feature in maturation for many viruses is the action of proteases. Proteolytic cleavages prepare virus particles for entry by facilitating their binding to cell receptors (e.g., Env clustering in HIV), setting up uncoating triggers (metastability, internal pressure), and facilitating trafficking (membrane crossing by lysis or fusion). Large conformational rearrangements often (tetra-, flavi-, retro-, herpesviruses, and tailed phage), but not always (noda-, alpha-, and PRD1-like viruses), accompany maturation. In recent years, methodological advances in structural and physical virology techniques have provided great advances in the detailed study of virus maturation.

However, many questions remain unanswered, particularly in the case of complex virus capsids. Although all NCLDV encode AdV-like proteases, little is known about their function and its consequences in the infectious cycle of these viruses. Studies on NCLDV and other members of the PRD1-like lineage are hampered by particle complexity and the consequent lack of in vitro assembly and maturation systems. The assembly process of a clinically relevant virus such as hepatitis C virus is only starting to be glimpsed, and even for viruses extensively studied such as HIV many fundamental questions are still open. Finally, novel maturation mechanisms are likely to be found in the largely untapped pool of archaeal viruses that propagate under extreme environmental conditions [201]. For example, an unusual morphological change might be related to maturation in the fusiform *Acidianus* two-tailed virus (ATV), whose lemon-shaped particles can grow two filamentous tails in the absence of the host cell [202]. How this remarkable change happens and what purposes it may serve in ATV propagation are questions that remain to be explored.

Acknowledgments Work in the San Martín lab is funded by grants BFU2013-41249-P and BIO2015-68990-REDT (the Spanish Adenovirus Network, AdenoNet), from the Spanish Ministry of Economy and Competitiveness, as well as BFU2016-74868-P, co-funded by the Spanish State Research Agency and the European Regional Development Fund.

References

1. Flint J, Racaniello VR, Rall GF, Skalka AM (2015) Principles of virology, volume I: molecular biology, 4th edn. American Society of Microbiology, Washington, DC
2. Mateu MG (2013) Assembly, stability and dynamics of virus capsids. Arch Biochem Biophys 531:65–79
3. Veesler D, Johnson JE (2012) Virus maturation. Annu Rev Biophys 41:473–496
4. Suomalainen M, Greber UF (2013) Uncoating of non-enveloped viruses. Curr Opin Virol 3:27–33
5. Yamauchi Y, Greber UF (2016) Principles of virus uncoating: cues and the snooker ball. Traffic
6. Tsai B (2007) Penetration of nonenveloped viruses into the cytoplasm. Annu Rev Cell Dev Biol 23:23–43
7. Verdaguer N, Garriga D, Fita I (2013) X-ray crystallography of viruses. Subcell Biochem 68:117–144
8. Ho PT, Reddy VS (2018) Rapid increase of near atomic resolution virus capsid structures determined by cryo-electron microscopy. J Struct Biol 201:1–4
9. Kaelber JT, Hryc CF, Chiu W (2017) Electron cryomicroscopy of viruses at near-atomic resolutions. Annu Rev Virol 4:287–308
10. Briggs JA (2013) Structural biology in situ – the potential of subtomogram averaging. Curr Opin Struct Biol 23:261–267
11. Roos WH, Bruinsma R, Wuite GJL (2010) Physical virology. Nat Phys 6:733–743
12. Greber UF (2016) Virus and host mechanics support membrane penetration and cell entry. J Virol 90:3802–3805
13. de Pablo PJ (2017) Atomic force microscopy of virus shells. Semin Cell Dev Biol 73:199–208
14. de Pablo PJ, Colchero J, Gómez-Herrero J, Baró AM (1998) Jumping mode scanning force microscopy. Appl Phys Lett 73:3300–3302

15. Ortega-Esteban A, Horcas I, Hernando-Pérez M, Ares P, Pérez-Berná AJ, San Martín C, Carrascosa JL, de Pablo PJ, Gómez-Herrero J (2012) Minimizing tip–sample forces in jumping mode atomic force microscopy in liquid. Ultramicroscopy 114:56–61
16. Klar TA, Jakobs S, Dyba M, Egner A, Hell SW (2000) Fluorescence microscopy with diffraction resolution barrier broken by stimulated emission. Proc Natl Acad Sci U S A 97:8206–8210
17. Lippe R (2017) Flow virometry: a powerful tool to functionally characterize viruses. J Virol 92 (3):e01765–e01717
18. Uetrecht C, Heck AJ (2011) Modern biomolecular mass spectrometry and its role in studying virus structure, dynamics, and assembly. Angew Chem Int Ed Engl 50:8248–8262
19. Abrescia NG, Bamford DH, Grimes JM, Stuart DI (2012) Structure unifies the viral universe. Annu Rev Biochem 81:795–822
20. Krupovic M, Bamford DH (2008) Virus evolution: how far does the double beta-barrel viral lineage extend? Nat Rev Microbiol 6:941–948
21. Abrescia NG, Cockburn JJ, Grimes JM, Sutton GC, Diprose JM, Butcher SJ, Fuller SD, San Martín C, Burnett RM, Stuart DI, Bamford DH, Bamford JK (2004) Insights into assembly from structural analysis of bacteriophage PRD1. Nature 432:68–74
22. Benson SD, Bamford JKH, Bamford DH, Burnett RM (1999) Viral evolution revealed by bacteriophage PRD1 and human adenovirus coat protein structures. Cell 98:825–833
23. San Martín C, Huiskonen JT, Bamford JK, Butcher SJ, Fuller SD, Bamford DH, Burnett RM (2002) Minor proteins, mobile arms and membrane-capsid interactions in the bacteriophage PRD1 capsid. Nat Struct Biol 9:756–763
24. Racaniello VR (2013) Picornaviridae: the viruses and their replication. In: Knipe DM, Howley PM (eds) Fields virology, vol 1. Wolters Kluwer/Lippincott Williams & Wilkins Health, Philadelphia, PA, pp 453–489
25. Berns KI, Parrish CR (2013) Parvoviridae. In: Knipe DM, Howley PM (eds) Fields virology, vol 1. Wolters Kluwer/Lippincott Williams & Wilkins Health, Philadelphia, PA, pp 1768–1791
26. Coulibaly F, Chevalier C, Gutsche I, Pous J, Navaza J, Bressanelli S, Delmas B, Rey FA (2005) The birnavirus crystal structure reveals structural relationships among icosahedral viruses. Cell 120:761–772
27. Friesen PD (2013) Insect viruses. In: Knipe DM, Howley PM (eds) Fields virology, vol 1. Wolters Kluwer/Lippincott Williams & Wilkins Health, Philadelphia, PA, pp 2326–2354
28. Schneemann A, Zhong W, Gallagher TM, Rueckert RR (1992) Maturation cleavage required for infectivity of a nodavirus. J Virol 66:6728–6734
29. Schneemann A, Gallagher TM, Rueckert RR (1994) Reconstitution of flock house provirions: a model system for studying structure and assembly. J Virol 68:4547–4556
30. Fisher AJ, Johnson JE (1993) Ordered duplex RNA controls capsid architecture in an icosahedral animal virus. Nature 361:176–179
31. Gallagher TM, Rueckert RR (1988) Assembly-dependent maturation cleavage in provirions of a small icosahedral insect ribovirus. J Virol 62:3399–3406
32. Nemecek D, Cheng N, Qiao J, Mindich L, Steven AC, Heymann JB (2011) Stepwise expansion of the bacteriophage varphi6 procapsid: possible packaging intermediates. J Mol Biol 414:260–271
33. Pettersen EF, Goddard TD, Huang CC, Couch GS, Greenblatt DM, Meng EC, Ferrin TE (2004) UCSF Chimera – a visualization system for exploratory research and analysis. J Comput Chem 25:1605–1612
34. Kearney BM, Johnson JE (2014) Assembly and maturation of a $T = 4$ quasi-equivalent virus is guided by electrostatic and mechanical forces. Viruses 6:3348–3362
35. Canady MA, Tihova M, Hanzlik TN, Johnson JE, Yeager M (2000) Large conformational changes in the maturation of a simple RNA virus, nudaurelia capensis omega virus (NomegaV). J Mol Biol 299:573–584

36. Helgstrand C, Munshi S, Johnson JE, Liljas L (2004) The refined structure of Nudaurelia capensis omega virus reveals control elements for a T = 4 capsid maturation. Virology 318:192–203
37. Tang J, Lee KK, Bothner B, Baker TS, Yeager M, Johnson JE (2009) Dynamics and stability in maturation of a T = 4 virus. J Mol Biol 392:803–812
38. Basavappa R, Syed R, Flore O, Icenogle JP, Filman DJ, Hogle JM (1994) Role and mechanism of the maturation cleavage of VP0 in poliovirus assembly: structure of the empty capsid assembly intermediate at 2.9 A resolution. Protein Sci 3:1651–1669
39. Bubeck D, Filman DJ, Cheng N, Steven AC, Hogle JM, Belnap DM (2005) The structure of the poliovirus 135S cell entry intermediate at 10-angstrom resolution reveals the location of an externalized polypeptide that binds to membranes. J Virol 79:7745–7755
40. Chow M, Newman JF, Filman D, Hogle JM, Rowlands DJ, Brown F (1987) Myristylation of picornavirus capsid protein VP4 and its structural significance. Nature 327:482–486
41. Marc D, Masson G, Girard M, van der Werf S (1990) Lack of myristoylation of poliovirus capsid polypeptide VP0 prevents the formation of virions or results in the assembly of noninfectious virus particles. J Virol 64:4099–4107
42. Moscufo N, Chow M (1992) Myristate-protein interactions in poliovirus: interactions of VP4 threonine 28 contribute to the structural conformation of assembly intermediates and the stability of assembled virions. J Virol 66:6849–6857
43. Strauss M, Filman DJ, Belnap DM, Cheng N, Noel RT, Hogle JM (2015) Nectin-like interactions between poliovirus and its receptor trigger conformational changes associated with cell entry. J Virol 89:4143–4157
44. Irigoyen N, Garriga D, Navarro A, Verdaguer N, Rodriguez JF, Caston JR (2009) Autoproteolytic activity derived from the infectious bursal disease virus capsid protein. J Biol Chem 284:8064–8072
45. Luque D, Saugar I, Rodríguez JF, Verdaguer N, Garriga D, San Martín C, Velázquez-Muriel JA, Trus BL, Carrascosa JL, Castón JR (2007) Infectious bursal disease virus capsid assembly and maturation by structural rearrangements of a transient molecular switch. J Virol 81:6869–6878
46. Saugar I, Luque D, Ona A, Rodriguez JF, Carrascosa JL, Trus BL, Caston JR (2005) Structural polymorphism of the major capsid protein of a double-stranded RNA virus: an amphipathic alpha helix as a molecular switch. Structure 13:1007–1017
47. Grimes JM, Burroughs JN, Gouet P, Diprose JM, Malby R, Zientara S, Mertens PP, Stuart DI (1998) The atomic structure of the bluetongue virus core. Nature 395:470–478
48. Dermody TS, Parker JSL, Sherry B (2013) Orthoreoviruses. In: Knipe DM, Howley PM (eds) Fields virology, vol 2. Wolters Kluwer/Lippincott Williams & Wilkins Health, Philadelphia, PA, pp 1304–1346
49. Ghabrial SA, Caston JR, Jiang D, Nibert ML, Suzuki N (2015) 50-plus years of fungal viruses. Virology 479–480:356–368
50. Poranen MM, Bamford DH (2012) Assembly of large icosahedral double-stranded RNA viruses. In: Rossmann MG, Rao VB (eds) Viral molecular machines. Springer, Boston, MA, pp 379–402
51. Caspar DLD, Klug A (1962) Physical principles in the construction of regular viruses. Cold Spring Harb Symp Quant Biol 27:1–24
52. Luque D, Gonzalez JM, Garriga D, Ghabrial SA, Havens WM, Trus B, Verdaguer N, Carrascosa JL, Caston JR (2010) The T=1 capsid protein of *Penicillium chrysogenum* virus is formed by a repeated helix-rich core indicative of gene duplication. J Virol 84:7256–7266
53. Long CP, McDonald SM (2017) Rotavirus genome replication: some assembly required. PLoS Pathog 13:e1006242
54. Roy P (2017) Bluetongue virus structure and assembly. Curr Opin Virol 24:115–123
55. Trask SD, McDonald SM, Patton JT (2012) Structural insights into the coupling of virion assembly and rotavirus replication. Nat Rev Microbiol 10:165–177

56. Boudreaux CE, Kelly DF, McDonald SM (2015) Electron microscopic analysis of rotavirus assembly-replication intermediates. Virology 477:32–41
57. Mindich L (2012) Packaging in dsRNA viruses. Adv Exp Med Biol 726:601–608
58. Poranen MM, Tuma R, Bamford DH (2005) Assembly of double-stranded RNA bacteriophages. Adv Virus Res 64:15–43
59. Poranen MM, Paatero AO, Tuma R, Bamford DH (2001) Self-assembly of a viral molecular machine from purified protein and RNA constituents. Mol Cell 7:845–854
60. Butcher SJ, Dokland T, Ojala PM, Bamford DH, Fuller SD (1997) Intermediates in the assembly pathway of the double-stranded RNA virus phi6. EMBO J 16:4477–4487
61. Huiskonen JT, de Haas F, Bubeck D, Bamford DH, Fuller SD, Butcher SJ (2006) Structure of the bacteriophage phi6 nucleocapsid suggests a mechanism for sequential RNA packaging. Structure 14:1039–1048
62. Nemecek D, Boura E, Wu W, Cheng N, Plevka P, Qiao J, Mindich L, Heymann JB, Hurley JH, Steven AC (2013) Subunit folds and maturation pathway of a dsRNA virus capsid. Structure 21:1374–1383
63. Fokine A, Rossmann MG (2014) Molecular architecture of tailed double-stranded DNA phages. Bacteriophage 4:e28281
64. Suttle CA (2005) Viruses in the sea. Nature 437:356–361
65. Baker ML, Jiang W, Rixon FJ, Chiu W (2005) Common ancestry of herpesviruses and tailed DNA bacteriophages. J Virol 79:14967–14970
66. Gelbart WM, Knobler CM (2009) Virology: pressurized viruses. Science 323:1682–1683
67. Johnson JE (2010) Virus particle maturation: insights into elegantly programmed nanomachines. Curr Opin Struct Biol 20:210–216
68. Wikoff WR, Liljas L, Duda RL, Tsuruta H, Hendrix RW, Johnson JE (2000) Topologically linked protein rings in the bacteriophage HK97 capsid. Science 289:2129–2133
69. Prevelige PE, Fane BA (2012) Building the machines: scaffolding protein functions during bacteriophage morphogenesis. Adv Exp Med Biol 726:325–350
70. Huang RK, Khayat R, Lee KK, Gertsman I, Duda RL, Hendrix RW, Johnson JE (2011) The Prohead-I structure of bacteriophage HK97: implications for scaffold-mediated control of particle assembly and maturation. J Mol Biol 408:541–554
71. Oh B, Moyer CL, Hendrix RW, Duda RL (2014) The delta domain of the HK97 major capsid protein is essential for assembly. Virology 456–457:171–178
72. Duda RL, Oh B, Hendrix RW (2013) Functional domains of the HK97 capsid maturation protease and the mechanisms of protein encapsidation. J Mol Biol 425:2765–2781
73. Gertsman I, Gan L, Guttman M, Lee K, Speir JA, Duda RL, Hendrix RW, Komives EA, Johnson JE (2009) An unexpected twist in viral capsid maturation. Nature 458:646–650
74. Veesler D, Khayat R, Krishnamurthy S, Snijder J, Huang RK, Heck AJ, Anand GS, Johnson JE (2014) Architecture of a dsDNA viral capsid in complex with its maturation protease. Structure 22:230–237
75. Smith DE, Tans SJ, Smith SB, Grimes S, Anderson DL, Bustamante C (2001) The bacteriophage phi29 portal motor can package DNA against a large internal force. Nature 413:748–752
76. Duda RL, Hempel J, Michel H, Shabanowitz J, Hunt D, Hendrix RW (1995) Structural transitions during bacteriophage HK97 head assembly. J Mol Biol 247:618–635
77. Lata R, Conway JF, Cheng N, Duda RL, Hendrix RW, Wikoff WR, Johnson JE, Tsuruta H, Steven AC (2000) Maturation dynamics of a viral capsid: visualization of transitional intermediate states. Cell 100:253–263
78. Lee KK, Gan L, Tsuruta H, Moyer C, Conway JF, Duda RL, Hendrix RW, Steven AC, Johnson JE (2008) Virus capsid expansion driven by the capture of mobile surface loops. Structure 16:1491–1502
79. Gertsman I, Komives EA, Johnson JE (2010a) HK97 maturation studied by crystallography and H/2H exchange reveals the structural basis for exothermic particle transitions. J Mol Biol 397:560–574

80. Gertsman I, Fu CY, Huang R, Komives EA, Johnson JE (2010b) Critical salt bridges guide capsid assembly, stability, and maturation behavior in bacteriophage HK97. Mol Cell Proteomics 9:1752–1763
81. Ross PD, Cheng N, Conway JF, Firek BA, Hendrix RW, Duda RL, Steven AC (2005) Crosslinking renders bacteriophage HK97 capsid maturation irreversible and effects an essential stabilization. EMBO J 24:1352–1363
82. Ross PD, Conway JF, Cheng N, Dierkes L, Firek BA, Hendrix RW, Steven AC, Duda RL (2006) A free energy cascade with locks drives assembly and maturation of bacteriophage HK97 capsid. J Mol Biol 364:512–525
83. Roos WH, Gertsman I, May ER, Brooks CL 3rd, Johnson JE, Wuite GJ (2012) Mechanics of bacteriophage maturation. Proc Natl Acad Sci U S A 109:2342–2347
84. Parent KN, Khayat R, Tu LH, Suhanovsky MM, Cortines JR, Teschke CM, Johnson JE, Baker TS (2010) P22 coat protein structures reveal a novel mechanism for capsid maturation: stability without auxiliary proteins or chemical crosslinks. Structure 18:390–401
85. Yang F, Forrer P, Dauter Z, Conway JF, Cheng N, Cerritelli ME, Steven AC, Pluckthun A, Wlodawer A (2000) Novel fold and capsid-binding properties of the lambda-phage display platform protein gpD. Nat Struct Biol 7:230–237
86. Grunewald K, Desai P, Winkler DC, Heymann JB, Belnap DM, Baumeister W, Steven AC (2003) Three-dimensional structure of herpes simplex virus from cryo-electron tomography. Science 302:1396–1398
87. Cardone G, Heymann JB, Cheng N, Trus BL, Steven AC (2012) Procapsid assembly, maturation, nuclear exit: dynamic steps in the production of infectious herpesvirions. Adv Exp Med Biol 726:423–439
88. Yu X, Jih J, Jiang J, Zhou ZH (2017a) Atomic structure of the human cytomegalovirus capsid with its securing tegument layer of pp150. Science 356(6345):eaam6892
89. Bauer DW, Huffman JB, Homa FL, Evilevitch A (2013) Herpes virus genome, the pressure is on. J Am Chem Soc 135:11216–11221
90. Newcomb WW, Juhas RM, Thomsen DR, Homa FL, Burch AD, Weller SK, Brown JC (2001) The UL6 gene product forms the portal for entry of DNA into the herpes simplex virus capsid. J Virol 75:10923–10932
91. Rochat RH, Liu X, Murata K, Nagayama K, Rixon FJ, Chiu W (2011) Seeing the portal in herpes simplex virus type 1 B capsids. J Virol 85:1871–1874
92. Liu F, Roizman B (1993) Characterization of the protease and other products of amino-terminus-proximal cleavage of the herpes simplex virus 1 UL26 protein. J Virol 67:1300–1309
93. Robertson BJ, McCann PJ 3rd, Matusick-Kumar L, Newcomb WW, Brown JC, Colonno RJ, Gao M (1996) Separate functional domains of the herpes simplex virus type 1 protease: evidence for cleavage inside capsids. J Virol 70:4317–4328
94. Heymann JB, Cheng N, Newcomb WW, Trus BL, Brown JC, Steven AC (2003) Dynamics of herpes simplex virus capsid maturation visualized by time-lapse cryo-electron microscopy. Nat Struct Mol Biol 10:334–341
95. Trus BL, Booy FP, Newcomb WW, Brown JC, Homa FL, Thomsen DR, Steven AC (1996) The herpes simplex virus procapsid: structure, conformational changes upon maturation, and roles of the triplex proteins VP19c and VP23 in assembly. J Mol Biol 263:447–462
96. Roos WH, Radtke K, Kniesmeijer E, Geertsema H, Sodeik B, Wuite GJ (2009) Scaffold expulsion and genome packaging trigger stabilization of herpes simplex virus capsids. Proc Natl Acad Sci U S A 106:9673–9678
97. Rux JJ, Burnett RM (2000) Type-specific epitope locations revealed by X-ray crystallographic study of adenovirus type 5 hexon. Mol Ther 1:18–30
98. Gil-Carton D, Jaakkola ST, Charro D, Peralta B, Castano-Diez D, Oksanen HM, Bamford DH, Abrescia NG (2015) Insight into the assembly of viruses with vertical single beta-barrel major capsid proteins. Structure 23:1866–1877

99. Huiskonen JT, Kivela HM, Bamford DH, Butcher SJ (2004) The PM2 virion has a novel organization with an internal membrane and pentameric receptor binding spikes. Nat Struct Mol Biol 11:850–856
100. Xiao C, Fischer MG, Bolotaulo DM, Ulloa-Rondeau N, Avila GA, Suttle CA (2017) Cryo-EM reconstruction of the *Cafeteria roenbergensis* virus capsid suggests novel assembly pathway for giant viruses. Sci Rep 7:5484
101. Xiao C, Kuznetsov YG, Sun S, Hafenstein SL, Kostyuchenko VA, Chipman PR, Suzan-Monti M, Raoult D, McPherson A, Rossmann MG (2009) Structural studies of the giant mimivirus. PLoS Biol 7:e92
102. Bahar MW, Graham SC, Stuart DI, Grimes JM (2011) Insights into the evolution of a complex virus from the crystal structure of vaccinia virus D13. Structure 19:1011–1020
103. Krupovic M, Koonin EV (2015) Polintons: a hotbed of eukaryotic virus, transposon and plasmid evolution. Nat Rev Microbiol 13:105–115
104. Zhang X, Sun S, Xiang Y, Wong J, Klose T, Raoult D, Rossmann MG (2012) Structure of Sputnik, a virophage, at 3.5-A resolution. Proc Natl Acad Sci U S A 109:18431–18436
105. Fischer MG, Suttle CA (2011) A virophage at the origin of large DNA transposons. Science 332:231–234
106. Condezo GN, Marabini R, Ayora S, Carazo JM, Alba R, Chillón M, San Martín C (2015) Structures of adenovirus incomplete particles clarify capsid architecture and show maturation changes of packaging protein L1 52/55k. J Virol 89:9653–9664
107. Butcher SJ, Bamford DH, Fuller SD (1995) DNA packaging orders the membrane of bacteriophage PRD1. EMBO J 14:6078–6086
108. San Martín C, Burnett RM, de Haas F, Heinkel R, Rutten T, Fuller SD, Butcher SJ, Bamford DH (2001) Combined EM/X-ray imaging yields a quasi-atomic model of the adenovirus-related bacteriophage PRD1, and shows key capsid and membrane interactions. Structure 9:917–930
109. Peralta B, Gil-Carton D, Castano-Diez D, Bertin A, Boulogne C, Oksanen HM, Bamford DH, Abrescia NG (2013) Mechanism of membranous tunnelling nanotube formation in viral genome delivery. PLoS Biol 11:e1001667
110. Santos-Perez I, Oksanen HM, Bamford DH, Goni FM, Reguera D, Abrescia NGA (2017) Membrane-assisted viral DNA ejection. Biochim Biophys Acta 1861:664–672
111. Condezo GN, San Martín C (2017) Localization of adenovirus morphogenesis players, together with visualization of assembly intermediates and failed products, favor a model where assembly and packaging occur concurrently at the periphery of the replication center. PLoS Pathog 13:e1006320
112. Hong C, Oksanen HM, Liu X, Jakana J, Bamford DH, Chiu W (2014) A structural model of the genome packaging process in a membrane-containing double stranded DNA virus. PLoS Biol 12:e1002024
113. Benevento M, Di Palma S, Snijder J, Moyer CL, Reddy VS, Nemerow GR, Heck AJ (2014) Adenovirus composition, proteolysis, and disassembly studied by in-depth qualitative and quantitative proteomics. J Biol Chem 289:11421–11430
114. San Martín C (2012) Latest insights on adenovirus structure and assembly. Viruses 4:847–877
115. Campos SK (2014) New structural model of adenoviral cement proteins is not yet concrete. Proc Natl Acad Sci U S A 111:E4542–E4543
116. Liu H, Jin L, Koh SB, Atanasov I, Schein S, Wu L, Zhou ZH (2010) Atomic structure of human adenovirus by cryo-EM reveals interactions among protein networks. Science 329:1038–1043
117. Reddy VS, Nemerow GR (2014a) Structures and organization of adenovirus cement proteins provide insights into the role of capsid maturation in virus entry and infection. Proc Natl Acad Sci U S A 111:11715–11720
118. Reddy VS, Nemerow GR (2014b) Reply to Campos: revised structures of adenovirus cement proteins represent a consensus model for understanding virus assembly and disassembly. Proc Natl Acad Sci U S A 111:E4544–E4545

119. Reddy VS, Natchiar SK, Stewart PL, Nemerow GR (2010) Crystal structure of human adenovirus at 3.5 A resolution. Science 329:1071–1075
120. Dai X, Wu L, Sun R, Zhou ZH (2017) Atomic structures of minor proteins VI and VII in the human adenovirus. J Virol 91(24):e00850–e00817
121. Yu X, Veesler D, Campbell MG, Barry ME, Asturias FJ, Barry MA, Reddy VS (2017b) Cryo-EM structure of human adenovirus D26 reveals the conservation of structural organization among human adenoviruses. Sci Adv 3:e1602670
122. Pérez-Berná AJ, Marion S, Chichón FJ, Fernández JJ, Winkler DC, Carrascosa JL, Steven AC, Šiber A, San Martín C (2015) Distribution of DNA-condensing protein complexes in the adenovirus core. Nucleic Acids Res 43:4274–4283
123. Weber J (1976) Genetic analysis of adenovirus type 2 III. Temperature sensitivity of processing viral proteins. J Virol 17:462–471
124. Blainey PC, Graziano V, Pérez-Berná AJ, McGrath WJ, Flint SJ, San Martín C, Xie XS, Mangel WF (2013) Regulation of a viral proteinase by a peptide and DNA in one-dimensional space: IV. Viral proteinase slides along DNA to locate and process its substrates. J Biol Chem 288:2092–2102
125. Graziano V, Luo G, Blainey PC, Pérez-Berná AJ, McGrath WJ, Flint SJ, San Martín C, Xie XS, Mangel WF (2013) Regulation of a viral proteinase by a peptide and DNA in one-dimensional space: II. Adenovirus proteinase is activated in an unusual one-dimensional biochemical reaction. J Biol Chem 288:2068–2080
126. Mangel WF, San Martín C (2014) Structure, function and dynamics in adenovirus maturation. Viruses 6:4536–4570
127. Mangel WF, McGrath WJ, Toledo DL, Anderson CW (1993) Viral DNA and a viral peptide can act as cofactors of adenovirus virion proteinase activity. Nature 361:274–275
128. Cotten M, Weber JM (1995) The adenovirus protease is required for virus entry into host cells. Virology 213:494–502
129. Gastaldelli M, Imelli N, Boucke K, Amstutz B, Meier O, Greber UF (2008) Infectious adenovirus type 2 transport through early but not late endosomes. Traffic 9:2265–2278
130. Greber UF, Willetts M, Webster P, Helenius A (1993) Stepwise dismantling of adenovirus 2 during entry into cells. Cell 75:477–486
131. Greber UF, Webster P, Weber J, Helenius A (1996) The role of the adenovirus protease on virus entry into cells. EMBO J 15:1766–1777
132. Wiethoff CM, Wodrich H, Gerace L, Nemerow GR (2005) Adenovirus protein VI mediates membrane disruption following capsid disassembly. J Virol 79:1992–2000
133. Ortega-Esteban A, Pérez-Berná AJ, Menéndez-Conejero R, Flint SJ, San Martín C, de Pablo PJ (2013) Monitoring dynamics of human adenovirus disassembly induced by mechanical fatigue. Sci Rep 3:1434. https://doi.org/10.1038/srep01434
134. Pérez-Berná AJ, Marabini R, Scheres SHW, Menéndez-Conejero R, Dmitriev IP, Curiel DT, Mangel WF, Flint SJ, San Martín C (2009) Structure and uncoating of immature adenovirus. J Mol Biol 392:547–557
135. Pérez-Berná AJ, Ortega-Esteban A, Menéndez-Conejero R, Winkler DC, Menéndez M, Steven AC, Flint SJ, de Pablo PJ, San Martín C (2012) The role of capsid maturation on adenovirus priming for sequential uncoating. J Biol Chem 287:31582–31595
136. Burckhardt CJ, Suomalainen M, Schoenenberger P, Boucke K, Hemmi S, Greber UF (2011) Drifting motions of the adenovirus receptor CAR and immobile integrins initiate virus uncoating and membrane lytic protein exposure. Cell Host Microbe 10:105–117
137. Luisoni S, Suomalainen M, Boucke K, Tanner LB, Wenk MR, Guan XL, Grzybek M, Coskun U, Greber UF (2015) Co-option of membrane wounding enables virus penetration into cells. Cell Host Microbe 18:75–85
138. Nakano MY, Boucke K, Suomalainen M, Stidwill RP, Greber UF (2000) The first step of adenovirus type 2 disassembly occurs at the cell surface, independently of endocytosis and escape to the cytosol. J Virol 74:7085–7095

139. Puntener D, Engelke MF, Ruzsics Z, Strunze S, Wilhelm C, Greber UF (2011) Stepwise loss of fluorescent core protein V from human adenovirus during entry into cells. J Virol 85:481–496
140. Ortega-Esteban A, Bodensiek K, San Martín C, Suomalainen M, Greber UF, de Pablo PJ, Schaap IA (2015a) Fluorescence tracking of genome release during mechanical unpacking of single viruses. ACS Nano 9:10571–10579
141. Silvestry M, Lindert S, Smith JG, Maier O, Wiethoff CM, Nemerow GR, Stewart PL (2009) Cryo-electron microscopy structure of adenovirus type 2 temperature-sensitive mutant 1 reveals insight into the cell entry defect. J Virol 83:7375–7383
142. Ortega-Esteban A, Condezo GN, Pérez-Berná AJ, Chillón M, Flint SJ, Reguera D, San Martín C, de Pablo PJ (2015b) Mechanics of viral chromatin reveals the pressurization of human adenovirus. ACS Nano 9:10826–10833
143. Moyer CL, Besser ES, Nemerow GR (2016) A single maturation cleavage site in adenovirus impacts cell entry and capsid assembly. J Virol 90:521–532
144. Guimet D, Hearing P (2013) The adenovirus L4-22K protein has distinct functions in the posttranscriptional regulation of gene expression and encapsidation of the viral genome. J Virol 87:7688–7699
145. Ostapchuk P, Almond M, Hearing P (2011) Characterization of empty adenovirus particles assembled in the absence of a functional adenovirus IVa2 protein. J Virol 85:5524–5531
146. Wohl BP, Hearing P (2008) Role for the L1-52/55K protein in the serotype specificity of adenovirus DNA packaging. J Virol 82:5089–5092
147. Wu K, Guimet D, Hearing P (2013) The adenovirus L4-33K protein regulates both late gene expression patterns and viral DNA packaging. J Virol 87:6739–6747
148. Pérez-Berná AJ, Mangel WF, McGrath WJ, Graziano V, Flint J, San Martín C (2014) Processing of the L1 52/55k protein by the adenovirus protease: a new substrate and new insights into virion maturation. J Virol 88:1513–1524
149. Cassany A, Ragues J, Guan T, Begu D, Wodrich H, Kann M, Nemerow GR, Gerace L (2015) Nuclear import of adenovirus DNA involves direct interaction of hexon with an N-terminal domain of the nucleoporin Nup214. J Virol 89:1719–1730
150. Greber UF, Suomalainen M, Stidwill RP, Boucke K, Ebersold MW, Helenius A (1997) The role of the nuclear pore complex in adenovirus DNA entry. EMBO J 16:5998–6007
151. Strunze S, Engelke MF, Wang IH, Puntener D, Boucke K, Schleich S, Way M, Schoenenberger P, Burckhardt CJ, Greber UF (2011) Kinesin-1-mediated capsid disassembly and disruption of the nuclear pore complex promote virus infection. Cell Host Microbe 10:210–223
152. Trotman LC, Mosberger N, Fornerod M, Stidwill RP, Greber UF (2001) Import of adenovirus DNA involves the nuclear pore complex receptor CAN/Nup214 and histone H1. Nat Cell Biol 3:1092–1100
153. Liu L, Cooper T, Howley PM, Hayball JD (2014) From crescent to mature virion: *Vaccinia virus* assembly and maturation. Viruses 6:3787–3808
154. Byrd CM, Hruby DE (2006) Vaccinia virus proteolysis – a review. Rev Med Virol 16:187–202
155. Marion S, San Martín C, Siber A (2017) Role of condensing particles in polymer confinement: a model for virus-packed "minichromosomes". Biophys J 113:1643–1653
156. Milrot E, Shimoni E, Dadosh T, Rechav K, Unger T, Van Etten JL, Minsky A (2017) Structural studies demonstrating a bacteriophage-like replication cycle of the eukaryote-infecting *Paramecium bursaria* chlorella virus-1. PLoS Pathog 13:e1006562
157. Griffin DE (2013) Alphaviruses. In: Knipe DM, Howley PM (eds) Fields virology, vol 1. Wolters Kluwer/Lippincott Williams & Wilkins Health, Philadelphia, PA, pp 651–686
158. Lindenbach BD, Murray CL, Thiel H-J, Rice CM (2013) Flaviviridae. In: Knipe DM, Howley PM (eds) Fields virology, vol 1. Wolters Kluwer/Lippincott Williams & Wilkins Health, Philadelphia, PA, pp 712–746
159. Jose J, Snyder JE, Kuhn RJ (2009) A structural and functional perspective of alphavirus replication and assembly. Future Microbiol 4:837–856

160. Pierson TC, Diamond MS (2012) Degrees of maturity: the complex structure and biology of flaviviruses. Curr Opin Virol 2:168–175
161. Ferlenghi I, Gowen B, de Haas F, Mancini EJ, Garoff H, Sjoberg M, Fuller SD (1998) The first step: activation of the Semliki Forest virus spike protein precursor causes a localized conformational change in the trimeric spike. J Mol Biol 283:71–81
162. Mancini EJ, Clarke M, Gowen BE, Rutten T, Fuller SD (2000) Cryo-electron microscopy reveals the functional organization of an enveloped virus, Semliki Forest virus. Mol Cell 5:255–266
163. Mukhopadhyay S, Zhang W, Gabler S, Chipman PR, Strauss EG, Strauss JH, Baker TS, Kuhn RJ, Rossmann MG (2006) Mapping the structure and function of the E1 and E2 glycoproteins in alphaviruses. Structure 14:63–73
164. Pletnev SV, Zhang W, Mukhopadhyay S, Fisher BR, Hernandez R, Brown DT, Baker TS, Rossmann MG, Kuhn RJ (2001) Locations of carbohydrate sites on alphavirus glycoproteins show that E1 forms an icosahedral scaffold. Cell 105:127–136
165. Zhang W, Mukhopadhyay S, Pletnev SV, Baker TS, Kuhn RJ, Rossmann MG (2002) Placement of the structural proteins in Sindbis virus. J Virol 76:11645–11658
166. Yap ML, Klose T, Urakami A, Hasan SS, Akahata W, Rossmann MG (2017) Structural studies of Chikungunya virus maturation. Proc Natl Acad Sci U S A 114:13703–13707
167. Kielian M, Chanel-Vos C, Liao M (2010) Alphavirus entry and membrane fusion. Viruses 2:796–825
168. Zhang W, Chipman PR, Corver J, Johnson PR, Zhang Y, Mukhopadhyay S, Baker TS, Strauss JH, Rossmann MG, Kuhn RJ (2003a) Visualization of membrane protein domains by cryo-electron microscopy of dengue virus. Nat Struct Biol 10(11):907
169. Zhang Y, Corver J, Chipman PR, Zhang W, Pletnev SV, Sedlak D, Baker TS, Strauss JH, Kuhn RJ, Rossmann MG (2003b) Structures of immature flavivirus particles. EMBO J 22:2604–2613
170. Kostyuchenko VA, Zhang Q, Tan JL, Ng TS, Lok SM (2013) Immature and mature dengue serotype 1 virus structures provide insight into the maturation process. J Virol 87:7700–7707
171. Li L, Lok SM, Yu IM, Zhang Y, Kuhn RJ, Chen J, Rossmann MG (2008) The flavivirus precursor membrane-envelope protein complex: structure and maturation. Science 319:1830–1834
172. Yu IM, Zhang W, Holdaway HA, Li L, Kostyuchenko VA, Chipman PR, Kuhn RJ, Rossmann MG, Chen J (2008) Structure of the immature dengue virus at low pH primes proteolytic maturation. Science 319:1834–1837
173. Kuhn RJ, Zhang W, Rossmann MG, Pletnev SV, Corver J, Lenches E, Jones CT, Mukhopadhyay S, Chipman PR, Strauss EG, Baker TS, Strauss JH (2002) Structure of dengue virus: implications for flavivirus organization, maturation, and fusion. Cell 108:717–725
174. Zhang X, Ge P, Yu X, Brannan JM, Bi G, Zhang Q, Schein S, Zhou ZH (2013) Cryo-EM structure of the mature dengue virus at 3.5-A resolution. Nat Struct Mol Biol 20:105–110
175. Plevka P, Battisti AJ, Junjhon J, Winkler DC, Holdaway HA, Keelapang P, Sittisombut N, Kuhn RJ, Steven AC, Rossmann MG (2011) Maturation of flaviviruses starts from one or more icosahedrally independent nucleation centres. EMBO Rep 12:602–606
176. Zicari S, Arakelyan A, Fitzgerald W, Zaitseva E, Chernomordik LV, Margolis L, Grivel JC (2016) Evaluation of the maturation of individual Dengue virions with flow virometry. Virology 488:20–27
177. Goff SP (2013) Retroviridae. In: Knipe DM, Howley PM (eds) Fields virology, vol 2. Wolters Kluwer/Lippincott Williams & Wilkins Health, Philadelphia, PA, pp 1424–1473
178. Freed EO (2015) HIV-1 assembly, release and maturation. Nat Rev Microbiol 13:484–496
179. Briggs JA, Simon MN, Gross I, Krausslich HG, Fuller SD, Vogt VM, Johnson MC (2004) The stoichiometry of Gag protein in HIV-1. Nat Struct Mol Biol 11:672–675
180. Briggs JA, Riches JD, Glass B, Bartonova V, Zanetti G, Krausslich HG (2009) Structure and assembly of immature HIV. Proc Natl Acad Sci U S A 106:11090–11095

181. Schur FK, Hagen WJ, Rumlova M, Ruml T, Muller B, Krausslich HG, Briggs JA (2015) Structure of the immature HIV-1 capsid in intact virus particles at 8.8 A resolution. Nature 517:505–508
182. Mattei S, Schur FK, Briggs JA (2016a) Retrovirus maturation-an extraordinary structural transformation. Curr Opin Virol 18:27–35
183. Lee SK, Potempa M, Swanstrom R (2012) The choreography of HIV-1 proteolytic processing and virion assembly. J Biol Chem 287:40867–40874
184. Fontana J, Jurado KA, Cheng N, Ly NL, Fuchs JR, Gorelick RJ, Engelman AN, Steven AC (2015) Distribution and redistribution of HIV-1 nucleocapsid protein in immature, mature, and integrase-inhibited virions: a role for integrase in maturation. J Virol 89:9765–9780
185. Cardone G, Purdy JG, Cheng N, Craven RC, Steven AC (2009) Visualization of a missing link in retrovirus capsid assembly. Nature 457:694–698
186. Gres AT, Kirby KA, KewalRamani VN, Tanner JJ, Pornillos O, Sarafianos SG (2015) Structural virology: X-ray crystal structures of native HIV-1 capsid protein reveal conformational variability. Science 349:99–103
187. Pornillos O, Ganser-Pornillos BK, Yeager M (2011) Atomic-level modelling of the HIV capsid. Nature 469:424–427
188. Zhao G, Perilla JR, Yufenyuy EL, Meng X, Chen B, Ning J, Ahn J, Gronenborn AM, Schulten K, Aiken C, Zhang P (2013) Mature HIV-1 capsid structure by cryo-electron microscopy and all-atom molecular dynamics. Nature 497:643–646
189. Ganser BK, Li S, Klishko VY, Finch JT, Sundquist WI (1999) Assembly and analysis of conical models for the HIV-1 core. Science 283:80–83
190. Mattei S, Glass B, Hagen WJ, Krausslich HG, Briggs JA (2016b) The structure and flexibility of conical HIV-1 capsids determined within intact virions. Science 354:1434–1437
191. Lanman J, Lam TT, Emmett MR, Marshall AG, Sakalian M, Prevelige PE Jr (2004) Key interactions in HIV-1 maturation identified by hydrogen-deuterium exchange. Nat Struct Mol Biol 11:676–677
192. Lanman J, Lam TT, Barnes S, Sakalian M, Emmett MR, Marshall AG, Prevelige PE Jr (2003) Identification of novel interactions in HIV-1 capsid protein assembly by high-resolution mass spectrometry. J Mol Biol 325:759–772
193. Monroe EB, Kang S, Kyere SK, Li R, Prevelige PE Jr (2010) Hydrogen/deuterium exchange analysis of HIV-1 capsid assembly and maturation. Structure 18:1483–1491
194. Hanne J, Gottfert F, Schimer J, Anders-Osswein M, Konvalinka J, Engelhardt J, Muller B, Hell SW, Krausslich HG (2016) Stimulated emission depletion nanoscopy reveals time-course of human immunodeficiency virus proteolytic maturation. ACS Nano 10:8215–8222
195. Kol N, Shi Y, Tsvitov M, Barlam D, Shneck RZ, Kay MS, Rousso I (2007) A stiffness switch in human immunodeficiency virus. Biophys J 92:1777–1783
196. Murakami T, Ablan S, Freed EO, Tanaka Y (2004) Regulation of human immunodeficiency virus type 1 Env-mediated membrane fusion by viral protease activity. J Virol 78:1026–1031
197. Pang HB, Hevroni L, Kol N, Eckert DM, Tsvitov M, Kay MS, Rousso I (2013) Virion stiffness regulates immature HIV-1 entry. Retrovirology 10:4
198. Wyma DJ, Jiang J, Shi J, Zhou J, Lineberger JE, Miller MD, Aiken C (2004) Coupling of human immunodeficiency virus type 1 fusion to virion maturation: a novel role of the gp41 cytoplasmic tail. J Virol 78:3429–3435
199. Chojnacki J, Staudt T, Glass B, Bingen P, Engelhardt J, Anders M, Schneider J, Muller B, Hell SW, Krausslich HG (2012) Maturation-dependent HIV-1 surface protein redistribution revealed by fluorescence nanoscopy. Science 338:524–528
200. Chojnacki J, Waithe D, Carravilla P, Huarte N, Galiani S, Enderlein J, Eggeling C (2017) Envelope glycoprotein mobility on HIV-1 particles depends on the virus maturation state. Nat Commun 8:545
201. Prangishvili D, Bamford DH, Forterre P, Iranzo J, Koonin EV, Krupovic M (2017) The enigmatic archaeal virosphere. Nat Rev Microbiol 15:724–739
202. Haring M, Vestergaard G, Rachel R, Chen L, Garrett RA, Prangishvili D (2005) Virology: independent virus development outside a host. Nature 436:1101–1102

Chapter 8
Atomic Force Microscopy of Viruses

P. J. de Pablo and I. A. T. Schaap

Abstract Atomic force microscopy employs a nanometric tip located at the end of a micro-cantilever to probe surface-mounted samples at nanometer resolution. Because the technique can also work in a liquid environment it offers unique possibilities to study individual viruses under conditions that mimic their natural milieu. Here, we review how AFM imaging can be used to study the surface structure of viruses including that of viruses lacking a well-defined symmetry. Beyond imaging, AFM enables the manipulation of single viruses by force spectroscopy experiments. Pulling experiments can provide information about the early events of virus–host interaction between the viral fibers and the cell membrane receptors. Pushing experiments measure the mechanical response of the viral capsid and its contents and can be used to show how virus maturation and exposure to different pH values change the mechanical response of the viruses and the interaction between the capsid and genome. Finally, we discuss how studying capsid rupture and self-healing events offers insight in virus uncoating pathways.

Keywords Protein · Shell · Cage · Capsid · Virus · Atomic force microscopy · Stiffness · Spring constant · Force curve · Nano-indentation · Tip · Cantilever · Topography · Rupture · Breaking · Fatigue · Elasticity

P. J. de Pablo (✉)
Department of Condensed Matter Physics and Solid Condensed Matter Institute IFIMAC, Universidad Autónoma de Madrid, Madrid, Spain
e-mail: p.j.depablo@uam.es

I. A. T. Schaap
SmarAct GmbH, Oldenburg, Germany
e-mail: schaap@smaract.com

U. F. Greber (ed.), *Physical Virology*, Advances in Experimental Medicine and Biology 1140, https://doi.org/10.1007/978-3-030-14741-9_8

Abbreviations

AFM	Atomic Force Microscopy
Fl	Lateral Force
Fn	Normal Force
FZ	Force vs. Distance
HAdV	human Adenovirus
HIV	Human Immunodeficiency Virus
HOPG	Highly Oriented Pyrolytic Graphite
JM	Jumping Mode
nN	nanoNewton
pN	picoNewton
TIRFM	Total Internal Reflection Fluorescence Microscopy
TMV	Tobacco Mosaic Virus

8.1 Introduction

A characterizing structural element in viruses is the protein capsid that can combine multiple functions, including recognition of the target cell and packaging of the viral genome. These capsids are constructed from protein subunits that form a closed shell with dimension of tens to hundreds of nanometer. Although virus capsids are the classic example of protein cages, non-viral structures such as bacterial microcompartments (BMCs) [1], vault particles [2], clathrin cages [3], and artificial virus-like structures [4–6] are other examples. Virus capsids are made up of repeating protein subunits (capsomers) that pack the viral genome [7] and are endorsed with meta-stable properties that allow a change of functionality during the viral life cycle [8]. These unique properties have made viral capsids a promising template to engineer carriers of drugs or other cargoes [9].

Protein cages, whether natural or artificial, have to protect their cargo against a variety of conditions, such as thermal and chemical changes [10], osmotic shocks [11], but also molecular impacts in highly crowded media [12]. To better understand the design of protein cages, methods are required that provide information about their structure and stability under the different conditions. To this end, structural biology techniques such as electron microscopy (EM) and X-ray crystallography are used to determine impressive high-resolution structures [13]. However, these methods require the averaging of thousands to millions of particles present in the electron micrographs or crystal. As a consequence, such reconstructed models provide limited information on structural differences that can exist between the individual particles in the population. This complicates, for example, structural studies of viruses that lack a well-defined symmetry such as the influenza virus [14]. In addition, these approaches require environments (vacuum, vitreous ice, etcetera) that are far away from the physiological conditions in which protein shells

normally operate and preclude the characterization of their dynamic properties in real time. The mechanical properties of a protein cage are defined by its molecular structure and a multitude of single molecule experiments has demonstrated a clear relation between mechanics and function [15]. Thus, the exploration of mechanical properties would complete the arsenal of structural biology methods to better understand the interplay between structure and function of protein cages.

Atomic force microscopy (AFM) allows the structural determination of individual protein particles at nanometric resolution in liquid milieu and can even monitor the highly dynamic entry and budding of individual viruses in the host. In addition, mechanical properties can be measured by manipulating the particles with the AFM probe. Environmental conditions, such as pH, can be varied within the AFM liquid cell to investigate the evolution of the protein shell structure and its mechanical properties. The ability of AFM to manipulate matter at the nanoscale allows also the dissection of protein shells to learn more about their (dis)assembly.

In this review, we provide a general overview of how AFM methods can be applied to better understand viruses. First, we introduce the most successful modes for the imaging of protein shells. Next, we explain how mechanical parameters, like stiffness and rupture force, can be measured by nano-indentation experiments. In this context, we also discuss self-healing properties and material fatigue of protein cages. We show how correlative microscopy, AFM with fluorescence, can be used to study genome release. In the last part, we present the effects of the pH conditions on virus mechanics and refer to AFM studies that monitored the entry and budding of individual virus particles.

8.2 Imaging Viruses with AFM

To examine a specimen with AFM, it needs to be immobilized to a solid substrate. Virus particles are normally attached by using physical interactions with the substrate, including polar, non-polar, and van der Waals forces [16]. The advantage of physisorption is that it does not require the formation of chemical bonds which may alter the structure of the sample. Hydrophobic patches or local charge densities that are present on the surface of the sample [17] can be exploited to immobilize the samples on substrates, such as mica, glass, and HOPG (highly oriented pyrolytic graphite) via hydrophobic or electrostatic interactions (see details in Moreno-Madrid et al. [18]). One could say that each type of virus has a preferred substrate, since each kind of protein cage exposes different residues.

Figure 8.1 shows human adenovirus (HAdV), herpes simplex, and P22 bacteriophage particles, adsorbed on mica, silanized glass, and HOPG, respectively [19–21]. These are examples of non-enveloped viruses with an icosahedral structure. Figure 8.1a–c shows that they can present three-fold, two-fold, and five-fold symmetry axes after adsorption. AFM can also image viruses with a less-defined geometry such as the HIV capsids [22] (Fig. 8.1d) and enveloped influenza viruses [23] (Fig. 8.1e). Figure 8.1f shows the cylindrical structure of tobacco mosaic virus (TMV) [24] and

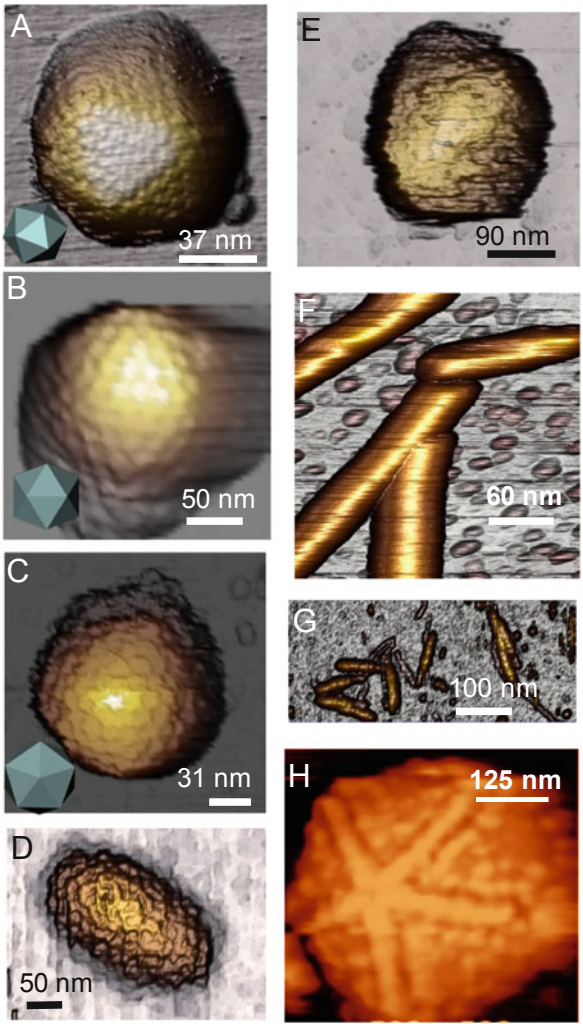

Fig. 8.1 AFM images of single viruses. (**a**) HAdV particle adsorbed on a triangular facet [19]. (**b**) Herpes simplex virus particle showing a two-fold orientation [20]. (**c**) P22 bacteriophage resting on its five-fold symmetry axis [21]. (**d**) Enveloped HIV virus [22]. (**e**) Enveloped influenza virus [23]. (**f**) TMV viruses [24]. (**g**) Viral fibers of T4 bacteriophage [25]. (**h**) Mimivirus [26]

Fig. 8.1g presents the AFM topography of T4 phage isolated fibers [25]. AFM can also scan huge viruses, such as mimivirus (Fig. 8.1h) [26].

In AFM, the tip mounted at the end of a flexible cantilever scans the sample in X, Y, and Z directions by using piezo actuators. While the X and Y scanners raster a square area, the interaction with the substrate and sample will lead to a bending of the cantilever. The cantilever deflects perpendicularly to the surface applying a normal force (F_n), and will also slightly twist due to lateral dragging forces parallel to the surface (F_l) [27]. To monitor F_n and F_l, a laser beam is focused at the end of the cantilever and reflected onto a four-quadrant photodiode, which gives out signals that are proportional to F_n and F_l. Thus, each pixel of the scanned area will be associated with certain bending values of the cantilever F_n and F_l. If the virus particle

is not strongly attached or if it is too soft, it will be easily displaced or damaged by the bending forces. To prevent this issue, a feedback loop is implemented to keep F_n at a constant level by moving the Z-piezo position. In this approach, known as contact mode, the AFM topography map will have X, Y, and Z coordinates, where Z is the displacement applied to the Z-piezo to keep F_n constant. However, the torsional bending force F_l of the cantilever is ~40 times higher than the flexural bending force F_n [28], which will lead to very high dragging forces. Although this is problemless with solid surfaces, like mica [29] or specimens which are held by close packing, such as purple membrane [30], isolated samples, such as DNA molecules, are prone to damage in contact mode [31]. Likewise, also protein cages are easily modified by too high lateral forces. The problem is made worse by the large topographical aspect ratio of the viruses (while scanning across a particle the tip "sees" uphill inclinations approaching 90°) which are difficult to track by the feedback loop and lead to an overshoot of F_n and F_l. To stabilize the sample against these forces, glutaraldehyde or other fixation agents can be used. Indeed, AFM has provided images under such conditions with a resolution that is comparable to that of EM images [32]. Nevertheless, since glutaraldehyde structurally reinforces the specimens [33, 34], it complicates the characterization of intact native viruses, such as disassembly or mechanical properties [35]. The developments of imaging modes that drastically reduce dragging forces have made it possible to investigate biological samples without chemical fixation. In jumping mode (JM), also called pulse force mode [36, 37], the lateral tip displacement occurs when the tip is retracted from the sample, which largely avoids dragging forces. In JM an approach-release cycle is performed at every pixel of the sample. In each cycle, known as a force versus distance (FZ) curve, the Z-piezo moves the tip to the sample until establishing mechanical contact and reaching a certain feedback force. After a few milliseconds, the Z-piezo retracts the tip for about 100 nm while the X–Y piezos move the tip laterally to the next pixel, and the process repeats [36, 38]. Especially in liquid milieu, where adhesion forces between tip and sample are largely absent, JM has proven very successful [39]. A further advantage is that mechanical sample properties such as stiffness can be obtained during imaging [40]. Variants of JM are now also increasingly implemented by multiple AFM manufacturers (PeakForce Tapping® QI™ mode). Nevertheless, the most common imaging mode for biological samples is still amplitude modulation mode. Here, the AFM cantilever is oscillated at a small amplitude (~10 nm) and when the tip comes close to the surface this amplitude will be modulated (reduced) by the tip–sample interaction. By using the oscillation amplitude as input for the feedback loop, the interaction forces with the sample are kept constant, while dragging forces are minimized because the tip spends most of its time away from the sample. A limitation of such AFM dynamic modes is that it is difficult to quantify the applied force in real time [41].

8.3 Nano-Indentation

The abilities of AFM are not limited to the topographical characterization of samples [42]. Because the AFM cantilever is a force transducer it can be used to manipulate matter at the atomic scale [43] including pulling and pushing on individual biomolecules [40, 44]. The number of mechanical studies of protein cages has seen a steep increase during the last decade. Virus mechanics have been found to depend on the packed genome [45–50], maturation state [19, 33, 51, 52], artificial cargo [21], and structural modification of the cage by protein engineering [53]. The internal pressure of viruses, caused by tightly packed DNA inside some bacteriophages [54] and helps during the first stages of genome translocation into the host [55], can be measured [56] and modulated by DNA counter-ions on individual particles [47]. Protein shells of non-viral origin have also been investigated, such as vault particles [57] and encapsulin [58].

The majority of AFM force spectroscopy experiments on viruses are performed by nano-indentation. Single FZ experiments are performed on top of a selected protein cage (Fig. 8.2a). The cantilever deflection can be transformed into a force by multiplying deflection with the spring constant of the cantilever. The indentation of the protein cage is given by the motion of the Z-piezo minus the bending of the cantilever. To find the top of the protein cage the particle is first imaged at high magnification (~50 nm × 50 nm) after which an FZ curve is performed on the central region of the particle. It is important to minimize the time between acquiring the image and performing the FZ curve so that drift, which can reach tens of nm per minute, does not affect the positioning of the AFM tip on the cage too much. Alternatively, an array of force curves can be performed on the particle from which a height image can be reconstructed after which the central curves can be selected for further analysis [23]. If elastic properties of the protein cage are studied, the FZ curves have to be performed slow enough to allow the water to leave the capsid during indentation, typically speeds between 50 nm/s and 1 μm/s are used [23, 60]. After the tip contacts the particle, the FZ curves behave approximately linearly, which denotes the indentation of the protein cage (Fig. 8.2b, label 2). Interestingly, an exponential increase in force that is expected because the contact area between the AFM tip and the cage will increase during indentation remains largely invisible in many experiments. This has been explained by the local compression of the protein layer directly under the tip and by buckling of the whole protein shell which both counteract this effect [40, 61].

When the indentation depth is kept small it is possible to perform repetitive FZ curves, and the particle deforms in a reversible way, which proves an elastic response. However, when the indentation surpasses the elastics limits, often at around 20% of the particle's height, the particle breaks which is visible as a sequence of irregular steps in the FZ curve due to the disassembly of the discrete building blocks that form the cage structure (Fig. 8.2b, label 3). Thin shell theory provides a stiffness for the protein shell of $k \approx E\frac{h^2}{R}$, where E is the Young's modulus, h the thickness of the shell, and R its radius [62]. k is obtained from the linear force

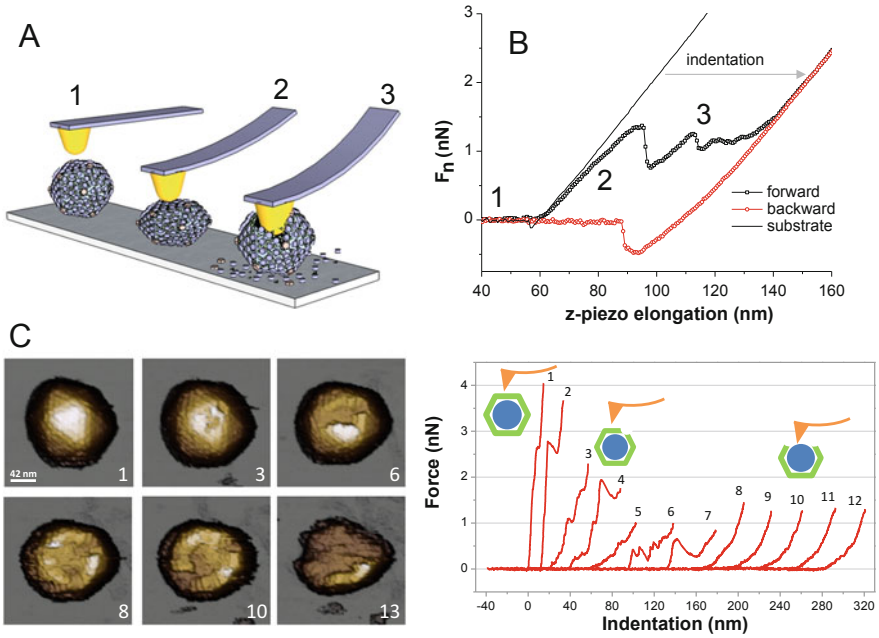

Fig. 8.2 Nano-indentation experiment. (**a**) The three main phases during a nano-indentation experiment on a protein cage: (1) before contact, (2) during indentation, and (3) after breaking. (**b**) F_n as function of the Z-piezo displacement, containing the three phases in the forward curve [adapted from [18]]. The cantilever deformation is obtained by performing an FZ on the substrate (Fig. b, solid line), and considering that it is much more rigid than the cantilever. The subtraction of the substrate curve from the sample curve gives the indentation of the cage. From the indentation curves both the stiffness or spring constant (by fitting the linear part) and the rupture force (visible as a sudden step) can be directly obtained. (**c**) AFM images (left) of a single HAdV wild-type particle that is subjected to 12 indentation curves (right) in the presence of spermidine. The number of the AFM images corresponds to the number of the indentation curve [adapted from [59]]

vs. indentation curves under the assumption of a spherical shell subjected to two opposing point forces and can thus be used to estimate the effective Young's modulus of viruses [63, 64]. To include more realistic contact boundary conditions that replace the point forces by a flat substrate and a rounded AFM tip, finite element analysis has proven very helpful [61].

However, when the viral genome contributes to the viral stiffness, the thin shell approximation breaks down and the response will show an exponential Hertzian behavior [59]. By performing consecutive FZ curves on the same virus it is possible to test the stiffness of the viral genome. Figure 8.2c shows an HAdV particle that has been indented 12 times [59]. After the third indentation (Fig. 8.2c, right graph) the shell broke (Fig. 8.2c, frame #3) which allowed the AFM tip to directly probe the virus core, which consists of dsDNA and condensing proteins [65]. Fitting the resulting exponential curves with the Hertz model [66] yields Young's moduli of 1.2 MPa and 0.3 MPa for the immature and mature cores, respectively. The higher

value suggests a highly condensed genome before maturation while the lower value indicates a less-condensed genome for the mature cores. This decondensation has been speculated to be important for the transport of the genome through the nuclear pore [59].

By performing FZ curves that exceed the elastic limits of the protein cage also the rupture events between the protein subunits can be studied [67]. For instance, in vault particles the stepped nonlinearities after the first rupture event were associated with the individual proteins unzipping while the particle was being disrupted during the nano-indentation experiment [68]. Most protein cages show a similar fracture behavior [51], which implies little plastic deformation before breaking like a brittle egg shell. However, in some cases a plastic behavior has been shown [69], i.e., a virus deforms like clay before breaking. In some cases, rupture events have been found to be reversible. For instance, both microtubule protein shells and vault particles have demonstrated self-healing capabilities [40, 68] (Fig. 8.3a). Such self-healing ability has also been demonstrated on monolayers of capsid protein of human immunodeficiency virus (HIV) [70]. Also reversible stepwise rupture events [71] in T7 bacteriophage ([71] (Fig. 8.3c, upper and middle) have been attributed to the reversible buckling of individual capsomers during the nano-indentation process (Fig. 8.3c, bottom).

Mechanical properties of virus capsids can also be modified by specific treatments or genetic engineering. When mature expanded capsids (EX) of P22 bacteriophage [53] are subjected to elevated temperatures they lose their pentons, leaving 12 vacancies in the shell that result in a "whiffle ball" (WB) [72]. WB structures are softer than EX, break before the intact P22 structures [69], and are chemically less resistant to sodium dodecyl sulfate. Interestingly, the stability of WB can be recovered by adding Dec proteins, a decoration protein of the bacteriophage L [73]. Binding of Dec protein to WB particles recuperates both their mechanical and chemical resistance [53]. Directed mutagenesis is another method that permits tailoring virus mechanics in the case of minute virus of mice [74, 75].

Often, mechanical parameters like stiffness, Young's modulus, and rupture forces of viral particles are directly associated with capsid stability. However, during transmission viruses are confronted with both mechanical and chemical attacks, such as pH variation [49] and osmotic shocks [11]. Therefore, a connection is expected between the capacity of protein cages to endure chemical and mechanical stresses. Indeed, for T7 bacteriophage it was found that mature capsids have a higher resistance to GuHCl and urea than immature T7 capsids. This increased chemical resistance coincides with an increased mechanical rigidity [51].

8.4 Mechanical Fatigue

The disassembly of many virus shells is thought to occur by the sequential release of capsomers in an ordered manner [76]. This process is difficult to investigate with AFM. As described above, the particle will break if a certain deformation threshold

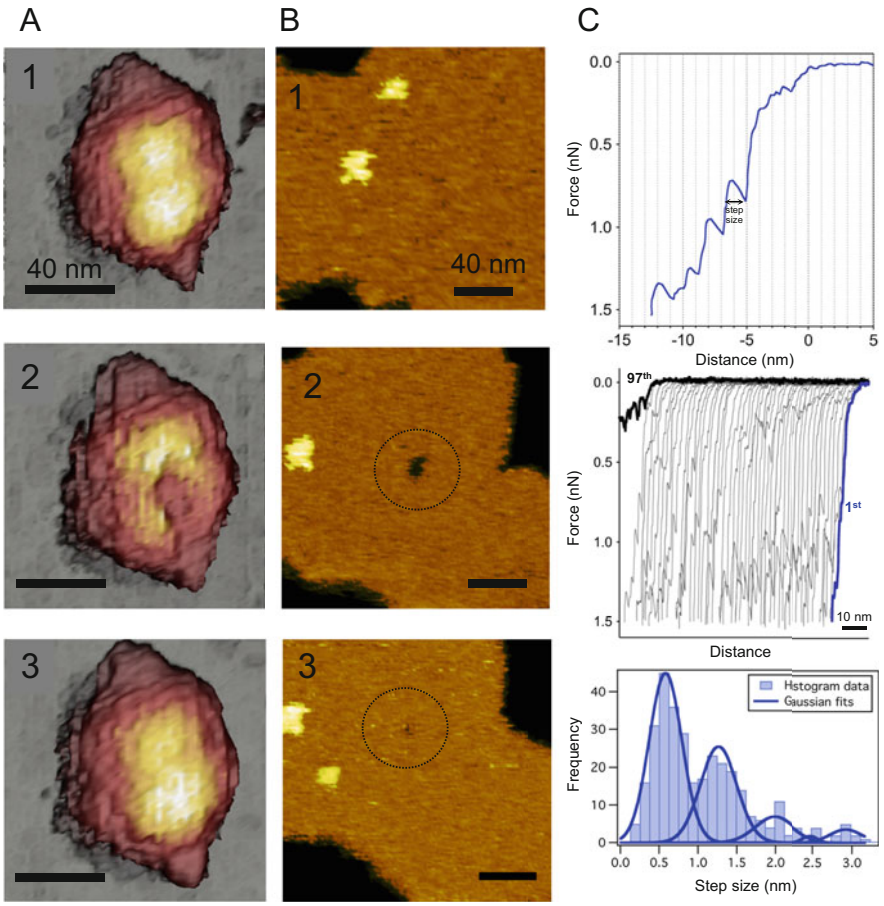

Fig. 8.3 Self-healing of protein shells. (**a**) Frame 1 shows an intact vault particle. In frame 2 the indentation experiment produced a conspicuous break. Frame 3 shows the same particle a few minutes later, the crack has disappeared [68]. (**b**) Frame 1 shows a monolayer of HIV proteins. Frame 2 shows a hole (indicated by a circle) induced by a nano-indentation experiment. Finally, frame 3 shows the healing process of this hole (circle) [70]. (**c**) Up. Indentation of T7 bacteriophage shell presenting discrete jumps in the force. Middle, tens of consecutive force curves performed on the same particle (grey) until it is broken (black). Bottom. Histogram of the steps, showing that the indentation reaches discrete values attributed to the reversible buckling of individual capsomers [adapted from [71]]

is exceeded which is signaled by a rapid sequence of irregular steps in the FZ curve. Due to this quick and uncontrolled disintegration of the structure it is nearly impossible to follow the actual disassembly sequence. An alternative approach to disassemble the virus capsid is to expose it to continuous deformations, induced by the AFM tip, that remain below the rupture threshold. In a way, this mimics the molecular collisions that the capsid would experience in crowded environments [77]. During AFM imaging in JM, the applied force at each pixel reaches about

100 pN [38]. A rough estimate indicates that ~10 k_BT is transferred to the particle at every cycle [78]. This is about ten times the energy that is transferred by a molecular collision ($\sim\frac{3}{2}k_BT$). As a consequence, natural disassembly pathways that are induced by molecular collisions will be accelerated by this imaging process at moderate energies. Such molecular fatigue experiments have been demonstrated to reproduce the natural pathway of adenovirus uncoating much more accurately than single nano-indentation experiments (Fig. 8.2c) could do at higher forces [19].

Let us exemplify the molecular fatigue methodology in the case study of lambda bacteriophage [78]. The mechanical environment that this virus experiences in the gut before infection is very different than that of the bacterial cytoplasm of its host due to differences in crowding and viscosity. The bacteriophage is normally decorated by gpD proteins that bind to the hydrophobic regions of the expanded mature capsid [79]. The fatigue experiments offer an excellent opportunity to probe the resistance of the lambda bacteriophage against disassembly by simulating macromolecular collisions. Figure 8.4 shows the evolution of defects in individual viruses during the imaging process. The label at each topography scan (Fig. 8.4a) indicates

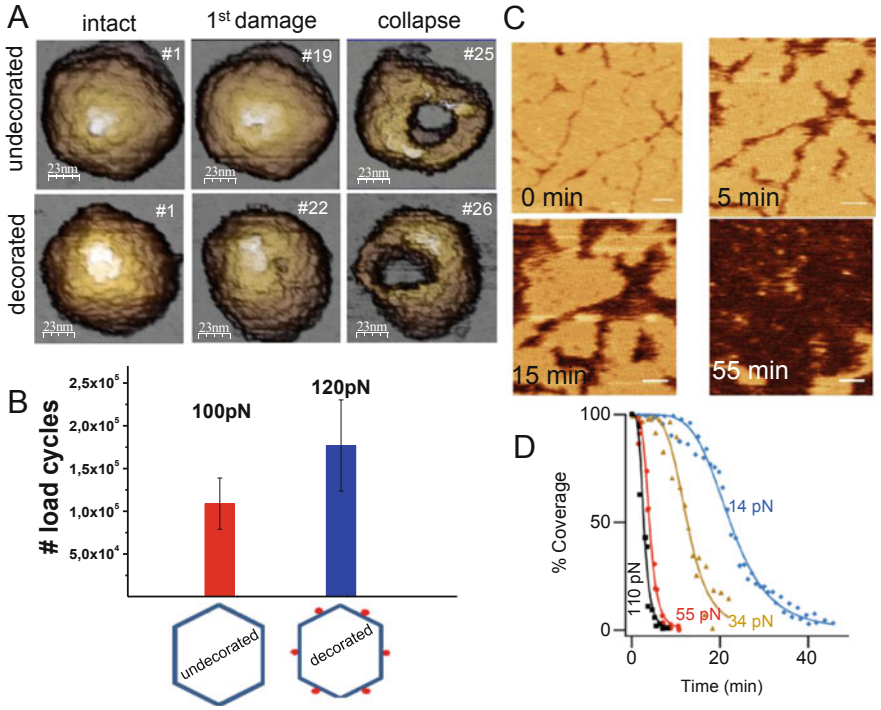

Fig. 8.4 Mechanical fatigue experiments. (**a**) Decorated and undecorated capsids imaged by AFM in different states of disassembly. The number of frames is indicated by the labels. (**b**) Required number of load cycles to create the first damage on decorated and undecorated particles [Adapted from [78]]. (**c**) Evolution of the disassembly of a monolayer of HIV proteins. (**d**) Variation of the protein coverage as a function of the applied force [70]

the times that the virus has been imaged. Seven and eight undecorated and decorated particles, respectively, are probed (Fig. 8.4b) to obtain the average number of loading cycles required for creating the first defect. Since 100 pN was not enough to induce any damage in decorated particles, the imaging force was increased to 120 pN [78]. The results show that the gpD proteins play a mechanical role by reinforcing the mature capsids which may be important to protect them against disassembly in crowded conditions.

Fatigue experiments have also been performed to induce disassembly of viral protein monolayers [80]. Figure 8.4c shows the disassembly of an HIV protein monolayer at imaging forces of 100 pN. The decrease of protein coverage (Fig. 8.4d) induced by the imaging at different forces shows that disassembly of the viral protein monolayer scales with the applied force. Mechanical fatigue experiments have also been applied to probe the stability of genetic cargo. Specifically, in birnavirus the height evolution during mechanical fatigue experiments has been attributed to the stabilization role of ribonucleotides dimers [81].

8.5 Probing the Viral Genome: Mechanics and Diffusion

AFM can be combined with other methods, such as mass spectrometry, to obtain a more complete picture of the biophysics of protein shells [49]. Here, we discuss the combination of AFM and total internal reflection fluorescence microscopy (TIRFM) to study the mechanical unpacking of protein shells. During infection, viruses have to release their genome at the right place and time. HAdV achieves this by disassembling in a stepwise manner while it travels through the cell. Finally, when HAdV particles reach the nuclear pores the dsDNA is released and enters the nucleus. The genomic core of HAdV consists of 35 kbps of dsDNA and 25 MDa of condensing proteins. During maturation, the condensing proteins are cleaved by a viral protease. In AFM uncoating experiments [19] the immature core appeared as a condensed blob, whereas it was not possible to clearly resolve the core of the mature virus. This suggests that the cores of the mature and immature particles have a different organization which could have consequences for the diffusive properties of the genome after disassembly of the virus capsid. Imaging of the genome release by AFM is difficult because of the diffusive nature of this process. However, fluorescence microscopy allows the imaging of moving biomolecules. By combining both techniques, AFM can be used to disassemble single capsids. At the same time, a DNA-specific intercalating fluorescent dye (YOYO-1) allows tracking the genome diffusion (Fig. 8.5a). By using TIRFM, only the fluorescence signal close to the surface is detected (~100 nm), which is exactly where the experiment takes place. Background fluorescence is largely avoided and also the tip apex and cantilever remain mostly out of the evanescent excitation field [83]. Figure 8.5b shows AFM and fluorescence images of an HAdV virus before and after a nano-indentation experiment: fluorescence emission becomes visible after the particle was disrupted. Figure 8.5c shows an FZ curve and the simultaneously recorded fluorescence signal:

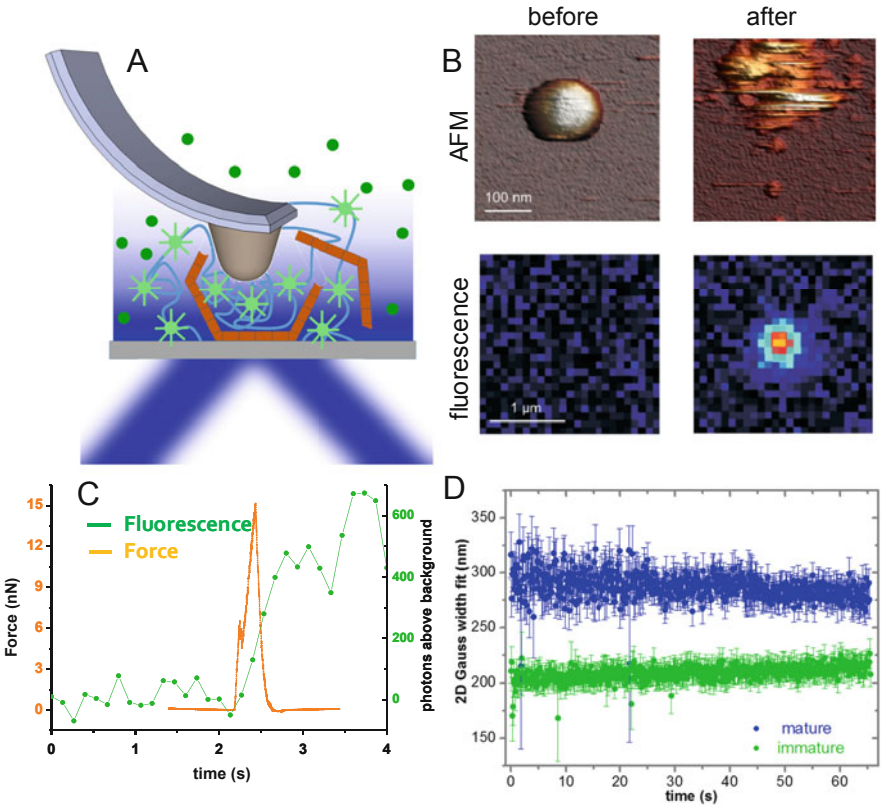

Fig. 8.5 Mechanical unpacking of viral genome. (**a**) Cartoon of the combined AFM-fluorescence system. (**b**) AFM and fluorescence frames of an HAdV capsid before and after the release of DNA. (**c**) Simultaneously acquired force (orange) and fluorescence (green) signals during a nano-indentation experiment that ruptured the capsid. (**d**) The emitted fluorescence as function of time after the rupture of mature (blue) and immature (green) particles [Adapted from [82]]

the fluorescence signal increases directly after the stepwise rupture event. Figure 8.5d shows how from measurements on multiple particles a difference is visible between mature and immature particles. The size of the fluorescence spot is larger for mature particles, suggesting that the structural change of the core during maturation allows the decondensation of DNA and makes it more accessible to the fluorophore [82]. This genome expansion may be an essential feature to allow diffusion through the nuclear pore.

8.6 pH Variation and Protein Shell Mechanics

From a multitude of nano-indentation experiments on different viruses the picture emerged that most viruses pack their genome in stiff symmetric protein shells that are hard to crack open. Although a tough shell may help to contain the densely packed genome and enhance the virus survival when it travels from host to host, it still will have to allow the release of the genome after entering the eukaryotic host cell. Changes in ionic conditions and pH that viruses encounter in the host cell have been early recognized as triggers for structural changes that eventually lead to disassembly of the capsid and the release of the viral genome [84–86]. AFM force spectroscopy can be employed to investigate such structural transitions [69]. To this end the changes in cellular environment that the virus encounters during infection need to be reproduced in the AFM liquid cell. In multiple experiments viruses have been studied at different pH values. To mimic the acidification in the endosomal pathway that influenza viruses experience on their way through the cell Li et al. measured the stiffness of influenza viruses subjected to a pH that was lowered from 7.4 to 5.0 [87]. Figure 8.6a shows that influenza viruses soften in a two-step process that correspond to the different pH values within the liposome when it evolves from the early to the late stage. The first softening step (pH 7.4–6.0), which is reversible, was attributed to a softening of the glycoprotein spike layer. The second softening step (pH 6.0–5.5), which is irreversible, was associated with the dissociation of the M1 protein layer from the inside of the viral lipid envelope. It was speculated that both steps are essential to time the release of the viral genomes and the fusion between the viral envelope and the liposome. It should be noted that the structure of the influenza virus differs considerably from that of most other viruses that have been studied with AFM. Most notably, the studied influenza strains lacked a well-defined symmetric protein capsid. Instead, the M1 protein coats the inside of the lipid envelope with a semi-continuous protein layer [89]. As a consequence, the stiffness is about 10 times less than that of other viral protein capsids. Because the influenza viruses can sustain much higher deformations, the force to break open the viruses is still comparable to that what is found for protein capsids [23, 90].

Intriguingly, the response of other viruses that have been tested at different pH values has shown a very different behavior and tends to weaken at high pH values instead of at low values. Snijder et al. showed that the force to break the capsid of a triatoma virus reduces a multifold when the pH was increased from 6.8 to 9.0 which was attributed to the loss of interaction between the genome and capsid which destabilized the latter [60]. Cowpea chlorotic mottle virus was found to swell and to soften when the pH was increased from 4.8 to 7.5 [91]. The inversed response at pH shifts of the triatoma virus and Cowpea chlorotic mottle virus as compared to that of the influenza virus may indicate a need to endure acidic environments. Both the triatoma virus and Cowpea chlorotic mottle virus use insects as transmission vectors and a high stability at low pH may be important to persist in the intestines of the insects. Studies of the mechanical changes of viruses as ionic changes other than pH

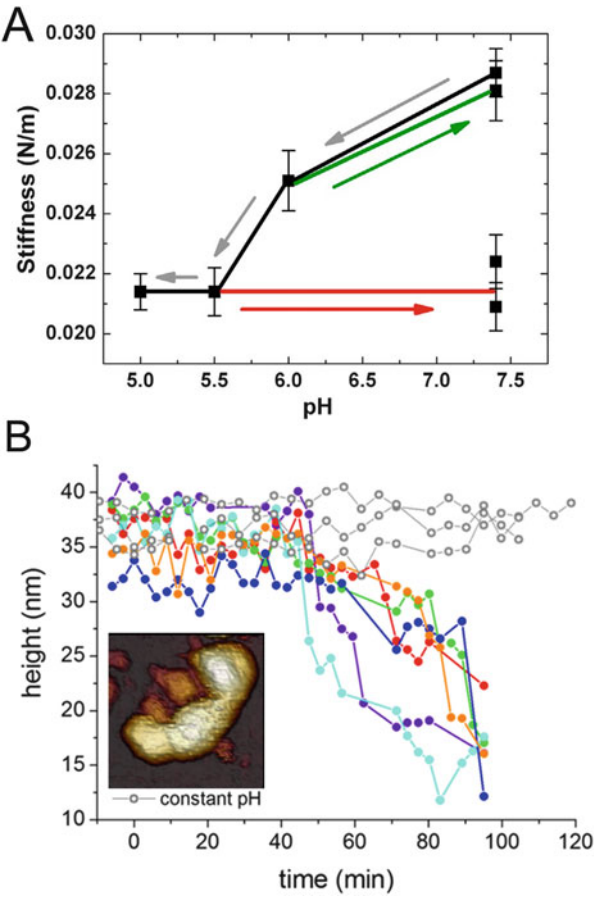

Fig. 8.6 pH Variation and protein shell mechanics. (**a**) Influenza viruses soften in a two-step process that corresponds to the different pH values. The green arrow indicated a reversible change, the red arrow an irreversible change in stiffness [adapted from [87]]. (**b**) Temporal evolution of some vault particles topographies when lowering the pH from 7.5 to 5.2 (colored curves) and at a constant pH of 7.5 (grey curves). Inset shows a vault particle at pH = 5.2 [adapted from [88]]

are rare but it is expected that these will be helpful to identify further subtleties in the uncoating processes of viruses.

Ionic conditions are also expected to affect other protein cages than viruses. For instance, it has been suggested that the acidification of the environment has a strong influence on vault particle dynamics by opening the particle into two halves [92]. AFM has been used to monitor the structural changes of individual vault particles while the pH was varied [88]. These experiments revealed that lowering the pH promotes a global destabilization of the particle governed by the weakening of inter-monomeric contacts. This destabilization results in the collapse of vault height when the pH was lowered from 7.5 to 5.2 (colored curves of Fig. 8.6b).

8.7 Monitoring Virus Transmission: Binding and Budding

So far, we have reviewed how the mechanics of viruses and other protein cages can be related to their stability and functionality. However, viruses are dynamic entities that will have to cross the cellular membrane (or penetrate the bacterial cell wall in case of bacteriophages) to deliver their genome inside the host cells. Once the genome has been replicated and expressed, new functional virus particles have to cross the cell membrane to leave the hosts. In eukaryotic viruses this process implies virus transport in and out of the host cells. Many viruses use the endocytotic pathway to enter the cell [7]. Before engulfment by the cellular membrane, viruses have to be trapped on the cell membrane via receptors that interact with virus fibers in a specific fashion. The interaction between HAdV fibers and CAR proteins in the membrane constitutes an illustrative example [65]. AFM allows measuring the force of these interactions [93]. In this experiment single viruses were covalently attached to the AFM tip (Fig. 8.7a, inset). The combination with confocal microscopy enables the co-localization of the cells in culturing conditions with the tip. Thus the AFM tip can scan the relevant area of the cell to obtain the adhesive force between the virus attached to the tip and the receptors in the membrane. The recording of this adhesion as function of time reveals binding events between the virus and the receptor (Fig. 8.7a). The colored steps correspond to the rupture forces of 1, 2, and 3 virus fibers, respectively. Such force spectroscopy experiments allow extracting parameters as k_{off} and the free energy of the fiber–receptor interaction. Also the binding of influenza viruses to cells has thus been characterized by a combination of AFM and optical trapping force spectroscopy [95].

Virus budding, the process by which enveloped viruses acquire their external membrane from the host cell membrane when they leave the cell, has also been studied with AFM [96]. In principle, AFM can also image the temporal evolution of

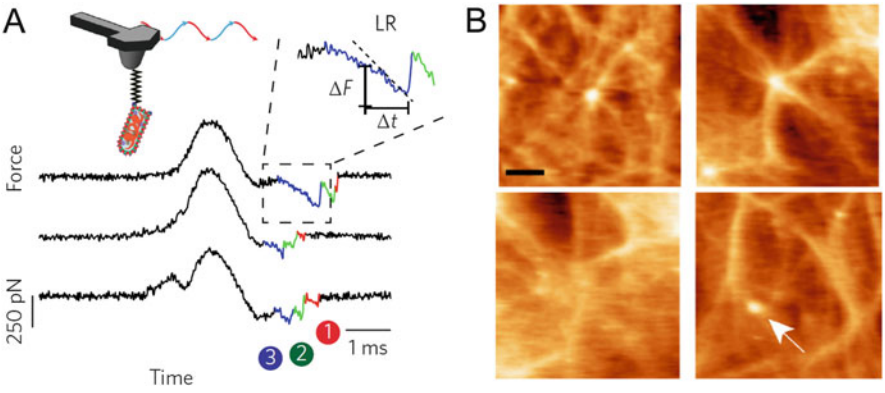

Fig. 8.7 Binding and budding of viruses. (**a**) The temporal evolution of the adhesion force between the fibers of a virus and the receptors of the cell membrane [adapted from [93]]. (**b**) Time evolution of the budding process of a single HIV virus with 10 min between frames (scale bar is 1.5 μm). Adapted from [94]

this process by recording sequential topographies of the cell surface. Figure 8.7b presents the evolution of the structural changes of the cell membrane attributed to the budding process of a single HIV virus particle [97]. In this case the budding process appears to be associated with a remodeling of the actin cortex under the cell membrane. Upper left shows the initial stage with a conspicuous blob (virus). Upper right presents the maximum bulge induced by the virus just before leaving the cell (bottom left). Finally, a new virus starts the budding process again (bottom right).

8.8 Conclusions

AFM enables unique possibilities for studying individual virus particles and other protein cages, complementing classical EM and X-ray diffraction studies. First, the high signal to noise ratio of AFM imaging allows obtaining nanometer resolution on single particles. This enables the identification of virus elements which are not symmetrically ordered [98]. Also, it opens the way to study dynamics and mechanics of single viruses. Second, because AFM can operate in buffer conditions, dynamic events, such as the response to ionic changes, and budding processes can be studied in real time. Third, structural virology studies are typically focused on establishing structure–function relationships [13]. Because AFM can measure mechanical properties of viral particles in real time, the above relationship can be extended to structure–function–mechanics. Current developments such as high-speed AFM [99] and combined approaches such as AFM with single molecule fluorescence [82] will greatly enhance our ability to study the structural dynamics of protein cages at shorter timescales which will help us to better understand their functionality.

Acknowledgements We acknowledge our students, former students, collaborators, and projects FIS2014-59562-R, FIS2015-71108-REDT, FIS2017-89549-R. Fundación BBVA and "María de Maeztu" Program for Units of Excellence in R&D (MDM-2014-0377).

References

1. Cheng S, Liu Y, Crowley CS, Yeates TO, Bobik TA (2008) Bacterial microcompartments: their properties and paradoxes. BioEssays 30:1084–1095
2. Querol-Audí J, Casañas A, Usón I, Luque D, Castón JR, Fita I, Verdaguer N (2009) The mechanism of vault opening from the high resolution structure of the N-terminal repeats of MVP. EMBO J 28:3450
3. Fotin A, Cheng Y, Sliz P, Grigorieff N, Harrison SC, Kirchhausen T, Walz T (2004) Molecular model for a complete clathrin lattice from electron cryomicroscopy. Nature 432:573
4. Lai Y-T, Reading E, Hura GL, Tsai K-L, Laganowsky A, Asturias FJ, Tainer JA, Robinson CV, Yeates TO (2014) Structure of a designed protein cage that self-assembles into a highly porous cube. Nat Chem 6:1065–1071

5. Wimmer E, Mueller S, Tumpey TM, Taubenberger JK (2009) Synthetic viruses: a new opportunity to understand and prevent viral disease. Nat Biotechnol 27:1163
6. Wörsdörfer B, Woycechowsky KJ, Hilvert D (2011) Directed evolution of a protein container. Science 331:589
7. Flint SJ, Enquist LW, Racaniello VR, Skalka AM (2004) Principles of virology. ASM Press, Washington D.C.
8. Mateu MGE (2013) Structure and physics of viruses. Springer, Dordrecht
9. Douglas T, Young M (1998) Host-guest encapsulation of materials by assembled virus protein cages. Nature 393:152–155
10. Agirre J, Aloria K, Arizmendi JM, Iloro I, Elortza F, Sánchez-Eugenia R, Marti GA, Neumann E, Rey FA, Guérin DMA (2011) Capsid protein identification and analysis of mature Triatoma virus (TrV) virions and naturally occurring empty particles. Virology 409:91–101
11. Cordova A, Deserno M, Gelbart WM, Ben-Shaul A (2003) Osmotic shock and the strength of viral capsids. Biophys J 85:70–74
12. Minton AP (2001) The influence of macromolecular crowding and macromolecular confinement on biochemical reactions in physiological media. J Biol Chem 276:10577–10580
13. Baker TS, Olson NH, Fuller SD (1999) Adding the third dimension to virus life cycles: three-dimensional reconstruction of icosahedral viruses from cryo-electron micrographs. Microbiol Mol Biol Rev 63:862–922
14. Calder LJ, Wasilewski S, Berriman JA, Rosenthal PB (2010) Structural organization of a filamentous influenza A virus. Proc Natl Acad Sci 107:10685–10690
15. Hinterdorfer P, van Oijen A (2009) Handbook of single-molecule biophysics. Springer, Dordrecht
16. Muller DJ, Amrein M, Engel A (1997) Adsorption of biological molecules to a solid support for scanning probe microscopy. J Struct Biol 119:172–188
17. Armanious A, Aeppli M, Jacak R, Refardt D, Sigstam T, Kohn T, Sander M (2016) Viruses at solid-water interfaces: a systematic assessment of interactions driving adsorption. Environ Sci Technol 50:732–743
18. Moreno-Madrid F, Martin-Gonzalez N, Llauro A, Ortega-Esteban A, Hernando-Perez M, Douglas T, Schaap IAT, de Pablo PJ (2017) Atomic force microscopy of virus shells. Biochem Soc Trans 45:499–511
19. Ortega-Esteban A, Perez-Berna AJ, Menendez-Conejero R, Flint SJ, Martin CS, de Pablo PJ (2013) Monitoring dynamics of human adenovirus disassembly induced by mechanical fatigue. Sci Rep 3:1434
20. Snijder J, Radtke K, Anderson F, Scholtes L, Corradini E, Baines J, Heck AJR, Wuite GJL, Sodeik B, Roos WH (2017) Vertex-specific proteins pUL17 and pUL25 mechanically reinforce herpes simplex virus capsids. J Virol 91:e00123–e00117
21. Llauro A, Luque D, Edwards E, Trus BL, Avera J, Reguera D, Douglas T, Pablo PJ, Caston JR (2016b) Cargo-shell and cargo-cargo couplings govern the mechanics of artificially loaded virus-derived cages. Nanoscale 8:9328–9336
22. Ramalho R, Rankovic S, Zhou J, Aiken C, Rousso I (2016) Analysis of the mechanical properties of wild type and hyperstable mutants of the HIV-1 capsid. Retrovirology 13:17
23. Li S, Eghiaian F, Sieben C, Herrmann A, Schaap IAT (2011) Bending and puncturing the influenza lipid envelope. Biophys J 100:637–645
24. Calo A, Eleta-Lopez A, Stoliar P, de Sancho D, Santos S, Verdaguer A, Bittner AM (2016) Multifrequency force microscopy of helical protein assembly on a virus. Sci Rep 6:21899
25. Ares P, Garcia-Doval C, Llauro A, Gomez-Herrero J, van Raaij MJ, de Pablo PJ (2014) Interplay between the mechanics of bacteriophage fibers and the strength of virus-host links. Phys Rev E Stat Nonlinear Soft Matter Phys 89:052710
26. Kuznetsov YG, Xiao CA, Sun SY, Raoult D, Rossmann M, Mcpherson A (2010) Atomic force microscopy investigation of the giant mimivirus. Virology 404:127–137
27. de Pablo PJ (2017) Atomic force microscopy of virus shells. Semin Cell Dev Biol 73:199–208

28. Carpick RW, Ogletree DF, Salmeron M (1997) Lateral stiffness: a new nanomechanical measurement for the determination of shear strengths with friction force microscopy. Appl Phys Lett 70:1548–1550
29. Ohnesorge F, Binnig G (1993) True atomic-resolution by atomic force microscopy through repulsive and attractive forces. Science 260:1451–1456
30. Butt HJ, Prater CB, Hansma PK (1991) Imaging purple membranes dry and in water with the atomic force microscope. J Vac Sci Technol B 9:1193–1196
31. Moreno-Herrero F, Colchero J, Gomez-Herrero J, Baro AM (2004) Atomic force microscopy contact, tapping, and jumping modes for imaging biological samples in liquids. Phys Rev E Stat Nonlinear Soft Matter Phys 69:031915
32. Xiao C, Kuznetsov YG, Sun SY, Hafenstein SL, Kostyuchenko VA, Chipman PR, Suzan-Monti M, Raoult D, Mcpherson A, Rossmann MG (2009) Structural studies of the giant mimivirus. PLoS Biol 7:958–966
33. Carrasco C, Luque A, Hernando-Perez M, Miranda R, Carrascosa JL, Serena PA, de Ridder M, Raman A, Gomez-Herrero J, Schaap IAT, Reguera D, de Pablo PJ (2011) Built-in mechanical stress in viral shells. Biophys J 100:1100–1108
34. Vinckier A, Heyvaert I, Dhoore A, Mckittrick T, Vanhaesendonck C, Engelborghs Y, Hellemans L (1995) Immobilizing and imaging microtubules by atomic-force microscopy. Ultramicroscopy 57:337–343
35. Roos WH, Bruinsma R, Wuite GJL (2010) Physical virology. Nat Phys 6:733–743
36. de Pablo PJ, Colchero J, Gomez-Herrero J, Baro AM (1998) Jumping mode scanning force microscopy. Appl Phys Lett 73:3300–3302
37. Miyatani T, Horii M, Rosa A, Fujihira M, Marti O (1997) Mapping of electrical double-layer force between tip and sample surfaces in water with pulsed-force-mode atomic force microscopy. Appl Phys Lett 71:2632–2634
38. Ortega-Esteban A, Horcas I, Hernando-Perez M, Ares P, Perez-Berna AJ, San Martin C, Carrascosa JL, de Pablo PJ, Gomez-Herrero J (2012) Minimizing tip-sample forces in jumping mode atomic force microscopy in liquid. Ultramicroscopy 114:56–61
39. de Pablo PJ (2013) Atomic force microscopy of viruses. Subcell Biochem 68:247–271
40. Schaap IAT, Carrasco C, de Pablo PJ, Mackintosh FC, Schmidt CF (2006) Elastic response, buckling, and instability of microtubules under radial indentation. Biophys J 91:1521–1531
41. Legleiter J, Park M, Cusick B, Kowalewski T (2006) Scanning probe acceleration microscopy (SPAM) in fluids: mapping mechanical properties of surfaces at the nanoscale. Proc Natl Acad Sci USA 103:4813–4818
42. Muller DJ, Janovjak H, Lehto T, Kuerschner L, Anderson K (2002) Observing structure, function and assembly of single proteins by AFM. Prog Biophys Mol Biol 79:1–43
43. Sugimoto Y, Abe M, Hirayama S, Oyabu N, Custance O, Morita S (2005) Atom inlays performed at room temperature using atomic force microscopy. Nat Mater 4:156
44. Rief M, Gautel M, Oesterhelt F, Fernandez JM, Gaub HE (1997) Reversible unfolding of individual titin immunoglobulin domains by AFM. Science 276:1109–1112
45. Carrasco C, Carreira A, Schaap IAT, Serena PA, Gomez-Herrero J, Mateu MG, de Pablo PJ (2006) DNA-mediated anisotropic mechanical reinforcement of a virus. Proc Natl Acad Sci USA 103:13706–13711
46. Carrasco C, Castellanos M, de Pablo PJ, Mateu MG (2008) Manipulation of the mechanical properties of a virus by protein engineering. Proc Natl Acad Sci USA 105:4150–4155
47. Hernando-Perez M, Miranda R, Aznar M, Carrascosa JL, Schaap IAT, Reguera D, de Pablo PJ (2012) Direct measurement of phage phi29 stiffness provides evidence of internal pressure. Small 8:2366–2370
48. Roos WH, Radtke K, Kniesmeijer E, Geertsema H, Sodeik B, Wuite GJL (2009) Scaffold expulsion and genome packaging trigger stabilization of herpes simplex virus capsids. Proc Natl Acad Sci USA 106:9673–9678

49. Snijder J, Uetrecht C, Rose RJ, Sanchez-Eugenia R, Marti GA, Agirre J, Guerin DM, Wuite GJ, Heck AJ, Roos WH (2013) Probing the biophysical interplay between a viral genome and its capsid. Nat Chem 5:502–509
50. Zeng C, Moller-Tank S, Asokan A, Dragnea B (2017) Probing the link among genomic cargo, contact mechanics, and nanoindentation in recombinant Adeno-associated virus 2. J Phys Chem B 121:1843–1853
51. Hernando-Perez M, Pascual E, Aznar M, Ionel A, Caston JR, Luque A, Carrascosa JL, Reguera D, de Pablo PJ (2014) The interplay between mechanics and stability of viral cages. Nanoscale 6:2702–2709
52. Roos WH, Gertsman I, May ER, Brooks CL, Johnson JE, Wuite GJL (2012) Mechanics of bacteriophage maturation. Proc Natl Acad Sci USA 109:2342–2347
53. Llauro A, Schwarz B, Koliyatt R, de Pablo PJ, Douglas T (2016c) Tuning viral capsid nanoparticle stability with symmetrical morphogenesis. ACS Nano 10:8465–8473
54. Purohit PK, Kondev J, Phillips R (2003) Mechanics of DNA packaging in viruses. Proc Natl Acad Sci USA 100:3173–3178
55. Gonzalez-Huici V, Salas M, Hermoso JM (2004) The push-pull mechanism of bacteriophage O29 DNA injection. Mol Microbiol 52:529–540
56. Smith DE, Tans SJ, Smith SB, Grimes S, Anderson DL, Bustamante C (2001) The bacteriophage phi 29 portal motor can package DNA against a large internal force. Nature 413:748–752
57. Llauró A, Guerra P, Irigoyen N, Rodríguez JF, Verdaguer N, de Pablo PJ (2014) Mechanical stability and reversible fracture of vault particles. Biophys J 106:687–695
58. Snijder J, Kononova O, Barbu IM, Uetrecht C, Rurup WF, Burnley RJ, Koay MS, Cornelissen JJ, Roos WH, Barsegov V, Wuite GJ, Heck AJ (2016) Assembly and mechanical properties of the cargo-free and cargo-loaded bacterial nanocompartment encapsulin. Biomacromolecules 17:2522–2529
59. Ortega-Esteban A, Condezo GN, Perez-Berna AJ, Chillon M, Flint SJ, Reguera D, San Martin C, de Pablo PJ (2015b) Mechanics of viral chromatin reveals the pressurization of human adenovirus. ACS Nano 9:10826–10833
60. Snijder J, Ivanovska IL, Baclayon M, Roos WH, Wuite GJ (2012) Probing the impact of loading rate on the mechanical properties of viral nanoparticles. Micron 43:1343–1350
61. Klug WS, Bruinsma RF, Michel JP, Knobler CM, Ivanovska IL, Schmidt CF, Wuite GJL (2006) Failure of viral shells. Phys Rev Lett 97:228101
62. Landau LD, Lifshizt E (1986) Theory of elasticity. Pergamon, London
63. Falvo MR, Washburn S, Superfine R, Finch M, Brooks FP, Chi V, Taylor RM (1997) Manipulation of individual viruses: friction and mechanical properties. Biophys J 72:1396–1403
64. Ivanovska IL, de Pablo PJ, Ibarra B, Sgalari G, Mackintosh FC, Carrascosa JL, Schmidt CF, Wuite GJL (2004) Bacteriophage capsids: tough nanoshells with complex elastic properties. Proc Natl Acad Sci USA 101:7600–7605
65. San Martín C (2012) Latest insights on adenovirus structure and assembly. Viruses 4:847–877
66. Dimitriadis EK, Horkay F, Maresca J, Kachar B, Chadwick RS (2002) Determination of elastic moduli of thin layers of soft material using the atomic force microscope. Biophys J 82:2798–2810
67. Ivanovska IL, Miranda R, Carrascosa JL, Wuite GJL, Schmidt CF (2011) Discrete fracture patterns of virus shells reveal mechanical building blocks. Proc Natl Acad Sci USA 108:12611–12616
68. Llauro A, Guerra P, Irigoyen N, Rodriguez JF, Verdaguer N, de Pablo PJ (2014) Mechanical stability and reversible fracture of vault particles. Biophys J 106:687–695
69. Llauro A, Coppari E, Imperatori F, Bizzarri AR, Caston JR, Santi L, Cannistraro S, de Pablo PJ (2015) Calcium ions modulate the mechanics of tomato bushy stunt virus. Biophys J 109:390–397
70. Valbuena A, Mateu MG (2015) Quantification and modification of the equilibrium dynamics and mechanics of a viral capsid lattice self-assembled as a protein nanocoating. Nanoscale 7:14953–14964
71. Voros Z, Csik G, Herenyi L, Kellermayer MSZ (2017) Stepwise reversible nanomechanical buckling in a viral capsid. Nanoscale 9:1136–1143

72. Uchida M, Douglas T (2013) Biophysical chemistry: unravelling capsid transformations. Nat Chem 5:444–445
73. Tang L, Gilcrease EB, Casjens SR, Johnson JE (2006) Highly discriminatory binding of capsid-cementing proteins in bacteriophage L. Structure 14:837–845
74. Carrillo PJ, Medrano M, Valbuena A, Rodriguez-Huete A, Castellanos M, Perez R, Mateu MG (2017) Amino acid side chains buried along intersubunit interfaces in a viral capsid preserve low mechanical stiffness associated with virus infectivity. ACS Nano 11:2194–2208
75. Castellanos M, Perez R, Carrasco C, Hernando-Perez M, Gomez-Herrero J, de Pablo PJ, Mateu MG (2012) Mechanical elasticity as a physical signature of conformational dynamics in a virus particle. Proc Natl Acad Sci USA 109:12028–12033
76. Greber UF, Willetts M, Webster P, Helenius A (1993) Stepwise dismantling of Adenovirus-2 during entry into cells. Cell 75:477–486
77. Zhou HX, Rivas G, Minton AP (2008) Macromolecular crowding and confinement: biochemical, biophysical, and potential physiological consequences. Annu Rev Biophys 37:375–397
78. Hernando-Pérez M, Lambert S, Nakatani-Webster E, Catalano CE, de Pablo PJ (2014) Cementing proteins provide extra mechanical stabilization to viral cages. Nat Commun 5:4520
79. Medina E, Nakatani E, Kruse S, Catalano CE (2012) Thermodynamic characterization of viral procapsid expansion into a functional capsid shell. J Mol Biol 418:167–180
80. Valbuena A, Mateu MG (2017) Kinetics of surface-driven self-assembly and fatigue-induced disassembly of a virus-based nanocoating. Biophys J 112:663–673
81. Mertens J, Casado S, Mata CP, Hernando-Perez M, de Pablo PJ, Carrascosa JL, Caston JR (2015) A protein with simultaneous capsid scaffolding and dsRNA-binding activities enhances the birnavirus capsid mechanical stability. Sci Rep 5:13486
82. Ortega-Esteban A, Bodensiek K, San Martin C, Suomalainen M, Greber UF, de Pablo PJ, Schaap IAT (2015a) Fluorescence tracking of genome release during mechanical unpacking of single viruses. ACS Nano 9:10571–10579
83. Gaiduk A, Kuhnemuth R, Antonik M, Seidel CA (2005) Optical characteristics of atomic force microscopy tips for single-molecule fluorescence applications. ChemPhysChem 6:976–983
84. Fontana J, Cardone G, Heymann JB, Winkler DC, Steven AC (2012) Structural changes in influenza virus at low pH characterized by cryo-electron tomography. J Virol 86:2919–2929
85. Suomalainen M, Greber UF (2013) Uncoating of non-enveloped viruses. Curr Opin Virol 3:27–33
86. Wetz K, Kucinski T (1991) Influence of different ionic and pH environments on structural alterations of poliovirus and their possible relation to virus uncoating. J Gen Virol 72:2541–2544
87. Li S, Sieben C, Ludwig K, Höfer CT, Chiantia S, Herrmann A, Eghiaian F, Schaap IAT (2014) pH-controlled two-step uncoating of influenza virus. Biophys J 106:1447–1456
88. Llauro A, Guerra P, Kant R, Bothner B, Verdaguer N, de Pablo PJ (2016a) Decrease in pH destabilizes individual vault nanocages by weakening the inter-protein lateral interaction. Sci Rep 6:34143
89. Harris A, Cardone G, Winkler DC, Heymann JB, Brecher M, White JM, Steven AC (2006) Influenza virus pleiomorphy characterized by cryoelectron tomography. Proc Natl Acad Sci 103:19123–19127
90. Schaap IAT, Eghiaian F, Des Georges A, Veigel C (2012) Effect of envelope proteins on the mechanical properties of influenza virus. J Biol Chem 287:41078–41088
91. Wilts BD, Schaap IA, Schmidt CF (2015) Swelling and softening of the cowpea chlorotic mottle virus in response to pH shifts. Biophys J 108:2541–2549
92. Goldsmith LE, Yu M, Rome LH, Monbouquette HG (2007) Vault nanocapsule dissociation into halves triggered at low pH. Biochemistry 46:2865–2875
93. Alsteens D, Newton R, Schubert R, Martinez-Martin D, Delguste M, Roska B, Muller DJ (2017) Nanomechanical mapping of first binding steps of a virus to animal cells. Nat Nanotechnol 12:177–183

94. Gladnikoff M, Rousso I (2008) Directly monitoring individual retrovirus budding events using atomic force microscopy. Biophys J 94:320–326
95. Sieben C, Kappel C, Zhu R, Wozniak A, Rankl C, Hinterdorfer P, Grubmüller H, Herrmann A (2012) Influenza virus binds its host cell using multiple dynamic interactions. Proc Natl Acad Sci USA 109:13626–13631
96. Kuznetsov YG, Datta S, Kothari NH, Greenwood A, Fan H, Mcpherson A (2002) Atomic force microscopy investigation of fibroblasts infected with wild-type and Mutant Murine Leukemia Virus (MuLV). Biophys J 83:3665–3674
97. Gladnikoff M, Shimoni E, Gov NS, Rousso I (2009) Retroviral assembly and budding occur through an actin-driven mechanism. Biophys J 97:2419–2428
98. Cartagena A, Hernando-Perez M, Carrascosa JL, de Pablo PJ, Raman A (2013) Mapping in vitro local material properties of intact and disrupted virions at high resolution using multi-harmonic atomic force microscopy. Nanoscale 5:4729–4736
99. Ando T, Kodera N, Naito Y, Kinoshita T, Furuta K, Toyoshima YY (2003) A high-speed atomic force microscope for studying biological macromolecules in action. ChemPhysChem 4:1196–1202

Chapter 9
Alkalinization of Icosahedral Non-enveloped Viral Capsid Interior Through Proton Channeling

Maria Marta Branda and Diego M. A. Guérin

Abstract Small icosahedral viruses have a compact capsid that apparently lacks holes through which solvents can be exchanged with the external milieu. However, due to the steric hindrance of amino acids, upon folding, capsid proteins form narrow cavities in which water and ions can be trapped. These occluded solvent molecules can form lines of water, called *water wires*, representing an arrangement with special features for proton conduction. In this chapter, we review the physico-chemical principles that permit proton conduction through protein cavities. We also describe how a combination of these elements found in an insect viral capsid can allow the virus to sense alkaline environments. Through this analysis, we stress the need to combine experimental and theoretical techniques when modeling complex biological systems.

Keywords Proton diode · Water wire · pH sensing · Grotthuss · *Triatoma virus*

9.1 Introduction

As a general concept, viral capsids are capsules that, among other functions, play two successive and opposite roles: initially, under specific conditions, they recognize and tightly enclose the genome, and ultimately, upon encountering one or more particular external stimulus, they destabilize and open to allow genome escape. Both

M. M. Branda
Departamento de Física, Universidad Nacional del Sur (DF-UNS), and GRUMASICA, IFISUR (UNS/CONICET), Bahía Blanca, Argentina

Present address: Instituto de Física Aplicada (INFAP, CONICET-UNSL), Ciudad de San Luis, Argentina

D. M. A. Guérin (✉)
Department of Biochemistry and Molecular Biology, Instituto Biofisika (UPV/EHU, CSIC), University of the Basque Country (EHU), Leioa, Vizcaya, Spain
e-mail: diego.guerin@ehu.eus

U. F. Greber (ed.), *Physical Virology*, Advances in Experimental Medicine and Biology 1140, https://doi.org/10.1007/978-3-030-14741-9_9

processes occur in the interior of the infected cell. In small icosahedral viruses, genome encapsidation is achieved spontaneously. Genome release, a process necessary to initiate infection, occurs after cell uptake upon receptor binding. This release can be triggered by different factors such as pH changes, and most likely these factors are specific for each virus. Nevertheless, the uptake mechanisms that many viruses employ rely on molecules and organelles that cells use for delivering nutrients into the cytosol. Indeed, these processes and molecules involved in the functions of all cells are highly conserved among organisms. In many divergent viruses, these pathways are required for uncoating as a final step under acidic conditions, and this acidification is associated with the expression of conserved genes [1]. In contrast, few known viruses are resistant to acidic conditions and require alkaline environments for genome uncoating. One example is *Helicoverpa armigera* stunt virus (HaSV; *Alphatetraviridae*; *Omegatetravirus*), which requires an alkaline pH value of nine for cell attachment and entry [2]. This virus is a pathogen of lepidopteran larvae, and such a high pH environment is reached in the midgut of the herbivorous insects it attacks. The requirement for an alkaline medium for infection of herbivorous pathogens most likely resulted from an evolutionary mechanism by which these viruses adapted their life cycle to evade the plant chemical defenses [2, 3]. Another insect virus that stands acidic conditions but requires an alkaline pH for genome externalization is *Triatoma virus* (TrV; *Dicistroviridae; Triatovirus*) [4–7]. TrV is structurally very similar to HaSV and to many plant and animal viruses [8, 9]. How the basic pH operates on the HaSV and TrV capsids to promote their destabilization is unclear.

In this chapter, we review the physical and structural features that explain how bridged water molecules buried into proteins can conduct protons. We also describe why a line of water molecules filling a narrow cavity that traverses the capsid of TrV can behave as a proton channel. Based on the atomic structure, quantum mechanic (QM) and molecular dynamic (MD) calculations, this ion channel was modeled and found that it behaves like a "proton diode." This feature could explain how the capsid of TrV can be sensitive to alkaline pH and insensitive to acidic pH [10].

9.2 Hypothesis of Ion Channels in Viral Capsids

The existence of ion channels as integral parts of the capsid of icosahedral viruses was an idea that emerged soon after the first atomic structures of viruses were solved [11, 12]. The hypothesis that viral capsids can be selective for ion permeation was postulated to explain the increase in virion densities observed in plant viruses. This change, due to the uptake of cesium ions, was observed when they were purified with isopycnic density gradients [12]. The hypothesis was coined even before the first atomic structure of a membrane ion channel was known [13] and served as an initial definition to approach the potential protein architectures of membrane channels [11]. The structural feature that provided support for the prediction of ion channels in viral capsids was the presence of cations located in the narrow pores formed by the assembly of symmetry-related structural proteins. Although these putative channels

have not yet been confirmed, it is clear that many of the functions played by the protein shell in the viral life cycle can be explained in terms of an interchange mechanism between the external solvent and the capsid interior. Such mechanisms can include selective ion permeation from the capsid exterior to assure genome neutrality or, conversely, to induce its destabilization by counterion leak to force capsid swelling, among others [12].

9.3 Small Icosahedral and Non-enveloped Capsid Viruses

Small, icosahedral, and non-enveloped virus (SINEV) represents a general set of characteristics that describe many viral pathogens of humans and all other living beings. *Small* refers to the size, which corresponds to a sphere of approximately 30 nm in diameter. *Icosahedral* means that the capsid is oligomeric, either composed of a single or of different proteins arranged according to strict icosahedral symmetry. By comparison with other more structurally complex viruses, *non-enveloped* indicates that the capsid of these viruses does not contain a lipidic membrane.

The genomes of SINEVs are enclosed in the capsid interior but are not packed according to the protein shell symmetry. Some prototypical human pathogens of this viral type are poliovirus (PV; [14]) and human rhinovirus 14 (HRV14, [15]). Their crystallographic structures show common features of all SINEV capsids: they are composed of 60 copies of four different peptides. All SINEV protein shells are compact and approximately 3 nm thick, with no apparent holes through which the internal contents can be exchanged with the surrounding milieu. The only exception to this hermetic feature is that the capsid has cavities that traverse along the three- and five-fold icosahedral axes (Fig. 9.1). These elongated regions are formed by the symmetry-related amino acid side chain that lines the cavities.

9.4 The Concept of pH and the Electrical Conductivity of Water

The pH (potential of hydrogen) is a numeric scale used to specify the acidity or basicity of aqueous solutions. The original concept of pH was developed in 1909 by a Danish chemist, Søren Peter Lauritz Sørensen, and it is widely assumed to be a convenient way to express acidity[1]: $pH = -\log [H^+]$.

The bare hydrogen ion (a proton) has an extremely high charge density and cannot exist freely in solution. The simplest hydration form of the proton is the hydroxonium ion (H_3O^+), and other species are also found in water solutions.

[1]This definition applies for dilute solutions. The general formula is as follows: $pH = -\log (aH^+)$, where aH^+ is the activity of H^+ (or effective H^+ concentration).

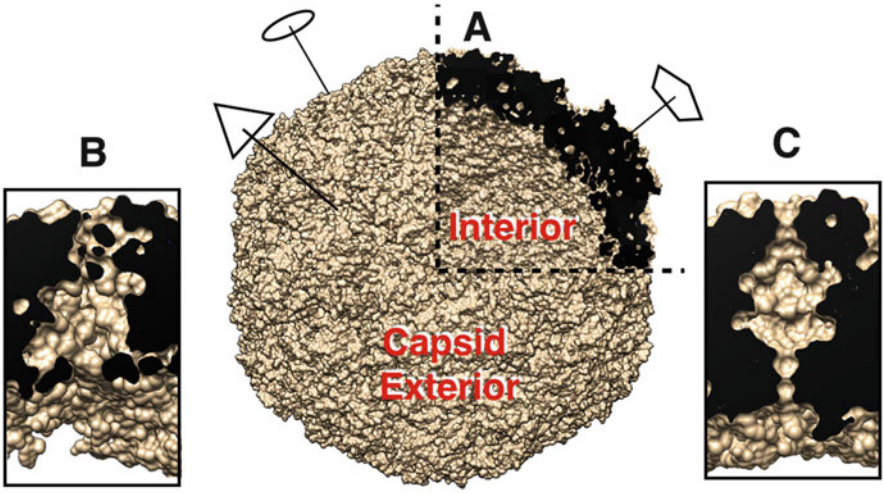

Fig. 9.1 Cavities traversing the protein shell in HRV14. (**a**) Surface representation of the structure of human rhinovirus 14 (RCSB PDB code 1HRV) showing the surface accessible to solvent. The oval, triangle, and pentagon symbols indicate the positions of the icosahedral symmetry axes. The upper right side of the capsid was removed to show the interior and the protein wall (black surface). (**b**) Cavity found along the three-fold axis. (**c**) Cavity found along the five-fold axis. The maximum constriction is approximately 0.4 nm. The image was prepared with UCSF Chimera (www.rbvi.ucsf.edu/chimera). The radius of the prove to draw the solvent accessible surface was 0.17 nm

Hydrogen molecular ions are expressed by the formula $H_3O^+(H_2O)_n$ and are formed by the addition of a proton to one or more water molecules. In particular, two hydrogen ions that are more stable than H_3O^+ are species known as Eigen ($H_9O_4^+$) and Zundel ($H_5O_2^+$) ions. These cations represent the ideal solvation structures of a proton [16–18].

In contrast, the hydroxide ion (OH^-) is the strongest base that can exist in aqueous solution. OH^- ions must be strongly hydrated, but the extent of this hydration is less clear than the hydrogen ions [17]. The tetrahedral $H_7O_4^-$ and $H_3O_2^-$ ions are probably the most stable hydrated hydroxide ions [19, 20].

One of the main properties of water in the liquid form is its capacity to dissolve substances that can dissociate into ions. Unlike the solid materials, in which electrical conduction is mainly due to the movement of electrons, ions dissolved in water are mainly responsible for electric conduction.

In addition to the conduction of water due to the mobility of dissolved ions, another mechanism of charge conduction is called Grotthuss. This mechanism relies on proton transfer between hydrogen-bonded water molecules (see below). The hydrogen ion H_3O^+ has similar solvation characteristics to the Na^+ ion [21]. Nevertheless, because the H^+ transfer between hydrogen-bonded molecules is fast and efficient, the apparent ionic mobility of protons in bulk water is 6–7 times higher than that of Na^+ [21].

The experimental value for the conductivity of pure water at 25 °C was found to be 5.5×10^{-10} S/m [22]. The diffusion rates of proton and hydroxide ions are

usually reduced since they are linked through hydrogen bridges to one or more water molecules. The successive transport involves the rotation and rupture of hydrogen bonds, and these processes decrease the transfer speed of both ions. At room temperature, protons diffuse almost twice as fast as hydroxide ions due to the activation energy required for hydroxide mobility (~3 kcal/mol), which is larger than that of the proton mobility by approximately 0.5 kcal/mol [19].

9.5 Atomic Models[2]

Currently, essential knowledge regarding the structure of proteins relies on the atomic positions of the constituent atoms of the amino acid chain, its ligands, and of other associated ions, in part because high-resolution techniques, such as X-ray crystallography, can assign positions to ordered atoms. If a non-protein atom can be identified in the electron density, such as "crystallographic waters" or ions coordinated to amino acid side chains, we refer to them as "structural" atoms. "To see" or "not to see" depends on the signal of an atom in the crystallographic map; that is, its electron density level. As a result, the background electron density and weak density bulges that could correspond to atoms in solution (or with low occupancy and/or high mobility) are absent in the atomic model. Thus, in such atomistic view, our interpretation of any function a protein can play is only based on "what we see" and overlooks "what we don't see." Within this modelization approach, we can make the tacit assumption that the sole role of the solvent medium is to provide the appropriate chemical environment to proteins, including pH and ionic strength, allowing them to fold and remain stable. We can imagine that these atomic models may be limited in terms of the biochemical functions of proteins that are directly linked to the solvent properties.[3]

As we will show next, modeling proteins in water aiming to describe processes or situations represented on the atomic scale can be cumbersome. For example, imagine we want to study a small peptide immersed in a solvent at neutral pH. The smallest system that can describe this situation must include at least 5.5×10^8 explicit water molecules[4], each composed of one oxygen and two H atoms. Among these molecules, only one has to be dissociated into one OH^- and one H^+. The sphere that can

[2]Many studies on protein structures have been motivated by the following biochemical paradigm: "The amino acid sequence is a form of information that directs the folding of the protein into its unique three-dimensional structure, and ultimately determines the function of the protein" [23]. It turn out that, in most cases, the atomic structure does not suffice to understand how a protein works.

[3]A similar limitation to these experimental models is found in theoretical simulations when the solvent is treated implicitly (isotropous and homogeneous), an approximation known as the "solvent effect" [24, 25].

[4]At neutral pH, $[H^+] = 10^{-7}$. This is equivalent to 10^{-7} mol H^+ per liter (L) of H_2O, that is, $1H^+$ per approx. 1.66×10^{-17} L. Finally, 1.66×10^{-17} L of liquid water corresponds to $\approx 5.5 \times 10^8$ water molecules.

contain all these atoms should be approximately 320 nm in diameter (~14×10^7 nm^3). This volume size is huge compared with the peptide of interest, and it is even 3–4 orders of magnitude larger than the volume corresponding to any large oligomeric protein such as a SINEV. If the portrayed solvent has a pH = 7.5, the model should include 1.8×10^9 explicit water molecules, corresponding to a volume three times greater than the volume required for a model at neutral pH. Moreover, a correct representation of a protein in a given physico-chemical situation will require the analysis of a large number of similar systems.

Based on these considerations, it becomes clear that there is no way to accurately represent the pH with an explicit solvent model in a small cavity or even one with a larger size similar to the interior of a virus (~6×10^4 nm^3). Similarly to pH, some other physico-chemical parameters and variables that are regularly used in biochemistry, such as temperature, pressure, and ionic strength, cannot be represented quantitatively on the atomic scale. Nevertheless, atomic models are always useful for qualitative descriptions in phenomena occurring on or approaching the atomic level.

9.6 Grotthuss Mechanism of Proton Conduction

Grotthuss described the movement of protons across liquid water more than 200 years ago [26, 27]. Although Grotthuss was using an incorrect empirical formula for water, since the water molecule was thought to be OH and not H_2O, his description of the proton transport proved to be prophetic.

A simplified scheme of proton transport in water, also named the "Grotthuss mechanism," can be displayed as follows (Fig. 9.2).

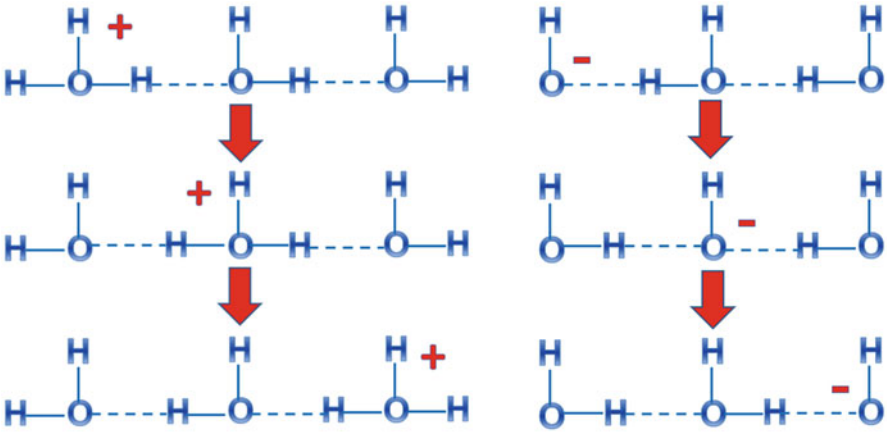

Fig. 9.2 Schematic representation of the Grotthuss mechanism of proton conduction and schematic representation of the Grotthuss-like mechanism of the proton hole conduction

It has been proposed that "water wires" with short hydrogen bonds may exhibit extremely rapid movement of protons due to quantum fluctuations [28]. Additionally, other authors have suggested that proton transfer can occur in a concerted manner by coupling to the structural fluctuations of the H bond network [29]. Stronger hydrogen bonding shortens the distance O–O, facilitating the necessary approach for transfer [30].

A limiting factor in the mobility of H^+ and OH^- ions is the rupture of hydrogen bonds in the outer hydration water layer. This process involves additional energy requirements to stretch the external hydrogen bonds [16]. The dissociation energy for the water dimer, H_4O_2, obtained from IR experimental data and quasi-classical trajectory (QCT) calculations, was ~3.6 kcal/mol [30, 31].

In contrast to proton conduction, proton hole transfer, which is termed the "Grotthuss-like mechanism," can basically be schematized as follows (Fig. 9.2).

The hydroxide anion OH^- in homogeneous bulk water, that is, the solvated "proton hole," is known to feature peculiar properties compared with the excess protons solvated therein. Using a QM/MM model, Riccardi et al. studied the proton transfers in two solution systems and carbonic anhydrase II, arguing that transfer of the "proton hole" is as important as the classical Grotthuss mechanism in many complex molecular systems [32].

9.7 Hydration of Narrow Protein Cavities

The main property that makes water the molecule of life is its ability to create three-dimensional hydrogen bonds [33]. Water in different states of aggregation displays hydrogen-bond networks that are intrinsic to each state. For instance, confinement of water molecules in narrow cavities is very cooperative, and the waters can behave very differently than in bulk [34]. Additionally, water in narrow hydrophobic cavities can exhibit liquid–vapor transitions [34–36]. Some protein structures have narrow hydrophobic cavities that are devoid of solvent, in which this architectural feature plays a key role in protein function. Examples of these structures are found in ion channels and transporters that regulate the flux through the protein pore via a mechanism termed "hydrophobic gating" [37].

Upon folding, many proteins display regions that are not occupied by atoms of their own amino acids. These regions are eventually filled with molecules that are taken up from the surrounding medium. As we will see in the next section, in some protein types, the incorporation of water molecules into narrow cavities allows the ensemble to acquire special properties.

9.8 Water Wires in Proteins

Long-distance proton transfer (>1 nm) mediated by proteins can be achieved through one-dimensional arrangements of water molecules known as "water wires" (also named "proton wires") [29, 38, 39]. There are many examples of membrane proteins that conduct protons through water wires, including the MotA flagellar motor torque generator [40], bacteriorhodopsin [41–44], gramicidin A [21, 45], F_o sector of ATPase [46], M2 proton channel of influenza A virus [47–49], carbonic anhydrase [50], and cytochrome C oxidase [51, 52] (Fig. 9.3).

Recent theoretical studies have served to model proton conduction through water wires. Hybrid DFT calculations were employed to analyze a single line of water molecules spanning lipid membranes. These studies have shown that in the presence of a proton gradient across the membrane, the water wire could transport protons (following the Grotthuss mechanism), and water molecules as well [53].

The Grotthuss-like mechanism has also been studied using ab initio MD simulations [54]. This study found that the nanoconfinement of alkaline aqueous solutions strongly affects key structural and dynamic properties of OH^-, compared to the volume limit.

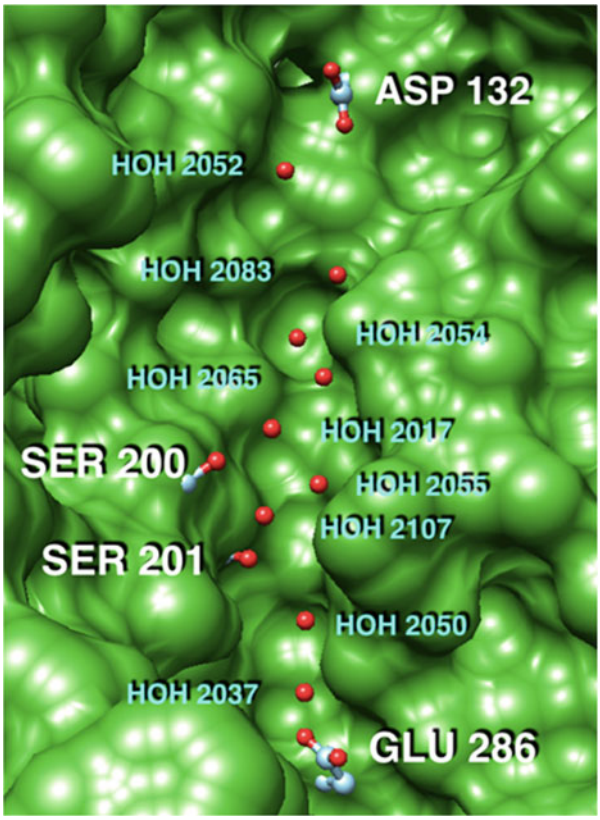

Fig. 9.3 Water wire in cytochrome c oxidase (CytcO). CytcO plays a key function in the respiratory chain, catalyzes the reduction of O_2 to H_2O while simultaneously pumping protons to maintain a transmembrane electrochemical gradient. The figure shows the amino acids and water molecules of the one of the two uptake-proton pathways, called F and D. The pathway D, of more than 3.0 nm length, starts near ASP 132 and leads to GLU 286 though water molecules resolved in the X-ray crystal structures [51]. The image was prepared with UCSF Chimera (www.rbvi.ucsf.edu/chimera). Amino acids 14–111 from CytcO chain A (RCSB PDB code 1M56) were removed to facilitate the visualization of the water wire

Interest in the potential technological application of proton conduction has motivated the performance of experiments that better characterize proton conduction through natural and synthetic water wires. A non-confined hydrogen-bonded water-chain formed along the peptide polytheonamide (pTB) (~4 nm long) was examined using single-channel current recordings in planar lipid bilayers [55]. One finding of this study was to observe whether this nanotube could asymmetrically conduct protons from one to the other side of the membrane. Proton flux from the C- to the N-terminus was 1.6 times higher than in the reverse direction.

Water wires confined by carbon nanotube can transport protons at rates that can exceed those of bulk water. Experimental proton conductivity values measured in 0.8-nm- and 1.5-nm-diameter tubes, respectively, are 9.2×10^{-10} S/m and 1.7×10^{-10} S/m [56]. The presence of water wires in biological systems is mainly associated with membrane proteins, probably due to the special attention dedicated over decades to the study of ion channels. However, the transduction functions played by proteins during the transmission of protons through water wires can be present elsewhere. Indeed, our recent study results examining hydration of the capsid of the insect virus TrV [10] predicted that a water wire can be formed along the narrow cavity traversing the capsid at the five-fold symmetry axis.

The generation of models using MD approach accounted for the full TrV atomic structure immersed in an explicit water bath (with a total of 8 M of non-hydrogen atoms). The results showed that a narrow region (of ~0.4 nm in diameter) lined by hydrophobic amino acids could became fully hydrated. This hydration process occurred only when a Mg ion was placed in a position coincident with a putative cation position observed by crystallography [9]. Subsequently, employing the hybrid's own n-layered integrated molecular orbital (ONIOM) calculations [24], we studied proton conduction through this water wire by mimicking a qualitatively basic pH at the capsid exterior. The calculations performed under three similar alkaline conditions showed that a concerted proton hole transfer occurred through the water wire [10]. This conduction happened downhill in energy, overcoming a low energetic barrier of thermal energy order, up to generate an OH^- at the end of the water wire. This proton hole *hopping* ends up transferring an OH^- from the external to the internal bulk solvent (see Fig. 9.4).

It is noteworthy that each proton jumps in the mentioned water wire provides the system an energy greater than the corresponding break in a hydrogen bridge [30, 31]. In this way, we can suspect that the energy provided to the system may be used to jump the mentioned barriers.

9.9 The Role of Ions in the Five-Fold Axis

Since the first structural studies run on small plant viruses, it has been known that a significant number of magnesium, calcium, and other cations are firmly bound to the virus structure and that these metal ions were crucial for viral integrity [57, 58]. When the very first crystal structures of spherical viruses were reported

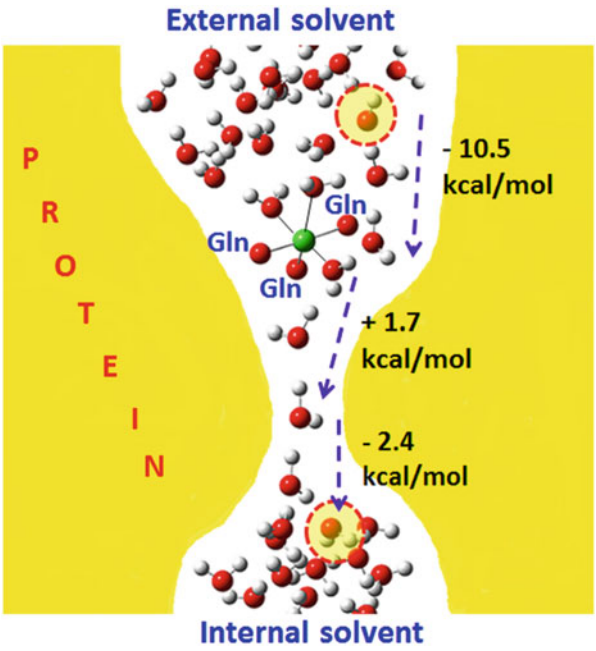

Fig. 9.4 Proton hole transfer through a Grotthuss-like mechanism. The image depicts the transit of a proton hole from the region of the external solvent to the interior. The protein lining the proton channel is indicated in yellow. Oxygen and hydrogen atoms from water molecules correspond to small red and white spheres, respectively. The Mg^{2+} cation is highlighted as a green sphere, and it is coordinated with three water and three Glutamine molecules through six O atoms. Blue arrows point to the movement of the proton hole indicating the energy changes. Translucent yellow circles indicate the first and last positions of the OH^- at the water wire ends. The Gln (blue color) represents the oxygen atoms of the glutamines to which the ion is coordinated

[59, 60], it was apparent that many ions were integral parts of the capsid shell. Successive crystallographic studies performed for many SINEVs have revealed that electron densities in positions coincident with the icosahedral axes are attributable to ions. Examples of plant viruses are southern bean mosaic virus (SBMV; [61]), tomato bushy stunt virus (TBSV; [62, 63]), and satellite tobacco necrosis virus (STNV; [64]). The same structural characteristics have been found in many vertebrate viruses such as human rhinovirus 14 (HRV14; [15]), HRV1A [65], HRV16 [66, 67] (Fig. 9.5), HRV3 [68], poliovirus type 1 [14] and type 3 [69], and coxsackievirus B3 [70]. More recently, the structure of the insect virus cricket paralysis virus (CrPV, [71]), TrV [9], and black queen cell virus (BQCV; [72]) has also exhibited ions blocking the cavity that traverses the capsid along the five-fold axis.

Experiments conducted in several of the previously mentioned viruses have shown that these metal ions are accessible from the external solvent and can be removed by chelating agents [61, 64, 73, 74]. These studies clearly show that capsid

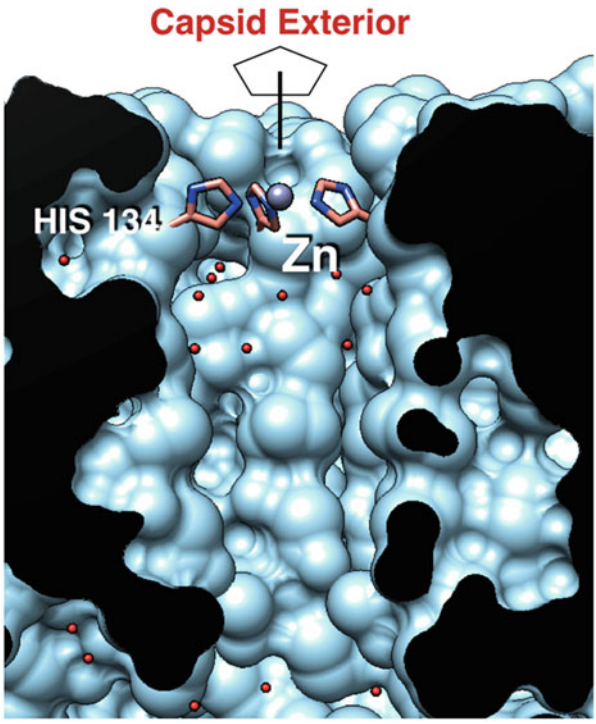

Fig. 9.5 Ion in the cavity at the five-fold axis in HRV16. The clipped image shows the external portion of the cavity in the structure of human rhinovirus 16 (RCSB PDB code 1AYM). A zinc ion (grey sphere) is coordinated to five symmetry-related His 134. Crystallographic water molecules are showed as red balls. The image was prepared with UCSF Chimera (www.rbvi.ucsf.edu/chimera). To draw the solvent accessible surface (in light blue) and facilitate the visualization of the His 134 side chains, a prove radius of 0.07 nm was used

stability and compactness rely on the roles of some of these ions [73]. Besides, other functions associated with pH sensitivity, hydration of narrow cavities, and ion channeling along the five-fold cavity are also linked to their presence [64]. In addition to these experimental results, some theoretical studies also postulate that the funnel shape of the five-fold cavity of SINEVs, together with the presence of internal ions in it, could be the expected architecture of the "at that moment" unknown membrane ion channels [11, 12, 75].

Recently, we reported results obtained for the TrV capsid using atomic force microscopy (AFM) experiments, which indicated that the ions located at the five-fold axis favor the leakage of solvent from the capsid interior [76]. This result is in agreement with the MD calculations performed for this virus [10]. As we mentioned in a previous section, the computational MD calculations showed that the Mg^{2+} ion creates a water wire that bridges the outer bulk solvent and the bulk solvent in the capsid interior. This water bridge most likely allows the water molecules to escape the capsid interior. This transit, in the absence of the cation, could be more difficult due to the hydrophobic gate effect.

9.10 Proton Diodes in Proteins (*I Am I and My Circumstance*)[5]

Voltage-dependent proton channels exist in diverse organisms, ranging from unicellular marine species to multicellular animals, and their functions are equally diverse ([77, 78] and references therein). The main role of voltage-dependent proton channels is to extrude protons from the intracellular medium when the proton concentration increases [79]. The key function of energy transducer membrane proteins is the creation of a proton gradient by directional proton transfer [44]. This mechanism of proteins is analogous to an electronic diode, which is also named a "proton diode."

Interestingly, in our study of proton conduction using the TrV capsid [10], we found the same conduction phenomenon as described for membrane proteins. We analyzed the influence of the external acidic pH by setting up a model similar to that employed in the situation of a basic external pH, and we computed the proton conduction through the water wire formed within the five-fold cavity. The external acid condition was mimicked by replacing the external OH^- with H_3O^+. Under this condition of acidic external pH, a classical Grotthuss occurred, but only for half way of the water wire. The proton migration stopped immediately before reaching the water molecule coordinated to the Mg^{2+} cation (see Fig. 9.6). The water wire near the metal ion became disrupted due to an important increase in distance between the hydronium and the inner water molecule. This disruption of connectivity was most likely a consequence of the electrostatic repulsion exerted by Mg^{2+} on the hydronium ion. The Mg^{2+} cation and its three coordinated water molecules formed a barrier that impeded the transit of protons into the internal solvent.

Thus, we can conclude that the two factors allowing the five-fold axis cavity to act as a proton diode are the limited space of the hydrophobic neck and the positive ion trapped within it. This finding is consistent with the sensitivity of TrV virions to alkaline environments and their resistance to an acidic pH [80, 7].

This supposed function of the five-fold cavity in the capsid of TrV could explain how the viral capsid senses the environmental pH, and the way this unidirectional proton permeation can promote the destabilization and opening of the protein shell under alkaline conditions [10].

[5]Ortega y Gaset wrote this *maxima*, and his phrase expresses—in some sense—that all of a person's life is strongly conditioned by the circumstances in which he or she lives. Analogously to humans, we assume that we can only understand how a protein functions as proton channel if we analyze the protein structure in a situation adequate for the internal putative "water wire" to conduct protons.

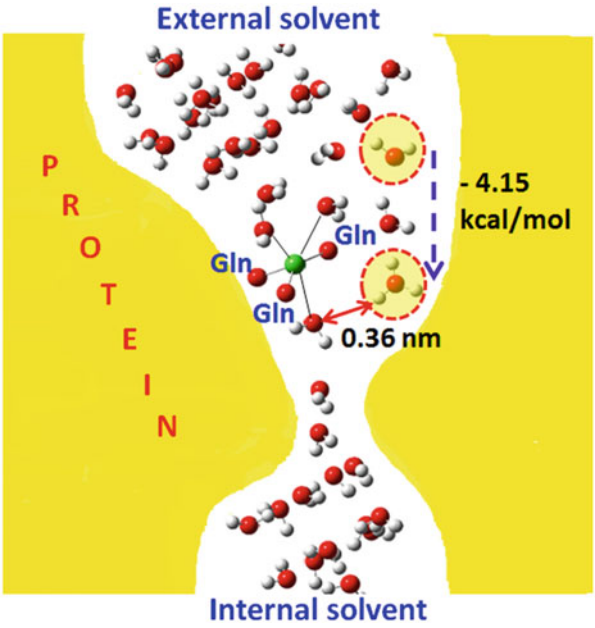

Fig. 9.6 Proton diode in the TrV capsid. When the region of the outer solvent has an acidic pH, proton migration occurs down till the most inner Mg^{2+}-coordinated water. There, the water wire is disrupted, most likely due to an electrostatic repulsion that force the distance between the hydronium and the inner water molecule to increase (~0.36 nm), thus hindering the proton to jump and reach the internal portion of the water wire. The dashed arrow indicates the two-step energy downhill jump of the proton (of about −4.15 kcal/mol). The initial and final hydronium positions are indicated as translucent yellow circles. Atom and protein are represented as in Fig. 9.4

9.11 Are Water Wires a General Phenomenon in SINEVs?

Despite many studies on closely related acid-stable and acid-labile viruses within the enterovirus and rhinovirus species have been done, these do not suffice to understand the molecular basis of these different properties. From the pioneer study on TrV [10], we can ask ourselves if the presence or absence of a proton-conducting wire could explain these differences. It is clear that in TrV virions a correlation exists between alkaline environment and capsid bursting allowing the genome exit, whereas the empty capsid is stable under this pH condition [7]. These same features have not been observed in picornaviruses and then there is no reason to generalize the proton conduction model proposed for TrV to other viruses. Moreover, it was found that some picornaviruses transitorily expose internal segments of their proteins [81], or even some RNA dyes can enter native virions [82, 83]. From this observations it is clear that some viral capsids can be highly dynamics allowing interchange its content with the surrounding without compromising its integrity. Such important conformational fluctuations will suffice for hydoxonium and other bigger ions to enter and exit the capsid shell via simple diffusion, even without liberating of their accompanying

hydration shell. Cavities exist at the five-fold axis in all icosahedral capsids. Therefore, the MD results found in TrV would suggest that water wires could be formed in other similar viruses. Although this is highly probable, this feature does not suffice to think that, in viruses displaying this water motif, protons are exchanged between the medium and the capsid interior.

Regarding capsid sensitivity to pH, we can ask ourselves: what would the water wire achieve that cannot be achieved with the protein itself? Water wires can facilitate the proton conduction by both mechanisms, Grotthuss (proton movement) and Grotthuss-like (proton hole jumping). These concerted mechanisms permit proton conduction along long distance by mean water wires. This feature is a consequence of the particular structure of the water molecules. For this reason it is unlikely that the amino acids could arrange in a motif with similar conduction properties as present in the water wires. Nevertheless, it is clear that amino acids like histidine can strongly impact on overall protein properties, as in stability of the food-and-mouth disease virus [84], and in ion selectivity of the membrane proton channel M2 [85, 86].

9.12 Conclusion

The viral capsid must, among other functions, carry the genome through the extracellular space. This process encompasses a long journey that can include ambient exposure and stringent aggressive environments, such as those encountered into the host digestive tract. Thus, the capsid is implied to protect the cargo from potentially dangerous lytic agents and other fortuitous chemical attacks. Part of this protective function is assured by the compactness of the capsid, which prevents the exchange of solute between the interior and the external milieu. This hermetism prevents the dehydration that could occur if internal water molecules escape, and it also impedes the diffusion of counter ions that could neutralize the encapsidated genome. However, once the virus has reached its target cell, to allow genome exit and initiate infection, this strong hermetic feature must be relaxed.

Due to the steric hindrance inherent to amino acid folding, the icosahedral viral capsids display narrow cavities that can be accessed by different types of molecules present in the surrounding medium. Some of these cavities are located in the three- and five-fold icosahedral axes, and in some cases these “empty” regions span the protein shell. During viral assembly, water molecules and ions enter these cavities, and their chemical properties can greatly influence the features of the ensemble. One of the astonishing features that water molecules acquire when are aligned is to boost the proton conduction.

In this chapter, we have reviewed the principles and structural characteristics that permit proton conduction through narrow hydrated cavities in proteins. We have also described how a combination of these elements found in the TrV capsid can permit unidirectional proton exit from the capsid interior. The existence of a proton diode as an integral part of the viral capsid of this virus provides a plausible explanation for

the sensitivity of the protein shell to alkaline but insensitivity to acidic environments. The analysis performed on the insect virus TrV showed how the integration of atomic models, along with MD and QM calculations, can describe a process that can only be understood when the protein structure and the surrounding medium are considered together. In this context, MD and QM allow modeling of the environment ("circumstance") in which the proton channel property can be found. Otherwise, unless an appropriate experiment confirms this hypothesis, this viral capsid property could never "be seen."

The presence of ion channels as integral part of the capsid of non-enveloped viruses would greatly further our understanding of the specific role of the amino acid residues lining the numerous cavities and channels in the protein shells. This hypothetical function of the protein envelope will also contribute to give a clue to open questions related to structural changes occurring during genome release.

Acknowledgements We thank Dieter Blaas, Medical University of Vienna, Vienna Biocenter, A-1030, Austria, for critical reading and useful comments of the manuscript. MMB is a member of the CONICET research staff, Argentina, and she thanks a permit from the CONICET and UNS to do sabbatical stage at DMAG's lab, Instituto Biofisika (CSIC, UPV/EHU). MMB thanks a traveling grant from the CYTED (216RT0506). This work was partially supported by a grant to DMAG from the Ministerio de Ciencia e Innovación (BFU2012-36241), and Gobierno Vasco (Elkartek KK-2017/00008), Spain.

References

1. Hackett BA, Yasunaga A, Panda D, Tartell MA, Hopkins KC, Hensley SE, Cherry S (2015) RNASEK is required for internalization of diverse acid-dependent viruses. PNAS 112 (25):7797–7802
2. Penkler DL, Jiwaji M, Domitrovic T, Short JR, Johnson JE, Dorrington RA (2016) Binding and entry of a non-enveloped T1/44 insect RNA virus is triggered by alkaline pH. Virology 498:277–287
3. Appell HM, Martin MM (1990) Gut redox conditions in herbivorous lepidopteran larvae. J Chem Ecol 16:3277–3290
4. Agirre J, Aloria K, Arizmendi JM, Iloro I, Elortza F, Marti GA, Neumann E, Rey FA, Guérin DMA (2011) Capsid protein identification and analysis of *Triatoma Virus* (TrV) mature virions and naturally occurring empty particles. Virology 409:91–101
5. Czibener C, La Torre JL, Muscio OA, Ugalde RA, Scodeller EA (2000) Nucleotide sequence analysis of *Triatoma virus* shows that it is a member of a novel group of insect RNA viruses. J Gen Virol 81:1149–1154
6. Muscio OA, La Torre JL, Scodeller EA (1987) Small nonoccluded viruses from triatomine bug *Triatoma infestans* (Hemiptera: Reduviidae). J Invertebr Pathol 49:218–220
7. Snijder J, Uetrecht C, Rose RJ, Sanchez-Eugenia R, Marti GA, Agirre J, Guérin DMA, Wuite GJL, Heck AJR, Roos WH (2013) Probing the biophysical interplay between a viral genome and its capsid. Nat Chem 5:502–509
8. Bonning BC, Miller WA (2010) Dicistroviruses. Annu Rev Entomol 55:129–150
9. Squires G, Pous J, Agirre J, Rozas-Dennis GS, Costabel MD, Marti GA, Navaza J, Bressanelli S, Guérin DM, Rey FA (2013) Structure of the *Triatoma virus* capsid. Acta Crystallogr D Biol Crystallogr 69(6):1026–1037

10. Viso J, Belelli PG, Machado M, González H, Pantano S, Amundarain MJ, Zamarreño F, Branda MM, Guérin DMA, Costabel MD (2018) Multiscale modelization in a small virus: mechanism of proton channeling and its role in triggering capsid disassembly. PLoS Comput Biol 14(4): e1006082. https://doi.org/10.1371/journal.pcbi.1006082
11. Eisenman G, Oberhauser A, Benzanilla F (1988) Ion selectivity and molecular structure of binding sites and channels in icosahedral viruses in the 21st Jerusalem Symposyum on quantum chemistry. In: Pullman A, Jortner J, Pullman B (eds) Transport through membrane: carriers, channels and pumps. Kluwer Academic, Dordrecht, pp 27–50
12. Silva AM, Cachau RE, Goldstein DJ (1987) Ion channels in southern bean mosaic virus capsid. Biophys J 52:595–592
13. Jiang Y, Lee A, Chen J, Ruta V, Cadene M, Chait BT, Mackinnon R (2003) X-ray structure of a voltage dependent K+ channel. Nature 423:33–41
14. Hogle JM, Chow M, Filman DJ (1985) Three-dimensional structure of poliovirus at 2.9 A resolution. Science 229:1358–1365
15. Rossmann MG, Arnold F, Erickson JW, Frankenberger EA, Grifith JP, Hecht HJ, Johnson JE, Kamer G, Luo M, Mosser AG, Rueckert RR, Sherry B, Vriend G (1985) Structure of a human common cold virus and functional relationship to other picornaviruses. Nature 317:145–153
16. Agmon N, Bakker HJ, Campen RK, Henchman RH, Pohl P, Roke S, Thämer M, Hassanali A (2016) Protons and hydroxide ions in aqueous systems. Chem Rev 116:7642–7672
17. Chaplin MF (2018) Structure and properties of water in its various states. In: Maurice PA (ed) Encyclopedia of water: science, technology, and society. Wiley (in press)
18. Marx D, Tuckerman ME, Hutter J, Parrinello M (1999) The nature of the hydrated excess proton in water. Nature 397(6720):601–604
19. Agmon N (2000) Mechanism of hydroxide mobility. Chem Phys Lett 319:247–252
20. Asthagiri D, Pratt LR, Kress JD, Gomez MA (2003) The hydration state of OH^- (aq). Chem Phys Lett 380:530–535
21. Wraight CA (2006) Chance and design-proton transfer in water, channels and bioenergetic proteins. Biochim Biophys Acta 1757:886–912
22. Light TS, Licht S, Bevilacqua AC, Morash KR (2005) The fundamental conductivity and resistivity of water. Electrochem Solid-State Lett 8(1):16–19
23. Lehninger AL, Nelson DL, Cox MM (2005) Lehninger principles of biochemistry, 4th edn. WH Freeman, New York, p 46
24. Chung LW, Sameera WMC, Ramozzi R, Page AJ, Hatanaka M, Petrova GP, Harris TV, Li X, Ke Z, Liu F, Li H-B, Ding L, Morokuma K (2015) The ONIOM method and its applications. Chem Rev 115:5678–5796
25. Simonson T, Carlsson J, Case DA (2004) Proton binding to proteins: pKa calculations with explicit and implicit solvent models. JACS 126:4167–4180
26. Cukierman SL (2006) Et tu, Grotthuss! and other unfinished stories. Biochim Biophys Acta Bioenerg 1757:876–885
27. de Grotthuss CJT (1806) Sur la décomposition de l'eau et des corps qu'elle tient en dissolution à l'aide de l'électricité galvanique (On the decomposition of water and of the bodies that it holds in solution by means of galvanic electricity). Ann Chim LVIII:54–74
28. Ceriotti M, Cuny J, Parrinello M, Manolopoulos DE (2013) Nuclear quantum effects and hydrogen bond fluctuations in water. Proc Natl Acad Sci 110:15591–15596
29. Hassanali A, Giberti F, Cuny J, Kühne TD, Parrinello M (2013) Proton transfer through the water gossamer. PNAS 110(34):13723–13728
30. Ruscic B (2013) Active thermochemical tables: water and water dimer. J Phys Chem A 117:11940–11953
31. Ch'ng LC, Samanta AK, Czakó G, Bowman JM, Reisler H (2012) Experimental and theoretical investigations of energy transfer and hydrogen-bond breaking in the water dimer. JACS 134:15430–15435

32. Riccardi D, Koňig P, Prat-Resina X, Yu H, Elstner M, Frauenheim T, Cui Q (2006) Proton holes in long-range proton transfer reactions in solution and enzymes: a theoretical analysis. JACS 128:16302–16311
33. Gordalla B, Müller MB, Frimmel FH (2007) The physicochemical properties of water and their relevance for life. In: Lozán JL, Grassl H, Hupfer P, Menzel L, Schönwiese C-D (eds) Global change: enough water for all? Wissenschaftliche Auswertungen, Hamburg. www.klima-warnsignale.uni-hamburg.de
34. Rasaiah JC, Garde S, Hummer G (2008) Water in nonpolar confinement: from nanotubes to proteins and beyond. Annu Rev Phys Chem 59:713–740
35. Beckstein O, Sansom MS (2003) Liquid–vapor oscillations of water in hydrophobic nanopores. Proc Natl Acad Sci U S A 100:7063–7068
36. Hummer G, Rasaiah JC, Noworyta JP (2001) Water conduction through the hydrophobic channel of a carbon nanotube. Nature 414:188–190
37. Aryal P, Sansom MSP, Tucker SJ (2015) Hydrophobic gating in ion channels. J Mol Biol 427:121–130
38. Karahka ML, Kreuzer HJ (2013) Charge transport along proton wires. Biointerphases 8(13):1–9
39. Miyake T, Rolandi M (2016) Grotthuss mechanisms: from proton transport in proton wires to bioprotonic devices. J Phys Condens Matter 28(023001):1–11
40. Zhou J, Sharp LL, Tang HL, Lloyd SA, Billings S, Braun TF, Blair DF (1998) Function of protonatable residues in the flagellar motor of *Escherichia coli*: a critical role for Asp 32 of MotB. J Bacteriol 180:2729–2735
41. Baudry J, Tajkhorshid E, Molnar F, Phillips J, Schulten K (2001) Molecular dynamics study of bacteriorhodopsin and the purple membrane. J Phys Chem B 105:905–918
42. Bondar AN, Baudry J, Suhai S, Fischer S, Smith JC (2008) Key role of active site wáter molecules in bacteriorhodopsin proton-transfer reactions. J Phys Chem B 112:14729–14741
43. Kandt C, Schlitter J, Gerwert K (2004) Dynamics of water molecules in the bacteriorhodopsin trimer in explicit lipid/water environment. Biophys J 86:705–717
44. Wolf S, Freier E, Potschies M, Hofmann E, Gerwert K (2010) Directional proton transfer in membrane proteins achieved through protonated protein-bound water molecules: a proton diode. Angew Chem Int Ed 49:6889–6893
45. Chernyshev A, Armstrong KM, Cukierman S (2003) Proton transfer in gramicidin channels is modulated by the thickness of monoglyceride bilayers. Biophys J 84(1):238–250
46. Aksimentiev A, Balabin IA, Fillingame RH, Schulten K (2004) Insights into the molecular mechanism of rotation in the Fo sector of ATP synthase. Biophys J 86:1332–1344
47. Gianti E, Carnevale V, de Grado WF, Klein ML, Fiorin G (2015) Hydrogen-bonded water molecules in the M2 channel of the influenza A virus guide the binding preferences of ammonium-based inhibitors. J Phys Chem B 119:1173–1183
48. Liang R, Li H, Swanson JMJ, Voth GA (2014) Multiscale simulation reveals a multifaceted mechanism of proton permeation through the influenza A M2 proton channel. PNAS 111 (26):9396–9401
49. Moffat JC, Vijayvergiya V, Gao PF, Cross TA, Woodbury DJ, Busath DD (2008) Proton transport through influenza a virus M2 protein reconstituted in vesicles. Biophys J 94:434–445
50. Maupin CM, Castillo N, Taraphder S, Tu C, McKenna R, Silverman DN, Voth GA (2011) Chemical rescue of enzymes: proton transfer in mutants of human carbonic anhydrase II. JACS 133:6223–6234
51. Lee HJ, Svahn E, Swanson JMJ, Lepp H, Voth GA, Brzezinski P, Gennis RB (2010) Intricate role of water in proton transport through cytochrome C oxidase. JACS 132:16225–16239
52. Xu J, Voth GA (2005) Computer simulation of explicit proton translocation in cytochrome C oxidase: the D pathway. PNAS 102(19):6795–6800
53. Zhao H, Sheng S, Hong Y, Zeng H (2014) Proton gradient-induced water transport mediated by water wires inside narrow aquapores of aquafoldamer molecules. JACS 136:14270–14276
54. Muñoz-Santiburcio D, Marx D (2016) On the complex structural diffusion of proton holes in nanoconfined alkaline solutions within slit pores. Nat Commun 7(12625):1–9

55. Matsuki Y, Iwamoto M, Mita K, Shigemi K, Matsunaga S, Oiki S (2016) Rectified proton Grotthuss conduction across a long water-wire in the test nanotube of the polytheonamide B channel. JACS 138:4168–4177
56. Tunuguntla RH, Allen FI, Kim K, Belliveau A, Noy A (2016) Ultrafast proton transport in sub-1-nm diameter carbon nanotube porins. Nat Nanotechnol 11:639–644
57. Hsu CH, Sehgal OP, Pickett EE (1976) Stabilizing effect of divalent metal ions on virions of southern bean mosaic virus. Virology 69:587–595
58. Hull R (1978) The stabilization of the particles of turnip rosette virus. III. Divalent cations. Virology 89(2):418–422
59. Abad-Zapatero C, Abdel-Meguid SS, Johnson JE, Leslie AGW, Rayment I, Rossmann MG, Suck D, Tsukihara T (1980) Structure of southern bean mosaic virus at 2.8 resolution. Nature 286:33–39
60. Harrison SC, Olson AJ, Schutt CE, Winkler FK, Bricogne G (1978) Tomato bushy stunt at 2.9 resolution. Nature 276:368–373
61. Abdel-Meguid SS, Yamane T, Fukuyama K, Rossmann MG (1981) The location of calcium ions in southern bean mosaic virus. Virology 114:81–85
62. Olson AJ, Bricogne G, Harrison SC (1983) Structure of tomato bushy stunt virus IV. The virus particle at 2.9 E resolution. J Mol Biol 171:61–93
63. Robinson IK, Harrison SC (1982) Structure of the expanded state of tomato bushy stunt virus. Nature 297:563–568
64. Montelius I, Liljas L, Unge T (1990) Sequential removal of Ca^{2+} from satellite tobacco necrosis virus. Crystal structure of two EDTA-treated forms. J Mol Biol 212:331–343
65. Kim S, Smith TJ, Chapman MS, Rossmann MG, Pevear DC, Dutko FJ, Felock PJ, Diana GD, McKinlay MA (1989) The crystal structure of human rhinovirus serotype 1A (HRV1A). J Mol Biol 210:91–111
66. Hadfield AT, Lee WM, Zhao R, Oliveira MA, Minor I, Rueckert RR, Rossmann MG (1997) The refined structure of human rhinovirus 16 at 2.15 Å resolution: implications for the viral life cycle. Structure 5:427–441
67. Oliveira MA, Zhao R, Lee WM, Kremer MJ, Minor I, Rueckert RR, Diana GD, Pevear DC, Dutko FJ, McKinlay MA, Rossmann MG (1993) The structure of human rhinovirus 16. Structure 1:51–68
68. Zhao R, Pevear DC, Kremer MJ, Giranda VL, Kofron JA, Kuhn RJ, Rossmann MG (1996) Human rhinovirus 3 at 3.0 Å resolution. Structure 4:1205–1220
69. Filman DJ, Syed R, Chow M, Macadam AJ, Minor PD, Hogle JM (1989) Structural factors that control conformational transitions and serotype specificity in type 3 poliovirus. EMBO J 8 (5):1567–1579
70. Muckelbauer JK, Kremer M, Minor I, Diana G, Dutko FJ, Groarke J, Pevear DC, Rossmann MG (1995) The structure of coxsackievirus B3 at 3.5 Å resolution. Structure 3:653–667
71. Tate J, Liljas L, Scotti P, Christian P, Lin T, Johnson JE (1999) The crystal structure of cricket paralysis virus: the first view of a new virus family. Nat Struct Biol 6:765–774
72. Spurny R, Přidal A, Pálková L, Khanh Tran Kiem H, de Miranda JR, Plevka P (2017) Virion structure of black queen cell virus, a common honeybee pathogen. J Virol 91(6):e02100–e02116. https://doi.org/10.1128/JVI.02100-16
73. Unge T, Montelius I, Liljas L, Öfverstedt L-G (1986) The EDTA-treated expanded satellite tobacco necrosis virus: biochemical properties and crystallisation. Virology 152:207–218
74. Zhao R, Hadfield AT, Kremer MJ, Rossmann MG (1997) Cations in human rhinoviruses. Virology 227:13–23
75. Kalko SG, Cachau RE, Silva AM (1992) Ion channels in icosahedral virus: a comparative analysis of the structures and binding sites at their five-fold axes. Biophys J 63:1133–1145
76. Martín-González N, Guérin Darvas SM, Durana A, Marti GA, Guérin DMA, de Pablo PJ (2018) Exploring the role of genome and structural ions in preventing viral capsid collapse during dehydration. J Phys Condens Matter 30(10):104001. https://doi.org/10.1088/1361-648X/aaa944

77. Cherny VV, Morgan D, Musset B, Chaves G, Smith SME, DeCoursey TE (2015) Tryptophan 207 is crucial to the unique properties of the human voltage-gated proton channel, hHV1. J Gen Physiol 146(5):343–356
78. DeCoursey TE, Morgan D, Musset B, Cherny VV (2016) Insights into the structure and function of HV1 from a meta-analysis of mutation studies. J Gen Physiol 148(2):97–118
79. Castillo K, Pupo A, Baez-Nieto D, Contreras GF, Morera FJ, Neely A, Latorre R, Gonzalez C (2015) Voltage-gated proton (Hv1) channels, a singular voltage sensing domain. FEBS Lett 589:3471–3478
80. Agirre J, Goret G, LeGoff M, Sánchez-Eugenia R, Marti GA, Navaza J, Guérin DMA, Neumann E (2013) Cryo-electron microscopy reconstructions of *Triatoma virus* particles: a clue to unravel genome delivery and capsid disassembly. J Gen Virol 94(Pt 5):1058–1068
81. Li Q, Yafal AG, Lee YM, Hogle J, Chow M (1994) Poliovirus neutralization by antibodies to internal epitopes of VP4 and VP1 results from reversible exposure of these sequences at physiological temperature. J Virol 68:3965–3970
82. Broo K, Wei J, Marshall D, Brown F, Smith TJ, Johnson JE, Schneemann A, Siuzdak G (2001) Viral capsid mobility: a dynamic conduit for inactivation. PNAS 98(5):2274–2277
83. Kremser L, Petsch M, Blaas D, Kenndler E (2004) Labeling of capsid proteins and genomic RNA of human rhinovirus with two different fluorescent dyes for selective detection by capillary electrophoresis. Anal Chem 76(24):7360–7365
84. Yuan H, Li P, Ma X, Lu Z, Sun P, Bai X, Zhang J, Bao H, Cao Y, Li D et al (2017) The pH stability of foot-and-mouth disease virus. Virol J 14:233
85. Acharya R et al (2010) Structure and mechanism of proton transport through the transmembrane tetrameric M2 protein bundle of the influenza A virus. Proc Natl Acad Sci U S A 107:15075–15080
86. Thomaston JL, Alfonso-Prieto M, Woldeyes RA, Fraser JS, Klein ML, Fiorin G, DeGrado WF (2015) High-resolution structures of the M2 channel from influenza A virus reveal dynamic pathways for proton stabilization and transduction. Proc Natl Acad Sci USA 112(46):14260–14265

Chapter 10
Computational Virology: Molecular Simulations of Virus Dynamics and Interactions

Elizabeth E. Jefferys and Mark S. P. Sansom

Abstract Molecular modelling and simulations play a key role in computational virology, allowing us to study viruses and their components. This allows experimental structures and related information to be integrated into a single coherent model, enabling predictions about the behaviour of a viral system to go beyond what could be obtained experimentally. In this way, computational approaches provide a powerful complement to more traditional experimental and structural methods. In this chapter, we describe three main areas of computational virology to showcase the power of methods within this field. We begin by describing relatively small simulation systems and focusing on the behaviour of fusion peptides. Then, extending to longer timescales and larger systems, we discuss computational studies of viral capsid assembly and genome encapsidation. Finally, we describe recent developments which allow entire viral particles to be simulated.

Keywords Fusion peptide · Capsid · Envelope · Molecular dynamics simulation

10.1 Introduction

Viruses are thought to be the most abundant and diverse group of biological systems on Earth [1]. With no known common ancestor, the biology of viruses from different families varies widely. And yet, within this diversity, there are a number of common processes—shared events found in most, if not all, viral replication cycles that are essential for productive infection (Fig. 10.1).

Disrupting any of these steps may prevent or impair viral propagation. Similarly, destabilising the infective virions before they are able to attack host cells can be an effective means to prevent propagation. From a therapeutic perspective, therefore, detailed molecular-level understanding of the dynamics at each of these stages, as

E. E. Jefferys · M. S. P. Sansom (✉)
Department of Biochemistry, University of Oxford, Oxford, UK
e-mail: mark.sansom@bioch.ox.ac.uk

U. F. Greber (ed.), *Physical Virology*, Advances in Experimental Medicine and Biology 1140, https://doi.org/10.1007/978-3-030-14741-9_10

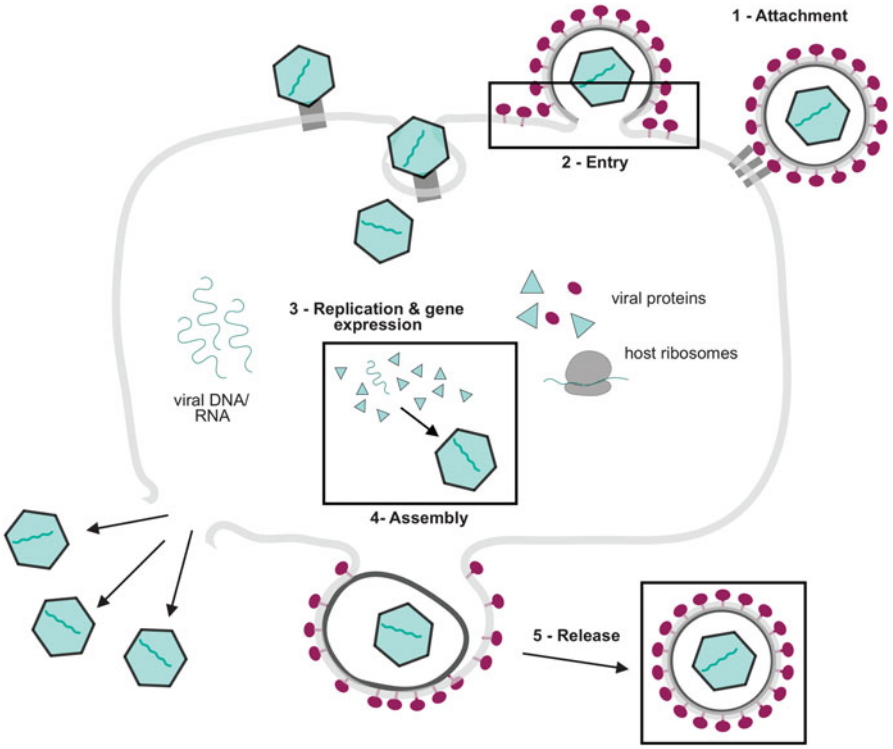

Fig. 10.1 A generalised viral replication cycle. Schematic viral replication cycle, showing the steps thought to be common to most viruses. Boxed steps have been studied using the computational methods discussed in this chapter

well as of the virions themselves, is of considerable interest. This is particularly true in view of emerging drug-resistant viral strains and new outbreaks of highly pathogenic species. In theory, if we can develop therapeutics that target multiple steps of viral replication cycles and/or critical processes with limited capacity for viable mutation, then the chances of any given virus developing resistance to the administered drugs should be reduced. Similarly, if we understand the structural and dynamic basis for drug resistance, antivirals could in principle be modified to account for the mutation.

Beyond the clear biomedical interest in characterising the molecular details of viruses and their replication cycles, there are possible technological benefits from this understanding. Viral nanoparticles (VNPs) and virus-like particles (VLPs)—differing primarily by the presence and absence of a genome, respectively [2]—are being developed as nanocontainers for drugs or imaging reagents for delivery to specific tissues [3]. This is enhanced by structure-guided approaches to shield from immune attack and to retarget virions to tissues of interest [4, 5]. Viral-based systems are also finding use as scaffolds for chemical synthesis and as components of composite materials [6]. In order to better develop VLPs and VNPs for practical applications

we need to understand how their naturally occurring antecessors assemble, disassemble, package cargo, and encounter and enter compatible host cells. This information can also be applied to aid the development of non-viral self-assembling systems for use in delivery and other applications [7].

As in many areas of biology, obtaining a comprehensive understanding of virus operation requires a multidisciplinary approach. Aided by advances in structural biology, computational methods have emerged as powerful tools which complement experimental techniques. In many cases, computational approaches can help to bridge the information gap between experiments by reporting in different spatial and temporal domains, as well as having considerable predictive power in their own right.

In this chapter, we focus on those aspects of computational virology which have a structural underpinning, specifically the use of molecular modelling and simulations in studying viral function [8]. As will be discussed, these methods allow the dissection of viral replication cycles at multiple levels, from the function of individual enzymes and glycoproteins to the assembly and dynamics of entire capsids or enveloped virions. It must be noted, however, that the field of computational virology extends beyond those approaches discussed here, to include an array of more inductive methods rooted in statistics and informatics (for example, the use of mathematical models to characterise the HIV-1 life cycle [9] and describe the development of drug resistance by this pathogen [10]). Also not discussed here, but of great value to virology research, are various online databases and web-based tools (reviewed in Ref. [11]).

We will also not discuss in any detail the many computational studies of viral enzymes, which have provided valuable information leading to the development and improvement of many effective antiviral drugs in clinical use today, choosing rather to focus on those simulation methods that are more specific to viral systems. For information on the former, the reader is referred to recent reviews (e.g. [12, 13]).

10.2 Molecular Simulations: A Primer

Before proceeding further, it is necessary to introduce some terminology and concepts that will be required to understand the computational studies subsequently presented. This section therefore provides a summary of some of the main computational techniques applied in the studies to be discussed.

Molecular simulations [14] lie at the heart of computational virology. There are a number of distinct methods for conducting molecular simulations, which vary primarily in how the system is represented and how its energy landscape is explored. The mainstay of biomolecular simulations is molecular dynamics (MD), in which Newton's equations of motion are iteratively solved for a system of interacting atoms or particles to build up a picture of how that system evolves with time. This can be thought of as 'breathing life' into (static) structures of biomolecules so that they behave as they may be expected to in their native environment.

Of the methods discussed in this chapter, MD is typically associated with the highest level of structural detail, at the cost of substantial computational demands. This limitation can be overcome to some extent by simplifying the system, reducing it from an atomistic (AT) to a coarse-grained (CG) resolution. Such coarse-graining can range from a near-atomic representation, such as the 4:1 mapping of non-hydrogen atoms to CG particles in the Martini force field [15, 16], through to representing, e.g. proteins or their domains as single particles, as in the trapezoid capsid assembly models pioneered by Rapaport and coworkers [17, 18], and to modelling solvent and bilayers as implicit (i.e. continuum) environments. Such simplification permits greater exploration of configurations available to the system, alongside access to longer timescales and larger system sizes. There are also various enhanced sampling variants of MD that can be used to explore the potential energy landscape more extensively, including metadynamics [19], accelerated MD [20], and adaptive biasing force sampling [21].

Langevin dynamics and Brownian dynamics (BD) simulations may be considered as a special case of CG methods. In these approaches, the solvent is not explicitly included. Instead, its effects on the other system components are accounted for using a stochastic force. This does not explicitly take into account electrostatic screening or the hydrophobic effect, but reproduces the random jostling of molecules caused by the solvent.

Monte Carlo (MC) simulations differ fundamentally from these approaches. MD simulations effectively explore the temporal evolution of configurations of a system, and thus are fundamentally deterministic: that is, given a set of starting positions and velocities, the system will evolve in the same way over time. However, a major limitation of classical MD is a tendency to only sample configurational space close to the initial conditions, often being unable to surmount high (relative to kT) energetic barriers between alternative configurations. MC simulations circumvent this problem by exploring the configurational landscape in a more effectively stochastic manner, allowing ‘leaps’ across the landscape to yield better overall coverage. At each step in a MC simulation, the particles are assigned new positions at random, and the new configuration is either accepted or rejected based on the Metropolis criterion, using a probability distribution weighted based on whether or not the new configuration is more energetically favourable than the previous one. This method of sampling the conformational landscape means that time-dependent phenomena cannot be explored.

With a combination of alternative simulation techniques and a range of resolutions available for molecular simulations, it has become possible to apply such methods to systems spanning a great range of length- and timescales (Fig. 10.2), putting many individual events in viral life cycles within the capabilities of computational investigation.

In addition to the structure-based approaches discussed above, a number of techniques with entirely distinct underpinnings have been applied to study various aspects of virus biology. For instance, equilibrium and reaction kinetic methods used in the early capsid assembly simulations of Zlotnick [25], and the predictions of retroviral capsid self-assembly behaviour by Nguyen et al. based on continuum

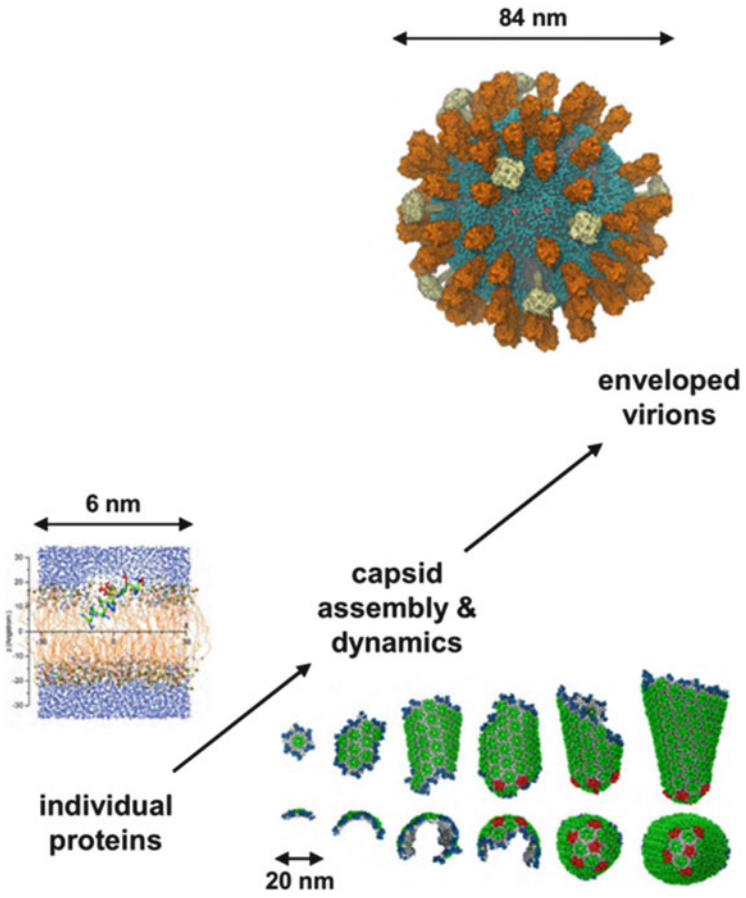

Fig. 10.2 Multiscale simulations. Illustration of the range of length scales accessible to molecular simulations through application of different computational techniques and model resolutions, from isolated viral components studied by all-atom MD simulations (modified from [22]), through modelling capsid assembly via interacting spheres (modified from [23]), to entire virions at coarse-grained resolution (from [24])

elastic theory [26]. A background discussion of these various more mathematics-based methods, and their relative merits and limitations, is beyond the scope of this chapter. However, their value in the overall field of computational virology cannot be overlooked, as they are able to provide information distinct from, yet complementary to, that obtained through the more structure-centred MD, MC, and BD simulations. For instance, the former often provide insight into fundamental physical and quantitative underpinnings of events, whereas the latter may provide more direct insight into molecular mechanisms.

10.3 Breaching the Host Barrier

To infect a host cell, viruses must be able to breach one or more cell membranes. In the case of enveloped viruses, this involves a merger between viral and host cell membrane lipid bilayers, a process brought about by an envelope glycoprotein, the fusogen. Viral fusogens fall into three classes which are best defined by shared structural features [27]. The majority of computational studies of viral fusion have focused on the prototypical class I fusogen of influenza A virus, haemagglutinin (HA), and on its fusion peptide. There have also been a number of computational investigations into membrane fusion in general, both protein-free and protein-mediated (e.g. [28–31]).

HA is a membrane-embedded glycoprotein, formed by three copies of a disulphide-linked HA1/HA2 heterodimer. HA1 mediates receptor binding to cellular sialic acid-containing membranes, while membrane fusion is catalysed by the HA2 subunit, and central to this is the 23-residue N-terminal fusion peptide (HAfp; Fig. 10.3) [32]. The

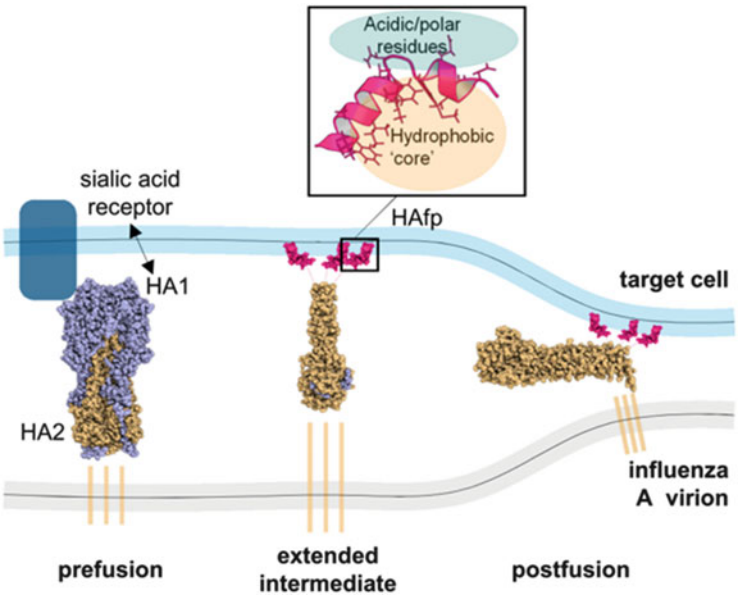

Fig. 10.3 Influenza haemagglutinin-mediated membrane fusion. The current model for membrane fusion mediated by haemagglutinin shown using structures of the fusogen determined in different states (PDB ids 1HGE, 1IBN, 1HTM, and 1QU1). The HA1 subunit first binds to sialic acid receptors on the target cell membrane and, following endocytosis and subsequent local pH drop, undergoes a conformational change during which HA1 is released and HA2 extends to insert the N-terminal fusion peptides (shown in the inset) into the target membrane. Subsequent reorganisation into a post-fusion hairpin brings the two membranes into close proximity to promote their merger. The fusion peptide is believed to help prime the target membrane for fusion, in addition to serving as a membrane anchor to help bring the two bilayers close together. All molecular models were rendered in Pymol [42]

HA2 transmembrane (TM) domain and fusion peptide, as well as conformational changes in the ectodomain, are all required to complete membrane fusion in vivo [33–36]. However, in vitro, HAfp alone is sufficient to induce lysis or vesicle fusion under suitable conditions [37–40]. Most of the computational studies of HA function have accordingly focused on just the fusion peptide, and more specifically on the, somewhat arbitrarily chosen [41], N-terminal 20 residue fragment (HAfp1-20).

It is difficult to characterise the mode of action of HAfp experimentally. The events that take place during fusion are thought to hinge upon the movements of individual lipid molecules [41, 43–46], thus occurring on a spatial scale too small for most time-resolved structural and biophysical techniques to access. Based on the available experimental and structural data, as well as models of protein-free membrane fusion mechanisms, HA-mediated fusion is believed to follow a standard stalk-hemifusion pathway [47–50]. However, as is true of many viral fusogens, despite it being well-established that HAfp plays a central role in the fusion process through its insertion into the target cell membrane, the exact details of how this contributes to the fusion reaction have yet to be elucidated. A number of models have been proposed, ranging from the peptide simply acting as an anchor in the host cell membrane, to it having a more dynamic role in the process, for instance, by increasing local lipid bilayer disorder, inducing positive membrane curvature, and promoting lipid tail extrusion [41, 43, 51, 52]. Experiments have, thus far, been unable to establish a conclusive mechanism.

Computer simulations can be used to model in detail the interactions of peptides and proteins with a lipid bilayer environment, and are therefore ideally suited for problems of this type [53–56]. Indeed, there have been a number of simulation studies directed towards establishing the location, structure, and dynamics of HAfp1-20 in association with lipid bilayers or with detergent micelles as a proxy for the former. It should be noted that the majority of computational studies into HA have focused exclusively on monomeric fragments of HAfp1-20. The interpretation of these studies must be undertaken with some caution as the behaviour of the protein may be different for the full-length, trimeric fusogen.

In the first study of this type, ATMD of HAfp1-20 in a dimyristoylphosphatidylcholine bilayer was carried out for 18 ns simulation time, revealing the peptide to sit in the interfacial region between the lipid headgroups and water, there adopting a kinked structure consistent with NMR data and other experimental secondary structure measurements [57]. Furthermore, and of importance in light of the physiological role of HA2, thinning of the lipid bilayer was seen in the vicinity of the peptide N-terminus, suggestive of functionally relevant membrane destabilisation. Subsequent ATMD simulations in various different lipid bilayers and detergent micelles have examined the impact of HAfp1-20 mutations and bilayer composition on behaviour of the peptide, leading to a model in which the peptide locally perturbs the bilayer lipids, forcing them to adjust to its presence, resulting in bilayer thinning, and induced local positive curvature [43, 51, 58–60]. Importantly, these results demonstrated that HAfp is not merely a hydrophobic membrane anchor, but likely plays a critical role in rendering the target membrane more fusion-competent.

In all of the afore-mentioned studies, there was a general agreement that the wild-type (WT) HAfp stably adopts an inverse-V conformation, as observed in the NMR structures [43, 51, 58–60], whilst non-fusogenic mutants created in silico tended to lose this conformation over the duration of the simulations, with a propensity towards a less distorted (i.e. un-kinked) helical organisation [51, 59, 60]. The inverse-V conformation was also stable in 2 ns-long ATMD of the peptide in dodecylphosphocholine micelles of two different sizes [58], supporting the validity of structures determined by NMR in detergent micelles as models for bilayer-associated HAfp. It could be observed from the simulations that hydrophobic residues around the kink region formed a rudimentary yet stable hydrophobic core (highlighted in Fig. 10.3), not only inserting into the bilayer, but also stabilising the inverse-V shape of the peptide. WT peptides also penetrated deeper into the bilayer core, with a greater angle of insertion relative to the plane of the bilayer (~30°), compared to non-fusogenic mutants [43, 51, 58–60]. This agrees well with experimental data that suggested insertion angles of ~30° for fusogenic HAfp1-20 [60].

The deep insertion of WT HAfp1-20 into the bilayer was associated with local reduction in lipid order, particularly in the *cis* leaflet (i.e. that into which the peptide was inserted), and thinning of the bilayer around the peptide [43, 58, 60]. Lipid order parameters can be analysed in detail from ATMD simulations. For instance, Lagüe and colleagues calculated the tail order parameters for lipids in the same and opposing leaflets as the peptide, and for first-, second-, and greater-neighbouring lipids [58]. Extracting the parameters for individual groups of lipids in this way is generally not possible experimentally, but from the simulations it could be shown that, while order parameters distant from the peptide were similar to those seen in a pure palmitoyloleoylphosphatidylcholine (POPC) bilayer, they were substantially lower for those lipids neighbouring the peptide in the *cis* leaflet, but higher for those neighbours in the *trans* leaflet. Furthermore, the authors could show that this was mostly due to conformational adjustments of the lipids rather than their tilting or overall membrane bending.

It was proposed that tilted insertion (~30° relative to the bilayer normal) may effectively destabilise vicinal lipid tail packing with a concomitant reduction in bilayer thickness [60], and promote lipid tail protrusion. AT and CG simulation studies of protein-free bilayer fusion have suggested that acyl tail dynamics are critical in initiating the reaction, with the limiting step being a splaying of lipid tails between the two membranes [44, 61–64]. It is therefore tempting to speculate that the ability of HAfp1-20 to induce local lipid tail extrusion may have some bearing on its physiological function. Investigating this idea further, Kasson and Larssen used the *Folding@Home* distributed computing network [65] to carry out extensive ATMD simulations of three different HAfp1-20 constructs, including WT, a non-fusogenic mutant, and a partially fusogenic mutant [43]. They performed 200 repeats per construct, with an average of ~200 ns per simulation. Such extensive simulation data allowed energetic parameters for each system to be estimated and relatively rare events of lipid tail protrusion to be examined. By computing the frequency of lipid tail protrusion for each construct, it was shown that this occurs most frequently for WT and least frequently for the non-fusogenic mutant, in line

with what would be expected based on experimental activities of these constructs and the purported role of lipid tail protrusion in fusion.

Given these findings, the authors proceeded to use tail protrusion as a metric for assessing the ability of a peptide to catalyse fusion stalk formation in order to look further into the importance of the inverse-V conformation in catalysing fusion. To do this, two alternative organisations of the peptide, a straight helix or a helical hairpin, were examined in addition to the inverse-V conformation. As these are not the usual stable structures of HAfp1-20, it was necessary to apply artificial restraints to hold the peptide in these conformations. The WT peptide in these different conformations was then simulated using ATMD in a POPC bilayer. It was found that lipid tail protrusions occurred most frequently with the inverse-V conformation, and least so with the straight helix. While this does not address the factors influencing peptide conformation, it does suggest that the kinked arrangement favours lipid protrusion more than the hairpin or straight helix conformations, consistent with earlier MD studies comparing the conformational dynamics of WT and mutant HAfp1-20 [51, 59, 60].

More recently, bias-exchange metadynamics—an enhanced sampling simulation technique—was used to study the behaviour of HAfp1-23 in lipid bilayers. This yielded results suggesting that the most favourable conformation of this longer peptide was the hairpin structure [66]. Whether or not this alternative conformation is a consequence of, e.g. either the additional three residues or more efficient simulation approach has yet to be addressed.

Whilst the ATMD simulations discussed so far have provided important insights into the potential structural features of HAfp1-20 that govern its fusogenic activity, they were unable to examine the process of fusion itself, which takes place over timescales typically inaccessible to ATMD. Although unforced merger of all but the most fusogenic bilayers typically still requires more time than is currently accessible to most CGMD simulations, coarse-graining the system does allow one to access certain events thought to take place within the overall fusion reaction.

Using the Martini CG force field, Risselada and coworkers studied the effect of HAfp1-20 on preformed fusion stalks [67]. In particular, they studied the properties of a pre-assembled stalk structure and the effects of mutant versus WT HAfp1-20 on stalk expansion. The simulations and associated free energy calculations suggested HA-mediated fusion may proceed through the formation of a membrane-spanning peptide bundle in the target membrane, in this way reducing the line-tension for stalk formation. Mutant peptides appeared to be non-fusogenic as a result of their interactions being of a strength outside the fine balance between strong enough to stabilise a bundle, and not so strong as to preclude formation of fusogenic intermediates.

This work did not address the process of stalk formation itself, focusing exclusively on how HAfp1-20 might stabilise an existing stalk and drive its expansion into the hemifusion diaphragm. Fuhrmans and Marrink started to consider this by using CGMD with the Martini force field to investigate the influence of HAfp1-20 on the lipid phase diagram and characterise in near-atomic detail the localisation of the peptide within these phases. To do this, they ran CG simulations in which lipid

molecules were allowed to spontaneously assemble themselves from a random dispersion into more ordered structures under a range of conditions, including different lipid types, hydrations, and temperatures, with or without HAfp1-20 WT, G1V, or W14A [68]. The results suggested that WT, but not the non-fusogenic mutants, could promote fusion by stabilising membrane pores, rather than stalks. Specifically, the WT peptide promoted positive curvature, indicating stabilisation of fusion pores or similar membrane architectures.

These two studies were able, by exploiting the greater timescales accessible to CGMD, to demonstrate the potential ability of HAfp1-20 to stabilise a fusogenic prefusion structure characterised by a large positive curvature [67] or the fusion pore itself so as to drive stalk elongation [68]. These two conclusions are not mutually exclusive, and are in some agreement with ATMD results indicating HAfp1-20 may promote positive membrane curvature, although no fusogenic membrane morphologies could be observed in these cases. This also agrees well with experimental data showing HAfp1-20 to stabilise neutral to weakly positively curved bilayers, corresponding in the fusion reaction to pores and dimples [59, 69, 70]. It is therefore possible that the peptides promote the formation of prefusion structures that can relax through the formation of a stalk over the course of the fusion reaction [67].

Following on from these detailed simulation studies of HAfp1-20, future studies may focus on the behaviour of fusion peptides and loops in the context of the full-length glycoproteins. This will substantially increase in computational cost, but should offer insights into the in vivo activity of these important viral proteins. Along this vein, if one seeks to actually computationally characterise the mechanism of action of fusogens, it will be necessary to develop novel techniques that will be able to effectively model the large-scale global conformational changes that fusogens are believed to undergo during their functional cycles. With structural information on the pre- and post-fusion states available for some fusogens, and several enhanced sampling simulation techniques available, this does not seem to be an entirely intractable problem.

10.4 Capsid Assembly and Disassembly

In order to form infectious virions, viruses must assemble their capsids correctly and spontaneously within the crowded host cell environment. Furthermore, they must do so in such a way so as to either simultaneously capture the viral genome or provide the means for its subsequent encapsidation. Upon entering the cytosol of a new host cell, the capsid must release the genetic material, be it through ejection or disassembly, in order for the replication cycle to continue. It follows that the processes of capsid assembly and genome encapsidation, as well as of genome release, should be potential targets for antiviral agents. Developing capsid-targeted therapeutics, however, requires a molecular-level understanding of these processes. Additionally, if we can dissect how viruses achieve high-fidelity and efficient assembly in vivo, it may help us to exploit these principles for nanofabrication and encapsidation

applications in engineering and medicine. While it has been suggested that capsid assembly is analogous to micellar assembly, this latter tends to yield polydisperse systems, whereas capsid proteins (CPs) tend to form more monodisperse assemblies, which are of considerable interest from a technological perspective [71].

From structural studies, we have a good understanding of the organisation of assembled capsids for many viruses, and the interactions between the CPs comprising them, but it remains difficult to infer from these stable lattices the routes by which they were formed. Experimentally, methods such as light scattering, cryoelectron microscopy (cryoEM), cryoelectron tomography (cryoET), and small-angle X-ray or light scattering may be used to follow the dynamics of capsid assembly in vitro. However, doing so is complicated by the presence of multiple transient and difficult to characterise intermediates along the assembly pathways. Computational methods can be used to help fill in the gaps left by experimental techniques, and to provide detailed information on not only the intermediate structures, but also the energetics of the process.

The self-assembly of viral capsids from their component proteins and nucleic acids was first demonstrated for tobacco mosaic virus (TMV) [72], and has since then been observed for many different viruses. The fact that many viral capsids can self-assemble reversibly in vitro suggests that this process should be amenable to examination using computer simulations; there are only a small number of different molecules that need to be simulated to capture the process, and it may not be essential to model an energetic driving force for the process to take place. Although there is evidence for participation of scaffolding proteins in the assembly of some capsids in vivo, it is not thought that these are absolutely necessary for formation or stability of the capsids in most cases [73]. However, given the timescales over which capsid assembly typically takes place (milliseconds to minutes or longer [74]), it is not possible to use ATMD to examine these processes. Therefore, it is invariably necessary to apply various degrees of coarse-graining to the CPs in order to use MD, BD, or MC simulations to characterise these events (Fig. 10.4). Alternatively, it is possible to use more abstract theoretical approaches, such as modelling the process by rate equations or the growing capsid as an elastic sheet, although such methods do not provide detailed molecular insights. The methodological details underlying simulations of capsid assembly, including both the structure-based and the more theoretical methods, are complex and deeply rooted in mathematics and fundamental biophysical principles. Although a description of these is beyond the scope of this chapter, readers are referred to a comprehensive review for more information on the methods [75].

10.4.1 Nucleic Acid-Free Capsid Assembly

Early work in computational virology focused on investigating the process of capsid self-assembly from the protein components alone, and the effects on this of molecular crowding, changes in capsomere concentration, and temperature. These studies

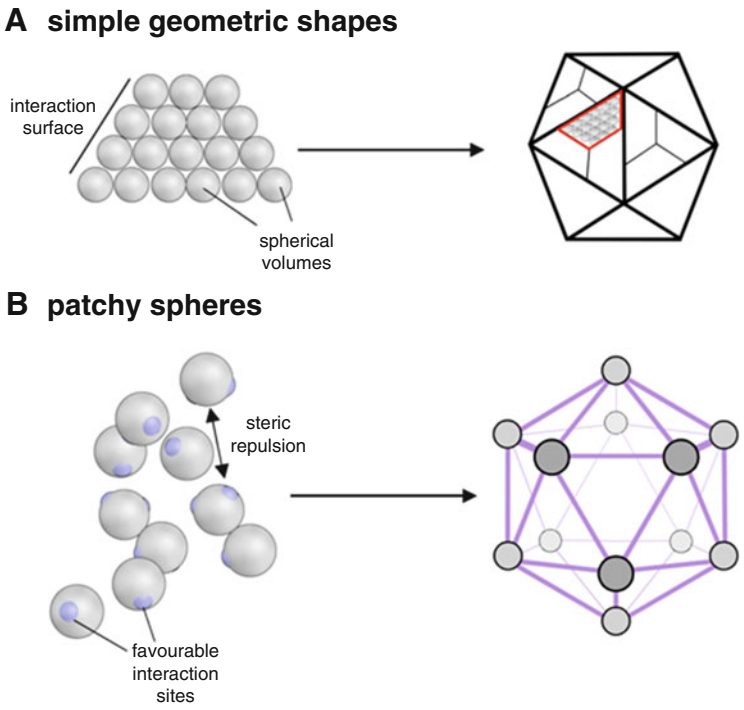

Fig. 10.4 The two common types of model used in capsid self-assembly simulations. (**a**) Capsomeres are represented as simple, rigid geometric shapes designed to assemble into the desired icosahedral structure. Each of these units is composed of an assembly of spherical volumes, with larger spheres to describe the overall shape of the subunit, and smaller spheres present to serve as attractive interaction sites. Overlap of the subunits is prevented through short-range Lennard-Jones repulsions [17, 18, 76]. (**b**) Each capsomere is modelled as a hard sphere adorned with 'sticky' patches, whose spatial arrangement encodes the desired capsid structure, and which effectively incorporate capsid protein shape and interactions [77, 78]

were in part prompted by the detection of noninfectious VLPs (virions with no genetic material) amidst the infectious progeny produced during viral infections. Combined with in vitro demonstration of icosahedral capsid assembly from isolated protein components for some viral species, this observation suggests that capsids can in some cases form and stably persist in the absence of the viral genome [17, 18]. Systems comprising a single protein component are more computationally tractable than those including nucleic acids, and there is clear biological relevance to studying protein-only capsid formation, which is also relevant from a bioengineering perspective, where one may wish to generate nanoparticles without any cargo.

The first studies to model capsid assembly using rate equations [25] and particle-based methods [79, 80] were limited by preconceptions of the assembly pathway and system dynamics. However, they provided preliminary demonstrations of the feasibility of modelling capsid self-assembly in silico. Subsequently, attempts to use MD

to study capsid self-assembly [17, 18] sought to capture the fundamentals of the process using a simple 'toy model' for the capsomeres: a triangle or trapezoid composed of hard spheres. These simulations imposed a number of ad hoc rules to ensure the formation of icosahedral assemblies, but did provide a precedent for an approach that informed much subsequent simulation work in the area, namely that by avoiding peripheral details it should be possible to extract salient features of capsid assembly in a computationally tractable manner. Subsequent simulations of capsid assembly have been carried out using models that are sufficiently realistic to remove the need to impose preconceived notions of the pathway or nonphysical assembly rules. These methods have enabled examination of possible intermediates in capsid self-assembly pathways. Such information is generally not available from experimental studies, but the results can be compared to data from light scattering or cryoEM in order to validate the computational findings. In most cases, a good agreement between the simulation and experiment has been seen.

In these studies, assembly was generally found to proceed according to a nucleation-growth mechanism in which new CPs were added progressively to a growing lattice, and nucleation tended to be the major roadblock to self-assembly [71, 76, 77, 81]. It was also found that dissociation events were as important as associations, and that the strength of interactions between CPs must be intermediate: too strong, and the system risks falling into kinetic traps corresponding to stable aberrant structures not conducive to capsid formation; too weak, and the proteins are unable to nucleate assembly or form a stable final capsid. Running the simulations at different temperatures demonstrated that kinetic trapping was common when the temperature of the system was too low, whilst high temperatures impeded capsid formation by preventing formation of stable substructures [71, 76, 81]. By incorporating the effect of state-activated inter-capsomere interactions into a patchy sphere model in BD simulations, it was shown that temporal variation in intermolecular capsomere interactions may be able to limit kinetic trapping [77]. Hierarchical assembly in which the reactivity of the CPs changes as assembly proceeds was found to outperform direct assembly for intermediate and high interaction strengths, where direct assembly would tend to lead to the system becoming trapped in aberrant intermediates. Extensive sets of simulations using discontinuous MD [76], BD [81], and MC [71] simulations have allowed extensive exploration of parameter space, and construction of phase diagrams for the assembly process, which may be used to identify conditions that favour the formation of off-target structures and dead-end products instead of complete capsids.

To date there has been rather less work looking at in silico assembly of specific viral capsids. Instead, the focus has been on understanding the fundamental features of capsid self-assembly using highly simplified toy models. There have been some attempts to carry out virus-specific analyses using a simulation-based data-fitting procedure [82]. Applying structure-based rule sets and data from light scattering experiments of in vitro self-assembly, it was demonstrated that the capsids of human papilloma virus (HPV), hepatitis B virus (HBV), and cowpea chlorotic mottle virus (CCMV) assemble according to distinguishable routes, suggesting that the mechanisms of capsid assembly may not fall into a shared pattern for all viruses. As

subsequently discussed, considerable computational effort has also been directed towards studying the assembly of pleomorphic retroviral, specifically HIV-1, capsids, which pose a multitude of additional challenges to molecular simulation.

10.4.2 Simulations of HIV-1 Capsid Assembly

The capsid assembly studies discussed thus far focused on extracting fundamental principles governing the spontaneous self-assembly of regular icosahedral structures. The highly simplified models did not seek to mimic any specific viruses, instead providing results of general relevance to the many viral families whose capsids conform to this symmetric architecture. However, some viruses, most notably the retroviruses, possess pleomorphic capsids that cannot be modelled according to the simple schemes employed in these studies.

The HIV-1 capsid has been subject to extensive investigation. During maturation to the infectious form, this enveloped retrovirus undergoes several morphological changes, including the cleavage of Gag polypeptide to release the capsid protein, CA. This can then self-assemble into the viral capsid, which is believed to adopt a fullerene cone arrangement constructed from CA hexamers and irregularly positioned pentamers. In vitro, however, the CA can spontaneously form a variety of morphologies, including cones, tubes, and planar sheets, all based on the same hexamer and pentamer units. High-resolution structural studies of CA have revealed the intermolecular interactions involved in hexamer and pentamer formation, but provided little information regarding the basis for forming such diverse lattice morphologies. Many computational studies have been carried out in the hopes of elucidating more details of this process. Collectively they provide an excellent illustration of the inevitable payoff in molecular simulations between accuracy and accessible length/timescales.

In a study addressing the role of protein–protein interactions in governing capsid morphology, a CG model of CA based on ATMD simulations was constructed and used as a basis for simulations of the capsid. This work demonstrated the importance of including molecular details in models for CA [83], as it showed that accurately representing the CA geometry is important for yielding results comparable to experiment. Following this, a number of simulations sought to use models that recapitulated the shape and interactions of CA. For example, using MC [84] and MD [85] methods, the assembly of CG models of CA dimers on 2D or quasi-2D surfaces was carried out. However, although the models were designed to capture the structure of CA or its dimers, they were ultimately rigid and therefore could not capture the NTD/CTD flexibility thought to be important in lattice assembly. To address this limitation, an ensemble of static structures in different conformations (identified using MD simulations) was used in MC simulations to examine 3D capsid assembly [86]. This more detailed CG model was limited to assembling into lattices of sizes about 20–40% of the complete HIV-1 capsid, demonstrating the computational cost of extending to more complex models. However, despite this

limitation, it was possible to show that hexameric lattices are the most favourable assembly products, forming a range of morphologies via a common assembly pathway involving a trimer-of-dimers intermediate as the dominant scaffold for lattice growth.

More recently, Voth and coworkers used CG simulations with a flexible CA model to investigate self-assembly under various conditions intended to recapitulate specific events in the viral replication cycle [23]. Lattice assembly was found to occur in a reversible, multistage manner, in which a trimer-of-dimers serves as a nucleus to seed lattice growth. The trimer-of-dimers building block was consistent with previous simulation results [84–86], obtained using different methods. This study demonstrated that, rather than the trimers assembling into the lattice, it is addition of CA dimers onto the trimer-of-dimer templates that serves as the means for lattice assembly.

Lattice growth could also be shown to be influenced by the CA concentration, local molecular crowding, and the CA conformational equilibria. For example, as seen for icosahedral capsid assembly, high levels of molecular crowding could effectively change the kinetics of assembly from being nucleation-limited to non-nucleation-limited [87]. As for the previous studies, however, the increased complexity of the CA model used meant that it was only possible to observe the nucleation and initial steps of capsid assembly.

At the other end of the resolution spectrum, both Hicks and Henley [88] and Levandosky and Zandi [89] simulated the nonequilibrium growth of elastic sheets, using a model in which, once a pentamer or hexamer was added to the growing sheet, its polymeric nature became fixed, thereby effectively reducing the number of degrees of freedom in the assembly pathway. In the latter study, CA was represented using a tapered triangular prism constructed from three layers of beads. The tapered structure caused the growing sheets to curve, and the accumulation of stress as they extended led to a need for pentameric units to relieve stress. As the curved sheets grew, the edges curled towards each other and eventually connected, before the top and bottom finally sealed to yield a conical morphology similar to that observed in experiments. Subsequent simulations of the nonequilibrium growth of elastic sheets revealed the formation of various unclosed structures, including rolls and curved sheets, as well as conical assemblies with unsealed holes at the tips, and seams along the length [90]. These various arrangements were subsequently observed in high-resolution cryoET data from intact viruses and purified cores, providing support for use of this elastic sheet model for HIV-1 capsid assembly. In line with the results from Levandosky and Zandi, these results suggest that capsid assembly involves the progressive growth of a curling sheet, which eventually meets at the edges.

At present, it is intractable to attempt to simulate the complete, reversible assembly of an HIV-1 capsid from flexible, high-resolution components, even using CG models. However, when supra-CG, nonequilibrium approaches are considered alongside those higher resolution, smaller scale studies, and both compared with experimental results, it should be possible to obtain a wealth of useful information about the dynamics of retroviral capsids during the viral replication cycle.

On discussing the role of computational methods in studying the HIV-1 capsid, it is worth noting the pivotal role played by MD in determining a high-resolution structure of the complete HIV-1 capsid [91]. MDFF, a flexible fitting method that effectively uses MD to relax high-resolution molecular structures as they are placed within low resolution electron density maps, was used to dock CA into density from cryoEM to create an atomic-resolution model for the capsid. This assembly was simulated for 100 ns equilibration, and remained stable over this time. However, the system is considerably large, and its stability over longer timescales could not be examined. During the equilibration phase, it is notable that a hydrophobic patch at the CA C-terminal domain pseudo three-fold axis was identified. This was suggested, and subsequently confirmed by mutagenesis, to be important in capsid assembly and viral infectivity.

10.5 Genome Encapsidation

For successful production of progeny virions, the viral genome must be packaged reliably and efficiently within the capsid shell. For small RNA viruses, this is believed to occur in concert with capsid assembly, and it may be that the genetic material is required during this process to act as 'electrostatic glue' [18]. In contrast, the double-stranded genomes of many DNA viruses cannot be packaged in this way owing to the high charge density and persistence length of dsDNA. In these cases, the capsid is first assembled as a stable entity, and the genome subsequently inserted through action of an ATP-dependent molecular motor [92, 93]. As with capsid assembly, a number of simulation models have been developed to investigate possible mechanisms of genome encapsidation. In addition to providing insights into viral assembly, simulations of this type can be used to predict the conformations of nucleic acids within viral capsids.

10.5.1 Capsid Assembly Around Cargo

Simulation methods to study self-assembly of capsids around nucleic acids are similar to those discussed previously for protein-only assembly, but include a model of the cargo being packaged. This may be treated as a (semi-)flexible polymer of particles, or more simply as an appropriately charged spherical volume.

Capsid assembly around nucleic acids is thought to be driven primarily by electrostatic interactions between nucleic acid phosphate groups and basic amino acid residues, often located in flexible tails termed arginine-rich motifs (ARMs). The net charge of these protein motifs has been correlated with genome length for many RNA viruses [94–97], typically with a ratio of nucleic acid negative charge to protein positive charge of ~2:1, leading to the idea that viruses are 'overcharged' such that the negative charge of the encapsidated nucleic acid exceeds the positive

charge of the capsid interior. A combination of BD simulations and continuum models have suggested that overcharging arises because only a fraction of the nucleic acid charges can reside within the electrostatic screening distance of the ARM charges, and that intramolecular RNA base-pairing increases overcharging [98]. Results from BD simulations modelling the assembly of pentagonal subunits on polyelectrolytes representing RNA suggested that this overcharging may arise as a consequence of geometry and electrostatic screening [99]. The latter limits the number of direct interactions that can exist between the CPs and RNA, leaving segments of nucleic acid that are not themselves screened by positive charges and form bridges to interconnect the positively charged regions. It is these bridges that were suggested to be the main origin of the overcharging.

It has been shown in vitro that, whilst CPs may be able to form a specific empty capsid structure with high fidelity [100–102], when assembling around cargo capsid morphology can be much more variable and may adapt to match the size of the encapsidated species [17, 103]. Understanding how such adaptability is achieved is particularly important for engineering vehicles for delivering drugs, imaging agents or other substances, and for controlling the sizes and morphologies of nanomaterials. Such capsid adaptability has been observed in both MD [104] and BD [99] simulations, assembling capsids from hard spheres or pentagonal assemblies thereof, respectively, around different anionic simplifications of the nucleic acid cargo. In both cases, it was apparent that the morphology of the assembled capsids varied depending on the size of the cargo [99, 104]. It was found that adaptive cargo encapsidation requires the interactions between cargo and capsid subunits to be of intermediate strength. Too strong and stable intermediates will form with curvatures unconducive to capsid assembly, whilst weaker interactions do not form stable lattices at all. Capsids formed most readily around cargo within a certain length range, outside of which the structures were malformed [99], suggesting that viral genomes might have co-evolved to optimally promote packaging into their cognate capsids (Fig. 10.5).

These studies did not address the in vivo high selectivity of viral genome packaging, which has been suggested may arise in part from interactions between the CPs and specific sequences within the RNA, termed packaging signals [99]. This has been investigated using a mathematical model of the assembly of pentagonal building blocks onto a hypothetical RNA molecule endowed with packaging signals that served as nucleation sites for interactions between individual CPs [105]. Depending on the nature of the packaging signals, a close correlation between assembly efficiency and packaging specificity could be demonstrated.

10.5.2 Genome Loading into Capsids

The use of ATP-dependent pumps to load the genome into the capsids of dsDNA viruses has been captured in novel simulation studies of the type illustrated in Fig. 10.6. Using this approach, it was shown that the structure of the DNA duplex

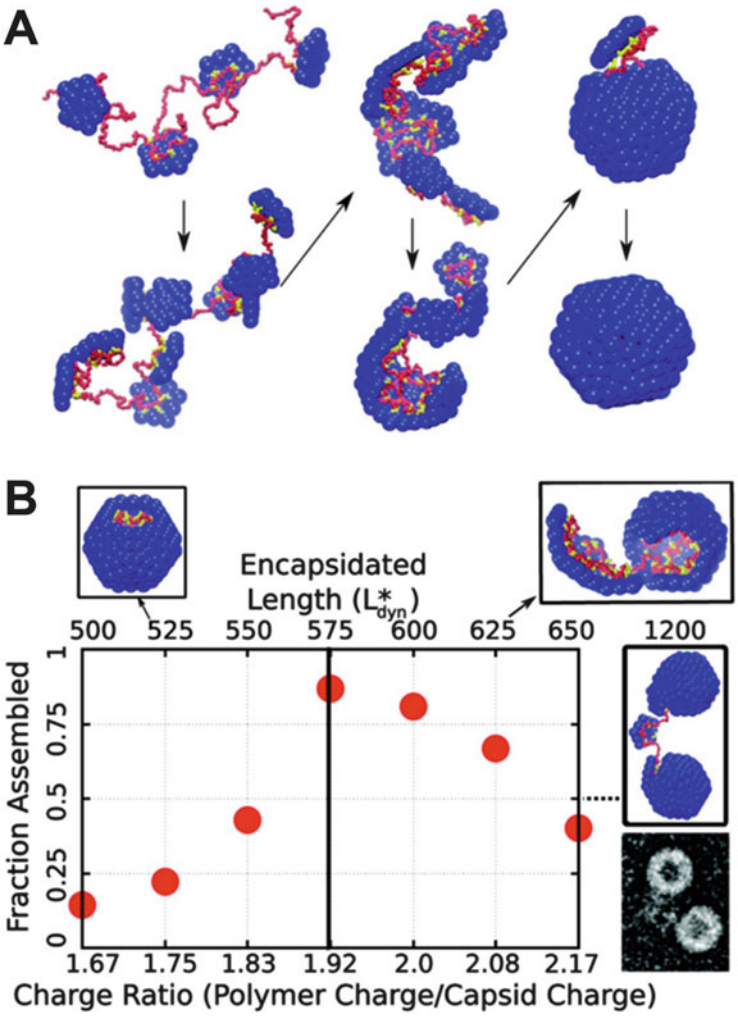

Fig. 10.5 Capsid assembly around a linear polyelectrolyte simulated at physiological salt concentration. (**a**) Representative snapshots taken along a BD simulation trajectory to illustrate the time course of assembly around a polyelectrolyte. (**b**) The fraction of trajectories culminating in assembly of a complete capsid is plotted as a function of polymer length (top axis) or charge ratio (bottom axis). Capsid assembly was optimal for a charge ratio (polymer to capsid) of ~1.9. Above this, the polymer tended not to be fully packaged (right-hand inset), whilst below this the polymer become encapsidated before the capsid forms a closed shell (left-hand inset). Reproduced from [99]

inside the capsid is determined by the size, shape, and core structures of the encasing protein shell, as well as the electrostatic properties of the capsid proteins and the local ionic strength. For example, spherical and icosahedral capsids without large core structures tended to favour a concentric spools model [106] whereas those with

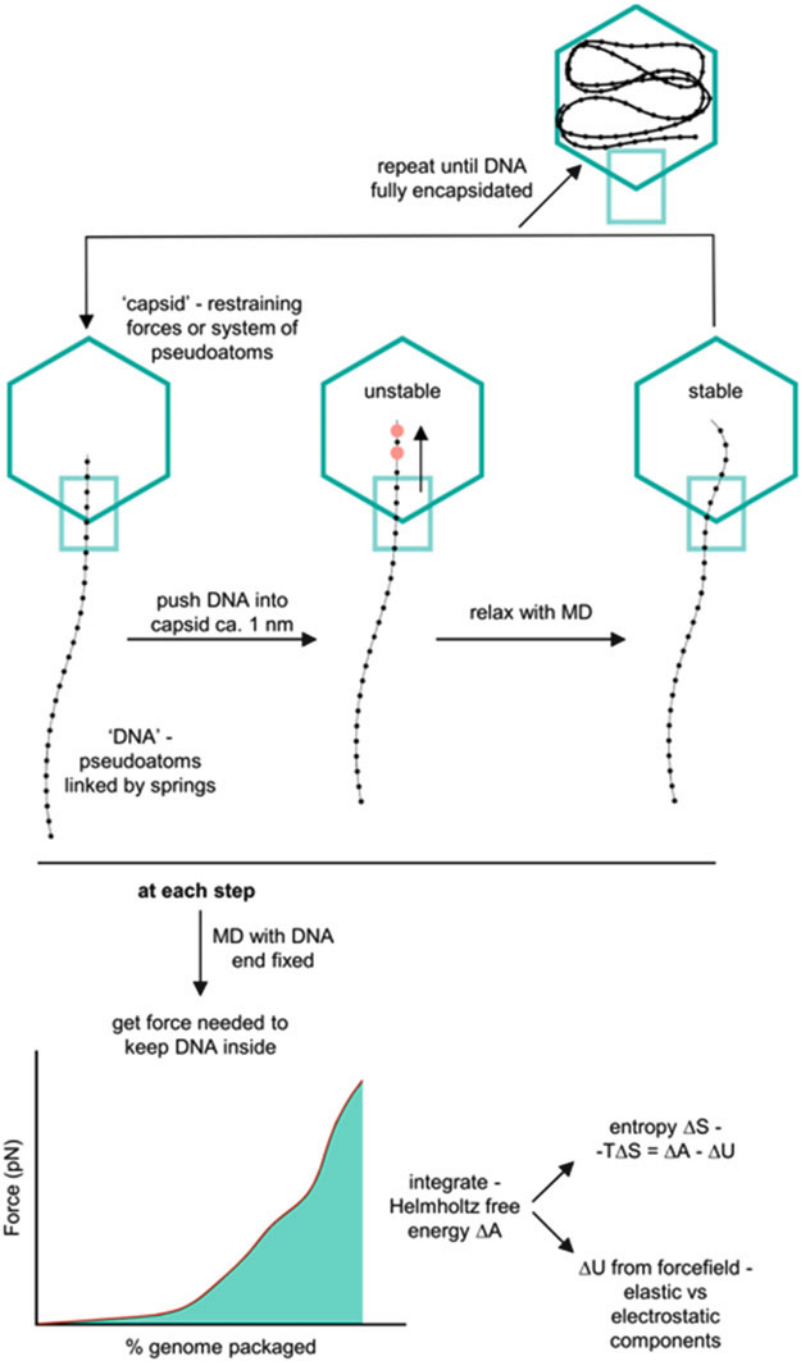

Fig. 10.6 Method for simulating DNA loading into capsids. DNA is represented as a series of pseudoatoms (one per ~6 base pairs) connected by springs designed to capture the flexibility of duplex DNA. The capsid is modelled as a simple repulsive potential that prevents the DNA from

large core structures favoured a coaxial spool model [107–110] for DNA organisation within phage particles. The ultimate structure of the packaged DNA was determined by a combination of capsid shape and elastic properties of the polymer, and within these constraints multiple individual conformations were found, which would be expected to be averaged out by static structural techniques.

Beyond such structural information, simulations of this type can also be used to estimate the force required to package dsDNA inside capsids, and to extract the energetic features of this process. For example, exploiting the availability of experimental data for the forces associated with DNA loading [112], Petrov and Harvey simulated the injection of dsDNA into bacteriophage ϕ29 [113]. Injecting the 19,272 bp genome into an elongated capsid is driven in vivo by an ATP-dependent motor situated at the bottom vertex of the capsid. Because the ϕ29 capsid is not believed to extend on genome packaging and maturation, it can be assumed that the capsid undergoes negligible extension over the course of the simulations. Critically, this method also assumes that packaging proceeds slowly enough for the DNA conformation to be more-or-less at equilibrium throughout the process. MD was chosen over BD or MC in this case because it is more efficient at equilibrating successive structures along the packaging trajectory. Using this method, it was found that the force required for insertion was almost zero until about half the DNA was packaged, and then increased to ~55 pN at 100% of packaged DNA, a force-distance behaviour in good agreement with single-molecule experimental results [110, 114, 115]. Importantly, the model used was not parameterised using data from experiments on viruses, aside from the capsid dimensions. This agreement with experimental data therefore provided post hoc evidence in support of the model parameters and simulation protocol. Overall, this study provides a good illustration of the capabilities of simulation methods to provide more than just qualitative information on time-dependent molecular structures.

10.6 Entire Virion Simulations

Over approximately four decades since the first atomic-resolution structure of a viral capsid was solved [116], there have been a number of simulations of complete viral capsids of nonenveloped virions. Concurrently, the development of computational

Fig. 10.6 (continued) crossing out of the region of the capsid or more explicitly using hard spheres in an appropriate geometry. At each step, the DNA is pushed into the capsid and then an MD simulation is run to allow the system to relax before the next packaging step takes place. In parallel, for each step MD simulations may be run with one end of the DNA fixed within the capsid, and the force required to maintain this state computed. By integrating the force as a function of percentage of the genome inserted over the course of the loading process, the free energy can be calculated, allowing the entropic contribution to DNA loading to be computed using the enthalpy directly available from the simulation force field [111]

virology has largely been facilitated by a number of technological and methodological advances in simulation hardware and tools, including increased computer power, improved simulation algorithms, development of CG and multiscale simulation approaches, and the emergence of novel methodologies for integrating diverse lines of experimental data into theoretical models [117]. However, even with these advances, simulation of complete virions represents a considerable computational challenge. Indeed, a desire to simulate entire virions has been cited as a key factor driving the implementation of GPUs in computer simulations [118]. More-or-less complete, high-resolution structures are now available for a number of viruses. Although these may lack data for part of the genome and for surface glycans, they serve as a starting point for simulations that can be used to 'breath life' into these static structures.

10.6.1 Nonenveloped Viruses

The first ATMD simulation of a complete virus particle was of satellite tobacco mosaic virus (STMV) with and without an RNA core [119]. This study revealed that, consistent with the apparent importance of RNA in capsid assembly, the capsid was much more stable in the presence of RNA. This was true even though the RNA used had an artificial sequence unrelated to the native STMV genome. This work was subsequently extended to include the native genomic sequence of STMV [120] providing the first all-atom model for the complete structure of a virus using its true genomic sequence. Consistent with the results from STMV, experiments have shown that cleavage of the Brome mosaic virus (BMV) CP N-terminal tails, thought to penetrate into the RNA core, is required for capsid disassembly, and after a 5 μs CGMD simulation of the BMV capsid with these tails removed, the capsid did indeed collapse [121].

However, in contrast to the above results, ATMD simulations of southern bean mosaic virus (SBMV) found it to be relatively stable during simulations of 10–20 ns even without a genome present [122]. Furthermore, in a series of long (1–25 μs) CGMD simulations of a range of highly simplified (~200:1 mapping) viral capsids [121], the capsids of three plant viruses, STMV, satellite panicum mosaic virus (SPMV), and STNV collapsed during simulations in the absence of a model for the genomic RNA, whereas the capsids of BMV, bacteriophage φX174, reovirus, and poliovirus were all stable in the absence of genetic material (Fig. 10.7). These results suggest that the genome is not the only factor influencing capsid stability. For instance, many nonenveloped viruses have been found to possess Ca^{2+}-binding sites at their icosahedral symmetry axes. Simulations of SBMV reveal changes in capsid nanomechanical properties upon calcium removal which may lead to opening of exit ports for RNA release [122]. A series of ATMD simulations of (at the time) previously unprecedented length (1 μs) were carried out for the plant virus STNV, revealing that without Ca^{2+}, the capsid transformed from a closed to open conformation, the lattice swelling due to increased water permeability [123].

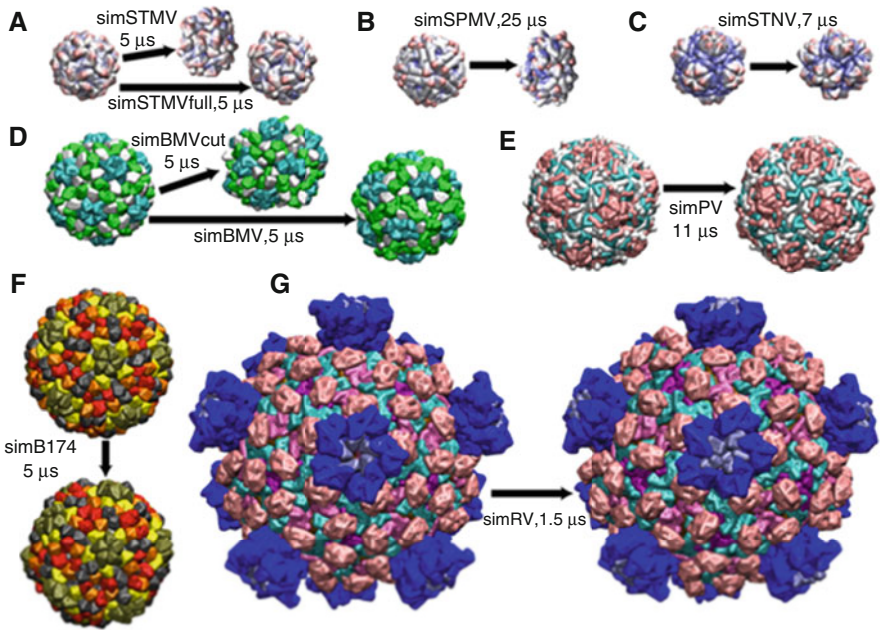

Fig. 10.7 Microsecond simulations of nonenveloped viruses. Initial and final structures from microsecond-timescale CG-MD simulations of the capsids from several nonenveloped viruses. (**a**) STMV. The capsid collapses in the absence of RNA (simSTMV), but is stable when the nucleic acid is included (simSTMVfull). (**b**, **c**) SPMV and STNV. Both capsids collapse within the simulation time. (**d**) BMV. Although the capsid was highly flexible and stable in simBMV, removing the N-terminal tails of the capsid proteins (simBMVcut) caused the capsid to collapse. (**e**–**g**) Poliovirus capsid, bacteriophage ϕX174 procapsid, and reovirus core. All were stable throughout the simulations. Reproduced from [121]

10.6.2 Enveloped Viruses

Enveloped viruses present a greater computational challenge. Not only is there a substantial increase in system size on addition of a bounding lipid bilayer, but the presence of this, envelope glycoproteins, and a matrix, in addition to the genome and capsid, adds several layers of complexity in terms of both initial model construction and subsequent simulations. It therefore becomes necessary to use CG representations and innovative approaches to both construct the virion models and subsequently simulate and analyse them (Fig. 10.8).

10.6.2.1 Influenza A Virus

The first microsecond-timescale simulation of a viral envelope [24] used the Martini CG force field to simulate a model of the influenza A virus envelope, providing insight into the influence of bilayer components and temperature on the stability of

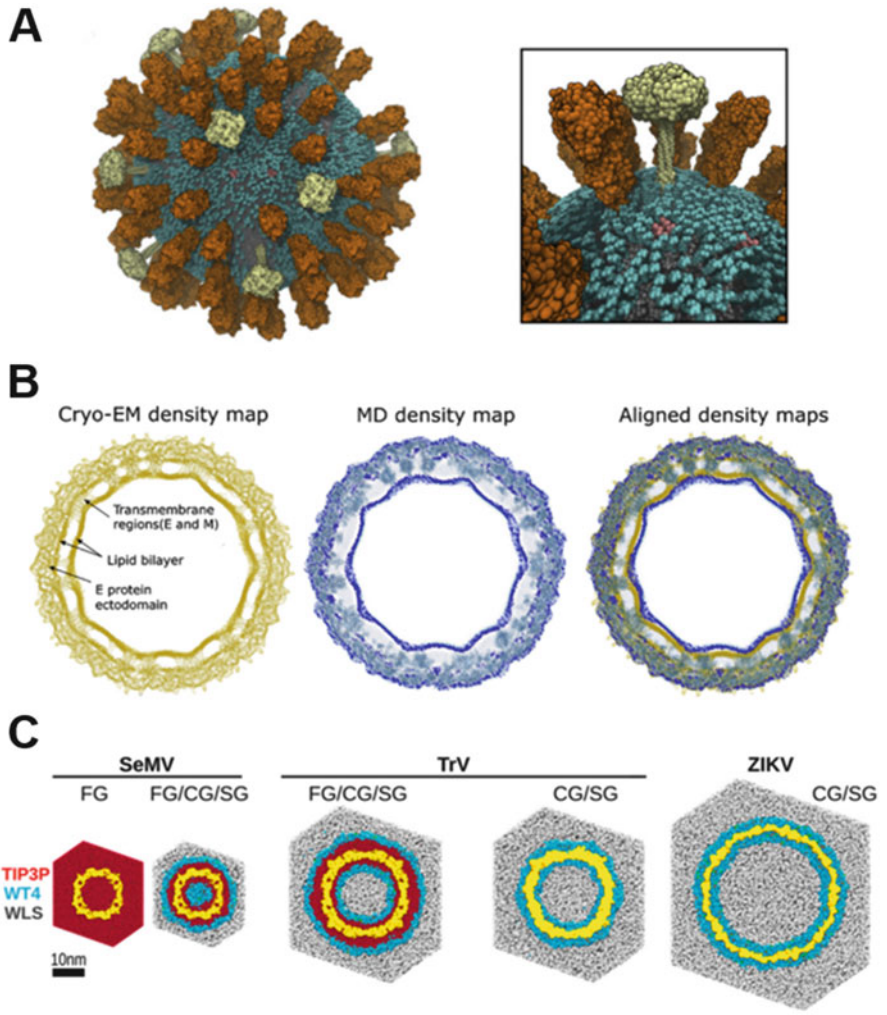

Fig. 10.8 Enveloped virus simulations. (**a**) Coarse-grained model of the influenza A virion shown in full and zoomed in, with the envelope proteins HA (orange), NA (white), and M2 (pink) embedded in the lipid vesicle (glycolipid in cyan; other lipids in grey). (**b**) The dengue virus envelope showing the alignment of experimental cryoEM maps with simulated averages of the envelope, illustrating the agreement between simulation and experiment. (**c**) Three VLPs simulated using hybrid methods. In each case, the VLP is shown as a yellow surface and the solvent particles as spheres (FG, fine-grained, i.e. atomistic). (**a**–**c**) reproduced from [24, 124], and [125], respectively

this medically important virus. By integrating data from X-ray crystallography, NMR spectroscopy, cryoEM, and lipidomics, the authors assembled a model for the viral envelope with inserted spike glycoproteins—HA and neuraminidase (NA)—and the M2 proton channel. Although there was no M1 protein matrix included, the presence of the ribonucleoprotein (RNP) core was treated using a

shell of position-restrained particles, and the influence of the matrix was modelled by applying position restraints to the centroids of the envelope proteins. Simulations were carried out at 295 K or 323 K, with or without glycolipid replacing two thirds of the sphingomyelin in the envelope, and with or without the proteins restrained (i.e. with or without the M1 matrix considered). From these simulations, it could be seen that the glycolipid covered the virion surface (Fig. 10.8a), and largely masked the M2 proton channel from the external surface, which could have implications for drugs such as adamantanes targeted against M2. In addition to affecting the volume of the virion surface accessible from the outside, the presence of glycolipid (and lower temperature) also appeared to reduce mobility of envelope components. Reduced mobility of envelope components is expected to increase physical robustness of the virion, which could contribute to the known stability of the virus under different environmental conditions [126, 127].

In addition to influencing translational dynamics, the glycolipid appeared to reduce clustering of the NA and HA spike glycoproteins, maintaining their roughly even surface distribution at a spacing that was suggested to be conducive to binding of bivalent IgGs, as well as the broadly neutralising antibody FI6 targeted against the HA stem. Not only are the observed spacings compatible with antibody binding, but they would also facilitate polyvalent interactions between HA and/or NA and host sialic acid residues, as would be required for strong virus–host interaction in spite of relatively weak affinity between HA and host receptors detected in vitro, and be important in progeny virion release.

10.6.2.2 Dengue Virus

The membrane envelope of the dengue virus (DENV) has also been simulated in two independent studies, again using the Martini CG force field. In the first study a combination of CG modelling and simulation was used to ‘add back’ the lipid bilayer to the cryoEM structure of the dengue virus envelope proteins [128]. This allowed estimation of the diffusive properties of lipids within the outer envelope of the DENV virion. The dense crowding of protein TM domains and the enclosure of the outer leaflet of the lipid bilayer within a protein shell resulted in lipid diffusive properties similar to those in the ‘raft-like’ influenza A virion membrane.

In a subsequent multiscale modelling study of the DENV envelope [124], a CG model of the DENV-2 envelope was constructed and validated through comparison with cryoEM maps. This model was used to explore the roles of protein domains and protein–lipid interactions in the envelope organisation and stability. There was good agreement between the cryoEM maps and the MD simulations (Fig. 10.8b). The MD simulations reproduced bilayer curvature and distortions around TM helices of the proteins observed in both leaflets from cryoEM. By changing the envelope lipid composition, it was further demonstrated that the proteins make numerous contacts with anionic lipids (phosphatidylserine) in the system, and that these interactions help to stabilise the viral particles. On this basis it was suggested that changes in the electrostatic environment during the viral life cycle would alter protein–lipid

interactions. For instance, histidine residues found to interact with lipid headgroups may become protonated in the endosome and phosphatidylserine headgroup carboxylates may also change ionisation state as the local pH falls, in both cases potentially leading to rearrangements in the envelope complex to promote fusion.

10.6.3 Hybrid Multiscale MD of Three Viruses

In the simulations discussed so far, the model resolution is invariant throughout the simulation, and so multiscale simulations require 'back-mapping' from CG to AT resolution models [129, 130]. However, it is in principle possible to combine multiple resolutions within the same simulation. Thus, a recent study used a hybrid multiscale approach with the SIRAH force field [131, 132] to study three different VLPs: the sesbania mosaic virus (SeMV) and tobacco rattle virus (TrV) capsids, and the envelope of zika virus (ZIKV) [125]. In this approach, parts of the system of particular interest were modelled using AT and/or CG resolution, and then those of less direct interest used instead a supra-CG (SG) resolution (Fig. 10.8c). The results from the ZIKV simulations were in good agreement not only with experimental data, but also with CG simulations of other flaviviruses, providing support for the general applicability of this method. This hybrid multiscale approach allows much more efficient simulation of biomolecular systems that include large amounts of bulk solvent, as is the case for virions and VLPs, enabling simulations to be run on modest computational resources and thereby rendering computational virology accessible to a wide range of researchers without access to supercomputing facilities.

10.7 Conclusion

The studies discussed in this chapter illustrate several roles for simulation methods in virology. As demonstrated by, e.g. the study of the influenza A virus model, simulations can effectively integrate data from multiple experimental sources to provide coherent and dynamic models. Such models can be used to explore scenarios which are difficult or impossible to address experimentally, as in the manipulation of lipid bilayer composition and protein structure to study the possible roles of protein–lipid interactions in the DENV envelope. Similarly, detailed examination of the conformations of individual lipids, important in understanding viral fusogen function, remains experimentally challenging, whilst being directly available via molecular simulations. Simulations can also unmask experimental averages, for instance, enabling the identification of intermediates observed in capsid self-assembly experiments or individual structures underlying the images seen using cryoET and cryoEM. Furthermore, simulations can offer insight into the energetics of biological events, as shown for, e.g. dsDNA loading into capsids. Finally, by simultaneously combining models at different resolutions to focus available computing power on specific components of

interest, it is in theory possible to use simulations to study viruses with relatively modest computing capacity, making computationally virology a potentially field-ready method.

Acknowledgements Work in M.S.P.S.'s group is supported by grants from BBSRC, EPSRC, the Leverhulme Trust, and Wellcome; EEJ is supported by Wellcome.

References

1. Hulo C, de Castro E, Masson P, Bougueleret L, Bairoch A, Xenarios I, Le Mercier P (2011) ViralZone: a knowledge resource to understand virus diversity. Nucleic Acids Res 39:D576–D582. https://doi.org/10.1093/nar/gkq901
2. Plummer EM, Manchester M (2011) Viral nanoparticles and virus-like particles: platforms for contemporary vaccine design. Wiley Interdiscip Rev Nanomed Nanobiotechnol 3(2):174–196. https://doi.org/10.1002/wnan.119
3. Yildiz I, Shukla S, Steinmetz NF (2011) Applications of viral nanoparticles in medicine. Curr Opin Biotechnol 22(6):901–908. https://doi.org/10.1016/j.copbio.2011.04.020
4. Cattaneo R, Russell SJ (2017) How to develop viruses into anticancer weapons. PLoS Pathog 13(3):e1006190. https://doi.org/10.1371/journal.ppat.1006190
5. Schmid M, Ernst P, Honegger A, Suomalainen M, Zimmermann M, Braun L, Stauffer S, Thom C, Dreier B, Eibauer M, Kipar A, Vogel V, Greber UF, Medalia O, Plückthun A (2018) Adenoviral vector with shield and adapter increases tumor specificity and escapes liver and immune control. Nat Commun 9:450. https://doi.org/10.1038/s41467-017-02707-6
6. Fischlechner M, Donath E (2007) Viruses as building blocks for materials and devices. Angew Chem Int Ed 46(18):3184–3193. https://doi.org/10.1002/anie.200603445
7. Butterfield GL, Lajoie MJ, Gustafson HH, Sellers DL, Nattermann U, Ellis D, Bale JB, Ke S, Lenz GH, Yehdego A, Ravichandran R, Pun SH, King NP, Baker D (2017) Evolution of a designed protein assembly encapsulating its own RNA genome. Nature 552:415–420. https://doi.org/10.1038/nature25157
8. Reddy T, Sansom MSP (2016a) Computational virology: from the inside out. BBA-Biomembranes 1858:1610–1618
9. Mohammadi P, Desfarges S, Bartha I, Joos B, Zangger N, Munoz M, Gunthard HF, Beerenwinkel N, Telenti A, Ciuffi A (2013) 24 hours in the life of HIV-1 in a T cell line. PLoS Pathog 9(1):e1003161. https://doi.org/10.1371/journal.ppat.1003161
10. Beerenwinkel N, Montazeri H, Schuhmacher H, Knupfer P, von Wyl V, Furrer H, Battegay M, Hirschel B, Cavassini M, Vernazza P, Bernasconi E, Yerly S, Boni J, Klimkait T, Cellerai C, Gunthard HF, Swiss HIVCS (2013) The individualized genetic barrier predicts treatment response in a large cohort of HIV-1 infected patients. PLoS Comput Biol 9(8):e1003203. https://doi.org/10.1371/journal.pcbi.1003203
11. Sharma D, Priyadarshini P, Vrati S (2015) Unraveling the web of viroinformatics: computational tools and databases in virus research. J Virol 89(3):1489–1501. https://doi.org/10.1128/jvi.02027-14
12. Leelananda SP, Lindert S (2016) Computational methods in drug discovery. Beilstein J Org Chem 12:2694–2718. https://doi.org/10.3762/bjoc.12.267
13. Mortier J, Rakers C, Bermudez M, Murgueitio MS, Riniker S, Wolber G (2015) The impact of molecular dynamics on drug design: applications for the characterization of ligand-macromolecule complexes. Drug Discov Today 20(6):686–702. https://doi.org/10.1016/j.drudis.2015.01.003
14. Allen MP, Tildesley DJ (2017) Computer simulation of liquids, 2nd edn. Oxford University Press, Oxford

15. Marrink SJ, Tieleman DP (2013) Perspective on the Martini model. Chem Soc Rev 42 (16):6801–6822. https://doi.org/10.1039/c3cs60093a
16. Marrink SJ, Risselada J, Yefimov S, Tieleman DP, de Vries AH (2007) The MARTINI force field: coarse grained model for biomolecular simulations. J Phys Chem B 111:7812–7824
17. Rapaport DC (2004) Self-assembly of polyhedral shells: a molecular dynamics study. Phys Rev E 70(5):051905. https://doi.org/10.1103/PhysRevE.70.051905
18. Rapaport DC, Johnson JE, Skolnick J (1999) Supramolecular self-assembly: molecular dynamics modeling of polyhedral shell formation. Comput Phys Commun 121:231–235. https://doi.org/10.1016/s0010-4655(99)00319-7
19. Laio A, Parrinello M (2002) Escaping free-energy minima. Proc Natl Acad Sci U S A 99 (20):12562–12566. https://doi.org/10.1073/pnas.202427399
20. Hamelberg D, Mongan J, McCammon JA (2004) Accelerated molecular dynamics: a promising and efficient simulation method for biomolecules. J Chem Phys 120(24):11919–11929. https://doi.org/10.1063/1.1755656
21. Darve E, Pohorille A (2001) Calculating free energies using average force. J Chem Phys 115 (20):9169–9183. https://doi.org/10.1063/1.1410978
22. Huang Q, Chen C-L, Herrmann A (2004) Bilayer conformation of fusion peptide of influenza virus hemagglutinin: a molecular dynamics simulation study. Biophys J 87(1):14–22. https://doi.org/10.1529/biophysj.103.024562
23. Grime JMA, Dama JF, Ganser-Pornillos BK, Woodward CL, Jensen GJ, Yeager M, Voth GA (2016) Coarse-grained simulation reveals key features of HIV-1 capsid self-assembly. Nat Commun 7:11568. https://doi.org/10.1038/ncomms11568
24. Reddy T, Shorthouse D, Parton DL, Jefferys E, Fowler PW, Chavent M, Baaden M, Sansom MS (2015) Nothing to sneeze at: a dynamic and integrative computational model of an influenza A virion. Structure 23(3):584–597. https://doi.org/10.1016/j.str.2014.12.019
25. Zlotnick A (1994) To build a virus capsid – an equilibrium-model of the self-assembly of polyhedral protein complexes. J Mol Biol 241(1):59–67. https://doi.org/10.1006/jmbi.1994.1473
26. Nguyen TT, Bruinsma RF, Gelbart WM (2006) Continuum theory of retroviral capsids. Phys Rev Lett 96(7):078102. https://doi.org/10.1103/PhysRevLett.96.078102
27. Harrison SC (2015) Viral membrane fusion. Virology 479:498–507. https://doi.org/10.1016/j.virol.2015.03.043
28. Issa ZK, Manke CW, Jena BP, Potoff JJ (2010) Ca^{2+} bridging of apposed phospholipid bilayers. J Phys Chem B 114(41):13249–13254. https://doi.org/10.1021/jp105781z
29. Knecht V, Marrink SJ (2007) Molecular dynamics simulations of lipid vesicle fusion in atomic detail. Biophys J 92(12):4254–4261. https://doi.org/10.1529/biophysj.106.103572
30. Risselada HJ, Grubmuller H (2012) How SNARE molecules mediate membrane fusion: recent insights from molecular simulations. Curr Opin Struct Biol 22(2):187–196. https://doi.org/10.1016/j.sbi.2012.01.007
31. Risselada HJ, Bubnis G, Grubmuller H (2014) Expansion of the fusion stalk and its implication for biological membrane fusion. Proc Natl Acad Sci U S A 111(30):11043–11048. https://doi.org/10.1073/pnas.1323221111
32. Calder LJ, Rosenthal PB (2016) Cryomicroscopy provides structural snapshots of influenza virus membrane fusion. Nat Struct Mol Biol 23(9):853–858. https://doi.org/10.1038/nsmb.3271
33. Armstrong RT, Kushnir AS, White JM (2000) The transmembrane domain of influenza hemagglutinin exhibits a stringent length requirement to support the hemifusion to fusion transition. J Cell Biol 151(2):425–437. https://doi.org/10.1083/jcb.151.2.425
34. Carr CM, Chaudhry C, Kim PS (1997) Influenza hemagglutinin is spring-loaded by a metastable native conformation. Proc Natl Acad Sci U S A 94(26):14306–14313. https://doi.org/10.1073/pnas.94.26.14306

35. Lai AL, Park H, White JM, Tamm LK (2006) Fusion peptide of influenza hemagglutinin requires a fixed angle boomerang structure for activity. J Biol Chem 281(9):5760–5770. https://doi.org/10.1074/jbc.M512280200
36. Steinhauer DA, Wharton SA, Skehel JJ, Wiley DC (1995) Studies of the membrane-fusion activities of fusion peptide mutants of influenza-virus hemagglutinin. J Virol 69 (11):6643–6651
37. Han X, Tamm LK (2000) A host-guest system to study structure-function relationships of membrane fusion peptides. Proc Natl Acad Sci U S A 97(24):13097–13102. https://doi.org/10.1073/pnas.230212097
38. Harter C, James P, Bachi T, Semenza G, Brunner J (1989) Hydrophobic binding of the ectodomain of influenza hemagglutinin to membranes occurs through the fusion peptide. J Biol Chem 264(11):6459–6464
39. Lear JD, Degrado WF (1987) Membrane-binding and conformational properties of peptides representing the NH2 terminus of influenza HA-2. J Biol Chem 262(14):6500–6505
40. Wharton SA, Martin SR, Ruigrok RWH, Skehel JJ, Wiley DC (1988) Membrane-fusion by peptide analogs of influenza-virus hemagglutinin. J Gen Virol 69:1847–1857. https://doi.org/10.1099/0022-1317-69-8-1847
41. Epand RM (2003) Fusion peptides and the mechanism of viral fusion. Biochim Biophys Acta 1614(1):116–121. https://doi.org/10.1016/s0005-2736(03)00169-x
42. Schrodinger, LLC (2010) The PyMOL molecular graphics system, Version 1.3r1
43. Larsson P, Kasson PM (2013) Lipid tail protrusion in simulations predicts fusogenic activity of influenza fusion peptide mutants and conformational models. PLoS Comput Biol 9(3): e1002950. https://doi.org/10.1371/journal.pcbi.1002950
44. Mirjanian D, Dickey AN, Hoh JH, Woolf TB, Stevens MJ (2010) Splaying of aliphatic tails plays a central role in barrier crossing during liposome fusion. J Phys Chem B 114 (34):11061–11068. https://doi.org/10.1021/jp1055182
45. Nishizawa M, Nishizawa K (2013) Molecular dynamics simulation analysis of membrane defects and pore propensity of hemifusion diaphragms. Biophys J 104(5):1038–1048. https://doi.org/10.1016/j.bpj.2013.01.022
46. Smeijers AF, Markvoort AJ, Pieterse K, Hilbers PAJ (2006) A detailed look at vesicle fusion. J Phys Chem B 110(26):13212–13219. https://doi.org/10.1021/jp060824o
47. Bonnafous P, Stegmann T (2000) Membrane perturbation and fusion pore formation in influenza hemagglutinin-mediated membrane fusion – a new model for fusion. J Biol Chem 275(9):6160–6166. https://doi.org/10.1074/jbc.275.9.6160
48. Donald JE, Zhang Y, Fiorin G, Carnevale V, Slochower DR, Gai F, Klein ML, DeGrado WF (2011) Transmembrane orientation and possible role of the fusogenic peptide from parainfluenza virus 5 (PIV5) in promoting fusion. Proc Natl Acad Sci U S A 108 (10):3958–3963. https://doi.org/10.1073/pnas.1019668108
49. Engel A, Walter P (2008) Membrane lysis during biological membrane fusion: collateral damage by misregulated fusion machines. J Cell Biol 183(2):181–186. https://doi.org/10.1083/jcb.200805182
50. Lee KK (2010) Architecture of a nascent viral fusion pore. EMBO J 29(7):1299–1311. https://doi.org/10.1038/emboj.2010.13
51. Legare S, Laggue P (2014) The influenza fusion peptide promotes lipid polar head intrusion through hydrogen bonding with phosphates and N-terminal membrane insertion depth. Proteins: Struct Funct Bioinf 82(9):2118–2127. https://doi.org/10.1002/prot.24568
52. Victor BL, Lousa D, Antunes JM, Soares CM (2015) Self-assembly molecular dynamics simulations shed light into the interaction of the influenza fusion peptide with a membrane bilayer. J Chem Inf Model 55(4):795–805. https://doi.org/10.1021/ci500756v
53. Ayton GA, Noid WG, Voth GA (2007) Multiscale modeling of biomolecular systems: in serial and in parallel. Curr Opin Struct Biol 17:192–198

54. Gurtovenko AA, Anwar J, Vattulainen I (2010) Defect-mediated trafficking across cell membranes: insights from in silico modeling. Chem Rev 110(10):6077–6103. https://doi.org/10.1021/cr1000783
55. Lindahl E, Sansom MSP (2008) Membrane proteins: molecular dynamics simulations. Curr Opin Struct Biol 18:425–431
56. Marrink SJ, de Vries AH, Tieleman DP (2009) Lipids on the move: simulations of membrane pores, domains, stalks and curves. Biochim Biophys Acta 1788:149–168
57. Bullough P, Hughson F, Skehel J, Wiley D (1994) Structure of influenza haemagglutinin at the pH of membrane fusion. Nature 371:37–42
58. Lague P, Roux B, Pastor RW (2005) Molecular dynamics simulations of the influenza hemagglutinin fusion peptide in micelles and bilayers: conformational analysis of peptide and lipids. J Mol Biol 354(5):1129–1141. https://doi.org/10.1016/j.jmb.2005.10.038
59. Li JY, Das P, Zhou RH (2010) Single mutation effects on conformational change and membrane deformation of influenza hemagglutinin fusion peptides. J Phys Chem B 114 (26):8799–8806. https://doi.org/10.1021/jp1029163
60. Vaccaro L, Cross KJ, Kleinjung J, Straus SK, Thomas DJ, Wharton SA, Skehel JJ, Fraternali F (2005) Plasticity of influenza haemagglutinin fusion peptides and their interaction with lipid bilayers. Biophys J 88(1):25–36. https://doi.org/10.1529/biophysj.104.044537
61. Kasson PM, Pande VS (2007) Control of membrane fusion mechanism by lipid composition: predictions from ensemble molecular dynamics. PLoS Comput Biol 3(11):2228–2238. https://doi.org/10.1371/journal.pcbi.0030220
62. Kasson PM, Lindahl E, Pande VS (2010) Atomic-resolution simulations predict a transition state for vesicle fusion defined by contact of a few lipid tails. PLoS Comput Biol 6(6): e1000829. https://doi.org/10.1371/journal.pcbi.1000829
63. Kawamoto S, Shinoda W (2014) Free energy analysis along the stalk mechanism of membrane fusion. Soft Matter 10(17):3048–3054. https://doi.org/10.1039/c3sm52344f
64. Pannuzzo M, De Jong DH, Raudino A, Marrink SJ (2014) Simulation of polyethylene glycol and calcium-mediated membrane fusion. J Chem Phys 140(12):124905. https://doi.org/10.1063/1.4869176
65. Shirts M, Pande VS (2000) Computing – screen savers of the world unite! Science 290 (5498):1903–1904. https://doi.org/10.1126/science.290.5498.1903
66. Lousa D, Pinto ART, Victor BL, Laio A, Veiga AS, Castanho M, Soares CM (2016) Fusing simulation and experiment: the effect of mutations on the structure and activity of the influenza fusion peptide. Sci Rep 6:28099. https://doi.org/10.1038/srep28099
67. Risselada HJ, Marelli G, Fuhrmans M, Smirnova YG, Grubmuller H, Marrink SJ, Muller M (2012) Line-tension controlled mechanism for influenza fusion. PLoS One 7(6):e38302. https://doi.org/10.1371/journal.pone.0038302
68. Fuhrmans M, Marrink SJ (2012) Molecular view of the role of fusion peptides in promoting positive membrane curvature. J Am Chem Soc 134(3):1543–1552. https://doi.org/10.1021/ja207290b
69. Li YL, Han X, Lai AL, Bushweller JH, Cafiso DS, Tamm LK (2005) Membrane structures of the hemifusion-inducing fusion peptide mutant G1S and the fusion-blocking mutant G1V of influenza virus hemagglutinin suggest a mechanism for pore opening in membrane fusion. J Virol 79(18):12065–12076. https://doi.org/10.1128/jvi.79.18.12065-12076.2005
70. Siegel DP, Epand RM (2000) Effect of influenza hemagglutinin fusion peptide on lamellar/inverted phase transitions in dipalmitoleoylphosphatidylethanolamine: implications for membrane fusion mechanisms. Biochim Biophys Acta 1468(1–2):87–98. https://doi.org/10.1016/s0005-2736(00)00246-7
71. Wilber AW, Doye JPK, Louis AA, Noya EG, Miller MA, Wong P (2007) Reversible self-assembly of patchy particles into monodisperse icosahedral clusters. J Chem Phys 127 (8):085106. https://doi.org/10.1063/1.2759922

72. Fraenkelconrat H, Williams RC (1955) Reconstitution of active tobacco mosaic virus from its inactive protein and nucleic acid components. Proc Natl Acad Sci U S A 41(10):690–698. https://doi.org/10.1073/pnas.41.10.690
73. Richards KE, Williams RC (1972) Assembly of tobacco mosaic virus in-vitro – effect of state of polymerization of protein component. Proc Natl Acad Sci U S A 69(5):1121–1124. https://doi.org/10.1073/pnas.69.5.1121
74. Harvey SC, Petrov AS, Devkota B, Boz MB (2009) Viral assembly: a molecular modeling perspective. Phys Chem Chem Phys 11(45):10553–10564. https://doi.org/10.1039/b912884k
75. Hagan MF (2014) Modeling viral capsid assembly. In: Rice SA, Dinner AR (eds) Advances in chemical physics, vol 155, pp 1–67
76. Nguyen HD, Reddy VS, Brooks CL (2007) Deciphering the kinetic mechanism of spontaneous self-assembly of icosahedral capsids. Nano Lett 7(2):338–344. https://doi.org/10.1021/nl062449h
77. Baschek JE, Klein HCR, Schwarz US (2012) Stochastic dynamics of virus capsid formation: direct versus hierarchical self-assembly. BMC Biophys 5(1):22. https://doi.org/10.1186/2046-1682-5-22
78. Boettcher MA, Klein HCR, Schwarz US (2015) Role of dynamic capsomere supply for viral capsid self-assembly. Phys Biol 12(1):016014. https://doi.org/10.1088/1478-3975/12/1/016014
79. Berger B, Shor PW, Tuckerkellogg L, King J (1994) Local rule-based theory of virus shell assembly. Proc Natl Acad Sci U S A 91(16):7732–7736. https://doi.org/10.1073/pnas.91.16.7732
80. Schwartz R, Shor PW, Prevelige PE, Berger B (1998) Local rules simulation of the kinetics of virus capsid self-assembly. Biophys J 75(6):2626–2636. https://doi.org/10.1016/s0006-3495(98)77708-2
81. Hagan MF, Chandler D (2006) Dynamic pathways for viral capsid assembly. Biophys J 91(1):42–54. https://doi.org/10.1529/biophysj.105.076851
82. Xie L, Smith GR, Feng X, Schwartz R (2012) Surveying capsid assembly pathways through simulation-based data fitting. Biophys J 103(7):1545–1554. https://doi.org/10.1016/j.bpj.2012.08.057
83. Krishna V, Ayton GS, Voth GA (2010) Role of protein interactions in defining HIV-1 viral capsid shape and stability: a coarse-grained analysis. Biophys J 98(1):18–26. https://doi.org/10.1016/j.bpj.2009.09.049
84. Chen B, Tycko R (2011) Simulated self-assembly of the HIV-1 capsid: protein shape and native contacts are sufficient for two-dimensional lattice formation. Biophys J 100(12):3035–3044. https://doi.org/10.1016/j.bpj.2011.05.025
85. Grime JMA, Voth GA (2012) Early stages of the HIV-1 capsid protein lattice formation. Biophys J 103(8):1774–1783. https://doi.org/10.1016/j.bpj.2012.09.007
86. Qiao X, Jean J, Weber J, Zhu FQ, Chen B (2015) Mechanism of polymorphism and curvature of HIV capsid assemblies probed by 3D simulations with a novel coarse grain model. Biochim Biophys Acta 1850(11):2353–2367. https://doi.org/10.1016/j.bbagen.2015.08.017
87. Smith GR, Xie L, Lee B, Schwartz R (2014) Applying molecular crowding models to simulations of virus capsid assembly in vitro. Biophys J 106(1):310–320. https://doi.org/10.1016/j.bpj.2013.11.022
88. Hicks SD, Henley CL (2006) Irreversible growth model for virus capsid assembly. Phys Rev E 74(3):031912. https://doi.org/10.1103/PhysRevE.74.031912
89. Levandovsky A, Zandi R (2009) Nonequilibirum assembly, retroviruses, and conical structures. Phys Rev Lett 102(19):198102. https://doi.org/10.1103/PhysRevLett.102.198102
90. Yu ZH, Dobro MJ, Woodward CL, Levandovsky A, Danielson CM, Sandrin V, Shi J, Aiken C, Zandi R, Hope TJ, Jensen GJ (2013) Unclosed HIV-1 capsids suggest a curled sheet model of assembly. J Mol Biol 425(1):112–123. https://doi.org/10.1016/j.jmb.2012.10.006

91. Zhao G, Perilla JR, Yufenyuy EL, Meng X, Chen B, Ning J, Ahn J, Gronenborn AM, Schulten K, Aiken C, Zhang P (2013) Mature HIV-1 capsid structure by cryo-electron microscopy and all-atom molecular dynamics. Nature 497(7451):643–646. https://doi.org/10.1038/nature12162
92. Bruinsma RF (2006) Physics of RNA and viral assembly. Eur Phys J E 19(3):303–310. https://doi.org/10.1140/epje/i2005-10071-1
93. Roos WH, Bruinsma R, Wuite GJL (2010) Physical virology. Nat Phys 6(10):733–743. https://doi.org/10.1038/nphys1797
94. Chang CB, Knobler CM, Gelbart WM, Mason TG (2008) Curvature dependence of viral protein structures on encapsidated nanoemulsion droplets. ACS Nano 2(2):281–286. https://doi.org/10.1021/nn700385z
95. Hu YF, Zandi R, Anavitarte A, Knobler CM, Gelbart WM (2008) Packaging of a polymer by a viral capsid: the interplay between polymer length and capsid size. Biophys J 94 (4):1428–1436. https://doi.org/10.1529/biophysj.107.117473
96. Johnson KN, Tang L, Johnson JE, Ball LA (2004) Heterologous RNA encapsidated in pariacoto virus-like particles forms a dodecahedral cage similar to genomic RNA in wild-type virions. J Virol 78(20):11371–11378. https://doi.org/10.1128/jvi.78.20.11371-11378.2004
97. Sun J, DuFort C, Daniel MC, Murali A, Chen C, Gopinath K, Stein B, De M, Rotello VM, Holzenburg A, Kao CC, Dragnea B (2007) Core-controlled polymorphism in virus-like particles. Proc Natl Acad Sci U S A 104(4):1354–1359. https://doi.org/10.1073/pnas.0610542104
98. ElSawy KM, Caves LSD, Twarock R (2011) On the origin of order in the genome organization of ssRNA viruses. Biophys J 101(4):774–780. https://doi.org/10.1016/j.bpj.2011.07.005
99. Perlmutter JD, Qiao C, Hagan MF (2013) Viral genome structures are optimal for capsid assembly. eLife 2:e00632. https://doi.org/10.7554/eLife.00632
100. Chen C, Kwak ES, Stein B, Kao CC, Dragnea B (2005) Packaging of gold particles in viral capsids. J Nanosci Nanotechnol 5(12):2029–2033. https://doi.org/10.1166/jnn.2005.506
101. Dixit SK, Goicochea NL, Daniel MC, Murali A, Bronstein L, De M, Stein B, Rotello VM, Kao CC, Dragnea B (2006) Quantum dot encapsulation in viral capsids. Nano Lett 6(9):1993–1999. https://doi.org/10.1021/nl061165u
102. Dragnea B, Chen C, Kwak ES, Stein B, Kao CC (2003) Gold nanoparticles as spectroscopic enhancers for in vitro studies on single viruses. J Am Chem Soc 125(21):6374–6375. https://doi.org/10.1021/ja0343609
103. Johnson JM, Tang JH, Nyame Y, Willits D, Young MJ, Zlotnick A (2005) Regulating self-assembly of spherical oligomers. Nano Lett 5(4):765–770. https://doi.org/10.1021/nl050274q
104. Elrad OM, Hagan MF (2008) Mechanisms of size control and polymorphism in viral capsid assembly. Nano Lett 8(11):3850–3857. https://doi.org/10.1021/nl802269a
105. Stockley PG, Twarock R, Bakker SE, Barker AM, Borodavka A, Dykeman E, Ford RJ, Pearson AR, Phillips SEV, Ranson NA, Tuma R (2013) Packaging signals in single-stranded RNA viruses: nature's alternative to a purely electrostatic assembly mechanism. J Biol Phys 39 (2):277–287. https://doi.org/10.1007/s10867-013-9313-0
106. Tsiang M, Niedziela-Majka A, Hung M, Jin DB, Hu E, Yant S, Samuel D, Liu XH, Sakowicz R (2012) A trimer of dimers is the basic building block for human immunodeficiency Virus-1 capsid assembly. Biochemistry 51(22):4416–4428. https://doi.org/10.1021/bi300052h
107. Grayson P, Evilevitch A, Inamdar MM, Purohit PK, Gelbart WM, Knobler CM, Phillips R (2006) The effect of genome length on ejection forces in bacteriophage lambda. Virology 348 (2):430–436. https://doi.org/10.1016/j.virol.2006.01.003
108. LaMarque JC, Le TVL, Harvey SC (2004) Packaging double-helical DNA into viral capsids. Biopolymers 73(3):348–355. https://doi.org/10.1002/bip.10529
109. Locker CR, Harvey SC (2006) A model for viral genome packing. Multiscale Model Simul 5 (4):1264–1279. https://doi.org/10.1137/060650684

110. Petrov AS, Lim-Hing K, Harvey SC (2007) Packaging of DNA by bacteriophage Epsilon15: structure, forces, and thermodynamics. Structure 15(7):807–812. https://doi.org/10.1016/j.str.2007.05.005
111. Petrov AS, Harvey SC (2008) Packaging double-helical DNA into viral capsids: structures, forces, and energetics. Biophys J 95(2):497–502. https://doi.org/10.1529/biophysj.108.131797
112. Smith DE, Tans SJ, Smith SB, Grimes S, Anderson DL, Bustamante C (2001) The bacteriophage phi 29 portal motor can package DNA against a large internal force. Nature 413 (6857):748–752. https://doi.org/10.1038/35099581
113. Petrov AS, Harvey SC (2007) Structural and thermodynamic principles of viral packaging. Structure 15(1):21–27. https://doi.org/10.1016/j.str2006.11.013
114. Forrey C, Muthukumar M (2006) Langevin dynamics simulations of genome packing in bacteriophage. Biophys J 91(1):25–41. https://doi.org/10.1529/biophysj.105.073429
115. Locker CR, Fuller SD, Harvey SC (2007) DNA organization and thermodynamics during viral packing. Biophys J 93(8):2861–2869. https://doi.org/10.1529/biophysj.106.094771
116. Harrison SC, Olson AJ, Schutt CE, Winkler FK, Bricogne G (1978) Tomato bushy stunt virus at 2.9 Å resolution. Nature 276(5686):368–373. https://doi.org/10.1038/276368a0
117. Huber RG, Marzinek JK, Holdbrook DA, Bond PJ (2017) Multiscale molecular dynamics simulation approaches to the structure and dynamics of viruses. Prog Biophys Mol Biol 128:121–132. https://doi.org/10.1016/j.pbiomolbio.2016.09.010
118. Stone JE, Phillips JC, Freddolino PL, Hardy DJ, Trabuco LG, Schulten K (2007) Accelerating molecular modeling applications with graphics processors. J Comput Chem 28 (16):2618–2640. https://doi.org/10.1002/jcc.20829
119. Freddolino PL, Arkhipov AS, Larson SB, McPherson A, Schulten K (2006) Molecular dynamics simulations of the complete satellite tobacco mosaic virus. Structure 14 (3):437–449. https://doi.org/10.1016/j.str.2005.11.014
120. Zeng YY, Larson SB, Heitsch CE, McPherson A, Harvey SC (2012) A model for the structure of satellite tobacco mosaic virus. J Struct Biol 180(1):110–116. https://doi.org/10.1016/j.jsb.2012.06.008
121. Arkhipov A, Freddolino PL, Schulten K (2006) Stability and dynamics of virus capsids described by coarse-grained modeling. Structure 14(12):1767–1777. https://doi.org/10.1016/j.str.2006.10.003
122. Zink M, Grubmuller H (2010) Primary changes of the mechanical properties of southern bean mosaic virus upon calcium removal. Biophys J 98(4):687–695. https://doi.org/10.1016/j.bpj.2009.10.047
123. Larsson DSD, Liljas L, van der Spoel D (2012) Virus capsid dissolution studied by microsecond molecular dynamics simulations. PLoS Comput Biol 8(5):e1002502. https://doi.org/10.1371/journal.pcbi.1002502
124. Marzinek JK, Holdbrook DA, Huber RG, Verma C, Bond PJ (2016) Pushing the envelope: dengue viral membrane coaxed into shape by molecular simulations. Structure 24 (8):1410–1420. https://doi.org/10.1016/j.str.2016.05.014
125. Machado MR, Gonzalez HC, Pantano S (2017) MD simulations of virus like particles with supra CG solvation affordable to desktop computers. J Chem Theory Comput 13 (10):5106–5116. https://doi.org/10.1021/acs.jctc.7b00659
126. Mihai ME, Tecu C, Ivanciuc AE, Necula G, Lupulescu E, Onu A (2011) Survival of H5N1 influenza virus in water and its inactivation by chemical methods. Roum Arch Microbiol Immunol 70:78–84
127. Stallknecht DE, Shane SM, Kearney MT, Zwank PJ (1990) Persistence of avian influenza-viruses in water. Avian Dis 34(2):406–411. https://doi.org/10.2307/1591428
128. Reddy T, Sansom MSP (2016b) The role of the membrane in the structure and biophysical robustness of the dengue virion envelope. Structure 24:375–382
129. Rzepiela AJ, Schäfer LV, Goga N, Risselada HJ, de Vries AH, Marrink SJ (2010) Reconstruction of atomistic details from coarse grained structures. J Comput Chem 31:1333–1343

130. Stansfeld PJ, Sansom MSP (2011) From coarse-grained to atomistic: a serial multi-scale approach to membrane protein simulations. J Chem Theory Comput 7:1157–1166
131. Barrera EE, Frigini EN, Porasso RD, Pantano S (2017) Modeling DMPC lipid membranes with SIRAH force-field. J Mol Model 23(9):259. https://doi.org/10.1007/s00894-017-3426-5
132. Darre L, Machado MR, Brandner AF, Gonzalez HC, Ferreira S, Pantano S (2015) SIRAH: a structurally unbiased coarse-grained force field for proteins with aqueous solvation and long-range electrostatics. J Chem Theory Comput 11(2):723–739. https://doi.org/10.1021/ct5007746